Roles for Nucleophiles and Hydrogen-Bonding Agents in the Decomposition of Phosphine-Free Ruthenium Metathesis Catalysts

Alexandre Goudreault

Thesis submitted to the
Faculty of Graduate and Postdoctoral Studies
University of Ottawa
in partial fulfillment of the requirements for the degree of

Master of Science

Center for Catalysis Research and Innovation
Department of Chemistry and Biomolecular Science
Ottawa-Carleton Chemistry Institute
Faculty of Science
University of Ottawa

Table of Contents

List of Figures

List of Schemes

Abstract

With its unrivaled versatility and atom economy, olefin metathesis is arguably the most powerful catalyst methodology now known for the construction of carbon-carbon bonds. When compared to palladium-catalyzed cross-coupling methodologies, however, catalyst productivity lags far behind, even for the "robust" ruthenium metathesis catalysts. Unexpected limitations to the robustness of these catalysts were first widely publicized by reports describing the implementation of metathesis in pharmaceutical manufacturing. Recurring discussion centered on low catalyst productivity resulting from decomposition of the Ru catalysts by impurities, including ppm-level contaminants in the technical-grade solvent. Over the past 7 years, a series of mechanistic studies from the Fogg group has uncovered the pathways by which common contaminants (or indeed reagents) trigger catalyst decomposition. Two principal pathways were identified: abstraction of the alkylidene or methylidene ligand by nucleophiles, and deprotonation of the metallacyclobutane intermediate by Bronsted base. Emerging applications, however, notably in chemical biology, highlight new challenges to catalyst productivity.

The first part of this thesis emphasizes the need for informed mechanistic insight as a guide to catalyst redesign. The widespread observation of a cyclometallated N-heterocyclic carbene (NHC) motif in crystal structures of catalyst decomposition products led to the presumption that activation of a C-H bond in the NHC ligand initiates catalyst decomposition. Reducing NHC bulk has therefore been proposed as critical to catalyst redesign. In experiments designed to probe the viability of this solution, the small NHC ligand IMe_4 (tetramethylimidazol-2-ylidene) was added to the resting-state methylidene complexes formed in metathesis by the first- and second-generation Grubbs catalysts ($RuCl_2(PCy_3)_2(=CH_2)$ **GIm** or $RuCl_2(H_2IMes)(PCy_3)(=CH_2)$ **GIIm**, respectively). The intended product, a resting-state methylidene species bearing a truncated NHC, was not formed, owing to immediate loss of the methylidene ligand. Methylidene loss is now shown to result from nucleophilic attack by the NHC – a small, highly potent nucleophile – on the methylidene. Density functional calculations indicate that IMe_4 abstracts the methylidene, generating the N-heterocyclic olefin $H_2C{=}IMe_4$. The latter is an even more potent nucleophile, which attacks a second methylidene, resulting in liberation of $[EtIMe_4]Cl$. These findings report indirectly on the original question concerning the impact of ligand truncation. The ease with which a small, potent nucleophile can abstract the key methylidene ligand from **GIm** and **GIIm** underscores the importance of *increasing* steric protection at the $[Ru]{=}CH_2$ site. This chemistry also suggests intriguing possibilities for efficient, selective, controlled methylidene abstraction to terminate metathesis activity while leaving the "$RuCl_2(H_2IMes)(PCy_3)$" core intact. This could prove an enabling strategy for tandem catalysis applications in which metathesis is the first step.

The second part of this thesis, inspired by the potential of olefin metathesis in chemical biology, focuses on the impact of hydroxide ion and water on the productivity of phosphine-free metathesis catalysts. In reactions with the important second-generation Hoveyda catalyst **HII**, hydroxide anion is found to engage in salt metathesis with the chloride ligands, rather than nucleophilic

attack. The resulting Ru-hydroxide complex is unreactive toward any olefins larger than ethylene, while ethylene itself causes rapid decomposition. Proposed as the decomposition pathway is bimolecular coupling promoted by the strong H-bonding character of the hydroxide ligands.

Lastly, the impact of the water on Ru-catalyzed olefin metathesis is examined. In a survey of normally facile metathesis reactions using state-of-the-art catalysts, even trace water (0.1% v/v) is found to be highly detrimental. The impact of water is shown to be greater at room temperature than previously established at 60 °C. Preliminary evidence strongly suggests that the mechanism by which water induces decomposition is temperature-dependent. Thus, at high temperature, decomposition of the metallacyclobutane intermediate appears to dominate, but this pathway is ruled out at ambient temperatures. Instead, water is proposed to promote bimolecular decomposition. Polyphenol resin, which can sequester water by H-bonding, is shown to offer an interim solution to the presence of trace water in organic media. These findings suggest that major avenues of investigation aimed at reducing intrinsic catalyst decomposition may likewise be relevant to the development of water-tolerant catalysts.

List of Contributions

Publications

1. S. A. Rufh, **A. Y. Goudreault**, M. Foscato, V. R. Jensen, and D. E. Fogg. "Rapid Decomposition of Olefin Metathesis Catalysts by a Truncated N-heterocyclic Carbene: Efficient Catalyst Quenching and N-Heterocyclic Carbene Vinylation." *ACS Catal.* **2018**, 11822–11826. (Communication)

2. **A. Y. Goudreault**, D. M. Walden, A. G. Botti, S. Steinmann, C. Michel, and D. E. Fogg. "Hydroxide-Induced Catalyst Deactivation in Olefin Metathesis." *ACS Catal.* (Submitted; Communication).

3. **A. Y. Goudreault**, A. G. Botti, and D. E. Fogg. "Water-Tolerant Olefin Metathesis: Hits and Myths." (Manuscript in preparation).

Presentations (O = Oral, P = Poster; presenting author in bold)

P4. **A. Y. Goudreault**, D. M. Walden, A. G. Botti, S. Steinmann, C. Michel, and D. E. Fogg. "Exploring the Effect of Hydroxide Ion in Metathesis." 102nd Canadian Society for Chemistry Conference, Quebec City, QC, June 3rd, 2019.

O3. **A. Y. Goudreault**, D. M. Walden, A. G. Botti, S. Steinmann, C. Michel, and D. E. Fogg. "Exploring the Effect of Hydroxide Ion on the Hoveyda-II Metathesis Catalyst: Decomposition or Deactivation?" Ottawa-Carleton Chemistry Institute (OCCI) Day, Ottawa, ON, May 23rd, 2019.

O2. **A. Y. Goudreault**, A. G. Botti, D. E. Fogg. "Re-examining the Role of Water in Olefin Metathesis: Innocuous, or Fatal?" Ottawa-Carleton Chemistry Institute (OCCI) Day, Ottawa, ON, May 22nd, 2019.

P1. **A. Y. Goudreault**, A. G. Botti, and D. E. Fogg. "Reaction of the Hoveyda Metathesis Catalyst with Hydroxide: Salt Metathesis vs. Nucleophilic Activation of the Benzylidene Ligand." 50th Inorganic Discussion Weekend (IDW), Ryerson University, Toronto, ON, November 3rd, 2017.

Acknowledgments

First and foremost, I would like to thank my supervisor Prof. Deryn Fogg for her guidance, support, and patience over the course of my graduate studies. I profoundly appreciate her training in how to think critically about science, and how to communicate ideas effectively. The skills and knowledge I gained during my time in her group I will use for the rest of my life.

I have greatly valued the support of the uOttawa NMR staff, Dr. Glenn Facey and Dr. Peter Pallister, who provided invaluable technical help and guidance over the years. I would also like to express my appreciation the assistance of Dr. Yun Liu and Roxanne Clément with electron microscopy and high-throughput experimentation, respectively. I also thank the Science Stores staff, especially Pierre Bisson, for their cheerful and expert assistance in procuring and shipping chemicals and materials.

To the lab members of the Fogg group, both past and present, it has been a truly unforgettable experience working with all of you. I thank Carolyn, Emma, and Gwen, for introducing me to the exciting world of research. Their enthusiasm first sparked my interest in organometallic chemistry. I thank Stephanie Ton and Stephanie Rufh for countless lunch and coffee breaks (and for letting me win at crib). Craig and Daniel, I cherish our friendship and I hope that we keep in touch. Xinrui, I appreciate your letting me hog the glovebox during desperate times. Andrew and Mason, I appreciate your always being willing to discuss and try out new ideas. To all of the others, I am grateful to have been colleagues during my time in the Fogg group.

To my family: Mom, Dad, Krystle (and the boys/Tiffany), Dominique, Andrew, and Brittany, my thanks for always being there for me. Lastly, to my best friend Jaymie, thank you for being by my side every step of the way, and for always believing in me - I truly could not have done it without you.

List of Compounds

Organic and main-group compounds

Compound	Structure	Compound	Structure
H_2IMes	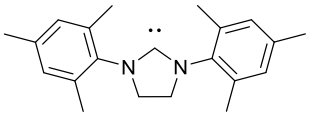	IMes	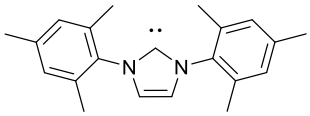
IMe_4	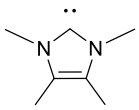	CAAC	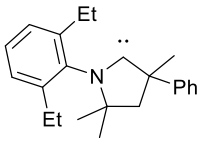
o-dianiline	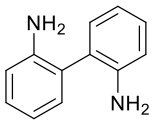	**1**	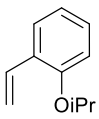
2		**3**	
4		**5**	[$MePCy_3$]Cl
6		**7**	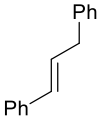
8	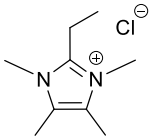	**9**	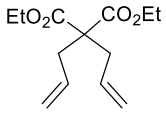
10	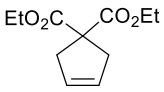	**11**	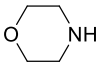
12	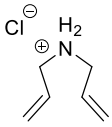	**13**	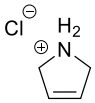
14	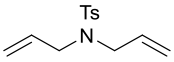	**15**	
16	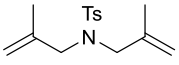	**17**	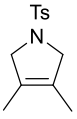

18	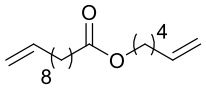	**19**	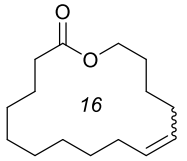
20	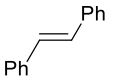	**21**	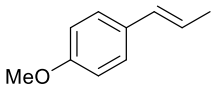
22	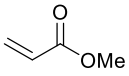	**23**	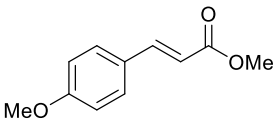

Transition-metal complexes

Compound	Structure	Compound	Structure
Ta-I	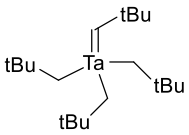	**W-I**	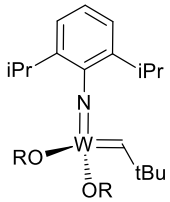
Mo-I	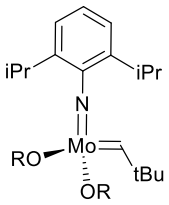	**Mo-II**	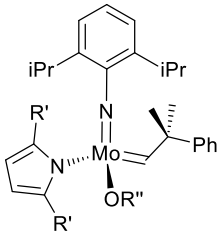
Mo-Im	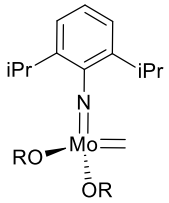	**GI**	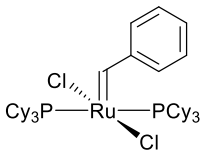
GII	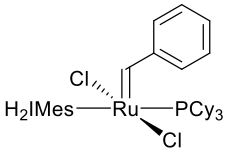	**HII**	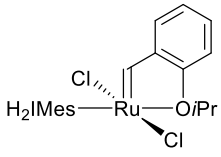

GIm	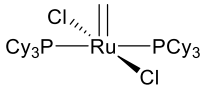	**GIIm**	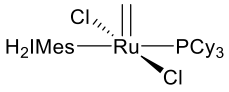
HII-OH	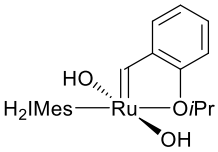	**PII**	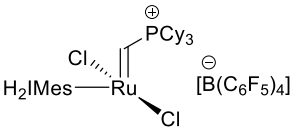
Caz-I	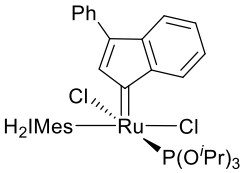	**Ind-II**	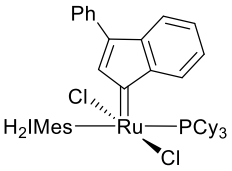
DA	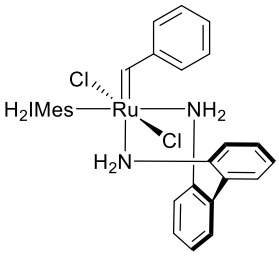	**nG**	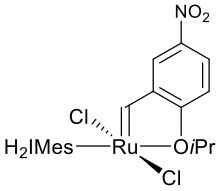
nGC	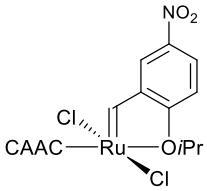	**Ru-1**	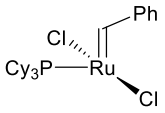
Ru-2	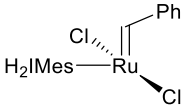	**Ru-3**	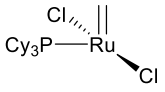
Ru-4	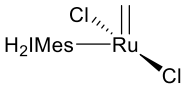	**Ru-5**	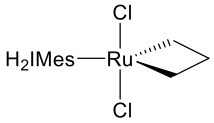
Ru-5'	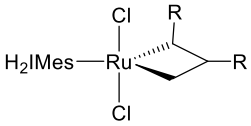	**Ru-6**	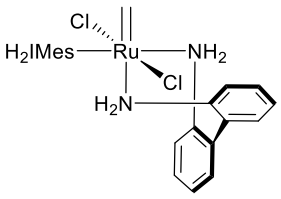

Ru-7	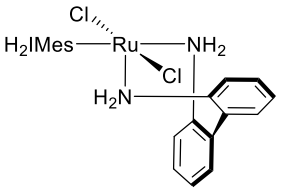	**Ru-8**	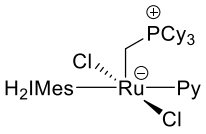
Ru-9	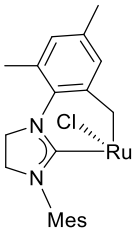	**Ru-10**	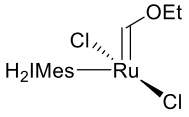
Ru-11	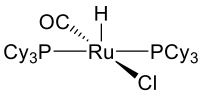	**Ru-12**	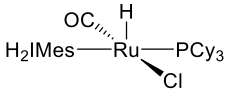
Ru-13	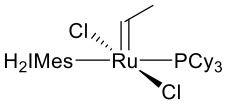	**Ru-14**	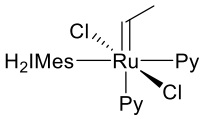
Ru-15	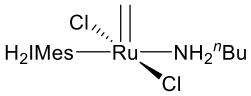	**Ru-16**	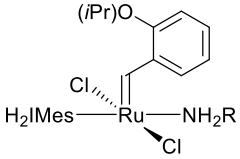
Ru-17	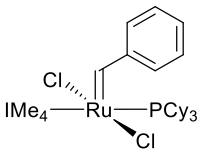	**Ru-18**	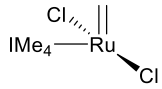
Ru-19	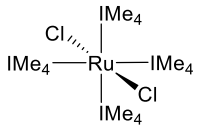	**Ru-20**	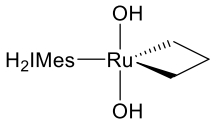
Ru-21	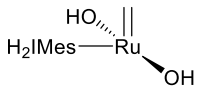	**Ru-22**	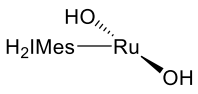

Ru-23	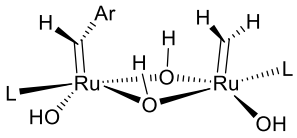	**Ru-24**	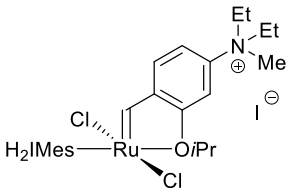
Ru-25	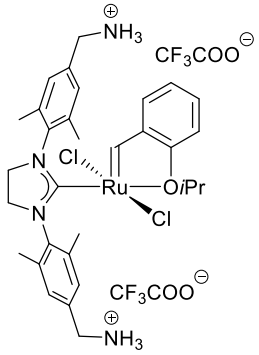	**Ru-26**	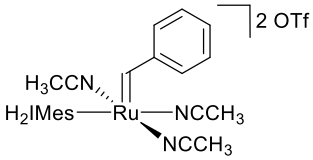
Ru-27	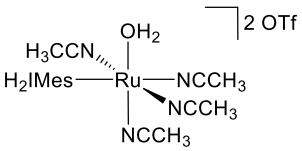	**Ru-28**	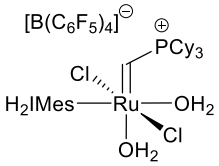
Ru-29	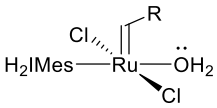	**Ru-30**	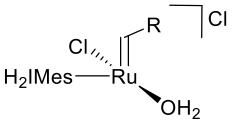

List of Abbreviations

ADMET	Acyclic diene metathesis
ATR	Attenuated total reflectance
BMC	Bimolecular coupling
CAAC	Cyclic alkyl amino carbene
CM	Cross-metathesis
DBU	1,8-Diazabicyclounde-7-ene
DDM	Diethyl diallylmalonate
DFT	Density functional theory
DMT	Dimethyl terephthalate
dppb	1,2-Bis(diphenylphosphino)butane
Equiv	Equivalents
FID	Flame-ionization detector
FT-IR	Fourier transform infra-red
GC	Gas chromatography
HPLC	High performance liquid chromatography
KTp	Potassium tris(1-pyrazolyl)borate
MALDI	Matrix-assisted laser desorption/ionization
MAP	Monoaryloxide pyrrolide
MCB	Metallacyclobutane
MeOH	Methanol
mRCM	Macrocyclic ring-closing metathesis
NHC	N-heterocyclic carbene
NHO	N-heterocyclic olefin
NMR	Nuclear magnetic resonance
PTFE	Polytetrafluoroethylene
PVP-MMA	Polyvinylphenol-methyl methacrylate
RCM	Ring-closing metathesis
ROMP	Ring-opening metathesis polymerization
SHOP	Shell higher olefin process
SM	Self-metathesis
THF	Tetrahydrofuran
TMSCl	Trimethylsilyl chloride
TOF	Time-of-flight
TON	Turnover number

Chapter 1. Introduction

1.1 Transition-Metal Catalysis

Catalysis revolutionized the landscape of synthetic chemistry over the 20th century, and represents a core technology for the sustainable production of chemicals and materials in the 21st century. Catalysis offers significant, in some cases enabling, reductions in energy and materials usage relative to traditional stoichiometric transformations.[1] Catalysts accelerate reactions by opening lower-energy reaction pathways, without being consumed in the process.[2] They can also contribute to the goal of full recyclability at the industrial level, where sustainable development is predicated on reducing waste and minimizing energy and materials usage.[3]

New catalytic methodologies based on molecular transition-metal complexes have helped expand the organic chemist's toolbox. Over the past two decades, three Nobel Prizes in chemistry have been awarded for transformative advances in the field of molecular catalysis. The first was awarded to Knowles, Noyori, and Sharpless in 2001 for their work in asymmetric hydrogenation and oxidation.[4-6] The second, in 2005, recognized Chauvin, Grubbs, and Schrock, for their contributions to the development of olefin metathesis for organic synthesis.[7-9] Lastly, in 2010, Heck, Negishi, and Suzuki were honoured for the development of palladium-catalyzed cross-couplings in organic synthesis.[10,11] The ubiquity of these methodologies highlights their global importance for synthetic "discovery" operations, as well as the potential of catalysis in pharmaceutical and specialty-chemicals manufacturing.

This importance notwithstanding, challenges to translation of metathesis methodologies into large-scale production are beginning to be more widely acknowledged. The issues have been highlighted in several leading reviews.[12-14] Both catalyst productivity (i.e. turnover number, TON) and consistent, reliable performance are integral to economic viability. In olefin metathesis, even where "robust" ruthenium catalysts are used, productivity and reliability are much more challenging than is the case in hydrogenation or cross-coupling catalysis. The identification of key decomposition pathways is a critical step toward developing longer-lived catalysts. Better understanding of catalyst vulnerabilities enables (in the short term) process redesign to curb decomposition. In the longer term, it provides an essential foundation for rational catalyst redesign.

1.2 Olefin Metathesis

1.2.1 General Background

Olefin metathesis is a chemical process that involves the rearrangement of carbon-carbon double bonds. Early, empirical reports utilized ill-defined catalysts.[15] From the 1950s to the 1970s, olefin metathesis was commonly carried out with heterogeneous mixtures of metal salts and alkylating agents.[16] Widely-used catalyst systems were based on group 6 (especially tungsten) salts or oxides and alkylaluminum reagents. These were highly active in ring-opening polymerization (ROMP) of cyclic olefins, in particular.[17,18] Supported W and Re oxides were also used in important

industrial applications involving cross-metathesis of unsaturated hydrocarbons, notably the Phillips Triolefin Process and the Shell Higher Olefins Process (SHOP).[19,20] All of these applications, importantly, are limited to *non-functionalized* hydrocarbons. Only with the development of more robust catalysts was the metathesis of functionalized olefins a possibility.

The search for well-defined catalysts (typically containing a [M]=CHR active site) saw intense research effort following acceptance of the Chauvin mechanism for olefin metathesis.[21] As shown in Scheme 1.1, the Chauvin mechanism postulates a series of [2+2] cycloaddition / cycloreversion equilibria, initiated by the reaction of a metal alkylidene catalyst with incoming olefin to form a metallacyclobutane (MCB) intermediate. Metal-alkylidene complexes were thus regarded as the most direct entry point into the catalytic cycle, and became a major focus of catalyst design efforts.

Scheme 1.1 Olefin metathesis reaction and the Chauvin mechanism.

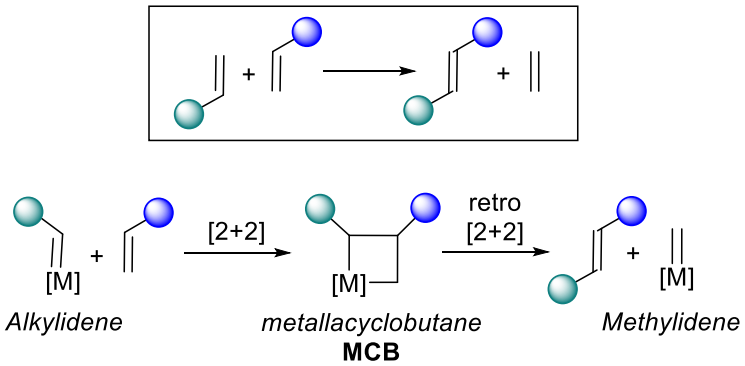

The first well-defined metal-alkylidene complex was designed and synthesized by Schrock in 1974.[22] This seminal report described the synthesis of the stable, isolable Ta(V) neopentylidene complex **Ta-I** (Chart 1.1). The high oxidation state of the metal results in a highly polarized M=CHR bond, with a partial positive charge at tantalum, and a partial negative charge at the alkylidene carbon. This and other such complexes are hence very reactive, and susceptible to unwanted side reactions with carbonyl functionalities, including ketones,[23] or protic groups such as alcohols or water. In addition, the complexes readily dimerize,[24] resulting in bimolecular decomposition, as discussed in Section 1.2.3.

Chart 1.1 Selected Schrock catalysts and (extreme right; **Mo-II**) a Schrock-Hoveyda mono-aryloxide pyrrolide (MAP) catalyst.

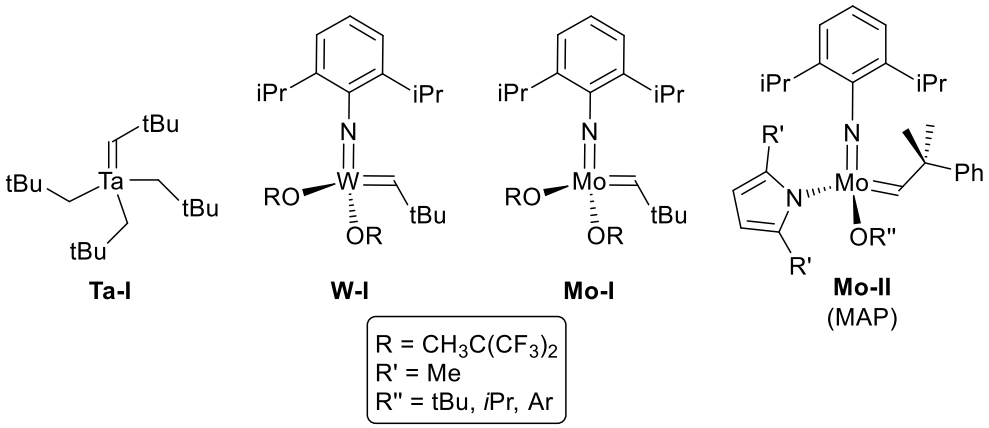

Subsequently-developed group 6 complexes were designed with steric protection of the alkylidene carbon in mind. In Schrock catalysts such as **W-I** and **Mo-I**, bulky imido and alkoxide (or aryloxide) ligands impede unwanted dimerization (Chart 1.1 above). The ease with which the substituents on these groups could be modified also confers a high level of steric and electronic tunability, and thus control over activity and stereoselectivity.[25,26] Replacing an alkoxide ligand with pyrrolide, in turn, generated the important MAP catalysts, one example of which is shown above. The latter are now regarded as the state of the art in the group 6 catalysts.[27]

For the four-coordinate Schrock catalysts, the ligand bulk is removed from the immediate vicinity of the metal center. These coordinatively unsaturated complexes therefore react with olefin via an associative pathway (Scheme 1.2).[27] They can also, however, bind other small molecules. While many of the Mo and W catalysts can exhibit high metathesis productivity in skilled hands, their sensitivity to oxygen and water (and in some cases their thermal sensitivity)[27] has limited widespread use. In contrast is the ease of handling of ruthenium catalysts described in the next section, which led to widespread adoption of olefin metathesis in organic synthesis.[28]

Scheme 1.2 Associative binding of olefin to **Mo-1** (C-N-O pocket highlighted in red).

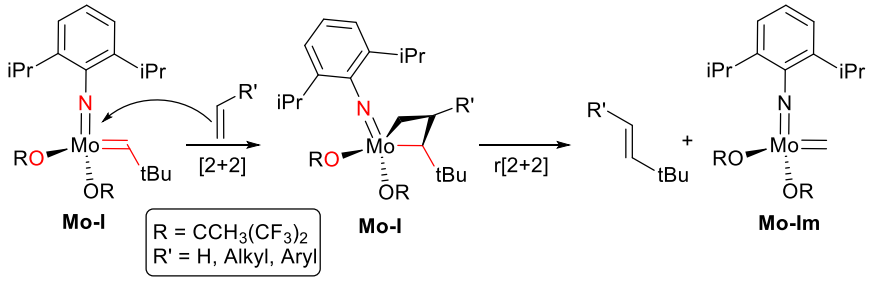

1.2.2 Ruthenium-Catalyzed Olefin Metathesis

Ruthenium metathesis catalysts with the general structure $RuX_2L_2(=CHR)$ are now ubiquitous in synthetic chemistry. While the first Ru-alkylidene catalyst was reported by Grubbs in 1992,[28] the

popularity of Ru-catalyzed olefin metathesis accelerated with the development of the first-generation Grubbs catalyst **GI** (Chart 1.2) in 1995.[29] Despite the lower activity of **GI** relative to the Mo and W catalysts, its improved stability to air, water, and functional groups put olefin metathesis, for the first time, into the hands of the practicing organic chemist.[28]

Chart 1.2 Widely used first- and second-generation ruthenium metathesis catalysts

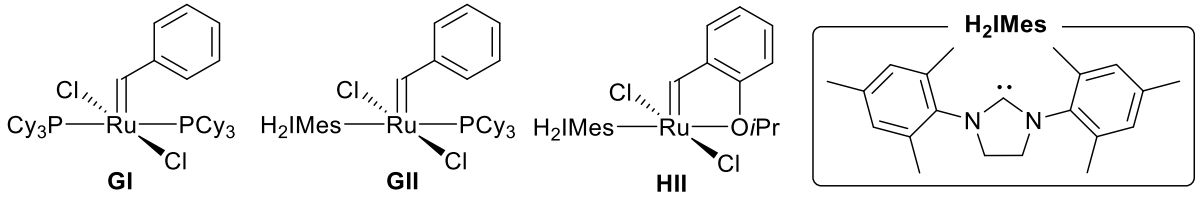

The tolerance of the catalysts for less rigorously anaerobic conditions led to the rapid deployment of **GI** in a variety of metathesis transformations (e.g. acyclic diene metathesis polymerization, ADMET; macrocyclic ring-closing metathesis, mRCM; and cross-metathesis, CM, Scheme 1.3).[30] A search for higher activity led to modifications to the neutral L-donor ligands. Most significantly, installation of an N-heterocyclic carbene (NHC) ligand in place of PCy_3 generated dramatically more reactive catalysts.[31] Among the first and most important of these was the second-generation Grubbs catalyst **GII**,[32] in which one PCy_3 ligand is replaced by the saturated H_2IMes ligand (see Chart 1.2 above). Even 20 years later, **GII** remains one of the most commonly used catalysts in academia, despite limitations discussed in the following Sections. Another leading catalyst is the phosphine-free variant **HII**, known as the Hoveyda catalyst.[33] **HII** initiates more readily[34] than **GII**: it is also free from the PCy_3-mediated decomposition pathway that plague **GII** and related catalysts (Section 1.2.3).

Scheme 1.3 Selected metathesis transformations. (a) Acyclic diene metathesis polymerization (ADMET). (b) Macrocyclic ring-closing metathesis (mRCM). (c) Cross-metathesis (CM).

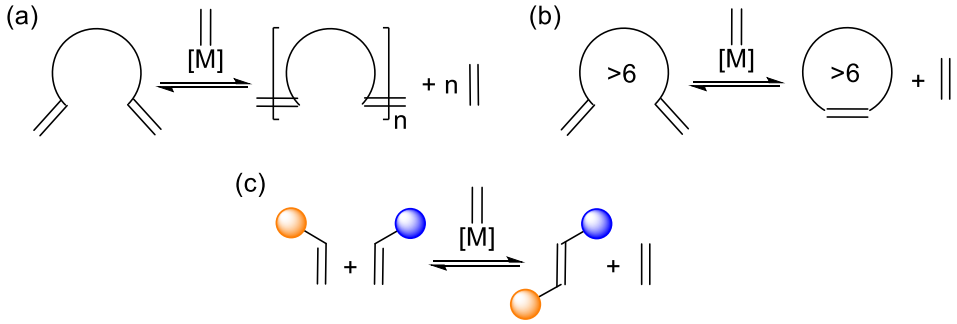

In contrast to the four-coordinate Schrock catalysts, the Ru catalysts are almost invariable *five-coordinate*, square pyramidal complexes, in which the high-trans-effect alkylidene ligand occupies the apical site. This necessitates ligand loss to generate a four-coordinate transition-state species (see **Ru-1**, **Ru-2**; Scheme 1.4). The latter can bind incoming olefin cis to the Ru=CHR bond, enabling cycloaddition to form the MCB intermediate.

Scheme 1.4 Catalytic cycle for metathesis by the first- and second-generation Grubbs catalysts, **GI** and **GII** (respectively)

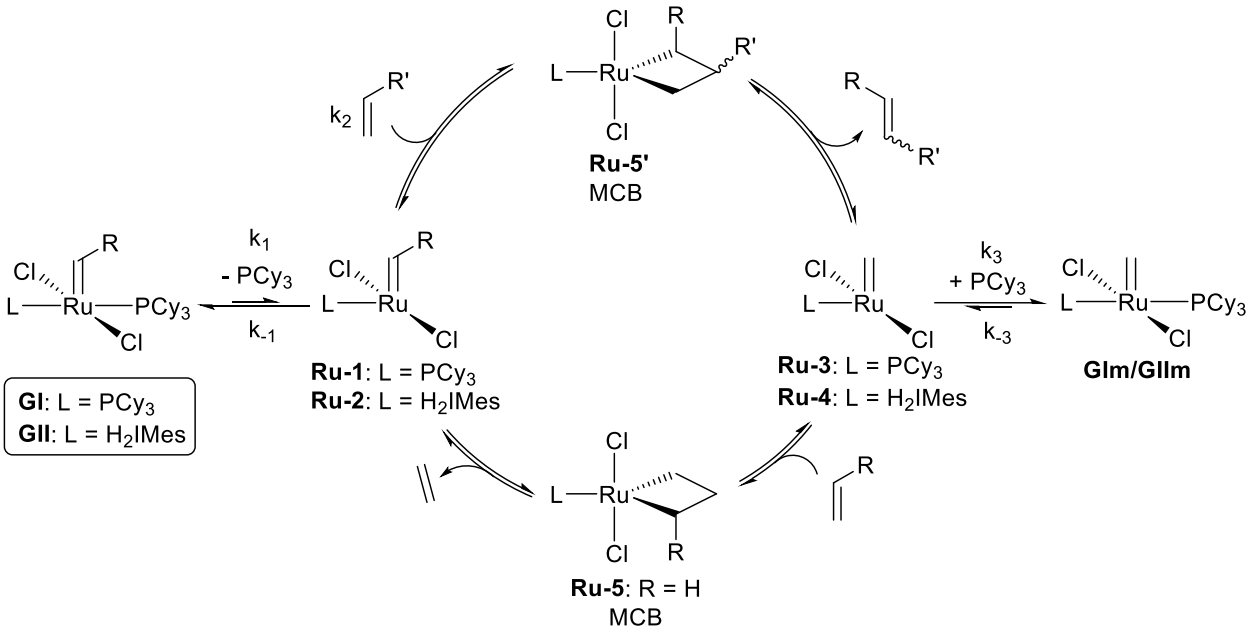

The need for ligand loss is particularly problematic for **GII**, given the very low lability of the PCy_3 ligand. This affects both initiation of the precatalyst **GII** (k_1 in Scheme 1.4)[35] and re-entry from the resting-state methylidene complex **GIIm**[36]: that is, k_{-3}. This was an unanticipated challenge in the Grubbs-class catalysts. Indeed, Grubbs originally attributed the higher activity of the second-generation catalysts to *labilization* of the PCy_3 ligand by the strong σ-donor NHC.[32] This idea was abandoned when **GII** was shown to undergo PCy_3 loss nearly 150 times slower than **GI** (Table 1.1).[37] The activating effect of the NHC ligand is now assigned to its strongly σ-donating character, which reduces the energy barrier to cycloaddition,[38] as well as a property described by Chen as "higher commitment".[39] That is, Ru-NHC catalysts undergo reaction with olefin faster than re-uptake of PCy_3 ($k_2 > k_{-1}$ for **GII**; Scheme 1.4).[37] Thus, although **GII** enters the catalytic cycle less readily than **GI**, it remains on-cycle longer.

Table 1.1 Relative rates of PCy_3 loss from the first- and second-generation Grubbs catalysts **GI** and **GII**, and their resting-state methylidene complexes **GIm** and **GIIm**. (Data from refs 36 and 39; Table reproduced from ref 39).

	k_1 or k_{-3} for PCy_3 loss (s^{-1})	k_{rel} (x slower vs. **GI**)
GI	9.6	1
GII	0.13	148
GIm	– [a]	– [a]
GIIm	4.7×10^{-4}	41,000 (ca. 275 x slower than **GII**)

[a] The rate of PCy_3 loss from **GIm** cannot be calculated, due to competing decomposition.

A powerful differentiation also exists between the benzylidene precatalyst, and the resting-state methylidene complex formed by re-uptake of PCy_3. Loss of PCy_3 from **GIIm**, the PCy_3-bound off-cycle resting state (Scheme 3 above), is ca. 275 times slower than from the parent **GII** (Table 1.1).[36] In consequence, the concentration of this deactivated methylidene species increases over time, reducing the effective catalyst charge.

An added concern is the vulnerability of this reservoir complex to loss of the metal-alkylidene bond. It is sterically protected, however, from direct attack at the methylidene carbon (except by small nucleophiles, such as H_2NnBu).[40] Four-coordinate **Ru-4** is much more readily attacked, but the low lability of the PCy_3 group impedes access to this species.[36] Discussed in Section 1.2.4 (under "induced decomposition pathways") is the accelerating effect of various donor groups on PCy_3 loss, which in turn accelerates intermolecular nucleophilic attack by PCy_3 on the methylidene ligand.[41]

Increasing the stability of the four-coordinate methylidene species **Ru-4** and the MCB intermediate **Ru-5** is key to high catalyst productivity. Noteworthy is that **Ru-4** is the same for all precatalysts for which L = H_2IMes. Differences in precatalyst structure therefore affect primarily the rate of formation of **Ru-4**. That is, faster-initiating catalysts such as **HII** enter the catalytic cycle more readily, but the active species **Ru-4** is the same (Scheme 1.5).[34] The faster uptake (at least with small olefins) of **HII** is due to its capacity to undergo *associative* initiation.[42-44] Faster entry is reinforced by the absence of a thermodynamically very stable resting state such as **GIIm**. For **HII**, the resting state is the **HII** precatalyst itself, formed by re-uptake of the styrenyl ether co-product **1**.[34] This so-called "boomerang mechanism", originally proposed by Hoveyda,[34] has been the subject of debate.[45] However, mechanistic labelling and kinetics studies by the Fogg and Diver groups demonstrated that it is indeed operative.[46,47]

Scheme 1.5 Catalytic cycle for initiation, operation, and "boomerang" recapture of the phosphine-free catalyst **HII**.

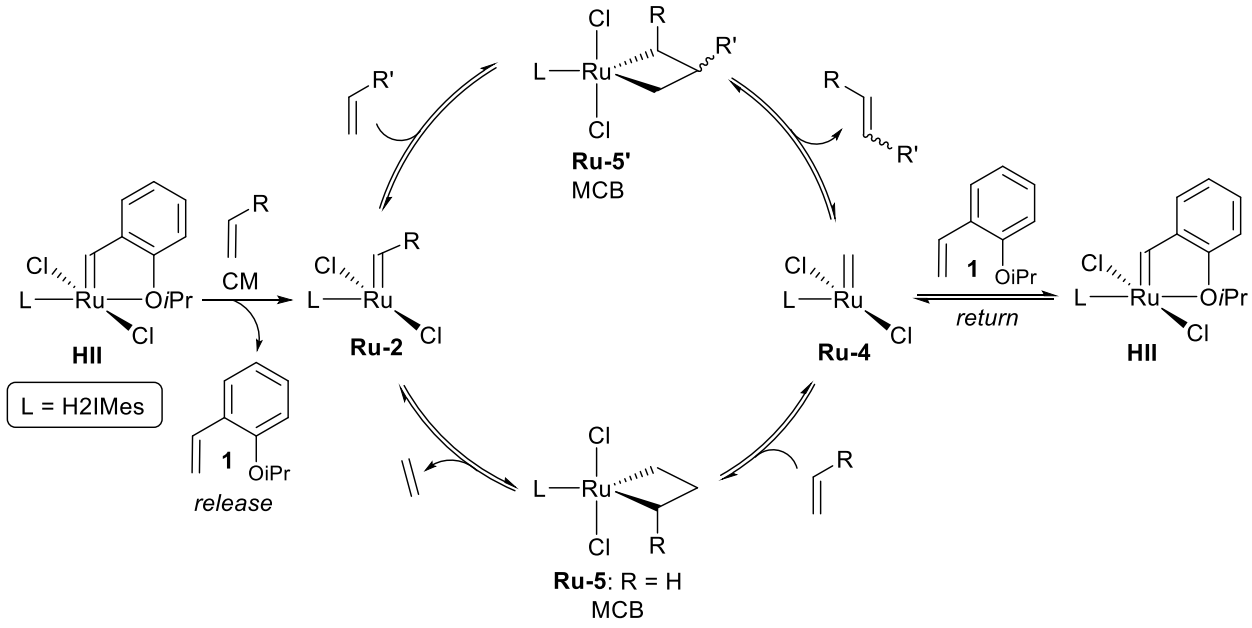

Methylidene **Ru-4** can be studied indirectly via its five-coordinate resting-state species. Most important of these is **GIIm**, study of which was greatly facilitated by Justin Lummiss's 2012 development of a high-yield synthetic route.[40,48] In comparison, the MCB intermediate (see **Ru-5**) has been less extensively examined, although computational evidence indicates that this is the on-cycle resting state.[49,50] For example, Solans-Monfort reported in a computational study that cycloreversion is the highest barrier in the cycle,[38] while Nelson and co-workers reported that substituted **Ru-5'** (where R = C_6H_4-*o*-O*i*Pr and R' = H) is more stable than the alkylidene or methylidene species **Ru-2** or **Ru-4**.[43]

For many years, the difficulty in studying the MCB intermediate was due to the five-coordinate nature of the Ru precatalysts. The problem lies in the fact that the fifth ligand that stabilizes the precatalyst can recapture the four-coordinate transition-state species $RuCl_2L(=CH_2)$ as a five-coordinate, off-cycle resting state (of which **GIIm** is just one example). Because these species were much more stable than the MCB, the latter – despite being the most stable *on-cycle* species[50] – could not be observed. In sharp contrast, the four-coordinate nature of the Schrock catalysts enables direct observation of the MCB intermediates by NMR methods at room temperature. Indeed, the unsubstituted tungstacyclobutane derived from **W-1** could even be isolated at 0 °C.[25]

Piers' development of a four-coordinate ruthenium catalyst was therefore a landmark accomplishment, which opened the door to direct study of the MCBs for the Ru catalysts.[51] The Piers catalysts are four-coordinate phosphonium alkylidene complexes (e.g. **PII**, Scheme 1.6) which undergo irreversible loss of the vinyl phosphonium salt on reaction with ethylene. This enables high-yield access to the ruthenacyclobutane **Ru-5**.[52] (In subsequent studies, the substituted

MCBs **Ru-5'** were also generated, by treating **PII** or its analogues with terminal olefins).[53] Romero and Piers were able to characterize **Ru-5** by NMR methods, and reported a strong C_α—C_β agostic interaction with the Ru center.[54] They also demonstrated that **Ru-5**, though stable at –40 °C, decomposed on warming to room temperature. The mechanistic basis of this pathway is discussed in the next Section.

Scheme 1.6 Generating the unsubstituted MCB **Ru-5** via second-generation Piers catalyst **PII**.

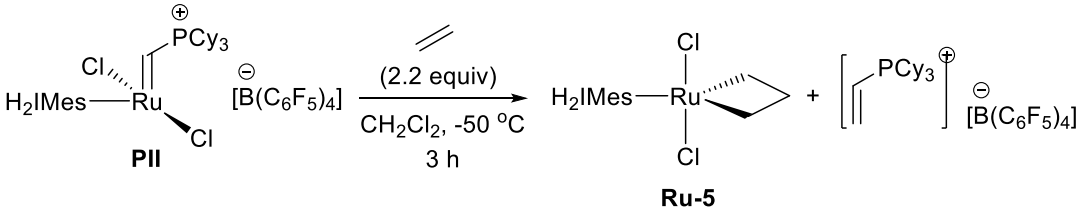

Understanding of Ru-catalyzed olefin metathesis is now at an advanced stage. A series of mechanistic studies, detailed below, established important guidelines for decomposition of Ru metathesis catalysts. Such studies are critical to identifying how and why certain functionalities or conditions limit catalyst performance. They enable rationalization of the large body of empirical evidence for functional-group tolerance or incompatibility in metathesis, and are ultimately the key to informed catalyst redesign. Discussed below are the major decomposition pathways identified to date. Considered first are pathways intrinsic to the Ru precatalyst or active species (Section 1.2.3). Alternative pathways induced by external agents, such as nucleophiles or Bronsted base, are then considered (Section 1.2.4).

1.2.3 Intrinsic Decomposition Pathways for Ru Metathesis Catalysts

Intrinsic decomposition pathways now known to be common to all metathesis catalysts are: (a) bimolecular coupling (BMC) of four-coordinate alkylidene species, such as **Ru-2/Ru-4**, and (b) decomposition of the MCB intermediate **Ru-5** via β-hydride elimination.

Pathway (a), established during the 1980s for group 6 and 7 transition-metal catalysts,[22,55-57] was only recently confirmed for the important Ru-NHC catalysts.[58] Coupling of four-coordinate $RuCl_2(L)(=CHR)$ intermediates was widely inferred for labile first-generation Ru catalysts (L = PCy_3 and other phosphines), based on the observed elimination of RCH=CHR products during catalyst synthesis or use.[59,60] It was considered unlikely for second-generation Ru catalysts,[61,62] an idea that has only recently been overturned.[58] Gwen Bailey of this research group brilliantly showed BMC of transiently stabilized methylidene complexes **Ru-6** by observation and quantitation of the ethylene liberated via coupling (Scheme 1.7). With Carolyn Higman, she found that increasing the bulk of the Ru-alkylidene group can greatly inhibit coupling, consistent with the behaviour of early metal catalysts.[58] Methylidene complexes such as **Ru-4** thus couple much more readily than their benzylidene counterparts. These findings cemented BMC as a major decomposition pathway for second-generation Ru-catalysts. Very recent work by Daniel do Nascimento of this research group demonstrated that even the benzylidene precatalysts are

vulnerable to decomposition by BMC, if the stabilizing ancillary ligand is abstracted to generate four-coordinate **Ru-2**.[63]

Scheme 1.7 Bimolecular coupling of transiently-stabilized methylidene complexes.

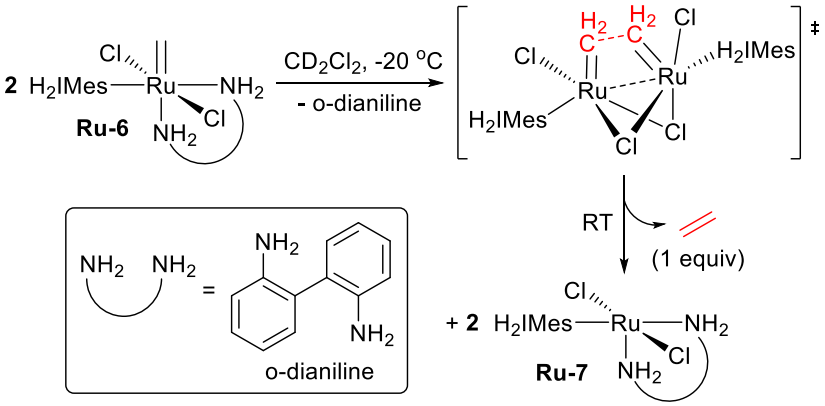

A second general decomposition pathway, again well established for the early transition-metals, is β-elimination of the MCB ring.[64] Here H-transfer from the MCB β-CH_2 group to the metal gives an allyl hydride intermediate, which can reductively eliminate a propene (H_2C=CHCHR **3** or RCH_2=$CHCH_3$ **4**, Scheme 1.8).[65] The strongest evidence for this pathway in the Ru systems was reported by Piers, who generated the ^{13}C-labelled MCB at -40 °C in CD_2Cl_2 and observed the labelled propene (albeit without quantitation) on warming to -10 °C.[52-54] For a monosubstituted MCB, decomposition instead generates a substituted propene.

The extent of β-elimination is maximized where the reaction conditions favour formation of unsubstituted **Ru-5**. Such conditions include ethenolysis reactions (in which internal olefins are converted to terminal olefins by CM with ethylene) or reactions in which poor mass transfer impedes volatilization of ethylene, ranging from high-throughput screening in small wellplates to process chemistry in pharma.

Scheme 1.8 Decomposition of MCB **Ru-5'** via β-hydride transfer and reductive elimination to liberate propenes **2, 3,** and **4**.

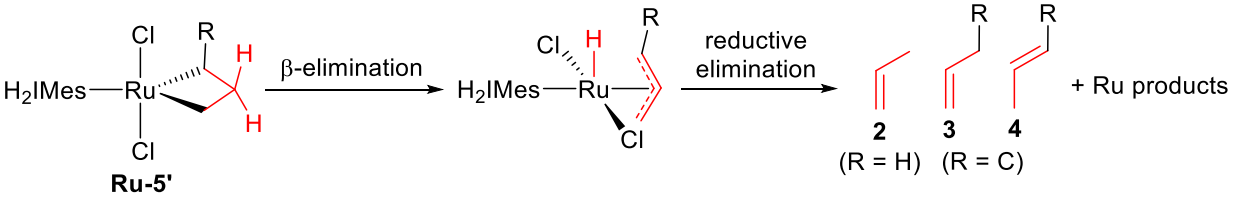

A final intrinsic decomposition pathway is specific to the Grubbs precatalysts, which are stabilized by a PCy_3 ligand. The role of PCy_3 is not limited to re-coordination to generate the resting state methylidene species, as shown above. It can also function as a nucleophile, attacking the Ru=CH_2 moiety (Scheme 1.9). As this indicates, the Ru=C bond is polarized toward Ru. The polarization of the M=C bond is thus opposite to that seen in the Schrock catalysts. The high nucleophilicity of

PCy_3, combined with the steric accessibility of the methylidene ligand, constitute a potent challenge to longevity for all Grubbs-class catalysts.

Liberation of $[MePCy_3]Cl$ **5** was first reported by Hong and Grubbs,[66] in a discovery widely celebrated for the wrong reasons. The key finding of this study is not the crystallographic identification of a Ru hydride as a decomposition product (widely, and incorrectly,[67] described as responsible for unwanted isomerization during metathesis reactions). Rather, the key finding was the observation that **5** is formed, albeit in unquantified amounts, via decomposition of **GIIm**. William McClennan and Justin Lummiss of this research group confirmed quantitative transformation of the methylidene ligand into the phosphonium salt $[MePCy_3]Cl$ **5** (Scheme 1.9).[68] In a careful labelling study, they reported spectroscopic evidence for the σ-alkyl intermediate **Ru-8**, and were able to isolate the corresponding pyridine adduct for the first-generation Grubbs catalyst.[68] For the NHC derivatives, the stability of the σ-alkyl intermediate is limited by facile C-H activation of the mesityl group, which effects rapid liberation of the phosphonium salt.

Scheme 1.9 Attack of PCy_3 on the methylidene ligand, and decomposition of the σ-alkyl intermediate **Ru-8**.

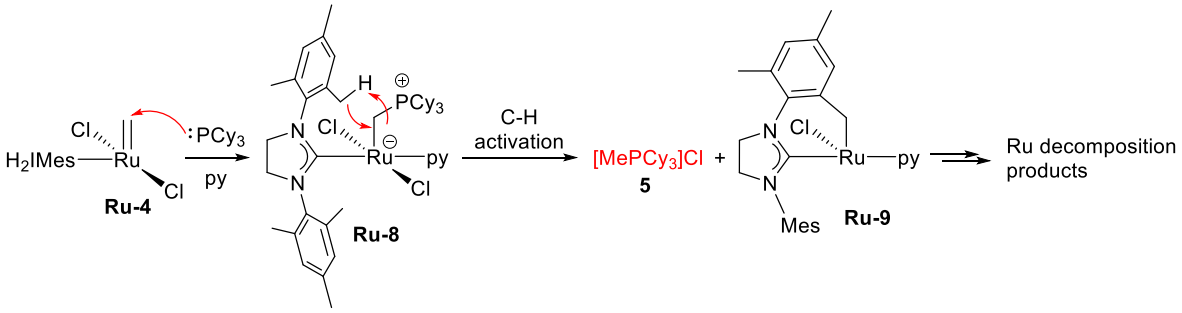

This protonolysis event was also examined. A kinetic isotope effect was observed in decomposition of the d_{22}-H_2IMes derivative **GIIm***, confirming involvement of the mesityl protons in liberation of $[MePCy_3]Cl$ **5**.[41] The Ru product contains a cyclometallated NHC of type **Ru-9**. Many reports have described the serendipitous crystallization of cyclometallated Ru products during decomposition of second-generation metathesis catalysts.[55,57,69] The Lummiss-McClennan studies were the first to indicate that cyclometallation is merely opportunistic. That is, nucleophilic attack on the methylidene carbon is the primary deactivation event: cyclometallation of the NHC merely provides a subsequent convenient proton.

It should be noted that the bimolecular nature of PCy_3-mediated decomposition means that this pathway will decrease in relevance as catalyst loadings are reduced. Moreover, in macrocyclization (which is necessarily carried out at high dilutions: e.g. 5 mM diene), the concentration of free PCy_3 is greatly reduced, and the significance of this pathway diminishes.[63,70] Importantly, however, it is greatly accelerated by the presence of external donor species.[41] The role of such contaminants in promoting this pathway is discussed in the next section.

1.2.4 Induced Decomposition of Ru Catalysts

Catalyst decomposition can be induced by contaminants, functional groups, additives, or even solvent, all of which may react with the precatalyst or the metathesis-active Ru intermediates. Loss of either the alkylidene ligand or the metallacyclobutane ring terminates metathesis activity. This section examines the contributions to decomposition of Lewis donors, nucleophiles, and Bronsted bases. Not considered are reactions with directly-functionalized olefins (for example vinyl ether **6**, which generate unreactive Fischer carbenes: Scheme 1.10).[37] The metathesis of directly-functionalized olefins remains a frontier area, and is discussed in detail in a recent review.[71]

Scheme 1.10 Reaction of **HII** with ethyl vinyl ether **6** to form the Fischer carbene **Ru-10**.

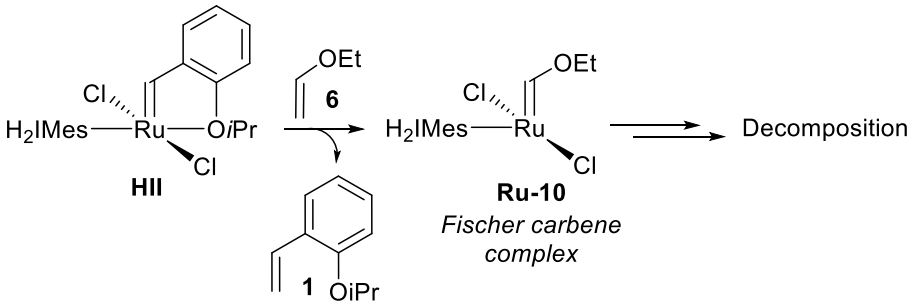

Several functional groups remain problematic for Ru metathesis catalysts. Groups that bind to Ru, such as alcohols,[72] amines (discussed later), thiols[73] and others[57] may retard metathesis. Protic functionalities are generally thought to be tolerated by the Ru catalysts, but several reports indicate otherwise, particularly where base is also present that can generate alkoxide species.[72,74-78] Reaction of the first- and second-generation Grubbs catalyst with methanol or methoxide generates hydrido-carbonyl Ru complexes (Scheme 1.11). Nicholas Beach of this research group demonstrated that decomposition by methanol alone is slow.[74] Thus, **GII'** was converted to $RuHCl(CO)(IMes)(PCy_3)$ only after heating at 60 °C for 4 h in CH_2Cl_2-MeOH. **GI** was even slower to react (8 h). In both cases, the alkylidene was liberated as the corresponding alkane.[74] Computational studies are consistent with this general picture.[79] Methanolysis is greatly accelerated by added base, owing to facile formation and β-elimination of Ru-alkoxide species.[72,74-78] Additional decomposition pathways enabled by Bronsted base, without alcohol, are considered later.

Scheme 1.11 Methanolysis of the first- and second-generation Grubbs catalysts to generate hydridocarbonyl complexes **Ru-11** and **Ru-12**.

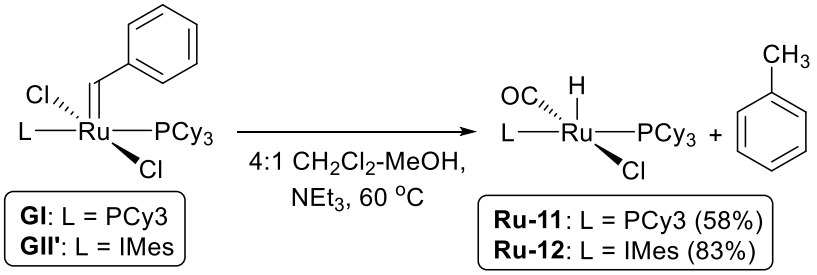

Most broadly deleterious to the PR_3-stabilized Grubbs catalysts are Lewis donors, which accelerate methylidene abstraction by phosphine.[41] William McClennan of this research group demonstrated the relevance of this pathway with a wide range of phosphine-stabilized catalysts (including PCy_3 and PPh_3 derivatives) and showed that it is promoted even by weak oxygen donors. Thus, as shown in Scheme 1.12a, up to 50% decomposition of the methylidene complex **GIIm** is induced by 100 equiv THF after only 2 h at 50 ºC. Abstraction of the methylidene ligand as the $[MePCy_3]Cl$ **5** salt was established. Moreover, this pathway was shown to be associative in donor, meaning that it will accelerate as the donor concentration increases. This accounts for the poor performance of (R)CM reactions using **GII** in THF and "green" ethereal solvents. Likewise problematic is the metathesis of terminal olefins in water, a subject considered in more detail in Chapter 4.

Scheme 1.12 (a) Donor-accelerated decomposition of the second-generation Grubbs methylidene complex **GIIm**. (b) Robustness of the ethylidene ligand to this decomposition manifold.

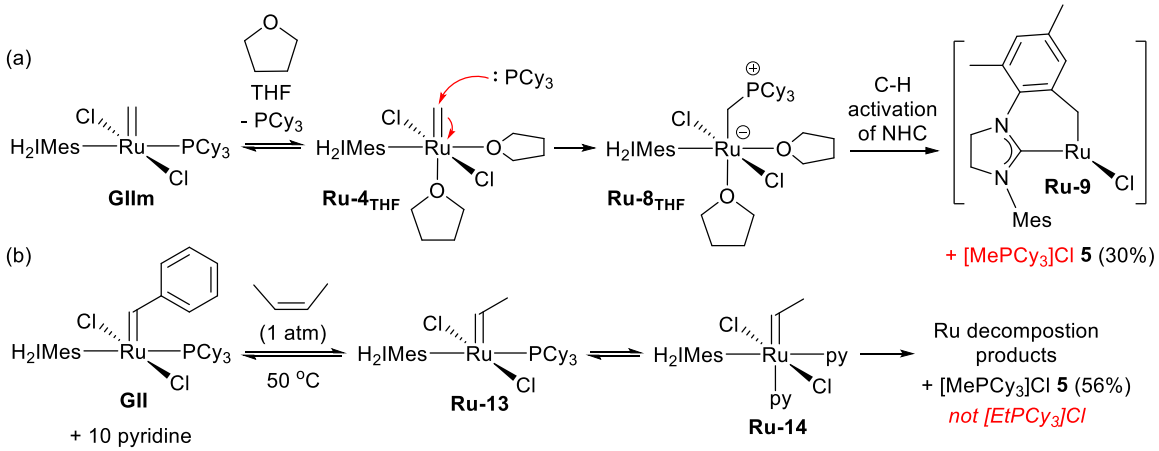

Of note, steric bulk at the alkylidene moiety can protect against nucleophilic attack by PCy_3. The ethylidene analogue of **GIIm** (Scheme 1.11b above) was shown by McClennan to undergo zero decomposition (hence zero release of $[EtPCy_3]Cl$) after 1 h at 50 °C in the presence of pyridine. Under the same conditions, liberation of **5** from **GIIm** was complete within minutes at RT.[41] This experiment offered the first clear insight into the superior metathesis performance attainable with **GII** when α-olefin substrates are replaced by β-methyl olefins.[30,80] Importantly, however, this is an incomplete solution to the problem of catalyst decomposition if isomerization can occur (as is the case with 2-butene), as the methylidene complex forms over time. [41]

While PCy_3 is a particularly strong nucleophile, primary aliphatic amines can likewise attack. Specifically, Justin Lummiss of this research group demonstrated that *n*-butyl amine rapidly abstracts not only the methylidene, but even the benzylidene functionality from **GII** and **GIIm**, respectively.[40,81] By utilizing ^{13}C-labelled **GIIm***, Lummiss was able to demonstrate that $NH_2{}^nBu$ can compete with PCy_3 for attack (Scheme 1.13a). NMR analysis indicated 30% liberation of $NH^nBu(^{13}CH_3)$ (formed via 1,2-H transfer) and 70% $[^{13}CH_3PCy_3]Cl$ **5***.[40]

Benjamin Ireland found similar behaviour with **HII** (Scheme 1.13b).[82] Both *n*-butylamine and benzylamine quantitatively abstracted the benzylidene ligand from **HII** within minutes at room temperature (Scheme 1.12b).[82] When the bulk of the primary amine or substitution number is increased, nucleophilic attack is shut down, and amine adducts are formed. Decomposition during metathesis ensues with these adducts, but via attack on the MCB intermediate, as discussed below.[82]

Scheme 1.13 (a) Abstraction of the methylidene ligand from ^{13}C-labelled **GIIm*** by n-butylamine. (b) Abstraction of the benzylidene ligand from **HII** by primary amines.

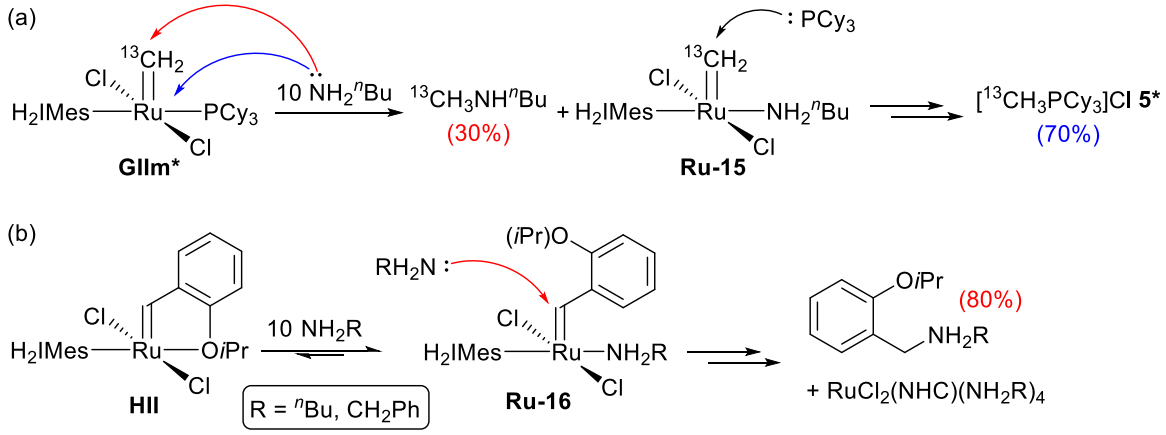

Molecular oxygen in air can also be problematic,[75,76,83] although (as discussed in Chapter 4) it is less aggressive than water.[84] In a mechanistic analysis, Stephanie Ton of this research group reported evidence for release of benzaldehyde via [2+2] addition of O_2 across the benzylidene bond.[83] A key additional pathway, at the 20 mM catalyst concentrations compatible with NMR analysis, was bimolecular decomposition following consumption of the PCy_3 ligand as the phosphine oxide.

One of the most important decomposition pathways, however, is induced by Bronsted base (Scheme 1.14). Deprotonation of the MCB at the β-site transforms the ring into a Ru-allyl species, which undergoes loss of propene following activation of a mesityl C-H bond[85] (cf. the intrinsic β-elimination pathway described in the preceding Section). As shown by Bailey and computational collaborators Foscato and Jensen, the relatively high acidity of the MCB β-CH_2 unit[85] enables deprotonation of the MCB by Bronsted bases ranging in strength from DBU down to NEt_3. Both were shown to be detrimental to **HII** even at room temperature.[82] After only 1 h, complete decomposition was observed on exposure to 10 equiv styrene and 1 equiv NEt_3, with >80% formation of β-methylstyrene **4** and 1,3-diphenylpropene **7**. Density functional theory (DFT) studies indicated that deprotonation of the MCB is thermodynamically preferred to deprotonation of the methylidene ligand.[85]

Scheme 1.14 β-deprotonation pathway for **HII** by added base during metathesis of styrene.

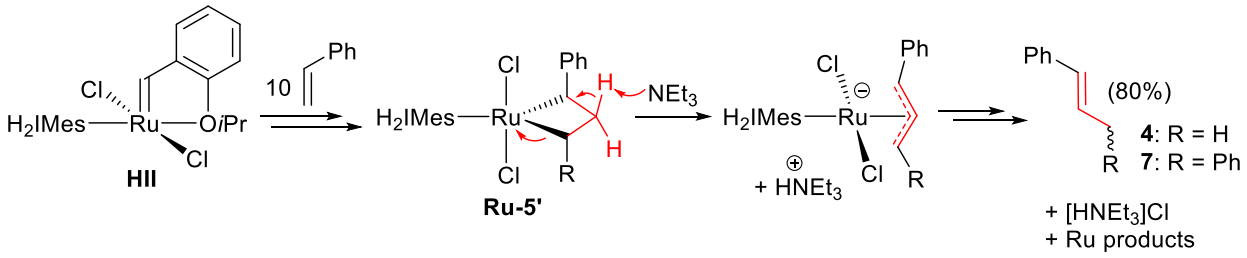

1.3 Scope of Thesis

Elucidating the mechanism by which catalyst decomposition occurs is the first step in determining how it can be prevented. Until recently, the majority of reports describing decomposition of Ru metathesis catalysts focused almost solely on the identity of Ru products identified by X-ray analysis of crystals that serendipitously deposited from reactions, typically in unknown yields. From these structures, hypotheses about decomposition pathways and solutions were widely formulated, but rarely examined.

Chapter 2 of this thesis set out to examine the impact of a specific ligand redesign strategy. "Slimming" of the NHC has been proposed based on the common observation of a cyclometallated H_2IMes ligand in second-generation catalysts. Prior work from the Fogg group sought to tackle the question of whether NHC truncation is beneficial, or detrimental, by undertaking synthesis of a methylidene analogue of **GIIm**, in which the H_2IMes ligand was truncated to an N-Me NHC. While the answer to the initial question appeared clear-cut and negative, the mechanistic details were unresolved. Chapter 2 adds critical, unexpected details that expand on these insights, and reveal new possibilities in tandem catalysis.

Examined in the next two Chapters is the impact of two specific contaminants on Ru-catalyzed olefin metathesis. Recent decomposition studies are distinguished by the mechanistic value placed on identification and quantitation of the organic products expelled from the catalyst. Such data were invaluable in elucidating the major pathways outlined above. This approach is adopted to determine the impact of hydroxide ion (Chapter 3) and water (Chapter 4). Both of these questions are relevant in multiple applications contexts. Arguably most exciting of these is chemical biology, but the literature clearly shows that metathesis in biologically relevant media has far to go in terms of catalyst performance. The negative impact of hydroxide anion is examined in Chapter 3, and a mechanism of deactivation is proposed. The more general question of the impact of H_2O on catalyst productivity is examined in Chapter 4. Finally, Chapter 5 highlights and reviews key findings, and suggests avenues for future work.

1.4 References

(1) Sheldon, R. A., *Green Chemistry and Catalysis*. Wiley-VCH: Chichester, 2007.

(2) Rothenberg, G., *Catalysis*. Wiley-VCH: Weinheim, 2008.

(3) Anastas, P.; Eghbali, N., Green Chemistry: Principles and Practice. *Chem. Soc. Rev.* **2010**, *39*, 301–312.

(4) Knowles, W. S., Asymmetric Hydrogenations (Nobel lecture). *Angew. Chem., Int. Ed.* **2002**, *41*, 1999–2007.

(5) Noyori, R., Nobel Lecture. *Angew. Chem., Int. Ed.* **2002**, *41*, 2008–2022.

(6) Sharpless, K. B., Searching for New Reactivity (Nobel lecture). *Angew. Chem., Int. Ed.* **2002**, *41*, 2024–2032.

(7) Chauvin, Y., Olefin Metathesis: The Early Days (Nobel Lecture). *Angew. Chem., Int. Ed.* **2006**, *45*, 3741–3747.

(8) Schrock, R. R., Multiple Metal-Carbon Bonds for Catalytic Metathesis Reactions (Nobel Lecture). *Angew. Chem., Int. Ed.* **2006**, *45*, 3748–3759.

(9) Grubbs, R. H., Olefin-Metathesis Catalysts for the Preparation of Molecules and Materials (Nobel Lecture). *Angew. Chem., Int. Ed.* **2006**, *45*, 3760–3765.

(10) Negishi, E.-i., Magical Power of Transition Metals: Past, Present, and Future (Nobel Lecture). *Angew. Chem., Int. Ed.* **2011**, *50*, 6738–6764.

(11) Suzuki, A., Cross-Coupling Reactions of Organoboranes: An Easy Way to Construct C-C Bonds (Nobel Lecture). *Angew. Chem., Int. Ed.* **2011**, *50*, 6722–6737.

(12) Higman, C. S.; Lummiss, J. A. M.; Fogg, D. E., Olefin Metathesis at the Dawn of Uptake in Pharmaceutical and Specialty Chemicals Manufacturing. *Angew. Chem., Int. Ed.* **2016**, *55*, 3552–3565.

(13) Farina, V.; Horváth, A., Ring-Closing Metathesis in the Large-Scale Synthesis of Pharmaceuticals. In *Handbook of Metathesis*, Grubbs, R. H.; Wenzel, A. G., Eds. Wiley-VCH: Weinheim, 2015; Vol. 2, pp 633–658.

(14) Fandrick, K. R.; Savoie, J.; Jinhua, N. Y.; Song, J. J.; Senanayake, C. H., Challenges and Opportunities for Scaling the Ring-Closing Metathesis Reaction in the Pharmaceutical Industry. In *Olefin Metathesis – Theory and Practice*, Grela, K., Ed. Wiley: Hoboken, 2014; pp 349-366.

(15) Grubbs, R. H., *Handbook of Metathesis*. Wiley-VCH: Weinheim, 2003.

(16) Ivin, K. J.; Mol, J. C., *Olefin Metathesis and Metathesis Polymerization*. Academic Press: New York, 1997.

(17) Banks, R. L.; Bailey, G. C., Olefin Disproportionation. A New Catalytic Process. *Ind. Eng. Chem. Prod. Res. Dev.* **1964**, *3*, 170–173.

(18) Natta, G.; Dall'Asta, G.; Mazzanti, G., Stereospecific Homopolymerization of Cyclopentene. *Angew. Chem., Int. Ed.* **1964**, *3*, 765–772.

(19) Keim, W., Oligomerization of Ethylene to α-Olefins: Discovery and Development of the Shell Higher Olefin Process (SHOP). *Angew. Chem., Int. Ed.* **2013**, *52*, 12492–12496.

(20) Mol, J. C., Industrial Applications of Olefin Metathesis. *J. Mol. Catal. A* **2004**, *213*, 39–45.

(21) Hérisson, J. L.; Chauvin, Y., Catalysis of Olefin Transformations by Tungsten Complexes. II. Telomerization of Cyclic Olefins in the Presence of Acyclic Olefins. *Makromol. Chem.* **1971**, *141*, 161–176.

(22) Schrock, R. R.; Copéret, C., Formation of High-Oxidation-State Metal–Carbon Double Bonds. *Organometallics* **2017**, *36*, 1884–1892.

(23) Schrock, R. R., Multiple Metal-Carbon Bonds. 5. The Reaction of Niobium and Tantalum Neopentylidene Complexes with the Carbonyl Function. *J. Am. Chem. Soc.* **1976**, *98*, 5399–5400.

(24) Schrock, R. R.; Sharp, P. R., Multiple Metal-Carbon Bonds. 7. Preparation and Characterization of $Ta(C_5H_5)_2(=CH_2)(CH_3)$, a Study of its Decomposition, and Some Simple Reactions. *J. Am. Chem. Soc.* **1978**, *100*, 2389–2399.

(25) Schrock, R. R.; DePue, R. T.; Feldman, J.; Schaverien, C. J.; Dewan, J. C.; Liu, A. H., Preparation and Reactivity of Several Alkylidene Complexes of the Type W(CHR')(N-2,6-C_6H_3-*iso*-Pr_2)$(OR)_2$ and Related Tungstacyclobutane Complexes. Controlling Metathesis Activity through the Choice of Alkoxide Ligand. *J. Am. Chem. Soc.* **1988**, *110*, 1423–1435.

(26) Schrock, R. R.; Murdzek, J. S.; Bazan, G. C.; Robbins, J.; DiMare, M.; O'Regan, M., Synthesis of Molybdenum Imido Alkylidene Complexes and some Reactions Involving Acyclic Olefins. *J. Am. Chem. Soc.* **1990**, *112*, 3875–3886.

(27) Schrock, R. R., Recent Advances in High Oxidation State Mo and W Imido Alkylidene Chemistry. *Chem. Rev.* **2009**, *109*, 3211–3226.

(28) Nguyen, S. T.; Grubbs, R. H.; Ziller, J. W., Synthesis and Activities of new single-component Ruthenium-Based Olefin Metathesis Catalysts conjugated PCy3 carbene complex. *J. Am. Chem. Soc.* **1993**, *115*, 9858–9859.

(29) Schwab, P.; France, M. B.; Ziller, J. W.; Grubbs, R. H., A Series of Well-Defined Metathesis Catalysts - Synthesis of $RuCl_2(=CHR')(PR_3)_2$ and their Reactions. *Angew. Chem., Int. Ed. Engl.* **1995**, *34*, 2039–41.

(30) Grela, K., *Olefin Metathesis-Theory and Practice*. Wiley: Hoboken, NJ, 2014.

(31) Vougioukalakis, G. C.; Grubbs, R. H., Ruthenium-Based Heterocyclic Carbene-Coordinated Olefin Metathesis Catalysts. *Chem. Rev.* **2010**, *110*, 1746–1787.

(32) Scholl, M.; Ding, S.; Lee, C. W.; Grubbs, R. H., Synthesis and Activity of a New Generation of Ruthenium-Based Olefin Metathesis Catalysts Coordinated with 1,3-Dimesityl-4,5-dihydroimidazol-2-ylidene Ligands. *Org. Lett.* **1999**, *1*, 953–956.

(33) Kingsbury, J. S.; Harrity, J. P. A.; Bonitatebus, P. J.; Hoveyda, A. H., A Recyclable Ru-Based Metathesis Catalyst. *J. Am. Chem. Soc.* **1999**, *121*, 791–799.

(34) Garber, S. B.; Kingsbury, J. S.; Gray, B. L.; Hoveyda, A. H., Efficient and Recyclable Monomeric and Dendritic Ru-Based Metathesis Catalysts. *J. Am. Chem. Soc.* **2000**, *122*, 8168–8179.

(35) Sanford, M. S.; Love, J. A., Mechanism of Ruthenium-Catalyzed Olefin Metathesis Reactions. In *Handbook of Metathesis*, Grubbs, R. H., Ed. Wiley-VCH: Weinheim, Germany, 2003; Vol. 1, pp 112–131.

(36) Lummiss, J. A. M.; Higman, C. S.; Fyson, D. L.; McDonald, R.; Fogg, D. E., The Divergent Effects of Strong NHC Donation in Catalysis. *Chem. Sci.* **2015**, *6*, 6739–6746.

(37) Sanford, M. S.; Love, J. A.; Grubbs, R. H., Mechanism and Activity of Ruthenium Olefin Metathesis Catalysts. *J. Am. Chem. Soc.* **2001**, *123*, 6543–6554.

(38) Paredes-Gil, K.; Solans-Monfort, X.; Rodriguez-Santiago, L.; Sodupe, M.; Jaque, P., DFT Study on the Relative Stabilities of Substituted Ruthenacyclobutane Intermediates Involved in Olefin Cross-Metathesis and Their Interconversion Pathways. *Organometallics* **2014**, *33*, 6065–6075.

(39) Adlhart, C.; Chen, P., Comparing Intrinsic Reactivities of the First- and Second-Generation Ruthenium Metathesis Catalysts in the Gas Phase. *Helv. Chim. Acta* **2003**, *86*, 941–949.

(40) Lummiss, J. A. M.; Botti, A. G. G.; Fogg, D. E., Isotopic Probes for Ruthenium-Catalyzed Olefin Metathesis. *Catal. Sci. Technol.* **2014**, *4*, 4210–4218.

(41) McClennan, W. L.; Rufh, S. A.; Lummiss, J. A. M.; Fogg, D. E., A General Decomposition Pathway for Phosphine-Stabilized Metathesis Catalysts: Lewis Donors Accelerate Methylidene Abstraction. *J. Am. Chem. Soc.* **2016**, *138*, 14668−14677.

(42) Vorfalt, T.; Wannowius, K. J.; Plenio, H., Probing the Mechanism of Olefin Metathesis in Hoveyda and Grela Type Complexes. *Angew. Chem., Int. Ed.* **2010**, *49*, 5533 –5536.

(43) Ashworth, I. W.; Hillier, I. H.; Nelson, D. J.; Percy, J. M.; Vincent, M. A., What is the Initiation Step of the Grubbs-Hoveyda Olefin Metathesis Catalyst? *Chem. Commun.* **2011**, *47*, 5428–5430.

(44) Thiel, V.; Hendann, M.; Wannowius, K.-J.; Plenio, H., On the Mechanism of the Initiation Reaction in Grubbs-Hoveyda Complexes. *J. Am. Chem. Soc.* **2012**, *134*, 1104–1114.

(45) Vorfalt, T.; Wannowius, K. J.; Thiel, V.; Plenio, H., How Important Is the Release–Return Mechanism in Olefin Metathesis? *Chem. – Eur. J.* **2010**, *16*, 12312–12315.

(46) Bates, J. M.; Lummiss, J. A. M.; Bailey, G. A.; Fogg, D. E., Operation of the Boomerang Mechanism in Olefin Metathesis Reactions Promoted by the Second-Generation Hoveyda Catalyst. *ACS Catal.* **2014**, *4*, 2387−2394.

(47) Griffiths, J. R.; Keister, J. B.; Diver, S. T., From Resting State to the Steady State: Mechanistic Studies of Ene−Yne Metathesis Promoted by the Hoveyda Complex. *J. Am. Chem. Soc.* **2016**, *138*, 5380−5391.

(48) Lummiss, J. A. M.; Beach, N. J.; Smith, J. C.; Fogg, D. E., Targeting an Achilles Heel In Olefin Metathesis: A Strategy For High-Yield Synthesis of Second-Generation Grubbs Methylidene Catalysts. *Catal. Sci. Technol.* **2012**, *2*, 1630–1632.

(49) Occhipinti, G.; Bjorsvik, H.-R.; Jensen, V. R., Quantitative Structure-Activity Relationships of Ruthenium Catalysts for Olefin Metathesis. *J. Am. Chem. Soc.* **2006**, *128*, 6952–6964.

(50) Cavallo, L., Ru-NHC Mechanism of Ruthenium-Catalyzed Olefin Metathesis Reactions from a Theoretical Perspective. *J. Am. Chem. Soc.* **2002**, *124*, 8965–8973.

(51) Romero, P. E.; Piers, W. E.; McDonald, R., Rapidly Initiating Ruthenium Olefin-Metathesis Catalyst. *Angew. Chem., Int. Ed.* **2004**, *43*, 6161–6165.

(52) Romero, P. E.; Piers, W. E., Direct Observation of a 14-Electron Ruthenacyclobutane Relevant to Olefin Metathesis. *J. Am. Chem. Soc.* **2005**, *127*, 5032–5033.

(53) van der Eide, E. F.; Piers, W. E., Mechanistic Insights Into the Ruthenium-Catalysed Diene Ring-Closing Metathesis Reaction. *Nature Chem.* **2010**, *2*, 571–576.

(54) Romero, P. E.; Piers, W. E., Mechanistic Studies on 14-Electron Ruthenacyclobutanes: Degenerate Exchange with Free Ethylene. *J. Am. Chem. Soc.* **2007**, *129*, 1698–1704.

(55) Chadwick, J. C.; Duchateau, R.; Freixa, Z.; van Leeuwen, P. W. N. M., *Homogeneous Catalysts: Activity – Stability – Deactivation*. Wiley-VCH: Weinheim, 2011.

(56) Merrifield, J. H.; Lin, G.-Y.; Kiel, W. A.; Gladysz, J. A., Mechanism of Coupling of $=CH_2$ to $H_2C=CH_2$ at a Homogeneous $(C_5H_5)Re(NO)(PPh_3)^+$ Center. Remarkable Enantiomer Self-Recognition. *J. Am. Chem. Soc.* **1983**, *105*, 5811–5819.

(57) Schrodi, Y., Mechanisms of Olefin Metathesis Catalyst Decomposition and Methods of Catalyst Reactivation. In *Handbook of Metathesis*, Grubbs, R. H.; Wenzel, A. G., Eds. Wiley-VCH: Weinheim, 2015; pp 323–342.

(58) Bailey, G. A.; Foscato, M.; Higman, C. S.; Day, C. S.; Jensen, V. R.; Fogg, D. E., Bimolecular Coupling as a Vector for Decomposition of Fast-Initiating Olefin Metathesis Catalysts. *J. Am. Chem. Soc.* **2018**, *140*, 6931–6944.

(59) Amoroso, D.; Snelgrove, J. L.; Conrad, J. C.; Drouin, S. D.; Yap, G. P. A.; Fogg, D. E., An Attractive Route to Olefin Metathesis Catalysts: Facile Synthesis of a Ruthenium Alkylidene Complex Containing Labile Phosphane Donors. *Adv. Synth. Catal.* **2002**, *344*, 757–763.

(60) Amoroso, D.; Yap, G. P. A.; Fogg, D. E., Deactivation of Ruthenium Metathesis Catalysts via Facile Formation of Face-Bridged Dimers. *Organometallics* **2002**, *21*, 3335–3343.

(61) Fürstner, A.; Ackermann, L.; Gabor, B.; Goddard, R.; Lehmann, C. W.; Mynott, R.; Stelzer, F.; Thiel, O. R., Comparative Investigation of Ruthenium-Based Metathesis Catalysts Bearing N-Heterocyclic Carbene (NHC) Ligands. *Chem. – Eur. J.* **2001**, *7*, 3236–3253.

(62) Huang, J.; Schanz, H.-J.; Stevens, E. D.; Nolan, S. P., Influence of Sterically Demanding Carbene Ligation on Catalytic Behavior and Thermal Stability of Ruthenium Olefin Metathesis Catalysts. *Organometallics* **1999**, *18*, 5375–5380.

(63) Nascimento, D. L.; Gawin, A.; Gawin, R.; Guńka, P. A.; Zachara, J.; Skowerski, K.; Fogg, D. E., A Highly Reactive Ruthenium-Indenylidene Catalyst for Olefin Metathesis. *J. Am. Chem. Soc.* **2019**, *141*, 10626–10631.

(64) Tsang, W. C. P.; Hultzsch, K. C.; Alexander, J. B.; Bonitatebus, P. J., Jr.; Schrock, R. R.; Hoveyda, A. H., Alkylidene and Metalacyclic Complexes of Tungsten that Contain a Chiral Biphenoxide Ligand. Synthesis, Asymmetric Ring-Closing Metathesis, and Mechanistic Investigations. [Erratum to document cited in CA138:287777]. *J. Am. Chem. Soc.* **2003**, *125*, 6337.

(65) van Rensburg, W. J.; Steynberg, P. J.; Meyer, W. H.; Kirk, M. M.; Forman, G. S., DFT Prediction and Experimental Observation of Substrate-Induced Catalyst Decomposition in Ruthenium-Catalyzed Olefin Metathesis. *J. Am. Chem. Soc.* **2004**, *126*, 14332–14333.

(66) Hong, S. H.; Day, M. W.; Grubbs, R. H., Decomposition of a Key Intermediate in Ruthenium-Catalyzed Olefin Metathesis Reactions. *J. Am. Chem. Soc.* **2004**, *126*, 7414–7415.

(67) Higman, C. S.; Plais, L.; Fogg, D. E., Isomerization During Olefin Metathesis: An Assessment of Potential Catalyst Culprits. *ChemCatChem* **2013**, *5*, 3548-3551.

(68) Lummiss, J. A. M.; McClennan, W. L.; McDonald, R.; Fogg, D. E., Donor-Induced Decomposition of the Grubbs Catalysts: An Intercepted Intermediate *Organometallics* **2014**, *33*, 6738–6741.

(69) Crabtree, R. H., Deactivation in Homogeneous Transition Metal Catalysis: Causes, Avoidance, and Cure. *Chem. Rev.* **2015**, *115*, 127–150.

(70) Higman, C. S.; Nascimento, D.; Ireland, B. J.; Audorsch, S.; Bailey, G. A.; Fogg, D. E., Chelate-Assisted Ring-Closing Metathesis: A Strategy for Accelerating Macrocyclization at Ambient Temperatures. *J. Am. Chem. Soc.* **2018**, *140*, 1604−1607.

(71) van Lierop, B. J.; Lummiss, J. A. M.; Fogg, D. E., Ring-Closing Metathesis. In *Olefin Metathesis-Theory and Practice*, Grela, K., Ed. Wiley: Hoboken, NJ, 2014; pp 85–152.

(72) Trnka, T. M.; Morgan, J. P.; Sanford, M. S.; Wilhelm, T. E.; Scholl, M.; Choi, T.-L.; Ding, S.; Day, M. W.; Grubbs, R. H., Synthesis and Activity of Ruthenium Alkylidene Complexes Coordinated with Phosphine and N-Heterocyclic Carbene Ligands. *J. Am. Chem. Soc.* **2003**, *125*, 2546–2558.

(73) Samojlowicz, C.; Grela, K., Olefin Metathesis Reactions of Sulfur-Containing Alkenes and Dienes. *Arkivoc* **2011**, 71–81.

(74) Beach, N. J.; Camm, K. D.; Fogg, D. E., Hydrogenolysis versus Methanolysis of First- and Second-Generation Grubbs Catalysts: Rates, Speciation, and Implications for Tandem Catalysis. *Organometallics* **2010**, *29*, 5450–5455.

(75) Dinger, M. B.; Mol, J. C., Degradation of the First-Generation Grubbs Metathesis Catalyst with Primary Alcohols, Water, and Oxygen. Formation and Catalytic Activity of Ruthenium(II) Monocarbonyl Species. *Organometallics* **2003**, *22*, 1089–1095.

(76) Dinger, M. B.; Mol, J. C., Degradation of the Second-Generation Grubbs Metathesis Catalyst with Primary Alcohols and Oxygen. *Eur. J. Inorg. Chem.* **2003**, 2827–2833.

(77) Schmidt, B.; Hauke, S., Cross Metathesis of Allyl Alcohols: How to Suppress and How to Promote Double Bond Isomerization. *Org. Biomol. Chem.* **2013**, *11*, 4194–4206.

(78) Beach, N. J.; Lummiss, J. A. M.; Bates, J. M.; Fogg, D. E., Reactions of Grubbs Catalysts with Excess Methoxide: Formation of Novel Methoxyhydride Complexes. *Organometallics* **2012**, *31*, 2349–2356.

(79) Ashworth, I. W.; Hillier, I. H.; Nelson, D. J.; Percy, J. M.; Vincent, M. A., Searching for the Hidden Hydrides: The Competition between Alkene Isomerization and Metathesis with Grubbs Catalysts. *Eur. J. Org. Chem.* **2012**, 5673-5677.

(80) Nickel, A.; Ung, T.; Mkrtumyan, G.; Uy, J.; Lee, C. W.; Stoianova, D.; Papazian, J.; Wei, W.-H.; Mallari, A.; Schrodi, Y.; Pederson, R. L., A Highly Efficient Olefin Metathesis Process for the Synthesis of Terminal Alkenes from Fatty Acid Esters. *Top. Catal.* **2012**, *55*, 518–523.

(81) Lummiss, J. A. M.; Ireland, B. J.; Sommers, J. M.; Fogg, D. E., Amine-Mediated Degradation in Olefin Metathesis Reactions that Employ the Second-Generation Grubbs Catalysts. *ChemCatChem* **2014**, *6*, 459–463.

(82) Ireland, B. J.; Dobigny, B. T.; Fogg, D. E., Decomposition of a Phosphine-Free Metathesis Catalyst by Amines and Other Nitrogen Bases: Metallacyclobutane Deprotonation as a Major Deactivation Pathway. *ACS Catal.* **2015**, *5*, 4690−4698.

(83) Ton, S. J.; Fogg, D. E., The Impact of Oxygen on Leading and Emerging Ru-Carbene Catalysts for Olefin Metathesis: An Unanticipated Correlation Between Robustness and Metathesis Activity *ACS Catal.* **2019**, in revision.

(84) Guidone, S.; Songis, O.; Nahra, F.; Cazin, C. S. J., Conducting Olefin Metathesis Reactions in Air: Breaking the Paradigm. *ACS Catal.* **2015**, *5*, 2697–2701.

(85) Bailey, G. A.; Lummiss, J. A. M.; Foscato, M.; Occhipinti, G.; McDonald, R.; Jensen, V. R.; Fogg, D. E., Decomposition of Olefin Metathesis Catalysts by Brønsted Base: Metallacyclobutane Deprotonation as a Primary Deactivating Event. *J. Am. Chem. Soc.* **2017**, *139*, 16446–16449.

Chapter 2. Catalyst Decomposition via a Truncated N-Heterocyclic Carbene

2.1 Context, Objectives, and Overview of Content

The 1999 discovery of the greatly enhanced metathesis activity of ruthenium catalysts bearing an N-heterocyclic carbene (NHC) led to a step-change in the synthetic relevance of olefin metathesis.[1-4] As a result, such "second-generation" complexes were widely adopted in academia, and are now beginning to be used in industrial processes.[5] Despite this popularity, catalysts such as **GII** (NHC = H_2IMes) deliver low turnover numbers in challenging transformations such as, e.g., acrylate cross-metathesis (CM)[6] and macrocyclic ring-closing metathesis (mRCM).[7,8] Efforts to improve performance generally focus on developing more active, more robust, metathesis catalysts. The Ru-NHC scaffold offers a well-established catalyst platform, and the relative ease with which NHC stereoelectronic properties can be tuned has led to the synthesis of hundreds of different NHC ligands.[4] However, attempts to design more efficient, more robust metathesis catalysts by modifying the NHC ligands have met with varying degrees of success. The challenge lies in the difficulty of redesign in the absence of rational design criteria. Limited understanding of the pathways by which the second-generation Ru catalysts decompose means that decomposition continues to plague their performance.

One phenomenon widely accepted as problematic for second-generation metathesis catalysts is NHC cyclometallation.[9,10] Activation of C-H bonds to form chelate complexes is seen for N-mesityl and other N-aryl NHCs,[11,12,13] as well as their N-isopropyl[14] counterparts. Cyclometallated NHCs are a common structural feature in ruthenium decomposition products formed by the second-generation catalysts. A suggested means of preventing such pathways is truncation of the N-substituents,[9] with the idea that cyclometallation should be precluded by reduced steric bulk.

The validity of this concept was originally investigated by Stephanie Rufh of the Fogg research group, who sought to examine the impact of replacing a PCy_3 ligand of the first-generation Grubbs catalyst **GI** with a truncated NHC. Given difficulties in the synthesis of the benzylidene complex,[15] she pursued this ligand-exchange reaction with methylidene complex **GIm**, the resting-state species formed by **GI**. The chosen NHC was 1,3,4,5-tetramethylimidazol-2-ylidene (IMe_4), which bears N-methyl groups in place of the N-mesityl substituents present in H_2IMes, as well as methyl groups on the backbone of the heterocyclic ring. Following the discovery that subjecting **GIm** to excess IMe_4 caused immediate loss of the methylidene functionality, she proposed in her MSc thesis that the small NHC facilitates bimolecular coupling (decomposition) of the methylidene intermediates. In subsequent work that forms the subject of this Chapter, a very different mechanistic pathway emerged. Described below is the mechanism by which **GIm** is in fact transformed by IMe_4, a pathway that centers on the accessibility and nucleophilicity of this small carbene. These findings point toward new potential opportunities enabled by truncated NHCs in tandem catalysis.

2.2 Published Contributions

Rapid Decomposition of Olefin Metathesis Catalysts by a Truncated N-heterocyclic Carbene: Efficient Catalyst Quenching and N-Heterocyclic Carbene Vinylation. S. A. Rufh,† A. Y. Goudreault,† M. Foscato,† V. R. Jensen, and D. E. Fogg.* *ACS Catal.* **2018**, 11822–11826. (Communication). †Equal Contributions. Copyright 2018 American Chemical Society. Reprinted with permission.

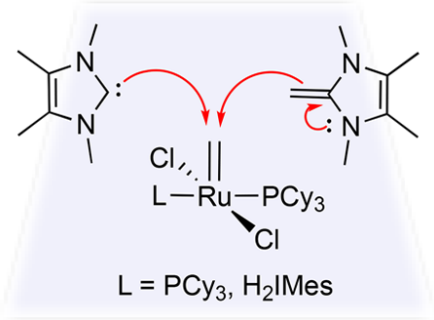

Abstract: The Grubbs methylidene $RuCl_2(PCy_3)_2(=CH_2)$ **GIm** is immediately decomposed by the small NHC tetramethylimidazol-2-ylidene (IMe_4), even at –80 °C. Labelling experiments with $RuCl_2(PCy_3)_2(=^{13}CH_2)$ reveal capture of the methylidene ligand as ethylimidazolium chloride $[^{13}CH_3{}^{13}CH_2–IMe_4]Cl$, **8***. Density functional calculations indicate that IMe_4 first abstracts methylidene from five-coordinate **GIm** (a pathway unavailable to bulkier NHCs), generating the N-heterocyclic olefin (NHO) $H_2C{=}IMe_4$. The latter attacks a second **GIm**; protonolysis of highly basic $[Ru]–CH_2CH_2IMe_4$ then liberates **8**. Identical, slightly slower, reactivity is seen for $RuCl_2(H_2IMes)(PCy_3)(=CH_2)$, **GIIm**. The high efficiency of this process opens up opportunities for tandem metathesis enabled by sterically accessible NHCs and NHOs.

Author Contributions: The reaction of GIm and its labelled isotopomer GIm* with IMe_4 was first conducted by SAR and was repeated by AYG. SAR was responsible for the initial observation of ethylimidazolium chloride 8, which was characterized and rigorously quantified by AYG. Low-temperature experiments, and experiments with GIIm were performed by AYG. All computational work was carried out by MF and VRJ. The initial draft of the manuscript was written by SAR and DEF. In light of new experimental and particularly computational evidence, uncovered in responding to a referee's comment, the manuscript was extensively revised by AYG and DEF. The revised version of the paper appears below.

2.3 Introduction

Olefin metathesis offers exceptionally versatile methodologies for the catalytic assembly of carbon-carbon bonds.[16] At the expanding frontiers of pharmaceutical manufacturing[17-19] and tandem catalysis,[20] catalyst transformation is a core issue. Critical in process chemistry is maximum catalyst lifetime, with complete termination of catalytic activity once metathesis is complete. In tandem catalysis – topical current examples being metathesis-dihydroxylation[21] and metathesis-transfer hydrogenation[22,23] – a complementary challenge is the efficient, controlled transformation of the metathesis-active species into the required oxidation or hydrogenation catalyst. The present work, originally aimed at exploring the common hypothesis that catalyst decomposition can be inhibited by truncation of the NHC ligand present in leading catalysts (Chart 2.1a),[9,24,25] instead revealed an unprecedentedly efficient means of terminating metathesis, with implications for both catalyst quenching and tandem catalysis.

Chart 2.1 (a) Key metathesis catalysts and active species **Ru-4**. (b) Exemplary cyclometallated decomposition product. (c) NHC ligands discussed.

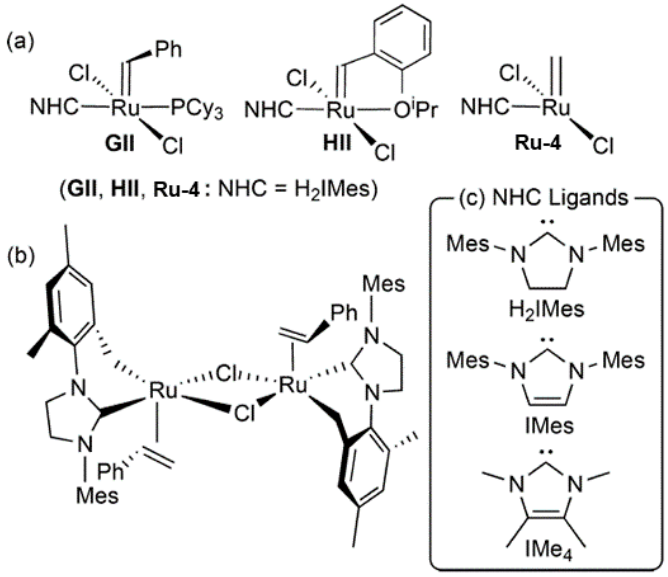

Within the initial context of catalyst decomposition, we queried the relevance of NHC bulk as a causal factor. Notwithstanding early analyses emphasizing the potentially protective role of bulky NHC[26] or anionic[27] ligands (buttressed by the observed susceptibility of H_2ITol derivatives to accelerated decomposition),[28,29,*] the widespread observation of cyclometallated NHCs in the ruthenium products of decomposition (Chart 2.1b)[33] has led to the presumption that NHC truncation may improve catalyst lifetimes.[9,24,25] Countering this view is the finding that NHC cyclometallation need not trigger catalyst deactivation,[34] and mechanistic evidence that in multiple

[*] More equivocal evidence is provided by the performance of H_2IPr catalysts. These are reported to show improved performance in some contexts[30,31] but which were shown to be less productive in others.[32]

scenarios, cyclometallation occurs *subsequent* to the key deactivating event.[29,35] We suspected that smaller NHC substituents might in fact *accelerate* catalyst decomposition, by increasing the accessibility of the Ru=CHR functionality to nucleophiles present on a substrate or in the reaction medium (Scheme 2.1).[35-37] Here we sought to assess whether ligand truncation accelerates methylidene abstraction, by generating a methylidene intermediate in which an N-methyl NHC (see IMe_4; Chart 2.1c) replaces the usual *N*-mesityl ligands. We report that attenuated NHC bulk indeed results in rapid decomposition, but via an unanticipated pathway that precedes ligand exchange.

Scheme 2.1 Abstraction of the [Ru]=CHR ligand.

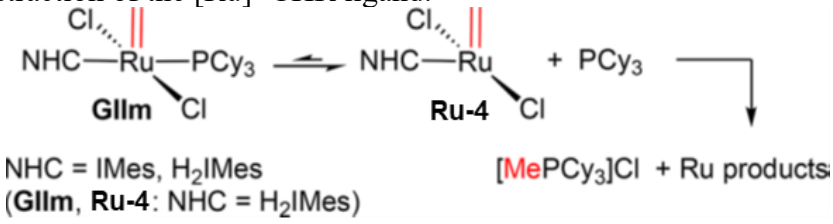

2.4 Results and Discussion

Known Ru–IMe_n complexes[33c,38-42] include "mixed-NHC" indenylidene and benzylidene catalysts.[43] However, access to $RuCl_2(IMe_4)(PCy_3)(=CHPh)$ **Ru-17** (the IMe_4 analogue of **GII**) is hampered by facile formation of an unreactive dimer,[15] the metathesis inactivity of which precludes access to the active species $RuCl_2(IMe_4)(=CH_2)$ **Ru-18**. As an alternative approach, we sought to effect ligand exchange of the resting-state Grubbs methylidene **GIm** with free IMe_4. This reaction led to the unexpected, near-instantaneous loss of both PCy_3 and methylidene ligands, as outlined below.

Addition of 1 equiv IMe_4 to a pink solution of **GIm** in C_6D_6 resulted in an immediate colour change to orange, and deposition of a grey precipitate. The ^1H NMR spectrum revealed loss of **GIm** (i.e. a decrease in the intensity of the methylidene singlet at 19.41 ppm). Identical behavior was seen at higher ratios of IMe_4, with full consumption of **GIm** on use of 4 equiv (Scheme 2.2). Reaction was then complete within minutes, even at –80 °C. No new methylidene signals were evident: even at the shortest reaction time that could be probed (5 min), the sole observable Ru species were the known[42] tetrakis-NHC complex $RuCl_2(IMe_4)_4$ (**Ru-19**), and traces of starting **GIm**. Importantly, **Ru-19** was present in 50% yield when reaction was complete, as indicated by integration against an internal standard. The degraded resolution of the spectrum as compared to the initial spectrum of **GIm** (Appendix A, Figures A1a, A1b) is consistent with formation of a paramagnetic Ru coproduct. Free PCy_3 was also present, in ca. 85% yield vs. **GIm**, as judged from quantitative $^{31}P\{^1H\}$ NMR analysis; the balance is presumably bound to Ru(III). Notably absent was $[MePCy_3]Cl$ **5**, ruling out nucleophilic abstraction of the methylidene ligand by PCy_3, the dominant pathway for decomposition of **GIIm** (Scheme 2.1).

Scheme 2.2 Reaction of **GIm** with IMe_4.

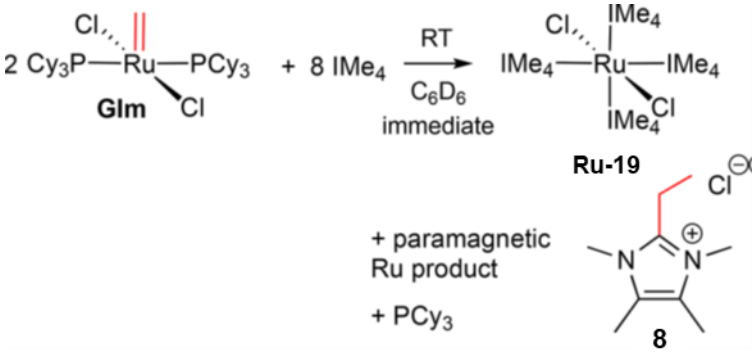

Further insight was afforded by ^{1}H NMR analysis of the precipitated byproducts in $CDCl_3$, which revealed an unexpected ethyl pattern (a quartet and triplet at 3.34 and 1.28 ppm, respectively; $^{3}J_{H\text{-}H}$ = 7.5 Hz). Assignment to ethylimidazolium salt **8** was supported by mass spectrometry, and confirmed by independent synthesis of **8**. Quantitation of **8** in the decomposition reaction is hampered by its low mass (just 8% vs. **GIm**, assuming 100% yield), and overlap of its ^{1}H NMR signals with those due to PCy_3. We were able to establish a lower limit of 65% **8**, based on starting **GIm**, by extracting **8** into D_2O containing a known concentration of $NaO_2S(CH_2)_3SiMe_3$ as integration standard. Repeating the reaction of Scheme 2.2 with **GIm***, in which the methylidene carbon is ^{13}C-labelled, indicated that the ethyl group of **8** originates in the methylidene ligand of **GIm**. $^{13}C\{^{1}H\}$ NMR analysis of the precipitate revealed a pair of doublets for the doubly-labelled ethyl carbons (Figure 2.1), arising from the rarely observed ^{1}J coupling of adjacent ^{13}C nuclei.*

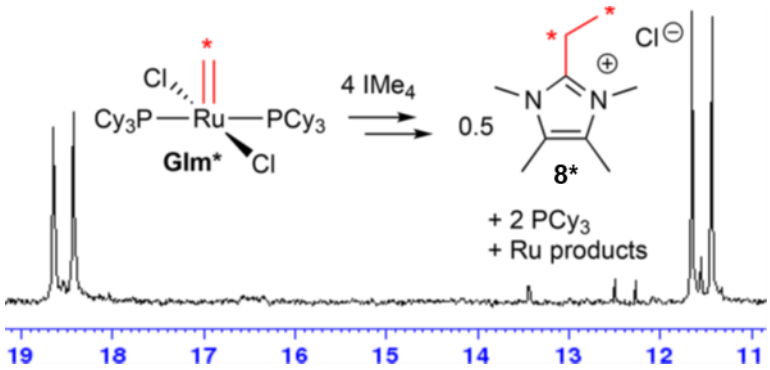

Figure 2.1 $^{13}C\{^{1}H\}$ NMR spectrum ($CDCl_3$, 151 MHz; ethyl region), showing the diagnostic ^{13}C–^{13}C doublet splitting pattern for **A*** ($^{1}J_{CC}$ = 33 Hz).

Formation of doubly-labeled **8*** suggests a mechanism involving bimolecular coupling of two Ru methylidene complexes.[35a,44] This possibility was explored by density functional theory (DFT) calculations: see Appendix E. Such coupling requires prior formation of methylidene complexes

* The corresponding reaction of IMe_4 with 1:1 **GIm** and **GIm*** afforded the labelled ethylimidazolium salts ($^{13}CH_2CH_3$, $CH_2{}^{13}CH_3$, and $^{13}CH_2{}^{13}CH_3$) in equal proportions, as judged by NMR analysis. (The unlabeled salt was also formed, but is masked by the labelled isotopomers)

with lower coordination numbers and less steric bulk than **GIm**. Initial dissociation of PCy_3, however, is incompatible with the known, very low lability of the PCy_3 ligand in **GIm**,* and the near-instantaneous reaction observed at –80 °C. DFT calculations confirm a high barrier for both dissociative and associative exchange of the PCy_3/IMe_4 ligands (>21.6 and 22.9 kcal/mol from **GIm**, respectively, at –80 °C). Neither is consistent with the observed rapidity of reaction at this temperature.

Instead, the calculations indicate a low barrier (16.4 kcal/mol at –80 °C) for nucleophilic attack of IMe_4 on the methylidene ligand to form intermediate **M13** (Scheme 2.3a). We had originally dismissed this possibility on the basis of the presence of solely ethylimidazolium salt **8** in the products: that is, the absence of the corresponding $[MeIMe_4]Cl$ salt. Overlooked in this consideration, however, is the dative nature of the $[Ru]–CH_2IMe_4$ linkage (see below), which favours elimination of the N-heterocyclic olefin (NHO) $H_2C{=}IMe_4$ over protonolysis and loss of $[MeIMe_4]Cl$. (It should be noted that **M13** may undergo PCy_3/IMe_4 exchange prior to eliminating NHO and forming tetrakis-IMe_4 product **Ru-19**).

Scheme 2.3 Decomposition via nucleophilic attack on five-coordinate methylidene complexes. (a) By NHC. (b) By NHO.[a]

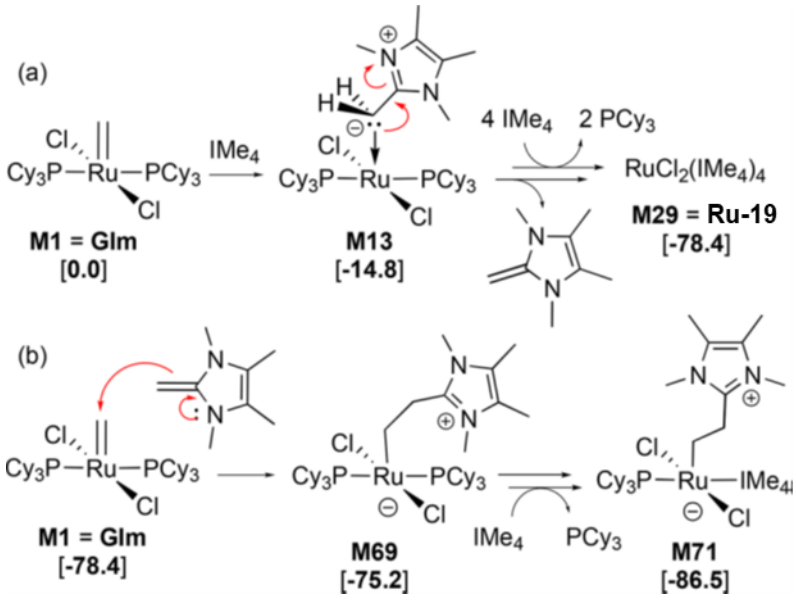

[a]Free energies (kcal/mol at RT) relative to **M1** = **GIm**. Labels starting with "**M**" define DFT-optimized intermediates and transition-states (see Appendix E).

NHOs such as $H_2C{=}IMe_4$ are potent nucleophiles, and indeed much current interest centers on their deployment in catalysis and polymer chemistry.[46-51] In the present work, the computational

* Sanford and Grubbs described **GIm** as an extremely poor initiator at ambient temperature.[45] Phosphine dissociation was identified as the slow step in its reactions, with a rate constant for initiation at 40 °C in toluene-d8 of 8.5×10^{-4} s^{-1}.

evidence supports nucleophilic attack of $H_2C{=}IMe_4$ on the methylidene ligand of a second **GIm** molecule (Scheme 2.3b), generating the [Ru]–$CH_2CH_2IMe_4$ complex **M69**. The latter is a true alkyl ligand, which is highly basic relative to the ylidic CH_2IMe_4 ligand in **M13**. Accordingly, it readily undergoes protonolysis to liberate **8**. As with the NHO elimination step, **M69** is likely to undergo PCy_3/IMe_4 exchange before protonolysis. Protonolysis necessitates C-H activation of a PCy_3 or IMe_4 ligand, with a higher barrier than ligand exchange.

Given the multitude of low-energy species, and the ambiguity of the additional Ru product(s), the protonolysis step was not examined in detail. However, the quantitative ^{31}P NMR data point toward deprotonation of a PCy_3 ligand as one significant contributor, with concomitant formation of a paramagnetic Ru-phosphine product. Hydrogen loss from a cyclohexyl ring of Ru-PCy_2R complexes (with, in some cases, formation of Ru(III) products) is well precedented.[52-55] Notwithstanding the ambiguity in the nature of the paramagnetic Ru species, the identity and yield of **8** confirm that NHC and NHO attack on the methylidene ligand of **GIm** represent the major vector for decomposition.

To test the generality of NHC/NHO-mediated methylidene abstraction, the corresponding reaction of **GIIm** with 4 equiv IMe_4 was carried out. Identical behaviour was observed, albeit at a slightly slower rate (e.g., 40% consumption of **GIIm** after 5 min at RT). Of note, the Ru product observed by ^1H NMR analysis was not $RuCl_2(H_2IMes)(IMe_4)_n$, as initially expected: rather, the IMe_4 ligand displaced the larger NHC, again affording the tetrakis-IMe_4 complex **Ru-19**.

NHC truncation thus indeed greatly accelerates catalyst decomposition, but not via the pathway we had originally set out to examine. Both **GIm** and **GIIm** are shown to be highly unstable with respect to loss of methylidene on treatment with a small NHC. Exceptionally rapid abstraction of the methylidene ligand essential to propagate metathesis is enabled by the small, highly nucleophilic NHC and NHO ligands.

The remarkable facility with which IMe_4 attacks the methylidene ligand is in striking contrast with the behavior of the classic, larger NHCs. The DFT calculations show that, whereas IMe_4 attack on methylidene to form **M13** is downhill by nearly 15 kcal/mol, the corresponding attack by H_2IMes introduces considerable geometric strain that costs almost 9 kcal/mol (see Appendix E). This difference explains why the second-generation Grubbs methylidene complex **GIIm** and its IMes analogue are accessible in near-quantitative yields via ligand exchange of **GIm** with the free carbene at elevated temperatures.[35f,56] These large NHCs function as Lewis bases for two reasons: because the bulk of the N-substituents flanking the carbene carbon suppresses their nucleophilicity, and because a coordination site is available at the metal. In the **GIm**-IMe_4 system, the combination of NHC truncation and blocked coordination (a function of the low bond lability in these methylidene complexes)[45,57] switches the reaction mode, enabling the NHC to function selectively as a nucleophile.

2.5 Conclusions

In transition-metal catalysis, the nucleophilicity of free NHCs is commonly masked by their strong Lewis basicity. In consequence, NHCs have been regarded almost exclusively as ligands. Emerging attention highlights the capacity of these electron-rich ligands to participate as nucleophiles that promote NHC coupling pathways.[58,59] The foregoing illustrates the heightened impact of unquenched carbene nucleophilicity when combined with minimal NHC bulk, showcased by the unprecedented attack of a small, accessible NHC on the methylidene ligand of *sterically protected*, five-coordinate complexes. Elimination of an N-heterocyclic olefin as the organic product of this reaction generates a further potent nucleophile, of a class that has recently attained fresh prominence for its potential in organocatalysis, in particular.[46-49] The facile olefination of an NHC by a resting-state metathesis catalyst is hence relevant not only to catalyst degradation, but to enabling alternative catalytic pathways.

Most obvious in the context of degradation are cases where small NHCs are released during metathesis, as in Herrmann-class bis-NHC metathesis catalysts.[*,43,60,61] Of perhaps keenest interest, however, are new opportunities arising from the potential of NHOs as selective methylidene-abstracting agents. Such reagents could offer new possibilities in tandem catalysis, via (e.g.) an NHO-triggered "flip" from metathesis to organo- or transition-metal catalysis, the latter enabled by the intact $RuCl_2(H_2IMes)$ core. The potent Lewis basicity and nucleophilicity of small NHCs, in contrast, offer complete, efficient quenching of Ru-based reactivity, by transforming the metathesis catalysis into a highly stable, coordinatively saturated Ru complex. Studies aimed at exploring these new opportunities are now in progress in our laboratories.

2.6 Experimental Details

2.6.1 General Procedures

Reactions were carried out in an N_2-filled glovebox at room temperature (RT, 25 ± 2 °C). HPLC-grade solvents were purified using a Glass Contour solvent purification system, then stored under N_2 in the glovebox over 4 Å molecular sieves for at least 24 h prior to use. NMR solvents were freeze/pump/thaw degassed (5x) and likewise stored over sieves, except for D_2O. Pyrene, anthracene, and 3-trimethylsilyl-1-propanesulfonic acid sodium salt (all 98% or 99%, Sigma-Aldrich), and TMSCl (Alfa Aeser, 98%) were used as received. Methylidene complex **GIm**,[56] its ^{13}C-labelled analogue **GIm***,[35f] and IMe_4[62] were prepared by literature methods.

NMR spectra were recorded on Avance II 300 or 600 NMR spectrometers at 23 ± 2 °C. Chemical shifts are given in ppm, and referenced to the residual proton or carbon signals of the solvent (^1H, ^{13}C), or (^{31}P) to 85% H_3PO_4, the latter via use of a capillary containing 72 mM PPh_3 in C_6D_6 (–

[*] Trace water may improve the performance of such catalysts, by preferential reaction with the free NHC. For evidence that catalysts of type **HII** and **GII** are degraded by water, see refs 29 and 61, and Chapter 4.

5.06 ppm relative to 85% H_3PO_4 at 0 ppm). Anaerobic MALDI-TOF mass spectra were collected on a Bruker UltrafleXtreme MALDI-TOF/TOF mass spectrometer interfaced to a glovebox, using the reported instrumental parameters.[63] Samples were prepared by the dried-droplet protocol, from solutions containing the charge-transfer matrix pyrene in benzene.[64]

2.6.2 Reaction of GIm with IMe_4

(a) A solution of pink **GIm** (6.6 mg, 0.0088 mmol) and dimethyl terephthalate (DMT; ca. 1 mg; internal standard) in 1 mL C_6D_6 was analyzed to establish the initial ^{1}H NMR integration ratio of **GIm** vs DMT. Addition of IMe_4 (4.5 mg, 0.036 mmol, 4 equiv) caused an immediate colour change from pink to bright orange, and deposition of a precipitate. NMR analysis of the supernatant at 10 min revealed solely free PCy_3 and **Ru-19**. No further change was apparent after 1 h (Figs. A1, A2 see Appendix A). The chemical shifts for **Ru-19** agree with reported[42] values. $^{31}P\{^1H\}$ NMR (121 MHz, C_6D_6): δ 10.5 (free PCy_3). ^{1}H NMR (300 MHz, C_6D_6): δ 8.00 (br s, DMT), 4.00 (br s, 1H, unassigned), 3.71 (s, 12H, NCH_3 of **Ru-19** 50% based on starting **GIm**), 3.43 (br s, DMT), 3.26 (br s, 1H, unassigned), 2.62−1.07 (m, Cy of PCy_3 + **Ru-19**), 1.79 (s, CCH_3 of **Ru-19**; overlaps with PCy_3 signals). MALDI-TOF MS (pyrene matrix; *m/z* 598.388 ($[M-2\ Cl]^+$; calcd 598.300). The signal for $C_{28}H_{48}Cl_2N_8Ru$; $[RuCl_2(IMe_4)_4]^{\bullet+}$ ($[M]^{\bullet+}$; 668.24) is not observed. For spectrum and assignment of other signals due to fragments, see Fig. C1.

This reaction was repeated on 56 mg scale to isolate the precipitate. The latter was filtered off and washed (benzene, hexanes) to remove free PCy_3, and dried under vacuum prior to ^{1}H NMR and MALDI-TOF analysis (Figs. A4, C2, respectively). Yield 23 mg (88% based on complete conversion to **8** and an Ru species of the form **Ru-19**–**8**; minor amounts of **Ru-19** may also be present). The identity of [Et–IMe_4]Cl **8** was confirmed on the basis of its independent synthesis: see below. MALDI-TOF MS (pyrene matrix): *m/z* 153.113 (calcd for $[C_9H_{17}N_2]^+$, $[M]^+$: 153.139). Other signals are indistinguishable from those due to **Ru-19**.

(b) Quantification of 2-Ethyl-1,3,4,5-Tetramethylimidazolution Chlorde, 8

A suspension of **GIm** (17.1 mg, 0.0228 mmol) and IMe_4 (11.5 mg, 0.0926 mmol, 4 equiv) in 3 mL C_6H_6 was stirred for 90 min to ensure complete reaction. As quantitation in $CDCl_3$ is hampered by signal overlap, a solution of 0.800 mL D_2O containing $NaO_3S(CH_2)_3SiMe_3$ (internal standard, I.S.; 3.00 mg, 0.0137 mmol, 1.2 equiv vs 100% theoretical yield of **8**) was added to the reaction flask, and the biphasic solution was stirred vigorously for 1 h to extract **8**. Yield of **8**: 65% **8** vs I.S. For spectrum, see Appendix A, Figure A4.

[Et–IMe_4]Cl **8**: ^{1}H NMR (300 MHz, D_2O): δ 3.69 (s, 6H, NCH_3), 2.96 (q, $^3J_{HH}$ = 7.71 Hz, 2H, CH_2CH$_3$), 2.20 (s, 6H, CCH_3), 1.20 (t, $^3J_{HH}$ = 7.68 Hz, 2H, CH$_2$CH_3). *Note*: small variations can arise from the concentration-dependence of these chemical shifts; see below.

$NaO_3S(CH_2)_3SiMe_3$, I.S.: ^{1}H NMR (300 MHz, D_2O): δ: 2.89 (m, 3H, SCH_2), 1.73 (m, 2H, CH$_2$CH_2CH$_2$), 0.62 (m, 2H, SiCH_2CH$_2$), –0.01 (s, 9H, Si(CH_3)$_3$; used for integration).

Additional, unassigned peaks: ^{1}H NMR (300 MHz, D_2O): δ 4.20-3.86 (br m), 2.43-2.00 (br m).

2.6.3 Decomposition of ^{13}C-Labelled GIm*: Identification of Doubly-Labelled 8*

In the glovebox, pink **GIm*** (10.1 mg, 0.0135 mmol) was dissolved in C_6D_6 (1 mL) in a J. Young NMR tube. Addition of IMe_4 (6.9 mg, 0.056 mmol, 4.1 equiv) caused a colour change to orange. The reaction mixture was allowed to stir at room temperature for 30 min to ensure complete consumption of **GIm***. The solvent was removed under vacuum, and the solid residue was redissolved in $CDCl_3$ (1 mL). $^{13}C\{^{1}H\}$ NMR (151 MHz, $CDCl_3$); δ 127.9 (C_6H_6), 31.6 (d, $^{1}J_{CC}$ = 15.5 Hz, PCy_3), 31.2 (d, $^{1}J_{CC}$ = 12.1 Hz, PCy_3), 27.7 (d, $^{1}J_{CC}$ = 9.3 Hz, PCy_3), 26.6 (s, PCy_3), 18.6 (d, $^{1}J_{CC}$ = 32.8 Hz, CH_2CH_3, **8***), 11.5 (d, $^{1}J_{CC}$ = 32.8 Hz, CH_2CH_3, **8***). For additional unassigned signals, see Appendix A, Figure A5. No signals for the ^{13}C-labelled methylimidazolium[49] analogue of **8*** were evident.

2.6.4 Decomposition of GIm*:GIm (1:1) by IMe_4: Identification of Labelled 8 salts

In the glovebox, solutions of **GIm** (11 mg, 0.014 mmol) and **GIm*** (10.9 mg, 0.014 mmol) in 1 mL C_6D_6 were prepared in two separate vials. Half of each solution was added to a J. Young NMR tube (total 0.0135 mmol Ru). IMe_4 (6.8 mg, 0.055 mmol, 4.1 equiv) was added. The reaction mixture was allowed to stir for 30 min at RT, after which the solvent was removed under vacuum for NMR analysis. $^{13}C\{^{1}H\}$ NMR (75 MHz, $CDCl_3$); δ 127.9 (C_6H_6), 31.6 (d, $^{1}J_{CC}$ = 15.5 Hz, PCy_3), 31.2 (d, $^{1}J_{CC}$ = 12.1 Hz, PCy_3), 27.7 (d, $^{1}J_{CC}$ = 9.3 Hz, PCy_3), 26.6 (s, PCy_3), 18.6 (d, $^{1}J_{CC}$ = 32.8 Hz, $^{13}CH_2{}^{13}CH_3$), 18.6 (s, $^{13}CH_2{}^{12}CH_3$), 11.5 (d, $^{1}J_{CC}$ = 32.8 Hz, $^{13}CH_2{}^{13}CH_3$), 11.5 (s, $^{12}CH_2{}^{13}CH_3$). For additional unassigned signals, see Appendix A, Figure A6.

2.6.5 Reaction of GIIm with IMe_4

In the glovebox, orange **GIIm** (7.4 mg, 0.0095 mmol) and anthracene (ca. 2.8 mg; internal standard, I.S.) were dissolved in 0.8 mL C_6D_6. A ^{1}H NMR spectrum was recorded to establish the initial ratio of **GIIm** to I.S. (see Appendix A, Figure A7a). Solid IMe_4 (4.7 mg, 0.038 mmol, 4 equiv) was added, causing an immediate colour change from orange to dark brown and deposition of a precipitate. Another ^{1}H NMR spectrum was collected after 5 min (Figure A7b). The reaction mixture was stirred for 24 h at RT, and re-analyzed (Figures A7c, A8). The precipitate was filtered off and washed with cold hexanes (2 x 2 mL). The combined filtrate was stripped of solvent and the precipitate was dissolved in $CDCl_3$ for ^{1}H NMR analysis (Figure A9).

(a) Filtrate. ^{1}H NMR (300 MHz, C_6D_6): δ 3.71 (s, NCH_3), 1.79 (s, CCH_3), 2.50–1.00 (m, free PCy_3). $^{31}P\{^{1}H\}$ NMR (121 MHz, C_6D_6): 10.5 (s, free PCy_3)

(b) Precipitate. ^{1}H NMR (300 MHz, $CDCl_3$): 3.82 (s, 6H, NCH_3), 3.37 (q, $^{3}J_{HH}$ = 7.8 Hz, 2H, CH_2), 2.26 (s, 6H, CCH_3), 1.29 (t, $^{3}J_{HH}$ = 7.7 Hz, 3H, CH_2CH_3).

2.6.6 Independent Synthesis of [EtIMe$_4$]Cl

A pale orange solution of IMe$_4$ (50.0 mg, 0.402 mmol) in 1 mL THF was added to ethereal 1-chloroethane (4.0 mL of a 2.0 M solution in Et_2O; 8.0 mmol, 20 equiv). The mixture was stirred for 18 h, after which the off-white precipitate was filtered off and dried under vacuum. Yield: 52 mg, 70%. Chemical shifts differ slightly from reported[65] values for the iodide salt, probably owing to differences in concentration. ^{1}H NMR (300 MHz, $CDCl_3$): δ 3.82 (s, 6H, NCH_3), 3.37 (q, $^3J_{HH}$ = 7.8 Hz, 2H, CH_2), 2.26 (s, 6H, CCH_3), 1.29 (t, $^3J_{HH}$ = 7.7 Hz, 3H, CH_2CH_3). ^{13}C{^{1}H} NMR (151 MHz, $CDCl_3$): δ 146.9 (N*C*N; correlates with CH_2CH_3 and NCH_3 by HMBC), 125.9 (*C*CH_3), 32.6 (N*C*H_3), 18.1 (*C*H_2CH_3), 11.4 (CH_2*C*H_3), 9.1 (C*C*H_3). See Appendix A, Figure A10.

2.6.7 Low-Temperature Decomposition of GIm by IMe$_4$

In the glovebox, pink **GIm** (5.8 mg, 0.0077 mmol) was dissolved in 0.7 mL C_7D_8, and the solution was transferred to a screw-cap NMR tube with a PTFE-lined septum seal. Separately, IMe$_4$ (4.0 mg, 0.031 mmol, 4 equiv) was dissolved in 200 μL C_7D_8, and withdrawn into a 250 μL gas-tight syringe which was then plugged with a rubber septum to exclude air. The NMR tube was inserted into a pre-chilled NMR probe (–80 °C) and allowed to equilibrate for 10 min, after which the initial ^{1}H NMR spectrum was recorded. The sample was then ejected, and the IMe$_4$ solution was dribbled down the cold internal surface of the NMR tube at –77 °C (acetone-dry ice) over ca. 1 min to enable cooling. The pierced PTFE septum was then quickly covered with Parafilm; the NMR tube was inverted to mix (causing a colour change from orange-red to light orange/yellow), and immediately reinserted into the NMR probe. ^{1}H NMR (300 MHz, C_7D_8, –80 °C); δ 3.77 (s, 24H, NCH_3 of **Ru-19**), 1.71 (s, 24H, CCH_3 of **Ru-19**, overlaps with PCy_3), 2.01–1.00 (m, Cy of PCy_3 + **Ru-19**). ^{31}P{^{1}H} NMR (121 MHz, C_7D_8, –80 °C); δ 10.5 (free PCy_3). For spectra, see Appendix A, Figure A11.

Repeating the procedure above in THF-d8 (6.0 mg **GIm**, 0.008 mmol; 4.0 mg IMe$_4$, 0.032 mmol, 4 equiv) gave similar results. ^{1}H NMR (300 MHz, THF-d8, –80 °C); δ 3.24 (s, 24H, NCH_3 of **Ru-2**), 2.10 (s, 24H, CCH_3 of **Ru-19**, overlaps with PCy_3), 2.28–1.03 (m, Cy of PCy_3 + **Ru-19**). ^{31}P{^{1}H} NMR (121 MHz, C_7D_8, –80 °C); δ 9.9 (free PCy_3). For spectra, see Appendix A, Figure A12.

2.6.8 Quantification of free PCy$_3$ from Decomposition of GIm by IMe$_4$

Note: All glassware used in this experiment was silanized by soaking overnight in neat TMSCl, then rinsed with copious CH_2Cl_2 and allowed to dry in the glovebox prior to use. Solid **GIm** (11 mg, 0.015 mmol was dissolved in 0.7 mL C_6D_6 and transferred to a J. Young NMR tube. A flame-sealed capillary containing 1,4-bis(diphenylphosphino)butane (dppb) was added to the NMR tube. A quantitative ^{31}P{^{1}H} NMR spectrum (delay time 60 s) was recorded to establish the starting ratio of **GIm** to dppb. The tube was returned to the glovebox, and IMe$_4$ (7.5 mg, 0.06 mmol, 4 equiv) was added in an additional 0.5 mL C_6D_6. The reaction was intermittently shaken gently

over the next 30 min, taking care not to damage the capillary inside. A quantitative $^{31}P\{^{1}H\}$ NMR spectrum was recorded to quantify the proportion of free PCy_3 using an inverse-gated 30° pulse sequence: in this case a 20 s relaxation delay was used (>3x T_1 for free PCy_3). Yield of free PCy_3: 87% based on starting **GIm**. For spectra, see Appendix A, Figure A13.

2.7 References

(1) Scholl, M.; Trnka, T. M.; Morgan, J. P.; Grubbs, R. H., Increased Ring Closing Metathesis Activity of Ruthenium-Based Olefin Metathesis Catalysts Coordinated with Imidazolin-2-Ylidene Ligands. *Tetrahedron Lett.* **1999**, *40*, 2247–2250.

(2) Huang, J.; Stevens, E. D.; Nolan, S. P.; Petersen, J. L., Olefin Metathesis-Active Ruthenium Complexes Bearing a Nucleophilic Carbene Ligand. *J. Am. Chem. Soc.* **1999**, *121*, 2674–2678.

(3) Weskamp, T.; Kohl, F. J.; Hieringer, W.; Gleich, D.; Herrmann, W. A., Highly Active Ruthenium Catalysts for Olefin Metathesis: The Synergy of N-Heterocyclic Carbenes and Coordinatively Labile Ligands. *Angew. Chem., Int. Ed.* **1999**, *38*, 2416–2419.

(4) Vougioukalakis, G. C.; Grubbs, R. H., Ruthenium-Based Heterocyclic Carbene-Coordinated Olefin Metathesis Catalysts. *Chem. Rev.* **2010**, *110*, 1746–1787.

(5) (a) Higman, C. S.; Lummiss, J. A. M.; Fogg, D. E. Olefin Metathesis at the Dawn of Uptake in Pharmaceutical and Specialty Chemicals Manufacturing. *Angew. Chem., Int. Ed.* **2016**, *55*, 3552–3565. (b) Grela, K., *Olefin Metathesis-Theory and Practice*. Wiley: Hoboken, NJ, 2014. (c) Grubbs, R. H.; Wenzel, A. G., *Handbook of Metathesis*. 2nd ed.; Wiley-VCH: Weinheim, 2015.

(6) Bailey, G. A.; Fogg, D. E., Acrylate Metathesis via the Second-Generation Grubbs Catalyst: Unexpected Pathways Enabled by a PCy_3-Generated Enolate. *J. Am. Chem. Soc.* **2015**, *137*, 7318–7321.

(7) Higman, C. S.; Nascimento, D.; Ireland, B. J.; Audorsch, S.; Bailey, G. A.; Fogg, D. E., Chelate-Assisted Ring-Closing Metathesis: A Strategy for Accelerating Macrocyclization at Ambient Temperatures. *J. Am. Chem. Soc.* **2018**, *140*, 1604−1607.

(8) Nascimento, D. L.; Gawin, A.; Gawin, R.; Guńka, P. A.; Zachara, J.; Skowerski, K.; Fogg, D. E., A Highly Reactive Ruthenium-Indenylidene Catalyst for Olefin Metathesis. *J. Am. Chem. Soc.* **2019**, *141*, 10626–10631.

(9) Crabtree, R. H., Deactivation in Homogeneous Transition Metal Catalysis: Causes, Avoidance, and Cure. *Chem. Rev.* **2015**, *115*, 127–150.

(10) Chadwick, J. C.; Duchateau, R.; Freixa, Z.; van Leeuwen, P. W. N. M., Alkene Metathesis. In *Homogeneous Catalysts: Activity – Stability – Deactivation*, Wiley-VCH: Weinheim, 2011; pp 347-396.

(11) Poater, A.; Ragone, F.; Correa, A.; Cavallo, L., Exploring the Reactivity of Ru-Based Metathesis Catalysts with a π-Acid Ligand Trans to the Ru-Ylidene Bond. *J. Am. Chem. Soc.* **2009**, *131*, 9000-9006.

(12) Hong, S. H.; Chlenov, A.; Day, M. W.; Grubbs, R. H., Double C-H Activation of an N-Heterocyclic Carbene Ligand in a Ruthenium Olefin Metathesis Catalyst. *Angew. Chem., Int. Ed.* **2007**, *46*, 5148–5151.

(13) Hong, S. H.; Wenzel, A. G.; Salguero, T. T.; Day, M. W.; Grubbs, R. H., Decomposition of Ruthenium Olefin Metathesis Catalysts. *J. Am. Chem. Soc.* **2007**, *129*, 7961–7968.

(14) Tang, C. Y.; Smith, W.; Vidovic, D.; Thompson, A. L.; Chaplin, A. B.; Aldridge, S., Sterically Encumbered Iridium Bis(N-heterocyclic carbene) Systems: Multiple C−H Activation Processes and Isomeric Normal/Abnormal Carbene Complexes. *Organometallics* **2009**, *28*, 3059–3066.

(15) Higman, C. S.; Rufh, S. A.; Fogg, D. E., Synthesis and Dynamic Behaviour of a Dimeric Ruthenium Benzylidene Complex Bearing a Truncated N-Heterocyclic Carbene Ligand. *J. Organomet. Chem.* **2017**, *847*, 162–166.

(16) (a) Grela, K., *Olefin Metathesis-Theory and Practice*. Wiley: Hoboken, NJ, 2014. (b) Grubbs, R. H.; Wenzel, A. G., *Handbook of Metathesis*. 2nd ed.; Wiley-VCH: Weinheim, 2015.

(17) Higman, C. S.; Lummiss, J. A. M.; Fogg, D. E., Olefin Metathesis at the Dawn of Uptake in Pharmaceutical and Specialty Chemicals Manufacturing. *Angew. Chem., Int. Ed.* **2016**, *55*, 3552–3565.

(18) Farina, V.; Horváth, A., Ring-Closing Metathesis in the Large-Scale Synthesis of Pharmaceuticals. In *Handbook of Metathesis*, Grubbs, R. H.; Wenzel, A. G., Eds. Wiley-VCH: Weinheim, 2015; Vol. 2, pp 633–658.

(19) Fandrick, K. R.; Savoie, J.; Jinhua, N. Y.; Song, J. J.; Senanayake, C. H., Challenges and Opportunities for Scaling the Ring-Closing Metathesis Reaction in the Pharmaceutical Industry. In *Olefin Metathesis – Theory and Practice*, Grela, K., Ed. Wiley: Hoboken, 2014; pp 349-366.

(20) Leading reviews: (a) Lohr, T. L.; Marks, T. J. Orthogonal Tandem Catalysis. *Nat. Chem.*, **2015**, *7*, 477–482; (b) Wasilke, J.-C.; Obrey, S. J.; Baker, R. T.; Bazan, G. C. Concurrent Tandem Catalysis. *Chem. Rev*., **2005**, *105*, 1001–1020; (c) Fogg, D. E.; dos Santos, E. N. Tandem Catalysis: A Taxonomy and Illustrative Review. *Coord. Chem. Rev*., **2004**, *248*, 2365–2379.

(21) Dornan, P. K.; Wickens, Z. K.; Grubbs, R. H., Tandem Z-Selective Cross-Metathesis/Dihydroxylation: Synthesis of anti-1,2-Diols. *Angew. Chem. Int. Ed.* **2015**, *54*, 7134 –7138.

(22) Zielinski, G. K.; Majtczak, J.; Gutowski, M.; Grela, K., A Selective and Functional Group-Tolerant Ruthenium-Catalyzed Olefin Metathesis/Transfer Hydrogenation Tandem Sequence Using Formic Acid as Hydrogen Source. *J. Org. Chem.* **2018**, *83*, 2542–2553.

(23) Renom-Carrasco, M.; Gajewski, P.; Pignataro, L.; de Vries, J. G.; Piarulli, U.; Gennari, C.; Lefort, L., Asymmetric Transfer Hydrogenation of Ketones with Modified Grubbs Metathesis Catalysts. *Adv. Synth. Catal.* **2016**, *358*, 515–519.

(24) Schrodi, Y., Mechanisms of Olefin Metathesis Catalyst Decomposition and Methods of Catalyst Reactivation. In *Handbook of Metathesis*, Grubbs, R. H.; Wenzel, A. G., Eds. Wiley-VCH: Weinheim, 2015; pp 323–342.

(25) Chadwick, J. C.; Duchateau, R.; Freixa, Z.; van Leeuwen, P. W. N. M., *Homogeneous Catalysts: Activity – Stability – Deactivation*. Wiley-VCH: Weinheim, 2011.

(26) Fürstner, A.; Ackermann, L.; Gabor, B.; Goddard, R.; Lehmann, C. W.; Mynott, R.; Stelzer, F.; Thiel, O. R., Comparative Investigation of Ruthenium-Based Metathesis Catalysts Bearing N-Heterocyclic Carbene (NHC) Ligands. *Chem. – Eur. J.* **2001**, *7*, 3236–3253.

(27) Conrad, J. C.; Parnas, H. H.; Snelgrove, J. L.; Fogg, D. E., Highly Efficient Ru-Pseudohalide Catalysts for Olefin Metathesis. *J. Am. Chem. Soc.* **2005**, *127*, 11882–11883.

(28) Kuhn, K. M.; Bourg, J.-B.; Chung, C. K.; Virgil, S. C.; Grubbs, R. H., Effects of NHC-Backbone Substitution on Efficiency in Ruthenium-Based Olefin Metathesis. *J. Am. Chem. Soc.* **2009**, *131*, 5313–5320.

(29) McClennan, W. L.; Rufh, S. A.; Lummiss, J. A. M.; Fogg, D. E., A General Decomposition Pathway for Phosphine-Stabilized Metathesis Catalysts: Lewis Donors Accelerate Methylidene Abstraction. *J. Am. Chem. Soc.* **2016**, *138*, 14668−14677.

(30) Manzini, S.; Urbina Blanco, C. A.; Slawin, A. M. Z.; Nolan, S. P., Effect of Ligand Bulk in Ruthenium-Catalyzed Olefin Metathesis: IPr* vs IPr. *Organometallics* **2012**, *31*, 6514−6517.

(31) Pump, E.; Leitgeb, A.; Kozłowska, A.; Torvisco, A.; Falivene, L.; Cavallo, L.; Grela, K.; Slugovc, C., Variation of the Sterical Properties of the N‑Heterocyclic Carbene Coligand in Thermally Triggerable Ruthenium-Based Olefin Metathesis Precatalysts/Initiators. *Organometallics* **2015**, *34*, 5383−5392.

(32) Occhipinti, G.; Bjorsvik, H.-R.; Jensen, V. R., Quantitative Structure-Activity Relationships of Ruthenium Catalysts for Olefin Metathesis. *J. Am. Chem. Soc.* **2006**, *128*, 6952–6964.

(33) Selected examples: (a) Hong, S. H.; Wenzel, A. G.; Salguero, T. T.; Day, M. W.; Grubbs, R. H., Decomposition of Ruthenium Olefin Metathesis Catalysts. *J. Am. Chem. Soc.* **2007**,

129, 7961–7968. (b) Leitao, E. M.; Dubberley, S. R.; Piers, W. E.; Wu, Q.; McDonald, R., Thermal Decomposition Modes for Four-Coordinate Ruthenium Phosphonium Alkylidene Olefin Metathesis Catalysts. *Chem. – Eur. J.* **2008**, *14*, 11565–11572. (c) Burling, S.; Paine, B. M.; Nama, D.; Brown, V. S.; Mahon, M. F.; Prior, T. J.; Pregosin, P. S.; Whittlesey, M. K.; Williams, J. M. J., C-H Activation Reactions of Ruthenium N-Heterocyclic Carbene Complexes: Application in a Catalytic Tandem Reaction Involving C-C Bond Formation from Alcohols. *J. Am. Chem. Soc.* **2007**, *129*, 1987–1995. (d) Abdur-Rashid, K.; Fedorkiw, T.; Lough, A. J.; Morris, R. H., Coordinatively Unsaturated Hydridoruthenium(II) Complexes of N-Heterocyclic Carbenes. *Organometallics* **2004**, *23*, 86–94. (e) Trnka, T. M.; Morgan, J. P.; Sanford, M. S.; Wilhelm, T. E.; Scholl, M.; Choi, T.-L.; Ding, S.; Day, M. W.; Grubbs, R. H., Synthesis and Activity of Ruthenium Alkylidene Complexes Coordinated with Phosphine and N-Heterocyclic Carbene Ligands. *J. Am. Chem. Soc.* **2003**, *125*, 2546–2558. (f) Hong, S. H.; Chlenov, A.; Day, M. W.; Grubbs, R. H., Double C-H Activation of an N-Heterocyclic Carbene Ligand in a Ruthenium Olefin Metathesis Catalyst. *Angew. Chem., Int. Ed.* **2007**, *46*, 5148–5151. (g) Vieille-Petit, L.; Luan, X.; Gatti, M.; Blumentritt, S.; Linden, A.; Clavier, H.; Nolan, S. P.; Dorta, R., Improving Grubbs' II Type Ruthenium Catalysts by Appropriately Modifying the N-Heterocyclic Carbene Ligand. *Chem. Commun.* **2009**, 3783–3785. (h) Vehlow, K.; Gessler, S.; Blechert, S., Deactivation of Ruthenium Olefin Metathesis Catalysts Through Intramolecular Carbene-Arene Bond Formation. *Angew. Chem., Int. Ed.* **2007**, *46*, 8082–8085. (i) Herbert, M. B.; Lan, Y.; Keitz, B. K.; Liu, P.; Endo, K.; Day, M. W.; Houk, K. N.; Grubbs, R. H., Decomposition Pathways of Z-Selective Ruthenium Metathesis Catalysts. *J. Am. Chem. Soc.* **2012**, *134*, 7861–7866.

(34) Herbert, M. B.; Grubbs, R. H., Z-Selective Cross Metathesis with Ruthenium Catalysts: Synthetic Applications and Mechanistic Implications. *Angew. Chem. Int. Ed.* **2015**, *54*, 5018–5024.

(35) (a) Bailey, G. A.; Foscato, M.; Higman, C. S.; Day, C. S.; Jensen, V. R.; Fogg, D. E., Bimolecular Coupling as a Vector for Decomposition of Fast-Initiating Olefin Metathesis Catalysts. *J. Am. Chem. Soc.* **2018**, *140*, 6931–6944. (b) Engel, J.; Smit, W.; Foscato, M.; Occhipinti, G.; Törnroos, K. W.; Jensen, V. R., Loss and Reformation of Ruthenium Alkylidene: Connecting Olefin Metathesis, Catalyst Deactivation, Regeneration, and Isomerization. *J. Am. Chem. Soc.* **2017**, *139*, 16609–16619. (c) Bailey, G. A.; Lummiss, J. A. M.; Foscato, M.; Occhipinti, G.; McDonald, R.; Jensen, V. R.; Fogg, D. E., Decomposition of Olefin Metathesis Catalysts by Brønsted Base: Metallacyclobutane Deprotonation as a Primary Deactivating Event. *J. Am. Chem. Soc.* **2017**, *139*, 16446–16449. (d) Bailey, G. A.; Fogg, D. E., Acrylate Metathesis via the Second-Generation Grubbs Catalyst: Unexpected Pathways Enabled by a PCy_3-Generated Enolate. *J. Am. Chem. Soc.* **2015**, *137*, 7318–7321. (e) Lummiss, J. A. M.; McClennan, W. L.; McDonald, R.; Fogg, D. E., Donor-Induced Decomposition of the Grubbs Catalysts: An Intercepted

Intermediate *Organometallics* **2014**, *33*, 6738–6741. (f) Lummiss, J. A. M.; Botti, A. G. G.; Fogg, D. E., Isotopic Probes for Ruthenium-Catalyzed Olefin Metathesis. *Catal. Sci. Technol.* **2014**, *4*, 4210–4218.

(36) Ireland, B. J.; Dobigny, B. T.; Fogg, D. E., Decomposition of a Phosphine-Free Metathesis Catalyst by Amines and Other Nitrogen Bases: Metallacyclobutane Deprotonation as a Major Deactivation Pathway. *ACS Catal.* **2015**, *5*, 4690−4698.

(37) Lummiss, J. A. M.; Ireland, B. J.; Sommers, J. M.; Fogg, D. E., Amine-Mediated Degradation in Olefin Metathesis Reactions that Employ the Second-Generation Grubbs Catalysts. *ChemCatChem* **2014**, *6*, 459–463.

(38) Reade, S. P.; Nama, D.; Mahon, M. F.; Pregosin, P. S.; Whittlesey, M. K., Synthesis and Reactivity of $RuHF(CO)(PPh_3)_3$ and the N-Heterocyclic Carbene Derivatives $RuHF(CO)(NHC)(PPh_3)_2$. *Organometallics* **2007**, *26*, 3484–3491.

(39) Davies, C. J. E.; Lowe, J. P.; Mahon, M. F.; Poulten, R. C.; Whittlesey, M. K., Synthesis and Small Molecule Reactivity of trans-Dihydride Isomers of $Ru(NHC)_2(PPh_3)_2H_2$. *Organometallics* **2013**, *32*, 4927–4937.

(40) Cybulski, M. K.; Nicholls, J. E.; Lowe, J. P.; Mahon, M. F.; Whittlesey, M. K., Catalytic Hydrodefluorination of Fluoroarenes Using $Ru(IMe_4)_2L_2H_2$ (IMe_4 = 1,3,4,5-Tetramethylimidazol-2-ylidene; L_2 = $(PPh_3)_2$, dppe, dppp, dppm) Complexes. *Organometallics* **2017**, *36*, 2308–2316.

(41) Burling, S.; Haller, L. J. L.; Mas-Marza, E.; Moreno, A.; MacGregor, S. A.; Mahon, M. F.; Pregosin, P. S.; Whittlesey, M. K., The Influence of N-Heterocyclic Carbenes (NHC) on the Reactivity of $[RuH(NHC)_4]^+$ with H_2, N_2, CO and O_2. *Chem. – Eur. J.* **2009**, *15*, 10912–10923.

(42) (a) Wolf, R.; Plois, M.; Hepp, A., Neutral and Cationic Hydridoruthenium Tetrakiscarbene Complexes. *Eur. J. Inorg. Chem.* **2017**, 4814–4814. (b) Wolf, R.; Plois, M.; Hepp, A., Neutral and Cationic Hydridoruthenium Tetrakiscarbene Complexes. *Eur. J. Inorg. Chem.* **2010**, 918–925.

(43) IMe_4 complexes: (a) Bantreil, X.; Randall, R. A. M.; Slawin, A. M. Z.; Nolan, S. P., Ruthenium Complexes Bearing Two N-Heterocyclic Carbene Ligands in Low Catalyst Loading Olefin Metathesis Reactions. *Organometallics* **2010**, *29*, 3007–3011. (b) Lujan, C.; Nolan, S. P., E/Z Selectivity in Ruthenium-Mediated Cross Metathesis. *Catal. Sci. Technol.* **2012**, *2*, 1027-1032. IMe_2 complexes: (c) Wolf, S.; Plenio, H., On the Ethenolysis of Natural Rubber and Squalene. *Green Chem.* **2011**, *13*, 2008–2012. (d) Sashuk, V.; Peeck, L. H.; Plenio, H., $[(NHC)(NHC_{ewg})RuCl_2(CHPh)]$ Complexes with Modified NHC_{ewg} Ligands for Efficient Ring-Closing Metathesis Leading to Tetrasubstituted Olefins. *Chem. – Eur. J.* **2010**, *16*, 3983–3993.

(44) Thiel, V.; Wannowius, K.-J.; Wolff, C.; Thiele, C. M.; Plenio, H., Ring-Closing Metathesis Reactions: Interpretation of Conversion–Time Data. *Chem. - Eur. J.* **2013**, *19*, 16403–16414.

(45) Sanford, M. S.; Love, J. A.; Grubbs, R. H., Mechanism and Activity of Ruthenium Olefin Metathesis Catalysts. *J. Am. Chem. Soc.* **2001**, *123*, 6543–6554.

(46) Roy, M. M. D.; Rivard, E., Pushing Chemical Boundaries with N‑Heterocyclic Olefins (NHOs): From Catalysis to Main Group Element Chemistry. *Acc. Chem. Res.* **2017**, *50*, 2017−2025.

(47) Crocker, R. D.; Nguyen, T. V., The Resurgence of the Highly Ylidic N-Heterocyclic Olefins as a New Class of Organocatalysts. *Chem. - Eur. J.* **2016**, *22*, 2208–2213.

(48) Blümel, M.; Crocker, R. D.; Harper, J. B.; Enders, D.; Nguyen, T. V., N-Heterocyclic Olefins as Efficient Phase-Transfer Catalysts for Base-Promoted Alkylation Reactions. *Chem. Comm.* **2016**, *52*, 7958–7961.

(49) Blümel, M.; Noy, J.-M.; Enders, D.; Stenzel, M. H.; Nguyen, T. V., Development and Applications of Transesterification Reactions Catalyzed by N-Heterocyclic Olefins. *Org. Lett.* **2016**, *18*, 2208–2211.

(50) Iturmendi, A.; García, N.; Jaseer, E. A.; Munárriz, J.; Miguel, P. J. S.; Polo, V.; Iglesias, M.; Oro, L. A., N-Heterocyclic olefins as Ancillary Ligands in Catalysis. *Dalton Trans.* **2016**, *45*, 12835–12845

(51) Walther, P.; Naumann, S., N‑Heterocyclic Olefin-Based (Co)polymerization of a Challenging Monomer: Homopolymerization of ω‑Pentadecalactone and Its Copolymers with γ‑Butyrolactone, δ‑Valerolactone, and ε-Caprolactone. *Macromolecules* **2017**, *50*, 8406–8416.

(52) Amoroso, D.; Yap, G. P. A.; Fogg, D. E., The Life, Death, and ROMP Activity of Ruthenium Complexes Containing the Basic, Chelating Diphosphine Bis(Dicyclohexyl)-1,4-Phosphinobutane. *Can. J. Chem.* **2001**, *79*, 958–963.

(53) Six, C.; Gabor, B.; Goerls, H.; Mynott, R.; Philipps, P.; Leitner, W., Inter- and Intramolecular Thermal Activation of sp^3 C-H Bonds with Ruthenium Bisallyl Complexes. *Organometallics* **1999**, *18*, 3316–3326.

(54) Christ, M. L.; Sabo-Etienne, S.; Chaudret, B., Highly Selective Dehydrogenative Silylation of Ethylene Using the Bis(dihydrogen) Complex $RuH_2(H_2)_2(PCy_3)_2$ as Catalyst Precursor. *Organometallics* **1995**, *14*, 1082–1084.

(55) Sabo-Etienne, S.; Chaudret, B., Chemistry of Bis(dihydrogen) Ruthenium Complexes and of their Derivative. *Coord. Chem. Rev.* **1998**, *178-180*, 381–407.

(56) Lummiss, J. A. M.; Beach, N. J.; Smith, J. C.; Fogg, D. E., Targeting an Achilles Heel In Olefin Metathesis: A Strategy For High-Yield Synthesis of Second-Generation Grubbs Methylidene Catalysts. *Catal. Sci. Technol.* **2012**, *2*, 1630–1632.

(57) Lummiss, J. A. M.; Higman, C. S.; Fyson, D. L.; McDonald, R.; Fogg, D. E., The Divergent Effects of Strong NHC Donation in Catalysis. *Chem. Sci.* **2015**, *6*, 6739–6746.

(58) Chernyshev, V. M.; Khazipov, O. V.; Shevchenko, M. A.; Chernenko, A. Y.; Astakhov, A. V.; Eremin, D. B.; Pasyukov, D. V.; Kashin, A. S.; Ananikov, V. P., Revealing the Unusual Role of Bases in Activation/Deactivation of Catalytic Systems: O–NHC Coupling in M/NHC Catalysis. *Chem. Sci.* **2018**, *9*, 5564–5577.

(59) Astakhov, A. V.; Khazipov, O. V.; Chernenko, A. Y.; Pasyukov, D. V.; Kashin, A. S.; Gordeev, E. G.; Khrustalev, V. N.; Chernyshev, V. M.; Ananikov, V. P., A New Mode of Operation of Pd-NHC Systems Studied in a Catalytic Mizoroki−Heck Reaction. *Organometallics* **2017**, *36*, 1981−1992.

(60) (a) Weskamp, T.; Schattenmann, W. C.; Spiegler, M.; Herrmann, W. A., A Novel Class of Ruthenium Catalysts for Olefin Metathesis. *Angew. Chem., Int. Ed.* **1998**, 37, 2490–2493. (b) Herrmann, W. A. Corrigendum. *Angew. Chem., Int. Ed.* **1999**, 38, 262.

(61) Guidone, S.; Songis, O.; Nahra, F.; Cazin, C. S. J., Conducting Olefin Metathesis Reactions in Air: Breaking the Paradigm. *ACS Catal.* **2015**, *5*, 2697–2701.

(62) Kuhn, N.; Kratz, T., Imidazole Chemistry. 2. Synthesis of Imidazol-2-ylidenes by Reduction of Imidazole-2(3H)-thiones. *Synthesis* **1993**, 561–562.

(63) Bailey, G. A.; Fogg, D. E., Confronting Neutrality: Maximizing Success in the Analysis of Transition-Metal Catalysts by MALDI Mass Spectrometry. *ACS Catal.* **2016**, *6*, 4962–4971.

(64) Eelman, M. D.; Blacquiere, J. M.; Moriarty, M. M.; Fogg, D. E., Shining New Light on an Old Problem: Retooling MALDI Mass Spectrometry for Organotransition-Metal Catalysis. *Angew. Chem., Int. Ed.* **2008**, *47*, 303–306.

(65) Chianese, A. R.; Zeglis, B. M.; Crabtree, R. H., Unexpected Oxidative C-C Cleavage in the Metallation of 2-Substituted Imidazolium Salts to Give N-Heterocyclic Carbene Complexes. *Chem. Commun.* **2004**, 2176–2177.

Chapter 3. Hydroxide-Induced Catalyst Deactivation in Olefin Metathesis

3.1 Published Contributions

Hydroxide-Induced Catalyst Deactivation in Olefin Metathesis. A. Y. Goudreault, D. M. Walden, A. G. Botti, S. Steinmann, C. Michel,* and D. E. Fogg.* Manuscript submitted to *ACS Catalysis*.

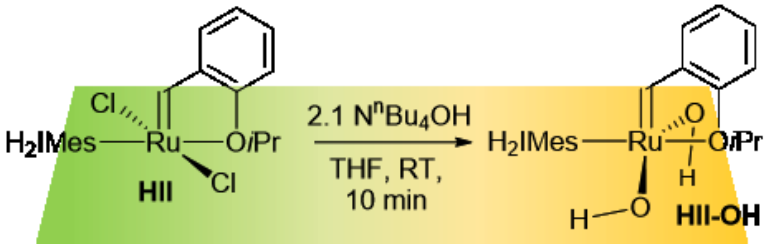

Abstract: Hydroxide ion is shown to be a potent disruptor of Ru-catalyzed olefin metathesis, in a study of the important second-generation Hoveyda catalyst **HII**. Ring-closing metathesis (RCM) reactivity was found to terminate immediately upon addition of [N^{n}Bu$_4$][OH], and was completely suppressed if the hydroxide ion was present from the outset of reaction. Termination is due to the formation of bis(hydroxide) complex **HII-OH**, which was synthesized for direct study by reacting **HII** with [N^{n}Bu$_4$][OH] in THF-water. On exposure to ethylene, **HII-OH** initiates very slowly (as expected from the inductive effect of the oxygen ligands), and decomposes in the first cycle of metathesis. Importantly, the decomposed Ru product(s) are shown to promote further decomposition of the precatalyst **HII-OH**. A bimolecular coupling pathway enabled by the H-bonding capacity of the hydroxide ligand is proposed, on the basis of experimental and density functional theory (DFT) studies.

Author Contributions: This manuscript was conceived and written by AYG and DEF. The original synthesis of **HII-OH** was conducted by AB. All other experiments were performed by AYG. Computational analysis was undertaken by DMW under the direction of SS and CM.

3.2 Introduction

Ruthenium-catalyzed olefin metathesis offers exceptionally powerful methodologies for the assembly of carbon-carbon bonds.[1] Emerging applications include pharmaceutical manufacturing[2] and chemical biology.[3] In both contexts, metathesis is typically carried out on densely-functionalized, polar substrates, in the presence of variable amounts of water (ranging from technical-grade, partially-dried organic solvents, to organic-aqueous mixtures). Understanding the unintended, non-metathetical reactions of the Ru=CHR bond under such conditions is hence of both fundamental and practical importance. The present work was aimed at assessing the impact of hydroxide on the productivity and fate of the second-generation Hoveyda catalyst **HII**, as an exemplary, widely used metathesis catalyst.

Nucleophiles and Bronsted base disrupt olefin metathesis via distinct pathways (Scheme 3.1). Nitrogen,* phosphine,† and carbon‡ nucleophiles are all known to attack the [Ru]=CHR carbon in **Ru-4**, while base can deprotonate metallacyclobutane (MCB) **Ru-5**.[6,13] The potential engagement of hydroxide ion in either manifold was anticipated.§

Unexpectedly, however, an alternative, hydroxide-promoted decomposition pathway was identified. Here we describe transformation of **HII** into bis-hydroxide complex **HII-OH**, and bimolecular decomposition of **HII-OH** during metathesis.

Scheme 3.1 Decomposition of metathesis-active species by an exemplary (a) Nucleophile; (b) Base.

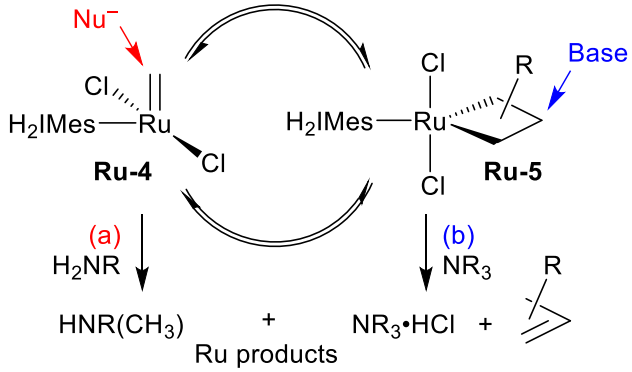

* Abstraction of the alkylidene ligand by nucleophilic amines[4-6] is shown in Scheme 3.1.

† Nucleophilic phosphines can likewise attack the [Ru]=CHR carbon. A mechanistic study demonstrated this pathway for a broad range of PR_3-stabilized benzylidene and indenylidene metathesis catalysts,[7] and the [Ru]–CH_2PCy_3 intermediate was isolated in the first-generation Grubbs system.[8] Loss of [$MePCy_3$]Cl was first reported by Hong and Grubbs, although elimination of the corresponding ylid has also been described.[9] Other examples of intra- or intermolecular attack on the benzylidene carbon have also been reported.[10,11]

‡ Nucleophilic attack of a free carbene at a methylidene carbon[12] is discussed in Chapter 2.

§ Nucleophilic attack of hydroxide ion on Ru-ligated groups is invoked in contexts ranging from the water-gas shift reaction (WGSR) in aqueous alkaline media, to catalyst synthesis and water oxidation catalysis.[14-16]

3.3 Results and Discussion

Our attention was initially drawn to the potential capacity of hydroxide ion to decompose Ru metathesis catalysts by studies examining the negative impact of adventitious enolate ion on metathesis.[13,17] Metathesis yields were significantly degraded by enolates, but were considerably worse when water was added as a sacrificial proton source to quench the enolate anion. In contrast, addition of phenols restored metathesis activity.[17]

Likewise suggestive was a survey of the impact of common contaminants on metathesis productivity. These experiments employed the readily-cyclized diene diethyl diallylmalonate (DDM, **9**; Figure 3.1), with the rationale that additives capable of disrupting this exceptionally facile ring-closing metathesis (RCM) reaction merit attention. As shown in Figure 3.1a, TONs were approximately halved by either water or morpholine (a basic contaminant present in technical grade toluene),[18,19] but dropped a further 50% when *both* water and morpholine were present (exact yields presented in Table 3.1, in Experimental Details Section 3.5).

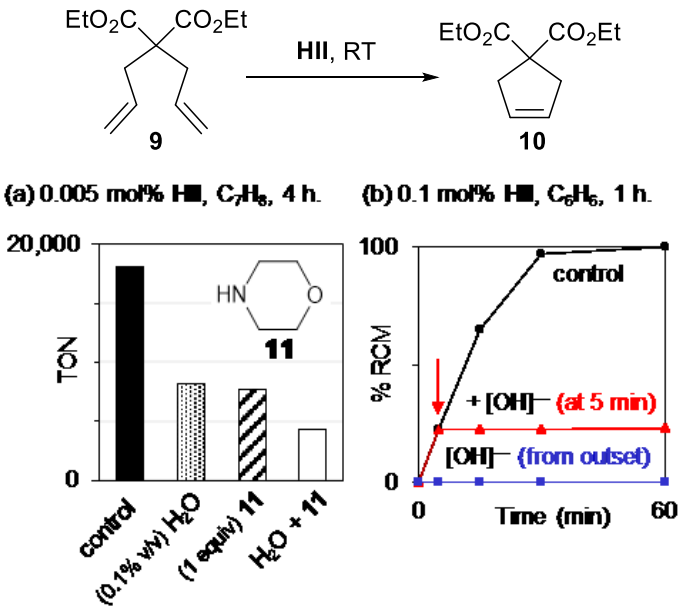

Figure 3.1 Impact of additives on RCM. (a) Water, morpholine **11**, or both. (b) [N^{n}Bu$_4$][OH] (2 equiv vs Ru).

The premise that hydroxide ion might be responsible was tested via a knockdown experiment (Figure 3.1b), in which [N^{n}Bu$_4$][OH], a soluble source of hydroxide,* was added during RCM. Metathesis activity immediately ceased (red line), even at catalyst loadings 20x higher than those used in the original screen. To assess whether this drop reflects attack on the active species **Ru-4**

* The [N^{n}Bu$_4$][OH] reagent was employed as a solution in degassed water, rather than as its alternative formulation as a solution in methanol, to circumvent formation of methoxide derivatives that rapidly decompose via β-elimination.[20,21]

or **Ru-5**, as opposed to the precatalyst **HII**, a second experiment was carried out, in which hydroxide was added prior to substrate. RCM activity was completely suppressed (blue line). We infer that the ruthenium product formed on reaction of **HII** with hydroxide ion is either completely inactive, or that it decomposes in the first cycle of metathesis.

Synthesis of the presumed hydroxide complex was undertaken for closer analysis. Accordingly, aqueous [N^{n}Bu$_4$][OH] was added to a solution of **HII** in THF (Scheme 3.2). As use of 1 equiv hydroxide resulted in only 50% consumption of **HII**, a 2:1 stoichiometry was employed. An immediate color change from green to red occurred, and NMR analysis revealed a new singlet for the benzylidene proton at 14.04 ppm (cf. 16.72 ppm for **HII**). Even on 200 mg scale, the reaction was complete in <10 min, and the bis-hydroxide product **HII-OH** was isolated in ca. 85% yield. Complete selectivity for salt metathesis was evident, in contrast with reactions of hydroxide with Ru-CO complexes,[14,15] but consistent with reactions of related Ru alkylidenes with aryloxide.[22-25]

The chemical shifts and signal multiplicities for all but the Ru=C*H*Ar protons in **HII-OH** accord closely with those of **HII**. Also present is a singlet for the Ru-O*H* protons at 1.1 ppm (assignment confirmed by exchange with degassed D_2O).[26] The distorted trigonal bipyramidal geometry* depicted in Scheme 3.2 (HO–Ru–OH = 139.6°) is based on density functional theory (DFT) analysis (see Appendix E). In comparison, a Cl-Ru-Cl angle of 156.5 is reported for **HII**.[28] This geometric difference has implications for reactivity, which are considered below.

Scheme 3.2 Synthesis of **HII-OH**.

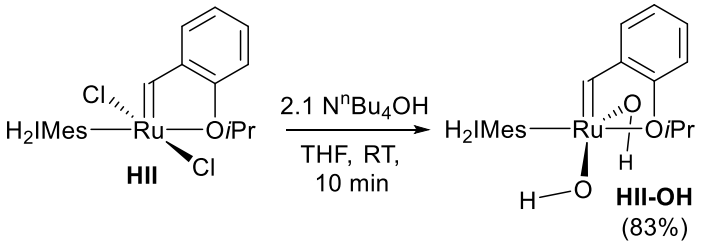

Consistent with the knockdown behaviour of Figure 3.1b, **HII-OH** was unreactive toward DDM **9**. Even on use of 10 mol% **HII-OH** at 60 °C, essentially no RCM was evident (<3%; cf. 100% within 15 min at RT on use of 1 mol% **HII** as catalyst). Slow initiation of **HII-OH** is expected from the the inductive withdrawal of electron density from the Ru center by the oxygen ligands: the departure from trans-anionic geometry of the complex may also be relevant, as cis-anionic structures have long been associated with slow initiation of Ru metathesis catalysts.[29] Both of these features, however, are present in Ru-catecholate metathesis catalysts, which are nevertheless

* Tau parameter analysis reveals a distorted trigonal bipyramidal geometry for **Ru-1**, as compared to distorted square pyramidal for **HII** (τ = 0.61 or 0.39, respectively; cf. values of 0 for a perfect square pyramid, and 1 for a perfect trigonal bipyramid).[27]

highly active in metathesis at 60 °C.[22,23] A deactivating effect is thus operative in both systems, but for **HII-OH**, deactivation appears to be exacerbated by rapid decomposition.

Of the two decomposition pathways discussed in the introduction, we exclude nucleophilic attack by hydroxide on the benzylidene carbon (cf. Scheme 3.1a). Such attack is expected to liberate the aldehyde HC(O)Ar (Ar = *o*-C_6H_4-O^{i}Pr) (Appendix A, Figure A17), which is not detected even after 24 h in solution. We therefore turned to examining whether the hydroxide ligand deprotonates the metallacyclobutane (MCB **Ru-5**; cf. Scheme 3.1b). In these experiments, we treated **HII-OH** with ethylene, and examined the disappearance of the benzylidene signal for **HII-OH**, as well as the emergence of organic products: styrenyl ether **1**, which reports on the extent to which **HII-OH** participates in metathesis (Scheme 3.3a), and propenes **3**/**4**, the yield of which reports on decomposition of the MCB **Ru-20** (Scheme 3.3b).

Loss of the [Ru]=C*H*Ar signal was quantitative by 24 h (see Figure 3.5 of Experimental Details for rate plots). Unexpectedly, however, uptake of **HII-OH** into metathesis was only ca. 40% (as judged from the yield of **1**),[30,31] and <10% propenes **3**/**4** were detected, indicating limited MCB deprotonation. Thus, puzzlingly, ca. 50% of the Ar tag is unaccounted for once disappearance of **HII-OH** is complete. We suspected that the key might lie in the non-metathetical reactivity of four-coordinate **Ru-21**, as described below. (Three-coordinate **Ru-22**, the co-product of MCB decomposition, may also contribute, but the low propene yield indicates that the proportion of this species is small).

Scheme 3.3 Reaction of **HII-OH** with C_2H_4. (a) Via metathesis. (b) Via MCB decomposition.[a]

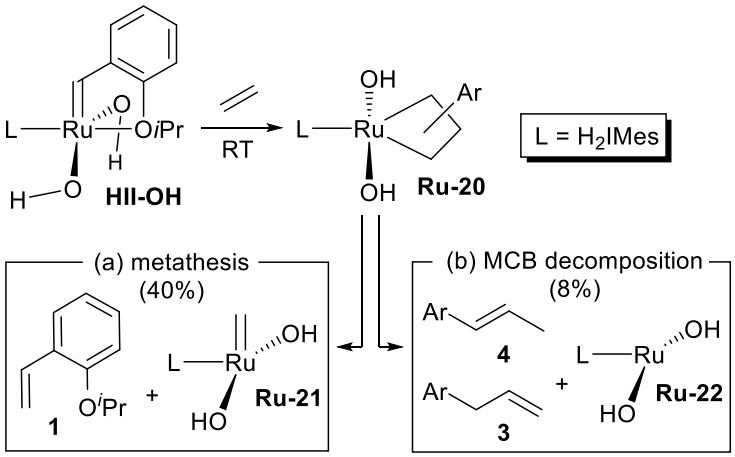

[a] The contribution of Path (a) is indicated by the yield of **1**, that of Path (b) by the yield of **3**+**4** (4% each).

In a recent study of fast-initiating metathesis catalysts,[32] we reported that rapid bimolecular coupling of four-coordinate intermediate **Ru-4** causes elimination of the methylidene ligands as ethylene. For **HII-OH**, slow initiation disfavours this pathway. However, it opens the door to *hetero*-coupling of **Ru-21** with **HII-OH** (Figure 3.2a). The plausibility of this reaction was

established by computational analysis: see below. Also revealed was an unanticipated resistance to bimolecular elimination of styrene **1** from the proposed dinuclear intermediate **Ru-23**, in contrast with facile elimination of ethylene via homocoupling of **Ru-4**. This is important in indicating that all **1** observed originates in metathesis.

To probe experimentally whether low-coordinate Ru species can decompose **HII-OH**, we treated the precatalyst with ethylene (Figure 3.2b), degassed the solution once decomposition was complete, then added fresh **HII-OH** (see arrows). Loss of **HII-OH** in the ensuing, ethylene-free reaction is faster than in the control reaction of **HII-OH** under N_2. As expected, it is slower than the initial decomposition of **HII-OH** under ethylene. Nevertheless, this experiment implies that **HII-OH** does indeed couple with low-coordinate Ru species formed via catalyst decomposition, presumably via hydrogen-bonding of the hydroxide ligands.

In striking contrast, the corresponding experiment with **HII** causes negligible decomposition of fresh **HII** (Figure 3.3). We infer that the H-bonding capacity of the hydroxide ligands is critical. The exceptional facility with which such ligands form hydroxy-bridged Ru species, and their capacity to engage in extended H-bonding, is well established.[33,34]

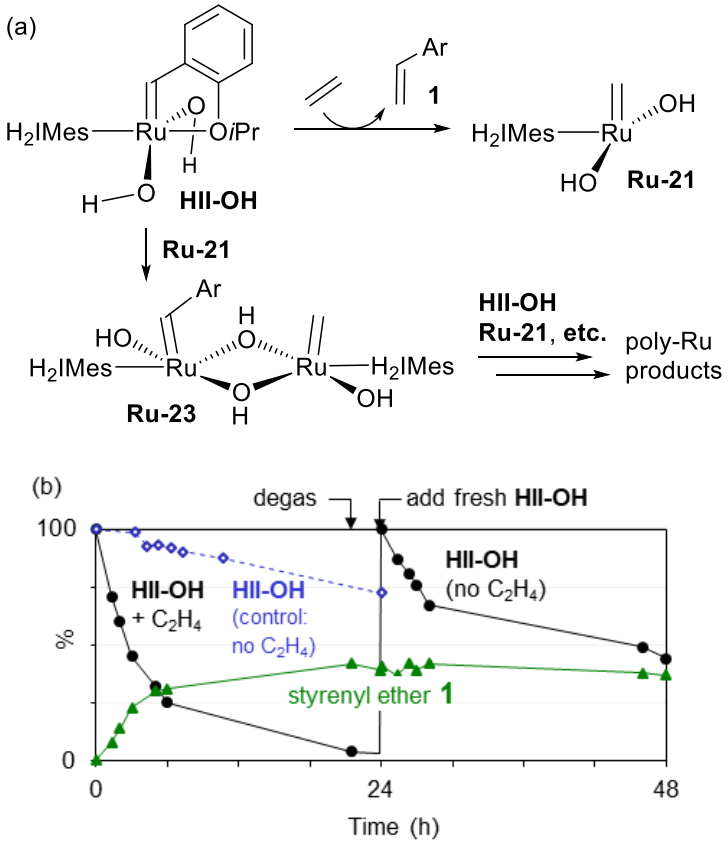

Figure 3.2 Accelerating effect of decomposed catalyst on the decomposition of **HII-OH**.

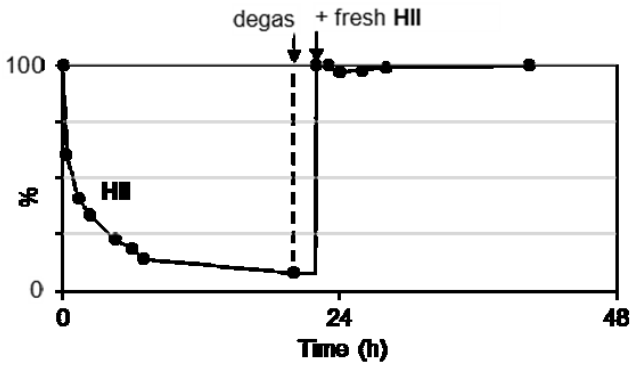

Figure 3.3 NMR experiment demonstrating that decomposed **HII** does not accelerate decomposition of pristine **HII** catalyst.

An important aspect of the **HII-OH** ethenolysis experiment is the absence of new olefinic species or (as noted above) any increase in the proportion of **1**. The Ru decomposition products thus consume **HII-OH** – presumably via hydroxide-promoted coupling – without eliminating the benzylidene and/or methylidene ligands. Moreover, no new alkylidene signals are observed, suggesting that the ultimate Ru products are paramagnetic (as indeed surmised from the decrease in signal-to-noise ratios over the 24 h timescale of decomposition: Appendix A; Figure A20). To test the validity of this picture, and to gain further insight, a computational study was undertaken.

Computational Analysis. We commenced computational analysis by considering initiation with ethylene as the olefin.[35] Most favorable is the dissociative pathway (Appendix D; Scheme D10). The basis for the low reactivity of **HII-OH** becomes evident at the stage of MCB formation. A 22.5 kcal/mol energy barrier must be surmounted to access the MCB for **HII-OH**, as compared with ca. 11 kcal/mol from **HII**. Slow initiation of **HII-OH** is thus unsurprising.

Computational analysis of the decomposition of **HII-OH** focused on methylidene intermediate **Ru-21**, the dominant product of the initial metathesis event (Scheme 3.3a). As discussed above, very slow initiation of **HII-OH** limits the concentration of this four-coordinate species, precluding homonuclear coupling. Favoured instead is coupling of **Ru-21** with the parent **HII-OH**, generating the hydroxo-bridged **Ru-23**. The latter complex is ca. 20 kcal/mol more stable for **HII-OH** than **HII**, a significantly greater thermodynamic driving force for **HII-OH**, and effectively precluded for **HII**.

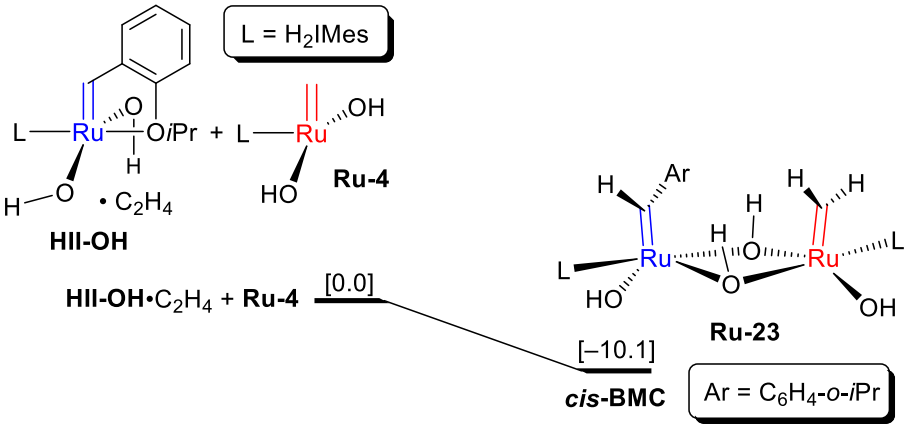

Figure 3.4 Formation of hydroxo-bridged dinuclear intermediate **Ru-23**.

3.4 Conclusions

The foregoing demonstrates that hydroxide ion is an unexpectedly potent disruptor of Ru-catalyzed olefin metathesis. Termination is traced to the slow initiation and rapid decomposition of the bis(hydroxide) complex **HII-OH**. A notable feature is the capacity of the decomposed Ru species to sequester and decompose the precatalyst **HII-OH**, behaviour that arises from the H-bonding capacity of the hydroxide ligand.

These results highlight previously unrecognized challenges to metathesis in aqueous solutions, and particularly in alkaline water. They also point toward the potential involvement in catalyst decomposition of low-coordinate Ru species that may themselves attack at otherwise catalytically competent Ru-benzylidene or -methylidene sites.

3.5 Experimental Details

3.5.1 General Procedures

All reactions were carried out in an N_2-filled glovebox or using a Schlenk line at room temperature (RT, 25 ± 2 °C). HPLC-grade solvents (C_6H_6, C_7H_8, and THF) were purified using a Glass Contour solvent purification system, then stored under N_2 in the glovebox over 4 Å molecular sieves for at least 16 h prior to use. Pentane (HPLC grade) was distilled over $MgSO_4$, then P_2O_5, and stored as above. C_6D_6 (Cambridge Isotopes) was freeze/pump/that degassed and stored as above. Diethyl diallylmalonate (Aldrich, 98%) and dodecane (internal standard for GC analysis, Aldrich, anhydrous 99%) were degassed by 5 freeze/pump/thaw cycles prior to use. Tetrabutylammonium hydroxide (N^nBu_4OH, 40% w/w in H_2O, Aldrich) was likewise degassed prior to use. Potassium tris(1-pyrazoloyl)borohydrate (KTp; TCI), was used as received to quench metathesis by the reported method.[36] Anthracene (Aldrich, 99%) and ethylene (BOC Gases; Linde group, 99.9% purity) were used as received. The second-generation Hoveyda catalyst **HII** was prepared according to a recent literature procedure.[37]

NMR spectra were recorded on Bruker Avance 300 MHz, Avance II 300 MHz, or Bruker Avance III 500 MHz spectrometers at 23 ± 2 °C. Chemical shifts are given in ppm and referenced to the residual proton or carbon signals of the solvent (^{1}H, ^{13}C). Air-sensitive NMR experiments were carried out using either screw-capped NMR tubes equipped with PTFE septa (Rotoflo, Norrell #S-5-300-SC), or valved J. Young NMR tubes (Norrell, #S-5-300-VT). Controlled mixing of solutions within the NMR tubes was achieved by attaching the tubes to a rotary motor with electrical tape.[32] Infrared (IR) analyses were performed with a Nicolet 6700 FT-IR spectrometer equipped with a attenuated total reflectance (ATR) accessory in the 4000-600 cm^{-1} range.

Metathesis experiments with diethyl diallyl malonate were analyzed by gas chromatography (GC) using an Agilent 7890A gas chromatograph equipped with an autosampler, a flame ionization detector (FID), and an Agilent HP-5 polysiloxane column (30 m length, 320 μm diameter). Calibration curves of peak areas versus concentration were established for the starting diene in the relevant concentration regimes, with ca. 1:1 (w/w) sample versus dodecane as internal standard. Yields were determined from the integrated peak areas vs. internal standard. The inlet temperature was maintained at 250 °C, with a split ratio of 10:1, and He (UHP grade) as the carrier gas. The FID was heated to 275 °C.

3.5.2 Synthesis of HII-OH from HII

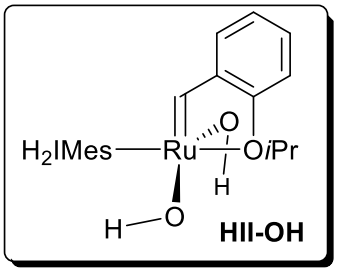

To a solution of green **HII** (200 mg, 0.32 mmol) in ca. 15 mL THF was added N^{n}Bu$_4$OH (40% w/w; 435 μL, 0.67 mmol, 2.10 equiv). An immediate color change to dark orange-red occurred. The reaction mixture was stirred at RT for 10 min, after which the solvent was removed under reduced pressure. The orange powder was suspended in cold pentane (5 mL), filtered off using a fine frit, resuspended in degassed H_2O (2 mL) and crushed with a spatula to maximize extraction of the salts. The product was filtered off, and the process was repeated twice, after which the bright orange product was washed with cold pentane (3 x 2 mL) and allowed to dry. Yield of **HII-OH**: 155 mg, 83%. ^{1}H NMR (300 MHz, C_6D_6): δ 14.04 (s, 1H, Ru=C*H*), 7.14 (dd, $^{3}J_{HH}$ = 7.7 Hz. $^{4}J_{HH}$ = 1.6 Hz, 1H, Ar*H*), 6.94 (td, $^{3}J_{HH}$ = 7.7 Hz, $^{4}J_{HH}$ = 1.6 Hz, 1H, Ar*H*), 6.93 (s, 4H, Mes *m*-C*H*) 6.83 (t, $^{3}J_{HH}$ = 7.4 Hz, 1H, Ar*H*), 6.37 (d, $^{3}J_{HH}$ = 8.0 Hz, 1H Ar*H*), 4.37 (sept, $^{3}J_{HH}$ = 6.3 Hz, 1H, C*H*Me$_2$), 3.42 (s, 4H, NHC NCH_2CH_2), 2.52 (s, 12H, Mes *o*-CH_3), 2.23 (s, 6H, Mes *p*-CH_3), 1.25 (d, $^{3}J_{HH}$ = 6.0 Hz, 6H, CH_3CHCH_3), 1.12 (s, 2H, Ru-O*H*; exchanges with D_2O). ^{13}C{^{1}H} NMR (125.5 MHz, C_6D_6): δ 235.3 (Ru=*C*H), 218.3 (C_{NHC}), 151.5 (Mes, *i*-C), 144.8 (*Ar*H), 138.7 (Mes, *o*-*C*), 138.3 (*Ar*H), 137.8 (Mes, *p*-*C*), 129.5 (Mes, *m*-*C*), 123.6 (*Ar*H), 122.9 (*Ar*H), 121.3 (*Ar*H), 112.4 (*Ar*H), 73.9 (CH$_3$*C*HCH$_3$), 51.4 (NHC, N*C*H$_2$), 21.2 (Mes, *p*-*C*H$_3$), 21.0 (*C*H$_3$CH*C*H$_2$), 18.9 (Mes, *o*-*C*H$_3$). IR (cm^{-1}): 3604 (s), 2970 (s), 2916 (m), 1473 (s), 1444 (s), 1394 (s), 1383 (s), 1240 (w), 1203 (s), 1115 (s), 1036 (s), 939 (s), 916 (s), 856 (s), 768 (s), 739 (s), 569 (s). ESI-MS (MeOH; *m/z* 591.17, [M+H]$^{+}$; calcd 591.21.

3.5.3 Representative Procedure for RCM of Diethyl Diallylmalonate at RT

(a) RCM of DDM with HII. A mixture of DDM (242 μL, 1.0 mmol) and dodecane (227 μL, 1.0 mmol, 1.0 equiv; internal standard for GC analysis) was diluted in 4.51 mL C_7H_8 to give a final concentration of 200 mM DDM. An aliquot was removed for GC-FID analysis to establish the starting ratio of substrate to dodecane. **HII** (19 μL of a stock solution of 10 mg **HII** in 6 mL C_7H_8; 0.050 μmol, 0.005 mol%) was then added. Aliquots were removed periodically, quenched with KTp in THF (10.0 mg/mL; 10 equiv vs starting Ru) and analyzed by GC-FID.

(b) RCM of DDM with HII with Added H_2O. As above, with the following modification: H_2O (4.5 μL, 0.25 mmol, 0.25 mol%) was added prior to adding the catalyst.

(c) RCM of DDM with HII with Added Morpholine. As above, with the following modification: morpholine was added (43 μL of a 12 mM stock solution; 0.050 μmol, 0.005 mol%) prior to addition of the catalyst. The 12 mM stock solution of morpholine was prepared by first diluting 10 μL morpholine in 10 mL toluene. Then, a 100 μL aliquot was removed and diluted 10x.

(d) RCM of DDM with HII with H_2O and Morpholine. As above, with the following modification: H_2O and morpholine stock solution both added prior to adding the catalyst.

3.5.4 RCM of DDM with HII and $[N^nBu_4]OH$: Present from Outset

A mixture of DDM (48.4 μL, 0.20 mmol) and dodecane (45 μL, 0.20 mmol) was diluted in 1.85 mL C_6H_6. An aliquot was removed for GC-FID analysis to establish the starting ratio of substrate to dodecane. $[N^nBu_4]OH$ (40 wt% in H_2O, 43 μL, 0.92 μM, 0.40 μmol) was then added, then **HII** (18 μL of a stock solution of 10.2 mg in 1.5 mL C_6H_6; 0.20 μM, 0.1 mol%). Aliquots were removed periodically for GC-FID analysis as above.

3.5.5 RCM of DDM with HII and $[N^nBu_4]OH$ Additive: Added after 5 Min

As above, with the following modification: $[N^nBu_4]OH$ was added from a stock solution 5 min after adding **HII**.

Table 3.1 Tabulated data for RCM experiments of Figure 3.1 (for entries 1-4 , see Figure 3.1a; for entries 5-7, see Figure 3.1b).

Entry	cat. (mol%)	T °C	Additive (equiv vs Ru)	Final Yield (%)
1	**HII** (0.005)	RT	none	90
2	**HII** (0.005)	RT	H_2O (5,000)	41
3	**HII** (0.005)	RT	Morpholine (1)	38
4	**HII** (0.005)	RT	H_2O (5,000) morpholine (1)	22
5	**HII** (0.1)	RT	none	100
6	**HII** (0.1)	RT	$[N^nBu_4]OH$ (2, added 5 min)	23
7	**HII** (0.1)	RT	$[N^nBu_4]OH$ (2, added outset)	0

3.5.6 NMR-Scale Experiment for the Stability of HII-OH

In a 4 mL vial, orange **HII-OH (**15.3 mg, 0.0260 mmol) and anthracene (I.S., 2.8 mg, 0.015 mmol, 0.57 equiv) was dissolved in 1.3 mL C_6D_6 (20 mM in Ru). The resulting solution was filtered through a pipette filter stuffed with a Kimwipe to remove any undissolved anthracene. 600 μL was removed and transferred to a J-Young NMR tube. A ^{1}H NMR spectrum was recorded to establish a starting ratio between **HII-OH** and anthracene, and then the timer started. The red solution was mixed in the NMR tube at RT, and ^{1}H NMR spectra were recorded periodically to track the decomposition of **HII-OH** over time.

The corresponding study of **HII** was omitted, in light of a literature study demonstrating that **HII** shows no decomposition after 12 h in toluene at 80 °C.[28]

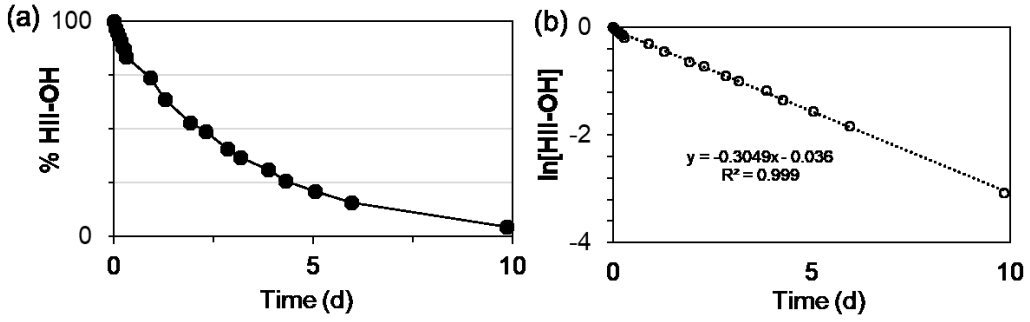

Figure 3.5 Background decomposition of **HII-OH** in C_6D_6 at RT. (a) Decay curve for **HII-OH**, monitored by ^{1}H NMR analysis relative to internal standard. (b) First-order plot.

3.5.7 Attempted RCM of DDM with HII-OH at RT: Monitoring Catalyst Decomposition

In a 4 mL vial, orange **HII-OH** (15.4 mg, 0.0260 mmol) and anthracene (I.S., 2.7 mg, 0.015 mmol, 0.57 equiv) were dissolved in 1.3 mL C_6D_6 to give a Ru concentration of 20 mM. The solution was filtered (pipette) to remove undissolved anthracene, and 600 μL was transferred to a J-Young NMR tube. A ^{1}H NMR spectrum was recorded to establish the initial ratio of **HII-OH** to anthracene. The sample was returned to the glovebox, where DDM **9** (29 μL, 0.12 mmol, 10 equiv) was added and a timer started. The resulting solution was mixed in the NMR tube at RT, and ^{1}H NMR spectra were recorded every hour to track decomposition of **HII-OH** over time. No RCM was observed. For final ^{1}H NMR spectrum showing ^{1}H NMR quantitation of Ru=CHR signal, see Appendix A, Figure A19.

3.5.8 Attempted RCM of DDM with HII-OH at 60 °C

A mixture of DDM (24 μL, 0.10 mmol) and dodecane (23 μL, 0.10 mmol, 1.0 equiv) was diluted in 1.26 mL C_6H_6 in a 2-neck round-bottom flask to give a final concentration of 50 mM DDM. An aliquot was removed for GC-FID analysis to establish the starting ratio of substrate to dodecane. The flask was removed to the Schlenk line and heated to 60 °C with stirring in a thermostatted oil bath. After 10 min for thermal equilibration, **HII-OH** (695 μL of a stock solution of 8.5 mg **HII-OH** in 1 mL C_6H_6; 0.010 mmol, 10 mol%) was added via gas-tight syringe against a flow of N_2. Aliquots were removed periodically for GC-FID analysis as above. No RCM was observed.

3.5.9 Decomposition of HII-OH by Ethylene

In a 4 mL vial, orange **HII-OH** (15.4 mg, 0.026 mmol) and anthracene (I.S., 2.7 mg, 0.015 mmol, 0.57 equiv) were dissolved in 1.3 mL C_6D_6 (20 mM Ru). The solution was filtered to remove undissolved anthracene, and 600 μL was transferred to a J-Young NMR tube. A ^{1}H NMR spectrum was recorded to establish a starting ratio of **HII-OH** to anthracene. The NMR sample was removed to the Schlenk line and degassed (4 freeze-pump-thaw cycles), then allowed to thaw under C_2H_4. The total thaw time was ca. 3 minutes, after which the tube was sealed, shaken, and the timer started. A ^{1}H NMR spectrum was immediately recorded to confirm the presence of ethylene (δ 5.25 ppm). Additional spectra were recorded every hour to track the decomposition of **HII-OH** over time. For final spectrum showing ^{1}H NMR quantitation of Ru=CHR proton and organic products, see Appendix A, Figure A17.

Decomposition of HII by ethylene. As above, but using a mixture of **HII** (8.9 mg, 0.014 mmol) and anthracene (2.4 mg, 0.019 mmol, 1.4 equiv) in 0.71 mL C_6D_6 (20 mM in **HII**). For final spectrum showing ^{1}H NMR quantitation of Ru=CHR proton and organic products, see Appendix A, Figure A18.

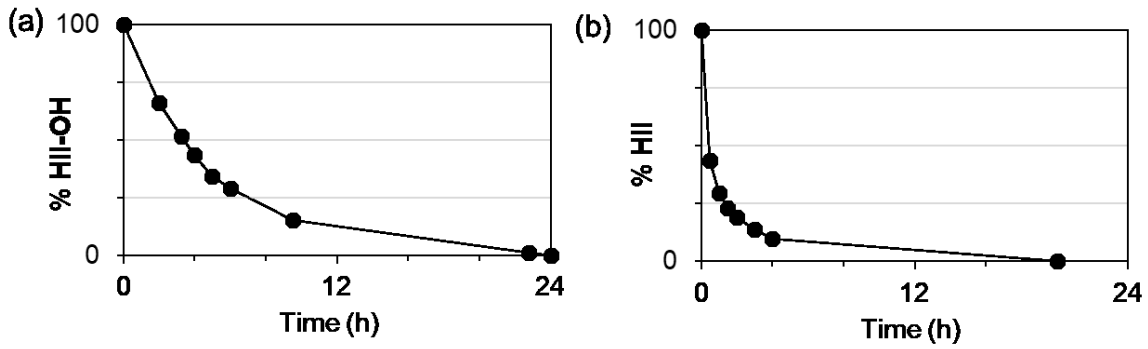

Figure 3.6 Rate plots for catalyst decomposition under ethylene. (a) **HII-OH**; (b) **HII**.

3.5.10 Accelerated Decomposition of HII-OH in the Presence of Already-Decomposed HII-OH

After complete decomposition of **HII-OH** over 22 h as described above, the NMR sample was returned to the glovebox and bubbled N_2 through the solution to remove ethylene (confirmed by ^{1}H NMR analysis). Fresh **HII-OH** (600 μL of a stock solution of 8.7 mg **HII-OH** in 0.74 mL C_6D_6; 0.012 mmol, 1 equiv) was then added. A ^{1}H NMR spectrum was recorded immediately to establish the starting ratio of fresh **HII-OH** to anthracene, and further spectra were recorded to track the decomposition of **HII-OH** over time. For spectra showing ^{1}H NMR quantitation based on integration of the Ru=C*H*Ar proton vs. IS, see Appendix A, Figure A20.

3.5.11 Stability of HII in the Presence of Decomposed HII

After complete decomposition of **HII** as described above, and degassing, fresh **HII** was added (600 μL of a stock solution of 8.9 mg **HII** in 0.71 mL C_6D_6; 0.012 mmol, 1 equiv) and the reaction was monitored as above. For rate plot, see Figure 3.3 above.

3.6 References

(1) (a) Grela, K., *Olefin Metathesis-Theory and Practice*. Wiley: Hoboken, NJ, 2014. (b) Grubbs, R. H.; Wenzel, A. G., *Handbook of Metathesis*. 2nd ed.; Wiley-VCH: Weinheim, 2015.

(2) (a) Higman, C. S.; Lummiss, J. A. M.; Fogg, D. E. Olefin Metathesis at the Dawn of Uptake in Pharmaceutical and Specialty Chemicals Manufacturing. *Angew. Chem., Int. Ed.* **2016**, *55*, 3552–3565. (b) Hughes, D.; Wheeler, P.; Ene, D., Olefin Metathesis in Drug Discovery and Development: Examples from Recent Patent Literature. *Org. Process Res. Dev.* **2017**, *21*, 1938−1962. (c) Fandrick, K. R.; Savoie, J.; Jinhua, N. Y.; Song, J. J.; Senanayake, C. H., Challenges and Opportunities for Scaling the Ring-Closing Metathesis Reaction in the Pharmaceutical Industry. In *Olefin Metathesis – Theory and Practice*, Grela, K., Ed. Wiley: Hoboken, 2014; pp 349-366. (d) Farina, V.; Horváth, A., Ring-Closing Metathesis in the Large-Scale Synthesis of Pharmaceuticals. In *Handbook of Metathesis*, Grubbs, R. H.; Wenzel, A. G., Eds. Wiley-VCH: Weinheim, 2015; Vol. 2, pp 633–658.

(3) For selected recent examples, see: (a) Bhushan, B.; Lin, Y. A.; Bak, M.; Phanumartwiwath, A.; Yang, N.; Bilyard, M. K.; Tanaka, T.; Hudson, K. L.; Lercher, L.; Stegmann, M.; Mohammed, S.; Davis, B. G., Genetic Incorporation of Olefin Cross-Metathesis Reaction Tags for Protein Modification. *J. Am. Chem. Soc.* **2018**, *140*, 14599–14603. (b) Lu, X.; Fan, L.; Phelps, C. B.; Davie, C. P.; Donahue, C. P., Ruthenium Promoted On-DNA Ring-Closing Metathesis and Cross-Metathesis. *Bioconjugate Chem.* **2017**, *28*, 1625–1629. (c) Grison, C. M.; Burslem, G. M.; Miles, J. A.; Pilsl, L. K. A.; Yeo, D. J.; Imani, Z.; Warriner, S. L.; Webb, M. E.; Wilson, A. J., Double Quick, Double Click Reversible Peptide "Stapling". *Chem. Sci.* **2017**, *8*, 5166–5171. (d) Cromm, P. M.; Spiegel, J.; Kuchler, P.; Dietrich, L.; Kriegesmann, J.; Wendt, M.; Goody, R. S.; Waldmann, H.; Grossmann, T. N., Protease-Resistant and Cell-Permeable Double-Stapled Peptides Targeting the Rab8a GTPase. *ACS Chem. Biol.* **2016**, *11*, 2375–2382. For recent and seminar early reviews, see: (e) Vinogradova, E. V., Organometallic Chemical Biology: An Organometallic Approach to Bioconjugation. *Pure Appl. Chem.* **2017**, *89*, 1619–1640. (f)) Chalker, J. M.; Bernardes, G. J. L.; Lin, Y. A.; Davis, B. G., Chemical Modification of Proteins at Cysteine: Opportunities in Chemistry and Biology. *Chem. – Asian J.* **2009**, *4*, 630–640. (g) Binder, J. B.; Raines, R. T., Olefin Metathesis for Chemical Biology. *Curr. Opin. Chem. Biol.* **2008**, *12*, 767–773.

(4) Lummiss, J. A. M.; Botti, A. G. G.; Fogg, D. E., Isotopic Probes for Ruthenium-Catalyzed Olefin Metathesis. *Catal. Sci. Technol.* **2014**, *4*, 4210–4218.

(5) Lummiss, J. A. M.; Ireland, B. J.; Sommers, J. M.; Fogg, D. E., Amine-Mediated Degradation in Olefin Metathesis Reactions that Employ the Second-Generation Grubbs Catalysts. *ChemCatChem* **2014**, *6*, 459–463.

(6) Ireland, B. J.; Dobigny, B. T.; Fogg, D. E., Decomposition of a Phosphine-Free Metathesis Catalyst by Amines and Other Nitrogen Bases: Metallacyclobutane Deprotonation as a Major Deactivation Pathway. *ACS Catal.* **2015**, *5*, 4690−4698.

(7) McClennan, W. L.; Rufh, S. A.; Lummiss, J. A. M.; Fogg, D. E., A General Decomposition Pathway for Phosphine-Stabilized Metathesis Catalysts: Lewis Donors Accelerate Methylidene Abstraction. *J. Am. Chem. Soc.* **2016**, *138*, 14668−14677.

(8) Lummiss, J. A. M.; McClennan, W. L.; McDonald, R.; Fogg, D. E., Donor-Induced Decomposition of the Grubbs Catalysts: An Intercepted Intermediate *Organometallics* **2014**, *33*, 6738–6741.

(9) Galan, B. R.; Pitak, M.; Keister, J. B.; Diver, S. T., Isocyanide-Promoted Ylidene Transfer to Phosphorus: Rearrangement in the First-Generation Grubbs Complex. *Organometallics* **2008**, *27*, 3630–3632.

(10) Werner, H.; Stuer, W.; Weberndorfer, B.; Wolf, J., Hydrido(carbonyl) and Hydrido(carbene) Complexes of Ruthenium. *Eur. J. Inorg. Chem.* **1999**, 1707–1713.

(11) Hansen, S. M.; Rominger, F.; Metz, M.; Hofmann, P., The First Grubbs-Type Metathesis Catalyst with Cis Stereochemistry: Synthesis of (h^2-dtbpm)$RuCl_2$(=CHCH=CMe_2) From a Novel, Coordinatively Unsaturated Dinuclear Ruthenium Dihydride. *Chem. – Eur. J.* **1999**, *5*, 557–566.

(12) Rufh, S.; Goudreault, A. Y.; Foscato, M.; Jensen, V. R.; Fogg, D. E., Rapid Decomposition of Olefin Metathesis Catalysts by a Truncated N-Heterocyclic Carbene (NHC): Unprecedentedly Efficient Catalyst Quenching and NHC Vinylation *ACS Catal.* **2018**, *8*, 11822−11826.

(13) Bailey, G. A.; Lummiss, J. A. M.; Foscato, M.; Occhipinti, G.; McDonald, R.; Jensen, V. R.; Fogg, D. E., Decomposition of Olefin Metathesis Catalysts by Brønsted Base: Metallacyclobutane Deprotonation as a Primary Deactivating Event. *J. Am. Chem. Soc.* **2017**, *139*, 16446–16449.

(14) Sinha, A.; Ghatak, T.; Bera, J. K., Hydroxycarbonyl Complexes as Key Intermediates in the Base-Assisted Reduction of Ruthenium Carbonyls. *Dalton Trans.* **2010**, *39*, 11301–11313.

(15) Sentets, S.; Rodriguez Martinez, M. d. C.; Vendier, L.; Donnadieu, B.; Huc, V.; Lugan, N.; Lavigne, G., Instant “Base-Promoted” Generation of Roper's-type Ru(0) Complexes $Ru(CO)_2(PR_3)_3$ from a Simple Carbonylchlororuthenium(II) Precursor. *J. Am .Chem. Soc.* **2005**, *127*, 14554–14555.

(16) Wang, Y.; Zhan, S.; Ahlquist, M. S. G., Nucleophilic Attack by OH_2 or OH–: A Detailed Investigation on pH-Dependent Performance of a Ru Catalyst. *Organometallics* **2019**, *38*, 1264–1268.

(17) Santos, A. G.; Bailey, G. A.; dos Santos, E. N.; Fogg, D. E., Overcoming Catalyst Decomposition in Acrylate Metathesis: Poly-phenol Resins as Enabling Agents for Phosphine-Stabilized Metathe-sis Catalysts. *ACS Catal.* **2017**, *7*, 3181−3189.

(18) Nicola, T.; Brenner, M.; Donsbach, K.; Kreye, P., First Scale-Up to Production Scale of a Ring Closing Metathesis Reaction Forming a 15-Membered Macrocycle as a Precursor of an Active Pharmaceutical Ingredient. *Org. Process Res. Dev.* **2005**, *9*, 513–515.

(19) Yee, N. K.; Farina, V.; Houpis, I. N.; Haddad, N.; Frutos, R. P.; Gallou, F.; Wang, X.-J.; Wei, X.; Simpson, R. D.; Feng, X.; Fuchs, V.; Xu, Y.; Tan, J.; Zhang, L.; Xu, J.; Smith-Keenan, L. L.; Vitous, J.; Ridges, M. D.; Spinelli, E. M.; Johnson, M.; Donsbach, K.; Nicola, T.; Brenner, M.; Winter, E.; Kreye, P.; Samstag, W., Efficient Large-Scale Synthesis of BILN 2061, a Potent HCV Protease Inhibitor, by a Convergent Approach Based on Ring-Closing Metathesis. *J. Org. Chem.* **2006**, *71*, 7133–7145.

(20) Beach, N. J.; Lummiss, J. A. M.; Bates, J. M.; Fogg, D. E., Reactions of Grubbs Catalysts with Excess Methoxide: Formation of Novel Methoxyhydride Complexes. *Organometallics* **2012**, *31*, 2349–2356.

(21) Dinger, M. B.; Mol, J. C., Degradation of the First-Generation Grubbs Metathesis Catalyst with Primary Alcohols, Water, and Oxygen. Formation and Catalytic Activity of Ruthenium(II) Monocarbonyl Species. *Organometallics* **2003**, *22*, 1089–1095.

(22) Monfette, S.; Camm, K. D.; Gorelsky, S. I.; Fogg, D. E., Electronic Effects of the Anionic Ligand in Ruthenium-Catalyzed Olefin Metathesis. *Organometallics* **2009**, *28*, 944–946.

(23) Monfette, S.; Fogg, D. E., Ruthenium Metathesis Catalysts Containing Chelating Aryloxide Ligands. *Organometallics* **2006**, *25*, 1940–1944.

(24) Conrad, J. C.; Amoroso, D.; Czechura, P.; Yap, G. P. A.; Fogg, D. E., The First Highly Active, Halide-Free Ruthenium Catalyst for Olefin Metathesis. *Organometallics* **2003**, *22*, 3634–3636.

(25) Conrad, J. C.; Parnas, H. H.; Snelgrove, J. L.; Fogg, D. E., Highly Efficient Ru-Pseudohalide Catalysts for Olefin Metathesis. *J. Am. Chem. Soc.* **2005**, *127*, 11882–11883.

(26) For detailed characterization data, see Appendix A, Figures A14-16.

(27) Addison, A. W.; Rao, T. N.; Reedijk, J.; Van Rijn, J.; Verschoor, G. C., Synthesis, Structure, and Spectroscopic Properties of Copper(II) Compounds Containing Nitrogen-Sulfur Donor Ligands. *J. Chem. Soc., Dalton Trans.* **1984**, 1349–1356.

(28) Garber, S. B.; Kingsbury, J. S.; Gray, B. L.; Hoveyda, A. H., Efficient and Recyclable Monomeric and Dendritic Ru-Based Metathesis Catalysts. *J. Am. Chem. Soc.* **2000**, *122*, 8168–8179.

(29) For an explicit discussion, see: (a) Kotyk, M. W.; Gorelsky, S. I.; Conrad, J. C.; Carra, C.; Fogg, D. E., Geometric and Electronic Structure of a C_1-Symmetric Ru-Aryloxide Metathesis Catalyst: An Experimental and Computational Study. *Organometallics* **2009**, *28*, 5424–5431. For early experimental evidence in cis-Cl2 systems, see: (b) Barbasiewicz, M.; Szadkowska, A.; Bujok, R.; Grela, K. *Organometallics* **2006**, *25*, 3599–3604. (c) Ung, T.; Hejl, A.; Grubbs, R. H.; Schrodi, Y. *Organometallics* **2004**, *23*, 5399–5401. (d) Slugovc, C.; Perner, B.; Stelzer, F.; Mereiter, K. *Organometallics* **2004**, *23*, 3622–3626. (e) Ben-Asuly, A.; Tzur, E.; Diesendruck, C. E.; Sigalov, M.; Goldberg, I.; Lemcoff, N. G. *Organometallics* **2008**, *27*, 811–813. For a computational study, see: (f) Benitez, D.; Goddard, W. A. *J. Am. Chem. Soc.* **2005**, *127*, 12218–12219. .

(30) Romero, P. E.; Piers, W. E., Mechanistic Studies on 14-Electron Ruthenacyclobutanes: Degenerate Exchange with Free Ethylene. *J. Am. Chem. Soc.* **2007**, *129*, 1698–1704.

(31) van Rensburg, W. J.; Steynberg, P. J.; Kirk, M. M.; Meyer, W. H.; Forman, G. S., Mechanistic comparison of ruthenium olefin metathesis catalysts: DFT insight into relative reactivity and decomposition behavior. *J. Organomet. Chem.* **2006**, *691*, 5312–5325.

(32) Bailey, G. A.; Foscato, M.; Higman, C. S.; Day, C. S.; Jensen, V. R.; Fogg, D. E., Bimolecular Coupling as a Vector for Decomposition of Fast-Initiating Olefin Metathesis Catalysts. *J. Am. Chem. Soc.* **2018**, *140*, 6931–6944.

(33) Nelson, D. J.; Nolan, S. P., Hydroxide Complexes of the Late Transition Metals: Organometallic Chemistry and Catalysis. *Coord. Chem. Rev.* **2017**, *353*, 278–294.

(34) Roesky, H. W.; Singh, S.; Yusuff, K. K. M.; Maguire, J. A.; Hosmane, N. S., Organometallic Hydroxides of Transition Elements. *Chem. Rev.* **2006**, *106*, 3813–3843.

(35) Ashworth, I. W.; Hillier, I. H.; Nelson, D. J.; Percy, J. M.; Vincent, M. A., Olefin Metathesis by Grubbs–Hoveyda Complexes: Computational and Experimental Studies of the Mechanism and Substrate-Dependent Kinetics. *ACS Catal.* **2013**, *3*, 1929-1939.

(36) Blacquiere, J. M.; Jurca, T.; Weiss, J.; Fogg, D. E., Time as a Dimension in High-Throughput Homogeneous Catalysis. *Adv. Synth. Catal.* **2008**, *350*, 2849–2855.

(37) Day, C. S.; Fogg, D. E., High-Yield Synthesis of a Long-Sought, Labile Ru-NHC Complex and Its Application to the Concise Synthesis of Second-Generation Olefin Metathesis Catalysts. *Organometallics* **2018**, *24*, 4551–4555.

Chapter 4. Examining the Impact of Water on Ruthenium-Catalyzed Olefin Metathesis

4.1 Statement of Contributions

This Chapter expands on preliminary findings described in the M.Sc. thesis of Adrian Botti, a former member of the Fogg group. AB examined the impact of water on the second-generation Grubbs and Hoveyda precatalysts (**GII** and **HII**, respectively) at 60 °C, and the impact on RCM and styrene metathesis at the same temperature. Decomposition of **GII** was attributed to a mechanism reported by William McClennan and Stephanie Rufh of this research group.[1] AYG reexamined the **HII** study: he confirmed that the MCB decomposes via β-elimination at elevated temperatures, and proposed a mechanistic explanation that takes into account recent findings by Gwen Bailey of this research group.[2,3] In collaboration with Daniel do Nascimento of this research group, AYG conducted a broad survey of the impact of additives (including water) on metathesis by various catalysts at RT, from which temperature-dependent decomposition pathways are proposed.

4.2 Introduction

The use of water as a reaction medium for olefin metathesis water has been pursued for two major reasons. A historical motivation was the use of water as the highest-ranked "green" solvent,* a function of its non-toxicity, non-flammability, and life cycle score.[4] In addition, metathesis in water enables access to products that are unattainable in organic solvents.[5] Prominent in the latter context are applications in chemical biology.[6]

However, metathesis in water is much more challenging than metathesis in traditional organic media. Recognized as a core problem is poor mass transfer arising from the limited solubility of ruthenium catalysts in water.[5] Two general strategies have been pursued to address this limitation. The first focuses on protocols to improve mass transfer for standard catalysts. These include use of surfactants,[7] emulsions,[8,9] and ultrasonication.[10] The second approach involves catalyst functionalization (or "tagging") to impart solubility in aqueous media. Of the many water-soluble metathesis catalysts now known,[11] many employ poly-ethylene glycol[12,13] or quaternary ammonium tags,[14] typically on the NHC ligand (e.g. **Ru-25** Figure 4.1).[14,15] More puzzlingly, tagged alkylidene ligands (e.g. **Ru-24**)[16] have also been used, despite loss of the "soluble" alkylidene group in the first cycle of metathesis.

Despite such efforts, turnover numbers (TONs) in water remain low relative to those attainable in organic media. For example, TONs of only 9 or 18, respectively, are achieved in RCM of the diene **12** using water-soluble **Ru-24** and **Ru-25** in H_2O/D_2O,[15,16] as compared with 11,600 for the neutral diene **14** using **Ru-26** in toluene.[17] While Thorpe-Ingold effects exerted by the tosyl protecting group could conceivably contribute to the ease of cyclization of **14**,[18,19] the difference in TONs remains very stark. The poor metathesis performance achieved even with water-soluble catalysts suggests that mass transfer is not the primary challenge to catalyst activity in water.

* Such "green" benefits are limited, however, by the production of organic-contaminated aqueous waste streams, which are costly to purify and impossible to combust.

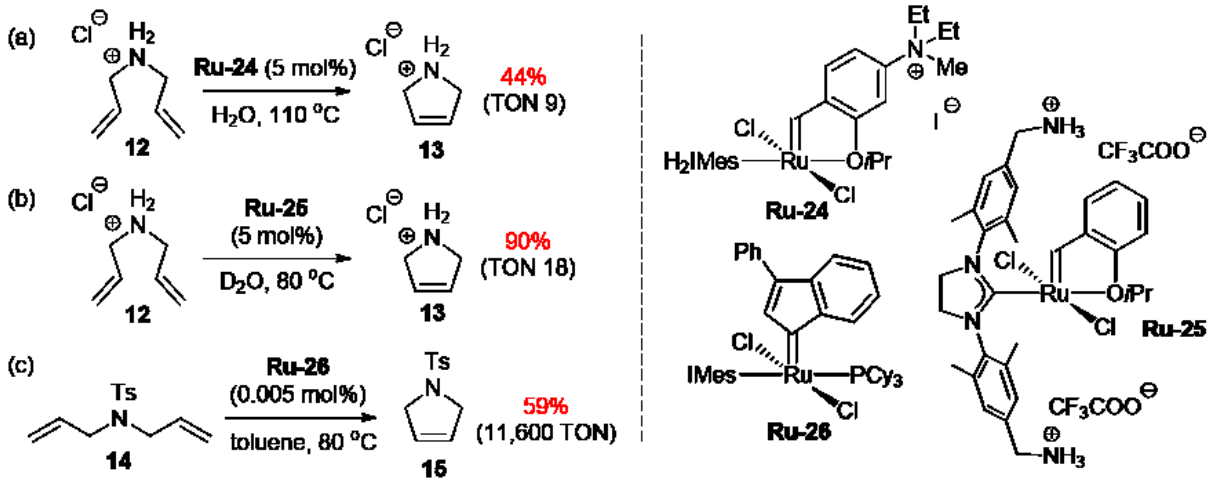

Figure 4.1 (a) RCM of **12** in water using a benzylidene-tagged catalyst **Ru-24** reported by Grela.[16] (b) RCM of **12** in deuterated water using NHC-tagged catalyst **Ru-25**, reported by Robinson.[15] (c) RCM of neutral diallylamine **14** in toluene using catalyst **Ru-26**, reported by Kadyrov.[17]

Only a handful of reports to date consider the possibility that water itself may exert a negative effect on Ru-catalyzed olefin metathesis.[1,20-23] In 2015, the Cazin group described the first direct study of the impact of water on RCM (Figure 4.2).[21] Water was identified as the most detrimental of the various components of air, in a study of a challenging RCM reaction (cyclization to give the tetrasubstituted olefin **17**). TONs were reported to drop by 50-70% in refluxing toluene containing 6% v/v H_2O, relative to the anhydrous control reaction. Catalyst decomposition was inferred, although not explored. Unlike most examples of metathesis in water, which are typically carried out using high catalyst loadings (e.g. 5 mol% Ru),[5,11] the Cazin experiments utilized 0.1 mol% Ru. This is important as excessive catalyst loadings can mask decomposition.

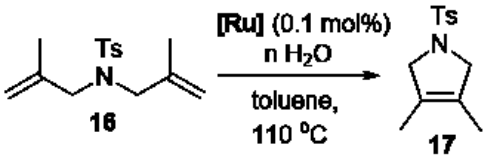

Yield 15 (%)		
	0 H_2O	6% v/v H_2O
Caz-1	90	18
Ind-II	68	10
HII	70	35

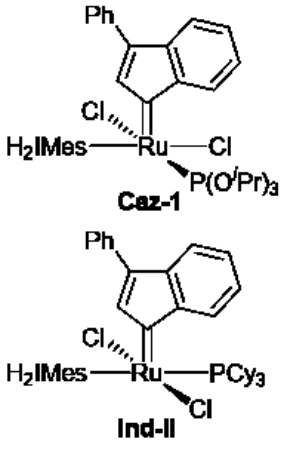

Figure 4.2 Cazin study showing the impact of H_2O on RCM of geminally-disubstituted substrate **16**.[21]

Of the catalysts in the Cazin study, PCy_3-stabilized **Ind-I** was more affected than phosphine-free **HII**. The mechanistic basis for this sensitivity can be rationalized from the insights developed by Mr. William McClennan of this research group, outlined in Chapter 1. His "donor-accelerated decomposition" mechanism is reproduced in Scheme 4.1a, for convenient reference. Here binding of water is shown to promote abstraction of the methylidene ligand by PCy_3,[1] leading to 50% decomposition of **GIIm** within 2 h at 50 °C, as compared to a base level of 10% in the absence of water. This is striking given the weak binding to the catalyst expected for water. The McClennan study was only the second report of the severely deleterious impact of water on Ru-catalyzed olefin metathesis, and the first to advance a mechanistic basis for this behavior. While it did not rule out additional avenues for catalyst degradation (as will become clear below), it clearly demonstrated that water significantly accelerates the methylidene-abstraction pathway.

Scheme 4.1 (a) Accelerated decomposition of **GIIm** in the presence of H_2O as a lewis donor.[1] (b) Decomposition of **GII** in the self-metathesis of styrene in the presence of H_2O. [a]

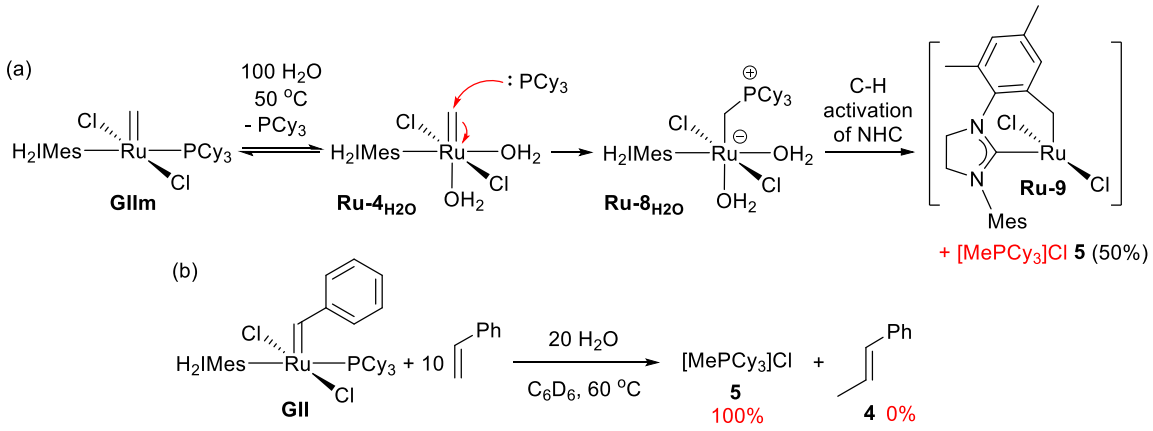

[a] Only [MePcy$_3$]Cl **5** is observed, indicating that donor-accelerated decomposition is the dominant pathway.

Indeed, unpublished results described in the M.Sc. thesis of Adrian Botti showed that donor-accelerated decomposition is the *major* pathway operative for phosphine-stabilized **GII** in the presence of water (Scheme 4.1b). Thus, 100% [$MePCy_3$]Cl **5** was observed on carrying out metathesis of styrene with **GII** in the presence of 20 equiv water. The absence of any propene **4** rules out any contribution of MCB β-elimination to catalyst decomposition.

Botti also examined the impact of water on phosphine-free **HII**, and demonstrated that even facile metathesis reactions are affected. Thus, RCM of the benchmark, readily-cyclized diene **9** using low loadings (0.005 mol%) of **HII** was examined in the presence and absence of water (Figure 4.3a). Yields decreased by 50% when 0.1% v/v H_2O was present. Decomposition of the MCB intermediate was inferred from an additional experiment (Figure 4.3b) in which styrene metathesis was carried out at 60 °C. Adding 20 equiv water quadrupled the proportion of propenes liberated, from 21 to 84%. (These experiments were repeated to evaluate the impact of temperature, as described in Section 4.3.2: the results were similar, although the propene yield was slightly lower).

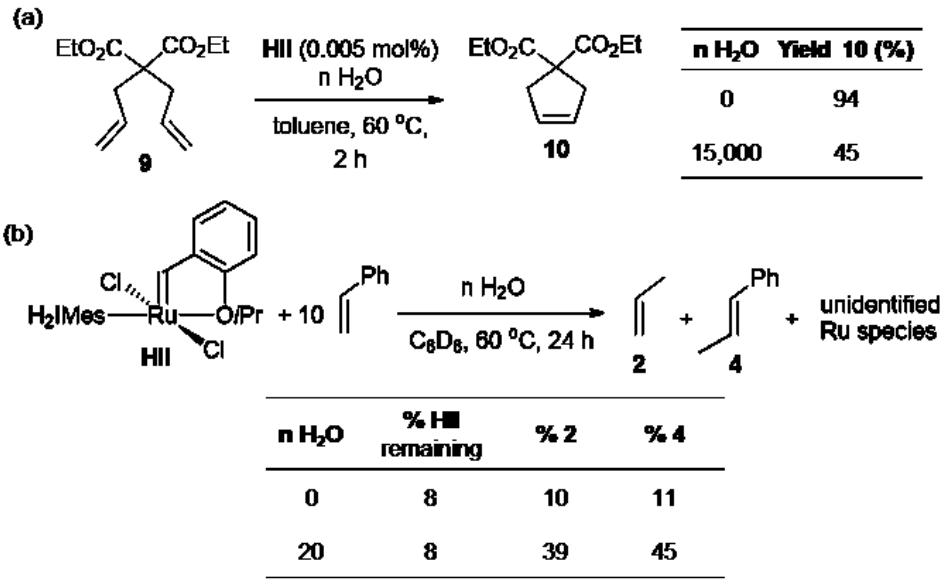

Figure 4.3 (a) Impact of H_2O on RCM of **9** using **HII** (0.005 mol%). (b) Impact of H_2O on the decomposition of **HII** in styrene metathesis. (Note identification of ca. 85% propenes from MCB decomposition). Data from M.Sc. thesis of Adrian Botti.

As noted above and in Chapter 1, propenes are a marker for decomposition of the MCB ring. The only prior experiments in which they were observed in such high amounts were styrene metathesis reactions in the presence of Bronsted base.[3,24] In the Bronsted base experiments, however, labelling and computational studied firmly identified propene elimination as due to deprotonation of the MCB at the β-hydrogen. The negligible basicity of H_2O precludes such a pathway. Thus, while the profoundly negative impact of water is clear, the mechanism of decomposition remained puzzling. While Botti speculated that water could increase the hydridic character of the β-hydrogen, this is ruled out by the unexpected acidity subsequently calculated for these protons.[3] A more plausible hypothesis may be water-mediated proton shuttling (Scheme 4.2), culminating in reductive elimination of the MCB hydrocarbons as propene.

Scheme 4.2 Potential role of water as a proton shuttle in the decomposition of the MCB **Ru-5**.

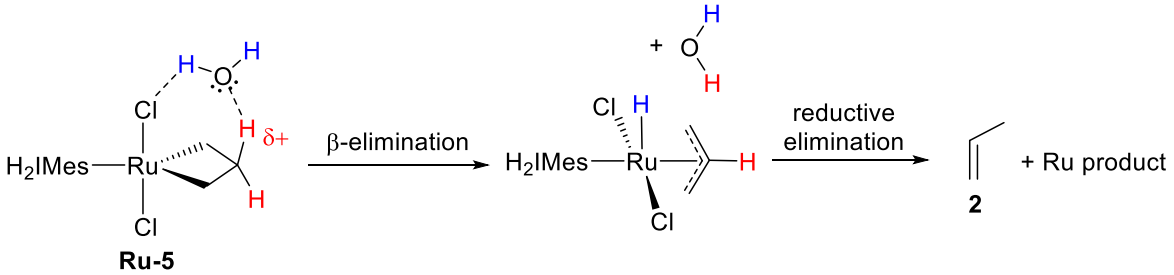

This Chapter describes additional studies of the impact of water on phosphine-free olefin metathesis catalysts. Mechanistic studies that offer initial insights into decomposition are described, and a strategy for scavenging water in standard organic media is presented.

4.3 Results and Discussion

4.3.1 Impact of Water on PCy_3-Free Catalysts at RT

A potentially important consideration in the studies described in the preceding Section is the impact of temperature. Use of higher temperatures is expected to increase productive metathesis events,[18,25] but could also supply the energy to access decomposition pathways. Establishing the impact of water at ambient temperatures was therefore a priority (and one that has particular prominence within the context of chemical biology).[6] As the major decomposition pathway for the Grubbs-class catalysts is now understood (see above), phosphine-free catalysts were chosen for study. These include the *o*-dianiline catalyst **DA**, **HII**, **nG,** and **nGC**, the structures of which are shown in Figures 4.4 and 4.5.

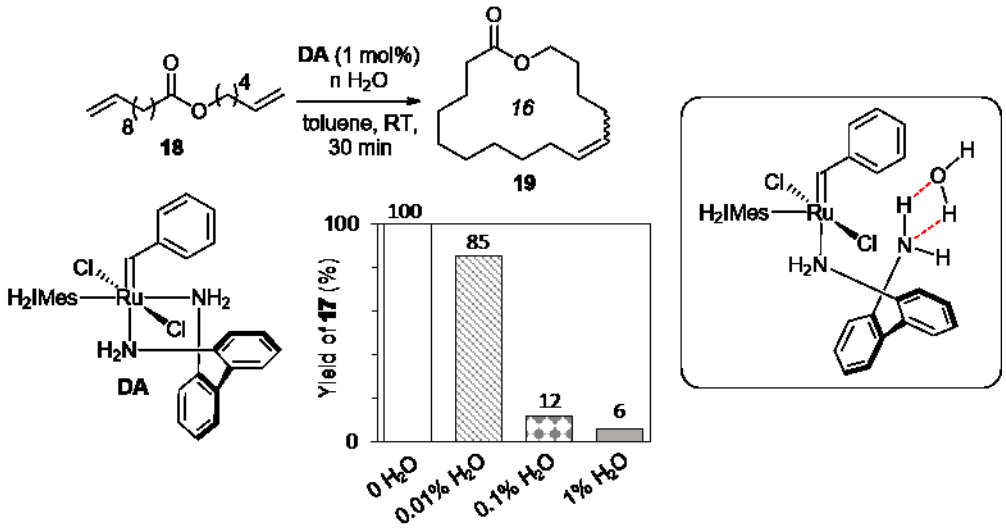

Figure 4.4 Impact of H_2O on the macrocyclization of prolactone **18** using 1 mol% **DA** catalyst at RT. Inset indicates H-bonding interaction between **DA** and H_2O.

The negative impact of H_2O on macrocyclic ring-closing metathesis (mRCM) was first observed in studies using **DA** (work carried out in collaboration with Daniel do Nascimento). Quantitative mRCM of diene **18** to form the 16-membered lactone **19** (a precursor to a leading synthetic musk)[26] was observed in dry toluene (Figure 4.4; RT, 1 mol% Ru). However, when even a relatively small amount of water was present (0.01% v/v), in situ mRCM yields dropped to 85%. Increasing the proportion of water tenfold (to 0.1% v/v) caused a much more dramatic drop, to ca. 10%. Further increases had a minor impact, unsurprisingly given that the solubility of H_2O in toluene is only 0.03% v/v.[22]

Clearly, added H_2O has a significant detrimental impact on the performance of **DA** even for this very easily cyclized substrate. The deleterious impact of water is consistent with the H-bonding capacity of the dianiline ligand, which greatly accelerates mRCM of dienes that bear polar groups (a discovery by Daniel do Nascimento).[27] H-Bonding between water and the *o*-dianiline NH_2 sites

is expected to promote coordination of H_2O (inset in Figure 4.4 above), and hence catalyst decomposition.

However, a broader catalyst screen (including **HII**, **nG**, and **nGC**; Figure 4.5) revealed significant negative impacts for all catalysts at 0.1% v/v water. H-Bonding via extended Cl···HOH interactions[28,29] is presumed (inset, Figure 4.5). Comparison of these results with those at 60 °C in Figure 4.3a suggests that the impact of water is lessened at elevated temperatures, presumably because metathesis is faster. Subsequent mechanistic experiments were conducted at RT, where the impact is greatest, and the lowest-energy decomposition pathway can be examined.

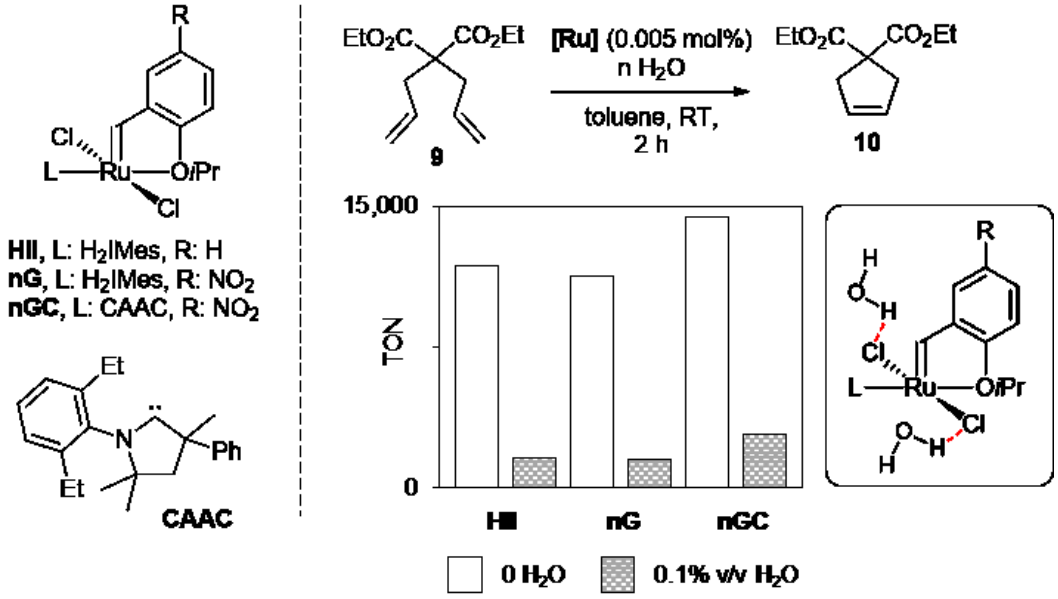

Figure 4.5 Impact of H_2O on the RCM of **9** using additional phosphine-free catalysts: **HII**, **nG** and **nGC.** Experiments performed via high-throughput screening at the Centre for Catalysis Research and Innovation (CCRI). Inset shows proposed H-bonding interactions with H_2O.

4.3.2 Reevaluating MCB Decomposition in the Presence of H_2O

The impact of temperature was examined more closely by carrying out styrene metathesis with **HII** at both 60 °C (i.e. the Botti conditions of Figure 4.3b) and 23 °C, and tracking the fate of the Ru=C*H*R alkylidene signal. The decay plots are shown in Figure 4.6. At 60 °C, decomposition of **HII** in the presence of 20 equiv H_2O was complete in 5 h (vs. 18 h under anhydrous conditions). Propenes were observed, as expected, although in lower proportions than reported by Botti (60%, vs. 84%), perhaps reflecting differences in the headspace volume, which would affect propene volatilization.

At RT, disappearance of **HII** is slower. More unexpectedly, *no* propenes were observed in the presence of water, despite liberation of 22% propenes in the water-free control reaction (Figure 4.6). That is, not only is there no evidence for β-elimination from the MCB at RT in the presence

of water, but water in fact appears to suppress this pathway. The latter is attributed to acceleration of an alternative decomposition pathway, rather than a protective effect. The disparity between the RT results and those at 60 °C points toward a temperature-dependent mechanism of decomposition. That is, MCB β-elimination appears to dominate at 60 °C, whereas at RT, an unknown pathway that precludes formation of propenes is operative.

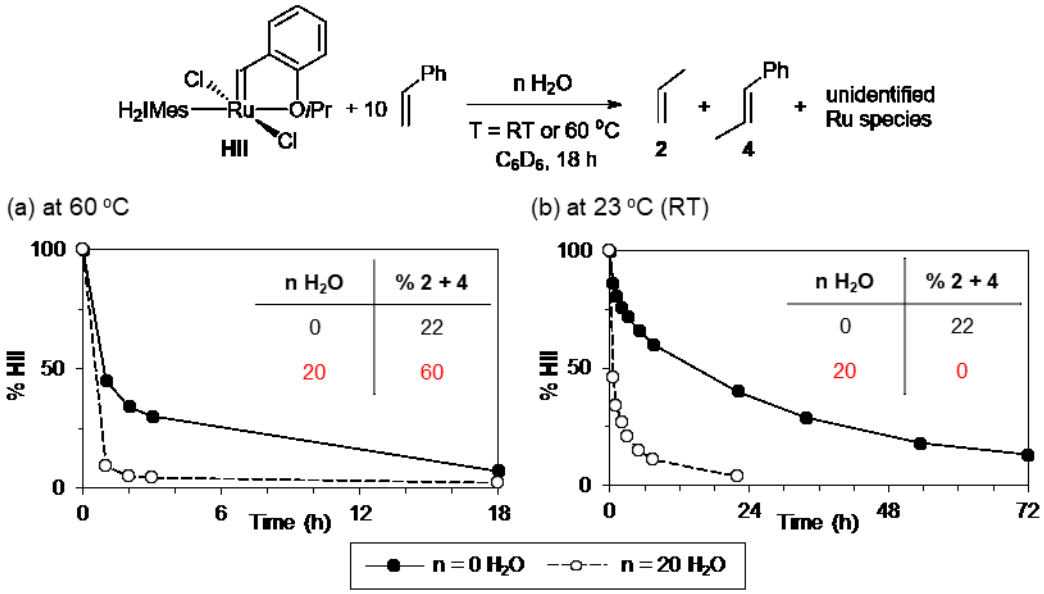

Figure 4.6 NMR-scale MCB decomposition experiments using **HII** (10 mol%). (a) at 60 °C. (b) at RT. Proportion of **2** and **4** determined following complete decomposition of **HII**.

Corroboration for the operation of an alternative decomposition pathway was provided by experiments with the state-of-the-art catalyst **nGC** (Figure 4.7). Present in **nGC** is a strongly σ-donating[30] cyclic alkyl amino carbene (CAAC) ligand. CAAC catalysts such as **nGC** have been shown to exhibit breakthrough TONs in challenging mRCM and ethenolysis reactions.[31-33] The sensitivity of **nGC** towards contaminants such as H_2O is therefore of significant interest.

In a preliminary screen, **nGC** was treated with styrene at 60 °C with and without added water (Figure 4.7). Decomposition was again faster in the presence of H_2O. ^1H NMR analysis after complete decomposition again reveals virtually zero propenes, with or without water. This indicates that MCB decomposition is not involved in either case, whereas Figure 4.6a above showed that at high temperatures, water did increase the proportion of propenes for **HII**. The fact that water accelerates decomposition of **nGC**, without yielding propenes, again suggests that water promotes a different decomposition pathway.

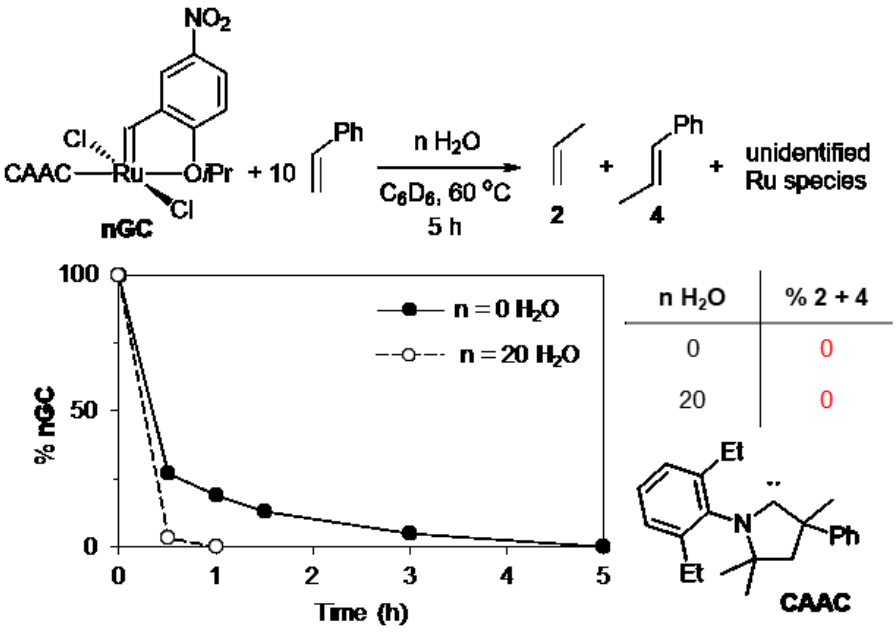

Figure 4.7 NMR-scale MCB decomposition experiments using **nGC** (10 mol%). No propenes were observed following complete decomposition of **nGC**.

Of other established decomposition pathways discussed in Chapter 1, nucleophilic attack at the methylidene carbon (Scheme 4.3a) is ruled out given the poor nucleophilicity of H_2O, and the absence of methanol, the presumed fate of the methylidene as ligand. Loss of the benzylidene as benzaldehyde, perhaps by nucleophilic attack, was reported in a mass spectrometric study by Lee and co-workers.[23] Thus, decomposition of cationic Ru benzylidene complex **Ru-26** by water in the presence of acetonitrile was described (Scheme 4.3b). While the mechanistic details were not probed, the cationic nature of the complex may activate the benzylidene ligand toward attack. (Of note, however, electron-deficient derivatives of **HII** more typically undergo Buchner expansion via insertion of the benzylidene carbon into a mesityl ring of the NHC).[34] In any case, no benzaldehyde was observed in the present work. A further, potentially more plausible pathway is presented next.

Scheme 4.3 (a) Potential nucleophilic attack at methylidene by H_2O, generating methanol (b) Decomposition of cationic Ru complex **Ru-26** by water, observed by Lee.[23]

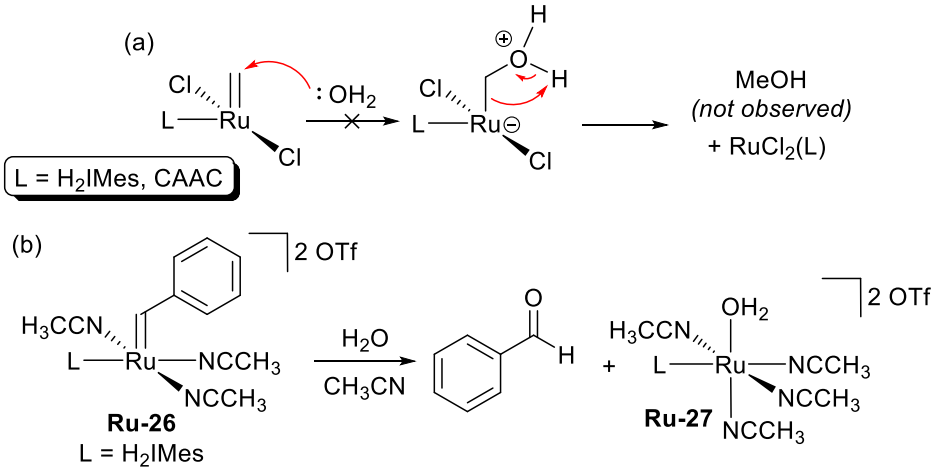

4.3.3 Potential Role for H_2O in Bimolecular Coupling

Considered in this Section is the possibility that water could promote bimolecular coupling (BMC). The importance of BMC in decomposition of Ru-NHC catalysts was recently demonstrated by Gwen Bailey of this research group (Chapter 1).[2] BMC was proposed to account for the balance of catalyst that does not decompose via β-elimination, and indeed up to ca. 65% ethylene was observed in careful quantitation experiments.[2] For the water experiments above, bimolecular reactions are favoured by the high catalyst concentrations (20 mM Ru) required to monitor decomposition by ^{1}H NMR analysis. As water is shown to accelerate decomposition, regardless of temperature, for all catalysts, one intriguing possibility is that it plays a role in promoting BMC.

The reduced proportion of propenes observed in the water RT experiment with **HII** suggests that decomposition occurs *before* MCB formation. As the pre-catalyst itself is stable to water (as shown in the M.Sc. thesis of Adrian Botti), the four-coordinate benzylidene **Ru-2** or methylidene **Ru-4** intermediates are most likely the vulnerable species. Bimolecular coupling could be enabled by Ru-OH_2 adducts of **Ru-2** or **Ru-4**. Binding of H_2O to these catalysts can clearly occur, as demonstrated in the donor-accelerated decomposition of the methylidene resting-state species **GIIm**.[1] Similarly, addition of H_2O to the four-coordinate Piers catalyst **PII** (Scheme 4.4) caused a shift in the location of the alkylidene ^{1}H NMR signal, which was attributed to reversible binding of H_2O at Ru.[35] (As specific chemical shifts were not reported, however, these experiments should be revisited).

Scheme 4.4 Coordination of H_2O to the second-generation piers catalyst **PII**.

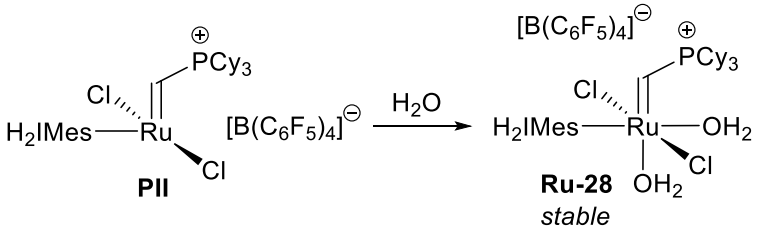

Formation of H_2O adducts of **Ru-2** or **Ru-4** could potentially enable homocoupling with the parent alkylidene complexes, or H-bonding to another Ru-aqua species **Ru-28** (Scheme 4.5). The potential for water to "bridge" two **Ru-28** molecules has precedents in Ru-catalyzed water oxidation chemistry, in which dimeric Ru-OH_2 intermediates have recently been identified.[36-38] Water could thus promote BMC by bringing two equiv of **Ru-2** and/or **Ru-4** in close proximity.

Scheme 4.5 Potential roles for Ru-aqua species **Ru-28** in water-mediated bimolecular decomposition. (a) H-bonding of **Ru-28** with **Ru-2**/**Ru-4**. (b) Dimerization of **Ru-28**.

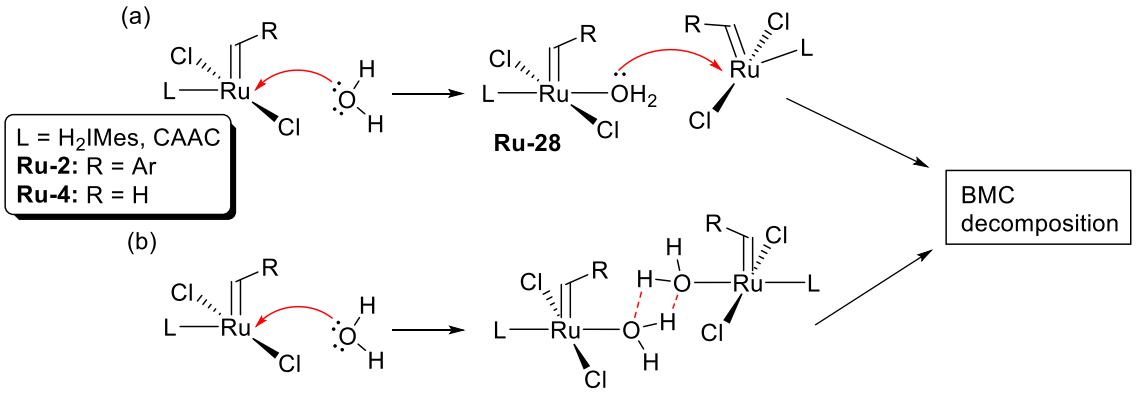

A related possibility involves aquation to generate cationic **Ru-29** (Scheme 4.6). Such complexes may then participate in H-bonding to other aqua complexes, setting the stage for BMC as above. Substitution of chloride ligands by H_2O is commonplace in ruthenium chemistry.[39] However, it is unclear how readily this can occur with 14-electron **Ru-2** or **Ru-4** intermediates (which might be expected to prefer lone pair donation from H_2O). To test this argument, bimolecular coupling was conducted with and without H_2O.

Scheme 4.6 Potential role for aqua complex **Ru-29** in water-mediated bimolecular coupling.

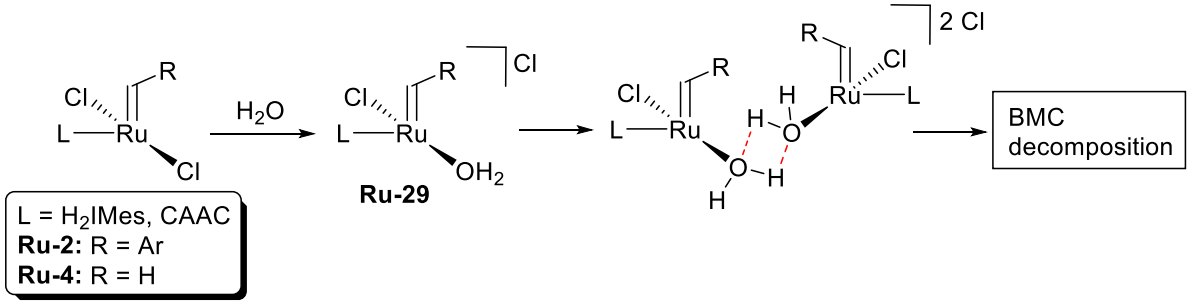

To assess the impact of H_2O on bimolecular coupling, a catalyst system is required for which BMC is the *only* (or major) decomposition pathway. Few catalyst systems meet this criterion. In Bailey's BMC study, transiently-stabilized phosphine-free methylidene complex **Ru-6** was used (Scheme 4.7a).[2] However, while the major decomposition for **Ru-6** was indeed BMC, the instability of this methylidene species led to rapid decomposition on warming above –10 °C. Low temperatures are problematic for experiments with water, as freezing of H_2O may impede mass transfer (already a problem for water in organic solvents such as CD_2Cl_2), or even inhibit reaction.

Scheme 4.7 BMC reactions studied using second-generation catalysts. (a) Of methylidene **Ru-6**, releasing ethylene.[2] (b) With **GIII**, releasing stilbene **20**.[2] (c) With **GII** and CuCl (but without internal standard: stilbene was reportedly a major product, but was not quantified).[33]

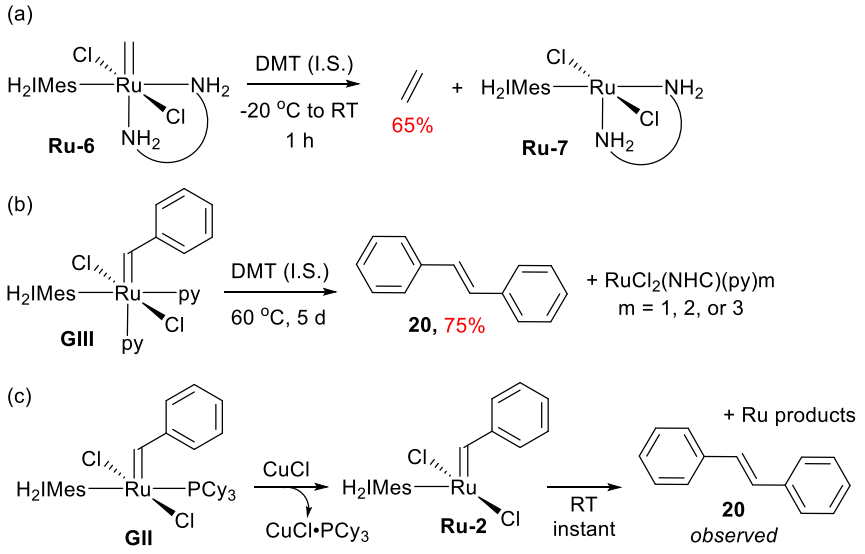

However, BMC has recently been shown to be unexpectedly facile even for benzylidene complexes. While Bailey and Higman reported that coupling of the **GIII** pre-catalyst liberated stilbene (74% yield) only over 5 days at 60 °C (Scheme 4.7b),[2] this is now known to be an artifact of low PCy_3 lability. In a 2019 report, do Nascimento showed that abstraction of the PCy_3 ligand from **GII** occurs within minutes on stirring with CuCl at 40 °C. Rapid BMC ensues, with liberation of stilbene (Scheme 4.7c).[33]

While BMC of **GII** in the presence of CuCl is more rapid than in the thermolysis of **GIII**, the potential for reaction of CuCl with water complicates the reaction. For this reason, the impact of water on BMC was undertaken via a thermolysis experiment, but using the more labile pyridine-functionalized catalyst **GIII** in place of **GII**. Such an experiment was previously carried out by Bailey.[2] Noted in her report, however, was considerable variation in the reaction rates of **GIII**, which is generated as a mixture of mono- and bis-py species (quantitation of which is severely hampered by the fact that the mixture gives a single alkylidene peak in the ^1H NMR spectrum). To ensure directly comparable conditions in the present work, the thermolysis experiment was

repeated using a common catalyst stock solution, which was divided into two portions, to one of which water was added.

As shown in Figure 4.8, heating **GIII** at 60 °C with 100 equiv H_2O caused complete loss of the Ru=C*H*Ph signal within 24 h. The yield of the stilbene coupling product reached ca. 70%, as judged by ^{1}H NMR integration relative to internal standard. In the water-free control experiment, only 55% stilbene was released (cf. 74% in the Bailey report).[2] The observation of 15% more stilbene **20** in the presence of water suggests that water does indeed promote BMC. However, the mass balance – that is, 30% of the starting catalyst charge is unaccounted for – indicates an additional pathway. One possibility, as demonstrated in Chapter 3 of this thesis, is that dimerization may be induced by decomposed Ru species without releasing a coupled olefinic product. This could account for reduced stilbene yields, particularly at elevated temperatures.

Thus, while these preliminary results suggest that H_2O may indeed promote dimerization of Ru intermediates, additional experiments at room temperature are required. Assessing the impact of added water on the rates and yields of stilbene release from catalysts that decompose via BMC at ambient temperatures would provide more information. This strategy is discussed under Future Work in Chapter 5.

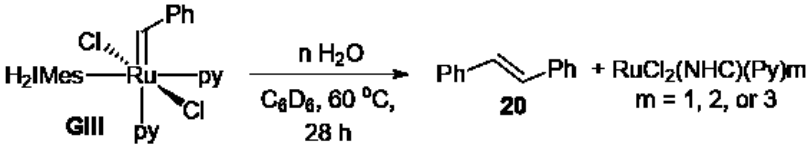

n H_2O	Time (h)	% 18
0	28	55
100	24	70

Figure 4.8 Impact of H_2O on bimolecular elimination of stilbene from the benzylidene catalyst **GIII**.

4.3.3 Strategies for Scavenging H_2O

While the primary goal in this work was to advance understanding of how water mediates decomposition of Ru metathesis catalysts, and thereby contribute design parameters for water-resistant catalysts, there is short-term value to water-scavenging protocols. These are clearly relevant only where water is a contaminant, rather than a solvent medium. Sequestering water during metathesis could improve the reliability of current catalysts. This approach could be particularly advantageous for the high-performing catalysts such as **DA**, which excels in the macrocyclization of polar dienes (see Figure 4.4),[27] but is highly sensitive to water.

Rigorous drying to remove water is time-consuming and can be costly.[40] Drying agents can offer greater convenience, and are commonly recyclable. Polyphenol resins were examined as water

scavengers in light of findings by Gwen Bailey (in collaboration with Prof. Eduardo dos Santos, Brazil) that established the utility of poly(4-vinylphenol-co-methyl methacrylate) (PVP-MMA) in acrylate metathesis.[22] As shown in Figure 4.9, PVP-MMA proved effective as a sacrificial proton source to quench highly basic phosphonium enolates generated by attack of PCy_3 on the acrylate olefin.[22] Use of water in place of the resin caused yields of **23** to drop further, probably because of hydroxide formation (see Chapter 3). However, use of the resin along with water restored metathesis yields. The phenolic resin may thus function not only as a sacrificial proton source, but also as a means of binding polar impurities (including water) present in the reaction medium.

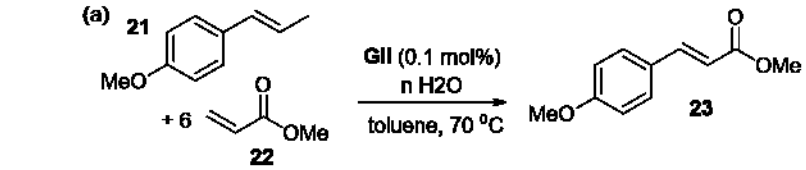

Entry	H_2O (ppm)	n PVP-MMA (equiv vs Ru)	Yield 21 (%)
1	-	-	55
2	300	-	23
3	-	100	95
4	300	100	82

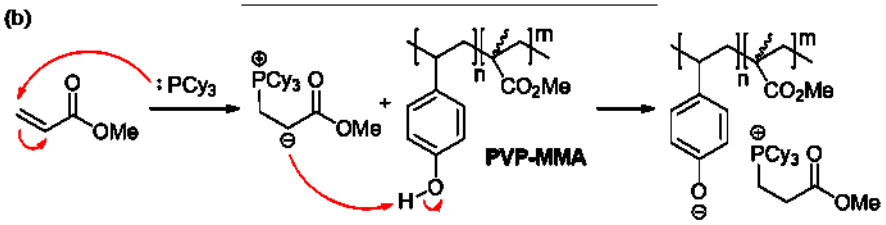

Figure 4.9 (a) Impact of PVP-MMA resin in the CM of **21** and **22** with added water. (b) Mechanism for enolate quenching by PVP-MMA resin.

The capacity of the resin to sequester water was therefore tested by adding PVP-MMA to mRCM reactions in the presence or absence of water (Figure 4.10). The catalysts used were **DA** and **nG**. Addition of 200 equiv vs Ru of H_2O (that is, only 0.02% v/v water) caused a significant drop in mRCM yield, as expected. The **DA** catalyst was more affected by H_2O than **nG**, consistent with H-bonding to the dianiline NH_2 groups, as described in Section 4.3.1 above. Addition of 50 equiv resin vs Ru (i.e. 50 repeat units) improved the yield for both **DA** and **nG**. Most notably, the performance of **DA** was almost completely restored (vs. only 10% increase for **nG**), suggesting that the phenolic resin outcompetes the dianiline ligand for H-bonding to water. (It should be noted, however, that the loading of the **DA** catalyst should be reduced, given that the control reaction reaches 100%, and some catalyst decomposition may therefore be masked).

Also of note, increasing the proportion of the resin to 200 equiv per Ru improved the performance of **nG**, but was detrimental to the performance of **DA** (Figure 4.10). For **nG**, it presumably reflects

uptake of all the H_2O by the resin. For **DA**, however, H-bonding of the precatalyst to the resin may cause catalyst deactivation.

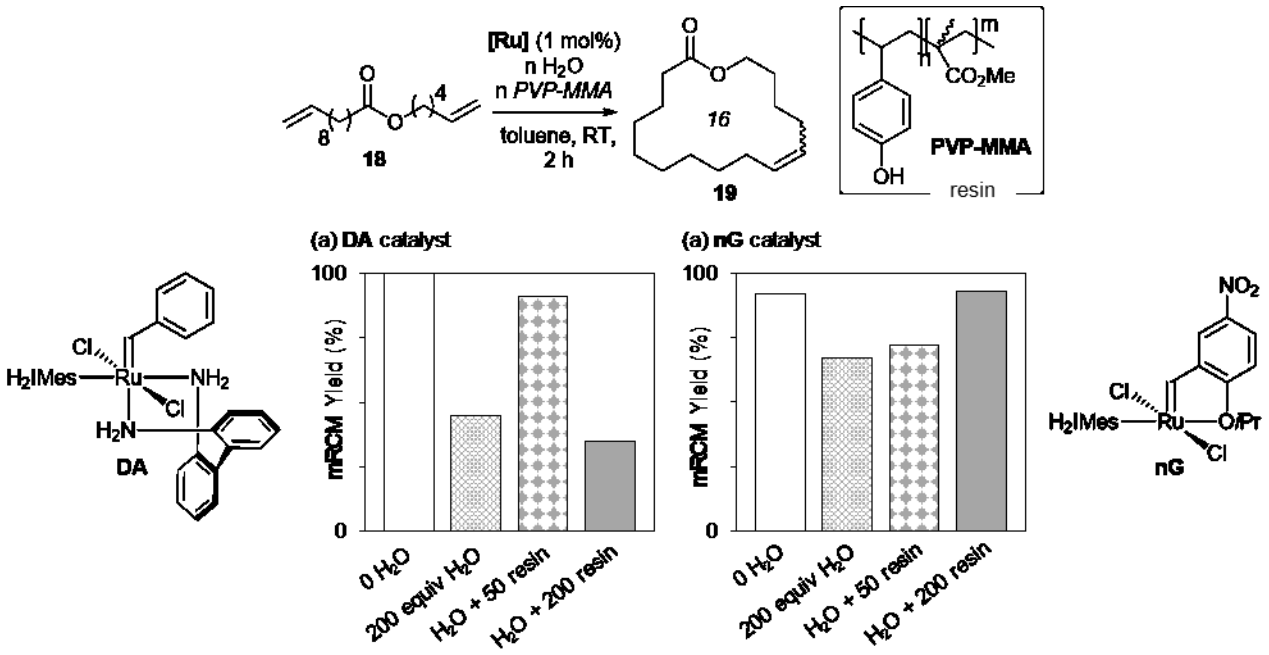

Figure 4.10 Protective effect of PVP-MMA resin on mRCM of **18** when water is present.

Given the inhibiting effect of excess PVP-MMA resin on metathesis with **DA**, sequestration of water by molecular phenols was also investigated. Phenols such as *p*-cresol have been shown to improve catalyst performance of phosphine-stabilized catalysts **GI** and **GII**.[29] The positive impact of phenol has been attributed to stabilization of the four-coordinate active species **Ru-2** or **Ru-4** by phenol.[29] Alternatively, a phenol–PCy_3 reaction could compete with re-uptake of PCy_3 by **Ru-4**, thus inhibiting formation of the deactivated resting-state methylidene species **GIm** and **GIIm**. The impact of phenol on PCy_3-free complexes, such as **DA** and **nG** is unknown.

Addition of *p*-cresol during mRCM did indeed increase yields of **19** in all cases (Figure 4.11), but the improvement is less drastic than with the phenolic resin. Of note, use of 200 equiv phenol (i.e. 1:1 vs. added H_2O) offered no improvement beyond that achieved using 50 equiv. This contrasts with the results seen above with the PVP-MMA resin, and suggests that the multivalent effect is critical to efficient H_2O sequestration.

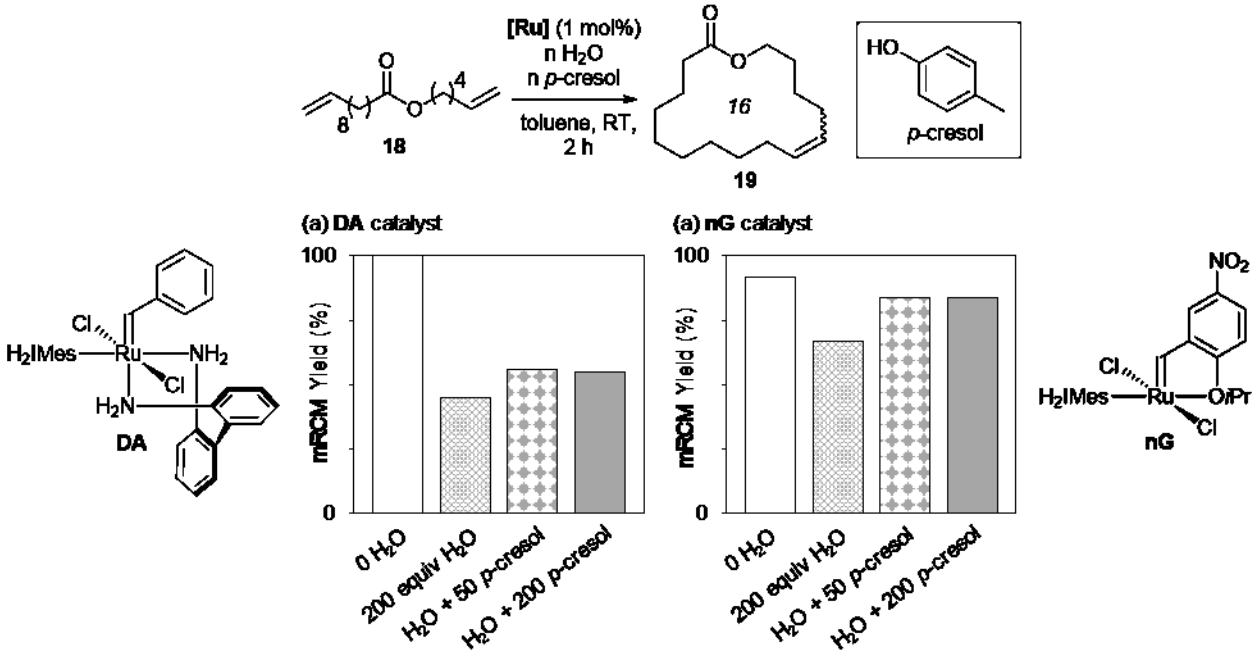

Figure 4.11 Impact of *p*-Cresol on mRCM yields for reactions in the presence of H_2O.

4.4 Conclusion

The foregoing demonstrates the deleterious impact of trace H_2O in ruthenium-catalyzed olefin metathesis. It was found that the negative effects of H_2O are more profound at ambient temperatures. While water has been previously shown to promote MCB decomposition at high temperature, a mechanistically different pathway appears operative at RT. Thus, while water accelerated decomposition of **HII** at RT, the propene markers for metallacyclobutane β-elimination are completely absent. Water-mediated bimolecular coupling is proposed as an alternative. Preliminary evidence supports the hypothesis that water promotes BMC decomposition, but this should be corroborated by further experiments under RT conditions. Finally, water can be sequestered via H-bonding to the phenol resin PVP-MMA, which was shown to restore catalyst activity in macrocyclization reactions.

These findings indicate that the mechanism of H_2O-induced decomposition is more complex than previously suspected. Nevertheless, these findings suggest that major avenues of investigation that are tackling the problem of intrinsic catalyst decomposition may likewise be relevant to the development of water-tolerant catalysts.

4.5 Experimental Procedures

4.5.1 General Procedures

General procedures conformed to those outlined in Section 3.5.1, with the following exceptions: reagents poly(4-vinylphenol-co-methylmethacrylate) resin (PVP-MMA, Sigma-Aldrich), p-

Cresol (99%, Sigma-Aldrich), and standards 1,3,5-trimethoxybenzene (TMB, Sigma-Aldrich), dimethyl terephthalate (DMT, >99%) were used as received. Styrene (99%, Sigma Aldrich) and deionized water were degassed by five consecutive freeze-pump-thaw cycles and stored under N_2 in the glovebox. Catalysts **nG** and **nGC** were graciously donated by Apeiron.

The following materials were prepared according to literature procedures: prolactone **18**,[41] the second-generation Grubbs catalyst **GII**,[42] the second-generation Hoveyda catalyst **HII**,[43] and the *o*-dianiline catalyst **DA**.[27]

High-through put experiments were run in a 96-well aluminum plate with stainless steel cover, sealed with a PFA sheet and two rubber sheets. Individual reactions were run in 8x40 mm glass shell vials (1 mL total volume), fitted with parylene-coated stir bars. Catalyst, substrate, and additive stock solutions were dispensed using an Unchained Labs CM3 sample processor. Injection of the catalysts (start points) and quenching agent (end points) were tracked through a software protocol designed to inject the quenching agent at the stipulated time-point. Yields were determined using the CCRI GC-FID chromatograph (Agilent 6850, HP-1 column).

4.5.2 Representative Procedure for the RCM of DDM with GII (High-Throughput Studies)

(a) A stock solution was prepared of DDM (1.2 mL, 4.9 mmol), dodecane (1.13 mL, 4.9 mmol) as internal standard in C_7H_8 (19.85 mL total volume, 250 mM in both DDM and dodecane). A 0.16 mM stock solution of quenching agent KTp (0.4 mL of a 10 mg/mL solution diluted to 10 mL) was made up in THF. A 0.078 mM stock solution of **GII** (1 mL of a 10 mg/15 mL solution, diluted to 10 mL C_7H_8) was prepared. Reaction components were added to the plate in the following order: substrate/internal standard stock, additive, then catalyst. Before addition of catalyst, the plate was sealed (see above) to prevent evaporation of solvent. Reactions were started and quenched via automated injection of catalyst and KTp after exactly 2 hours.

Amount dispensed from each stock for a given well: 0.20 mL of substrate/internal standard solution, 0.27 mL C_7H_8, and 32 µL of catalyst stock.

Final conditions: 100 mM DDM, 100 mM dodecane, 0.005 mol% catalyst, 500 µL reaction volume in C_7H_8.

(b) With added H_2O: As above, with the following modification: H_2O (4.8 µL, 0.26 mmol, 100,000 equiv) was added by hand (via micropipette) prior to sealing the plate, and adding catalyst.

4.5.3 Representative Procedure for the Macrocyclization of Prolactone

(a) A mixture of prolactone (11.9 µL, 0.05 mmol) and dodecane (11.4 µL, 0.05 mmol, 1 equiv; internal standard for GC analysis) was diluted in 9.95 mL C_7H_8 to give a final concentration 5 mM prolactone. An aliquot was removed for GC-FID analysis to establish the starting ratio of prolactone to dodecane. **DA** (35.8 µL of a stock solution of 10.5 mg in 1.0 mL C_7H_8; 0.5 µmol, 1 1 mol%) was added to the stirred solution. Aliquots were removed periodically, quenched with KTp in THF (10.0 mg/mL; 10 equiv vs. starting Ru), and analyzed by GC-FID.

(b) With added H_2O: As above, with the following modification: H_2O (9.9 µL, 0.55 mmol, 1100 equiv) was added prior to adding the catalyst.

(c) With added PVP-MMA resin: As above, with the following modification: PVP-MMA resin (22 mg, 0.10 mmol, 200 equiv of phenol repeating unit)

4.5.4 Representative Procedure for the Quantification of Propenes Formed During Styrene Metathesis

(a) In a 4 mL vial, green **HII** (15.1 mg, 0.024 mmol) and anthracene (2.4 mg, 0.013 mmol, 0.5 equiv; internal standard) were dissolved in 1.2 mL C_6D_6 to give a 20 mM solution in **HII**. 550 µL was transferred to a J-Young NMR tube, and a ^{1}H NMR spectrum recorded to establish a starting ratio of **HII** to anthracene. The tube was returned to the glovebox, and styrene (12.5 µL, 0.11 mmol, 10 equiv) was added. The resulting solution was mixed in the NMR tube at RT, and ^{1}H NMR spectra were recorded periodically to track the decomposition of **HII** and yield of propenes over time.

(b) With added H_2O: As above, with the following modification: H_2O (4 µL, 0.22 mmol, 20 equiv) was added prior to addition of styrene.

Key ^{1}H NMR data for propenyl products:

Propene **2**: ^{1}H NMR (C_6D_6, 300 MHz): δ 5.72 (m, 1H, =C*H*CH$_3$), 5.01 (dm, $^3J_{HH}$ = 17 Hz, 1H, =CH$_a$*H*$_b$; overlaps with =C*H*$_a$H$_b$), 4.95 (dm, $^3J_{HH}$ = 10 Hz, 1H, =C*H*$_a$H$_b$; overlaps with =CH$_a$*H*$_b$), 1.55 (dt, $^3J_{HH}$ = 6.4 Hz, $^3J_{HH}$ = 1.5 Hz, 3H, =CHC*H*$_3$).

β-Methylstyrene **4**: ^{1}H NMR (C_6D_6, 300 MHz): δ 6.29 dq, $^3J_{HH}$ = 15.8 Hz, $^4J_{HH}$ = 2.0 Hz, 1H, Ph*H*C=), 6.03 (dq, $^3J_{HH}$ = 15.8 Hz, $^3J_{HH}$ = 6.7 Hz, 1H, =C*H*CH$_2$Ph), 1.65 (dd, $^3J_{HH}$ = 7 Hz, $^4J_{HH}$ = 2.0 Hz, 3H, =CHC*H*$_3$). The observed shifts are in good agreement with reported values.

4.5.5 Representative Procedure for the Thermolysis of GIII

(a) In a 4 mL vial, green **GIII** (17.5 mg, 0.024 mmol) and anthracene (2.4 mg, 0.013 mmol, 0.5 equiv: internal standard) were dissolved in 1.2 mL C_6D_6 to give a 20 mM solution in **GIII**. 550 µL was transferred to a J-Young NMR tube, and a ^{1}H NMR spectrum recorded to establish a starting ratio of **GIII** to anthracene. The sample was then placed in a pre-heated 60 ^{o}C oil bath, and a timer started. The solution was mixed every 5 minutes for 2 h, and then once every hour. ^{1}H NMR spectra were recorded periodically to track the decomposition of **GIII** and yield of stilbene over time.

(b) With added water: As above, with the following modification: H_2O (20 µL, 1.1 mmol, 100 equiv) was added prior to placing in oil bath.

4.6 References

(1) McClennan, W. L.; Rufh, S. A.; Lummiss, J. A. M.; Fogg, D. E., A General Decomposition Pathway for Phosphine-Stabilized Metathesis Catalysts: Lewis Donors Accelerate Methylidene Abstraction. *J. Am. Chem. Soc.* **2016**, *138*, 14668−14677.

(2) Bailey, G. A.; Foscato, M.; Higman, C. S.; Day, C. S.; Jensen, V. R.; Fogg, D. E., Bimolecular Coupling as a Vector for Decomposition of Fast-Initiating Olefin Metathesis Catalysts. *J. Am. Chem. Soc.* **2018**, *140*, 6931–6944.

(3) Bailey, G. A.; Lummiss, J. A. M.; Foscato, M.; Occhipinti, G.; McDonald, R.; Jensen, V. R.; Fogg, D. E., Decomposition of Olefin Metathesis Catalysts by Brønsted Base: Metallacyclobutane Deprotonation as a Primary Deactivating Event. *J. Am. Chem. Soc.* **2017**, *139*, 16446–16449.

(4) Henderson, R. K.; Jiménez-González, C.; Constable, D. J. C.; Alston, S. R.; Inglis, G. G. A.; Fisher, G.; Sherwood, J.; Binks, S. P.; Curzons, A. D., Expanding GSK's Solvent Selection Guide – Embedding Sustainability Into Solvent Selection Starting at Medicinal Chemistry. *Green Chem.* **2011**, *13*, 854–862.

(5) Lipshutz, B. H., Ghorai, S., Olefin Metathesis in Water and Aqueous Media. In *Olefin Metathesis – Theory and Practice*, Grela, K., Ed. 2014; pp 515-521.

(6) Binder, J. B.; Raines, R. T., Olefin Metathesis for Chemical Biology. *Curr. Opin. Chem. Biol.* **2008**, *12*, 767–773.

(7) Davis, K. J.; Sinou, D., Ring Closing Metathesis in Water With or Without Surfactants in the Presence of RuCl2(PPh3)2(CHPh). *J. Mol. Catal. A: Chem.* **2002**, *177*, 173–178.

(8) Connon, S. J.; Rivard, M.; Zaja, M.; Blechert, S., Ru-NHC Practical olefin metathesis in protic media under an air atmosphere. *Adv. Synth. Catal.* **2003**, *345*, 572–575.

(9) Lynn, D. M.; Kanaoka, S.; Grubbs, R. H., Living Ring-Opening Metathesis Polymerization in Aqueous Media Catalyzed by Well-Defined Ruthenium Carbene Complexes. *J. Am. Chem. Soc.* **1996**, *118*, 784–790.

(10) Gulajski, L.; Sledz, P.; Lupa, A.; Grela, K., Olefin Metathesis in Water using Acoustic Emulsification. *Green Chem.* **2008**, *10*, 271–274.

(11) Burtscher, D.; Grela, K., Aqueous Olefin Metathesis. *Angew. Chem., Int. Ed.* **2009**, *48*, 442–454.

(12) Gallivan, J. P.; Jordan, J. P.; Grubbs, R. H., A Neutral, Water-Soluble Olefin Metathesis Catalyst Based on an N-Heterocyclic Carbene Ligand. *Tetrahedron Lett.* **2005**, *46*, 2577–2580.

(13) Hong, S. H.; Grubbs, R. H., Highly Active Water-Soluble Olefin Metathesis Catalyst. *J. Am. Chem. Soc.* **2006**, *128*, 3508–3509.

(14) Jordan, J. P.; Grubbs, R. H., Small-Molecule N-Heterocyclic-Carbene-Containing Olefin-Metathesis Catalysts for use in Water. *Angew. Chem., Int. Ed.* **2007**, *46*, 5152–5155.

(15) Wang, Z. J.; Jackson, W. R.; Robinson, A. J., A Simple and Practical Preparation of an Efficient Water Soluble Olefin Metathesis Catalyst. *Green Chem.* **2015**, *17*, 3407–3414.

(16) Michrowska, A.; Gulajski, L.; Kaczmarska, Z.; Mennecke, K.; Kirschning, A.; Grela, K., A Green Catalyst for Green Chem.: Synthesis and Application of an Olefin Metathesis Catalyst Bearing a Quaternary Ammonium Group. *Green Chem.* **2006**, *8*, 685–688.

(17) Kadyrov, R., Low Catalyst Loading in Ring-Closing Metathesis Reactions. *Chem. – Eur. J.* **2013**, *19*, 1002–1012.

(18) van Lierop, B. J.; Lummiss, J. A. M.; Fogg, D. E., Ring-Closing Metathesis. In *Olefin Metathesis-Theory and Practice*, Grela, K., Ed. Wiley: Hoboken, NJ, 2014; pp 85–152.

(19) Compain, P., Olefin Metathesis of Amine-Containing Systems: Beyond the Current Consensus. *Adv. Synth. Catal.* **2007**, *349*, 1829–1846.

(20) Camm, K. D.; Fogg, D. E., From Drug Cocktails to Tissue Engineering: Synthesis of ROMP Polymers for Biological Applications. In *NATO Sci. Ser. II*, Imamoglu, Y.; Dragutan, V., Eds. Springer Verlag: Berlin, 2007; Vol. 243, pp 285–303.

(21) Guidone, S.; Songis, O.; Nahra, F.; Cazin, C. S. J., Conducting Olefin Metathesis Reactions in Air: Breaking the Paradigm. *ACS Catal.* **2015**, *5*, 2697–2701.

(22) Santos, A. G.; Bailey, G. A.; dos Santos, E. N.; Fogg, D. E., Overcoming Catalyst Decomposition in Acrylate Metathesis: Poly-phenol Resins as Enabling Agents for Phosphine-Stabilized Metathe-sis Catalysts. *ACS Catal.* **2017**, *7*, 3181−3189.

(23) Kim, M.; Eum, M. S.; Jin, M. Y.; Jun, K. W.; Lee, C. W.; Kuen, K. A.; Kim, C. H.; Chin, C. S., Reactions of Ruthenium Benzylidenes with H2O to give Benzaldehyde and (Aqua)Ruthenium Complex. *J. Organomet. Chem.* **2004**, *689*, 3535–3540.

(24) Ireland, B. J.; Dobigny, B. T.; Fogg, D. E., Decomposition of a Phosphine-Free Metathesis Catalyst by Amines and Other Nitrogen Bases: Metallacyclobutane Deprotonation as a Major Deactivation Pathway. *ACS Catal.* **2015**, *5*, 4690−4698.

(25) Monfette, S.; Eyholzer, M.; Roberge, D. M.; Fogg, D. E., Getting RCM Off the Bench: Reaction-Reactor Matching Transforms Metathesis Efficiency in the Assembly of Large Rings. *Chem. – Eur. J.* **2010**, *16*, 11720–11725.

(26) Kraft, P., Aroma Chemicals IV: Musks. In *Chemistry and Technology of Flavors and Fragrances*, Rowe, D. J., Ed. CRC Press: Boca Raton, 2005; pp 143–168.

(27) Higman, C. S.; Nascimento, D.; Ireland, B. J.; Audorsch, S.; Bailey, G. A.; Fogg, D. E., Chelate-Assisted Ring-Closing Metathesis: A Strategy for Accelerating Macrocyclization at Ambient Temperatures. *J. Am. Chem. Soc.* **2018**, *140*, 1604−1607.

(28) Gavette, J. V.; Klug, C. M.; Zakharov, L. N.; Shores, M. P.; Haley, M. M.; Johnson, D. W., Intramolecular N–H···Cl Hydrogen Bonds in the Outer Coordination Sphere of a Bipyridyl Bisurea-Based Ligand Stabilize a Tetrahedral FeLCl2 Complex. *Chem. Commun.* **2014**, *50*, 7173–7175.

(29) Forman, G. S.; McConnell, A. E.; Tooze, R. P.; van Rensburg, W. J.; Meyer, W. H.; Kirk, M. M.; Dwyer, C. L.; Serfontein, D. W., A Convenient System for Improving the Efficiency of First-Generation Ruthenium Olefin Metathesis Catalysts. *Organometallics* **2005**, *24*, 4528–4542.

(30) Soleilhavoup, M.; Bertrand, G., Cyclic (Alkyl)(Amino)Carbenes (CAACs): Stable Carbenes on the Rise. *Acc. Chem. Res.* **2015**, *48*, 256–266.

(31) Gawin, R.; Tracz, A.; Chwalba, M.; Kozakiewicz, A.; Trzaskowski, B.; Skowerski, K., Cyclic Alkyl Amino Ruthenium Complexes—Efficient Catalysts for Macrocyclization and Acrylonitrile Cross Metathesis. *ACS Catal.* **2017**, *7*, 5443–5449.

(32) Marx, V. M.; Sullivan, A. H.; Melaimi, M.; Virgil, S. C.; Keitz, B. K.; Weinberger, D. S.; Bertrand, G.; Grubbs, R. H., Cyclic Alkyl Amino Carbene (CAAC) Ruthenium Complexes as Remarkably Active Catalysts for Ethenolysis. *Angew. Chem., Int. Ed.* **2015**, *54*, 1919–1923.

(33) Nascimento, D. L.; Gawin, A.; Gawin, R.; Guńka, P. A.; Zachara, J.; Skowerski, K.; Fogg, D. E., A Highly Reactive Ruthenium-Indenylidene Catalyst for Olefin Metathesis. *J. Am. Chem. Soc.* **2019**, *141*, 10626–10631.

(34) (a) Griffiths, J. R.; Hofman, E. J.; Keister, J. B.; Diver, S. T., Kinetics and Mechanism of Isocyanide-Promoted Carbene Insertion into the Aryl Substituent of an N-Heterocyclic Carbene Ligand in Ruthenium-Based Metathesis Catalysts. *Organometallics* **2017**, *36*, 3043–3052. (b) Galan, B. R.; Pitak, M.; Gembicky, M.; Keister, J. B.; Diver, S. T., Ligand-Promoted Carbene Insertion into the Aryl Substituent of an N-Heterocyclic Carbene Ligand in Ruthenium-Based Metathesis Catalysts. *J. Am. Chem. Soc.* **2009**, *131*, 6822–6832. (c) Galan, B. R.; Gembicky, M.; Dominiak, P. M.; Keister, J. B.; Diver, S. T., Carbon Monoxide-Promoted Carbene Insertion in the Aryl Substituent of an N-Heterocyclic Carbene Ligand: Buchner Reaction in a Ruthenium Carbene Complex. *J. Am. Chem. Soc.* **2005**, *127*, 15702–15703.

(35) Romero, P. E.; Piers, W. E.; McDonald, R., Rapidly Initiating Ruthenium Olefin-Metathesis Catalysts. *Angew. Chem., Int. Ed.* **2004**, *43*, 6161–6165.

(36) Gersten, S. W.; Samuels, G. J.; Meyer, T. J., Catalytic Oxidation of Water by an Oxo-Bridged Ruthenium Dimer. *J. Am. Chem. Soc.* **1982**, *104*, 4029–4030.

(37) Hirahara, M.; Nagai, S.; Takahashi, K.; Saito, K.; Yui, T.; Yagi, M., New Series of Dinuclear Ruthenium(II) Complexes Synthesized Using Photoisomerization for Efficient Water Oxidation Catalysis. *Inorg. Chem.* **2015**, *54*, 7627–7635.

(38) Duan, L.; Fischer, A.; Xu, Y.; Sun, L., Isolated Seven-Coordinate Ru(IV) Dimer Complex with [HOHOH]− Bridging Ligand as an Intermediate for Catalytic Water Oxidation. *J. Am. Chem. Soc.* **2009**, *131*, 10397–10399.

(39) Süss-Fink, G., Water-Soluble Arene Ruthenium Complexes: From Serendipity to Catalysis and Drug Design. *J. Organomet. Chem.* **2014**, *751*, 2–19.

(40) Williams, D. B. G.; Lawton, M., Drying of Organic Solvents: Quantitative Evaluation of the Efficiency of Several Desiccants. *J. Org. Chem.* **2010**, *75*, 8351–8354.

(41) Fürstner, A.; Langemann, K., Macrocycles by Ring-Closing Metathesis. *Synthesis* **1997**, 792–803.

(42) van Lierop, B. J.; Reckling, A. M.; Lummiss, J. A. M.; Fogg, D. E., High-Yield, High-Purity Routes to Second-Generation Ru Metathesis Catalysts from Commercially Available Precursors. *ChemCatChem* **2012**, *4*, 2020–2025.

(43) Day, C. S.; Fogg, D. E., High-Yield Synthesis of a Long-Sought, Labile Ru-NHC Complex and Its Application to the Concise Synthesis of Second-Generation Olefin Metathesis Catalysts. *Organometallics* **2018**, *24*, 4551–4555.

Chapter 5. Conclusions and Future Work

Understanding the pathways by which the M=C or M–C bonds are lost from the active species in olefin metathesis is critical for the development of higher-performing catalysts. Within the last decade, a series of important mechanistic studies has helped establish the intrinsic decomposition pathways operative for the important Ru catalysts, and advances have been made toward inhibiting these pathways. Nevertheless, catalyst productivity is challenged by sensitivity to contaminants. In the critical context of chemical manufacturing, even ppm levels of impurities may be detrimental to batch-to-batch reproducibility, while chemical biology – that is, metathesis in water, in the presence of surfactants, buffers, and densely-functionalized biomolecules – remains a frontier.

Mechanistic studies, however, are far fewer than reports in which a series of decomposition events is inferred from the crystal structure of a decomposition product. The common occurrence of a cyclometallated NHC ligand in such structures has drawn much attention, and led to the widespread inference that attack on (e.g.) the mesityl *o*-methyl groups in the commonly-used H_2IMes metathesis catalysts is key to catalyst decomposition. Reducing the bulk of the NHC ligand has thus been recommended in leading reviews as an obvious target for catalyst redesign. This forms a partial context for the present thesis work. The research question that set the backdrop for Chapter 2 was whether NHC truncation is beneficial, or detrimental. As described in a previous M.Sc. thesis from the Fogg group, Ms. Stephanie Rufh observed rapid, complete loss of the methylidene ligand when the very small NHC ligand IMe_4 was added to the precursor complex $RuCl_2(PCy_3)(=CH_2)$ **GIm** in an attempt to synthesize a resting-state methylidene species bearing a truncated NHC. Described in Chapter 2 of this thesis is the unexpected discovery that the **GIm**–IMe_4 reaction occurs even at cryogenic temperatures (–80 °C), and that it involves nucleophilic attack of the small NHC at the methylidene ligand, rather than ligand exchange. The liberated N-heterocyclic olefin is itself a potent nucleophile, which itself attacks at the [Ru]=CH_2 carbon, resulting in liberation of the ethylimidazolium salt [EtIMe_4]Cl. The same pathway was observed on adding IMe_4 to the second-generation Grubbs methylidene $RuCl_2(H_2IMes)(PCy_3)(=CH_2)$ **GIIm**, albeit at a slower rate.

These findings report indirectly on the original question concerning the impact of ligand truncation. The sensitivity of both **GIm** and **GIIm** to abstraction of the methylidene by a small, potent nucleophile underscores the importance of steric protection at the key [Ru]=CH_2 site. An intriguing further implication is drawn from the selectivity of this reaction, which points toward IMe_4 as a potentially very efficient catalyst quenching agent. Moreover, the capacity of this NHC to effect *controlled* abstraction of the methylidene ligand, leaving the "$RuCl_2(H_2IMes)(PCy_3)$" core intact, could be invaluable for tandem catalysis applications in which metathesis is the first step.

The following two Chapters turn to the question of decomposition of leading metathesis catalysts within contexts that have gone largely ignored, but which are critical to the expanding applications in chemical biology noted above. While many reviews have been written on aqueous metathesis, problems of decomposition by water are just beginning to be acknowledged. A single mechanistic study exists in the literature, a study from the Fogg group focusing on the mechanism by which water promotes decomposition of phosphine-stabilized Grubbs-class catalysts. Chapters 3 and 4 consider the impact of water on phosphine-free catalysts. Examined in Chapter 3, in light of data showing that the negative impact of water on the performance of **HII** is greatly magnified when Bronsted base is also present, is the impact of hydroxide ion. Deliberately adding a soluble source of the hydroxide anion at any point during RCM was indeed found to immediately halt metathesis. Rather than attacking on an active species, however, salt metathesis to form a bis-hydroxide complex **HII-OH** was observed. The latter complex, though unreactive towards bulkier substrates, decomposed in the presence of ethylene at room temperature. Proposed as the deactivating event is bimolecular coupling of the four-coordinate methylidene species with the precatalyst, a pathway promoted by the strong H-bonding capacity of the hydroxide ligand. DFT studies revealed that the geometry of the resulting dinuclear intermediate hampers methylidene/benzylidene coupling to liberate olefin. Strong H-bonding of the hydroxide ligands also appears to promote further agglomeration.

Chapter 4 considers the impact of water itself on olefin metathesis promoted by phosphine-free catalysts. As noted above, despite extensive reports of aqueous metathesis, water is now emerging as unexpectedly deleterious to the productivity even of the "robust" Ru catalysts. In Chapter 4, metathesis yields are shown to decrease by 50% or more on addition of just 0.1% v/v water to the reaction medium. This drop is observed in room-temperature reactions for leading metathesis catalysts of the Hoveyda and Grela classes, including recent and highly productive CAAC derivatives. The mechanism of decomposition was examined. An initial hypothesis, based on prior unpublished work, centered on the capacity of water to promote β-elimination of the MCB intermediate by acting as a proton shuttle. While this may be the case for reactions at elevated temperatures, based on the release of propenes, no propene products were observed at room temperature. Instead, a role for water in bimolecular coupling is suggested. Of note, water-scavenging resins can be used to restore metathesis yields in organic media. Macrocyclization reactions using a dianiline catalyst, which avidly takes up water, were shown to afford yields comparable to anhydrous controls in the presence of 0.02% v/v water and resin.

From the perspective of aqueous metathesis, important questions have just begun to be posed. Most obviously, the mechanism by which water decomposes the catalyst requires further examination: insight into the nature of the problem may then lead to the identification of design criteria to protect against it. Deuterium labelling studies using D_2O may prove useful in determining the validity of the proposed, high-temperature "proton shuttle" mechanism. Kinetics experiments should be undertaken to determine the order of the decomposition reaction with respect to ruthenium and water. The hypothesis that bimolecular coupling is operative at room

temperature should be probed by examining labile catalysts that readily undergo this decomposition pathway, but which resist nucleophilic attack.

As discussed in the preceding chapters, ethylidene complexes are resistant to nucleophilic attack. Addition of water to such catalysts could therefore offer a probe of this pathway unobscured by nucleophilic attack. The pyridine-stabilized complex **Ru-14** used in the Bailey work is a good candidate. Relevant clues are both the proportion of butene evolved from BMC, and the rate of decomposition. As shown in Chapter 3, bimolecular coupling does not necessarily liberate an olefin. The proportion of butenes liberated may thus under-report BMC. Ambient-temperature conditions, or perhaps metathesis in donor solvents that can inhibit Ru coupling, are therefore important avenues for study.

Repeating the added water metathesis experiments of Chapter 4 at higher dilution may also give insights. Of interest is the possibility that reducing the concentration of catalyst and substrate could give higher TONs (even if turnover frequencies suffer), owing to reduced rates of BMC. The pseudohalide catalysts first developed by Jay Conrad of the Fogg group may offer additional, intriguing opportunities to inhibit bimolecular coupling of metathesis catalysts in either water-rich or water-free media.

A final suggestion for future work centers on structure-activity relationships for different metathesis catalysts in the presence of water. This would be valuable in revealing which catalysts are more tolerant, and which are more vulnerable to water. As shown in Chapter 4, the CAAC catalyst **nGC** performs better than both H_2IMes containing complexes **HII** and **nG** in the presence of water. Such catalyst also resist MCB β-elimination (a topic that is currently being studied in more detail by Daniel do Nascimento of this research group). If the σ-donating character of the CAAC ligand is responsible, ligand modifications to enhance this character may result in even more robust and water-tolerant catalysts.

6. Appendices

A. NMR Spectra

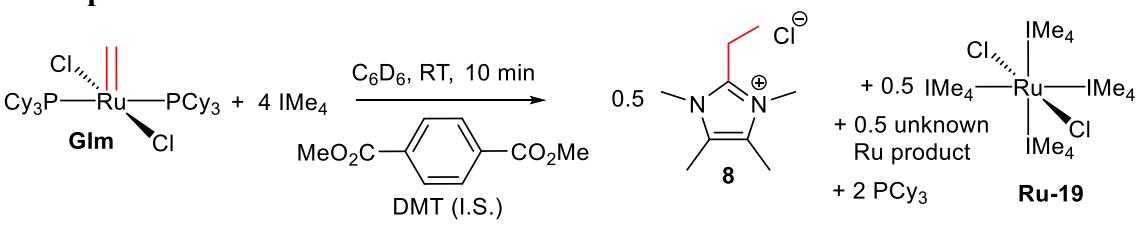

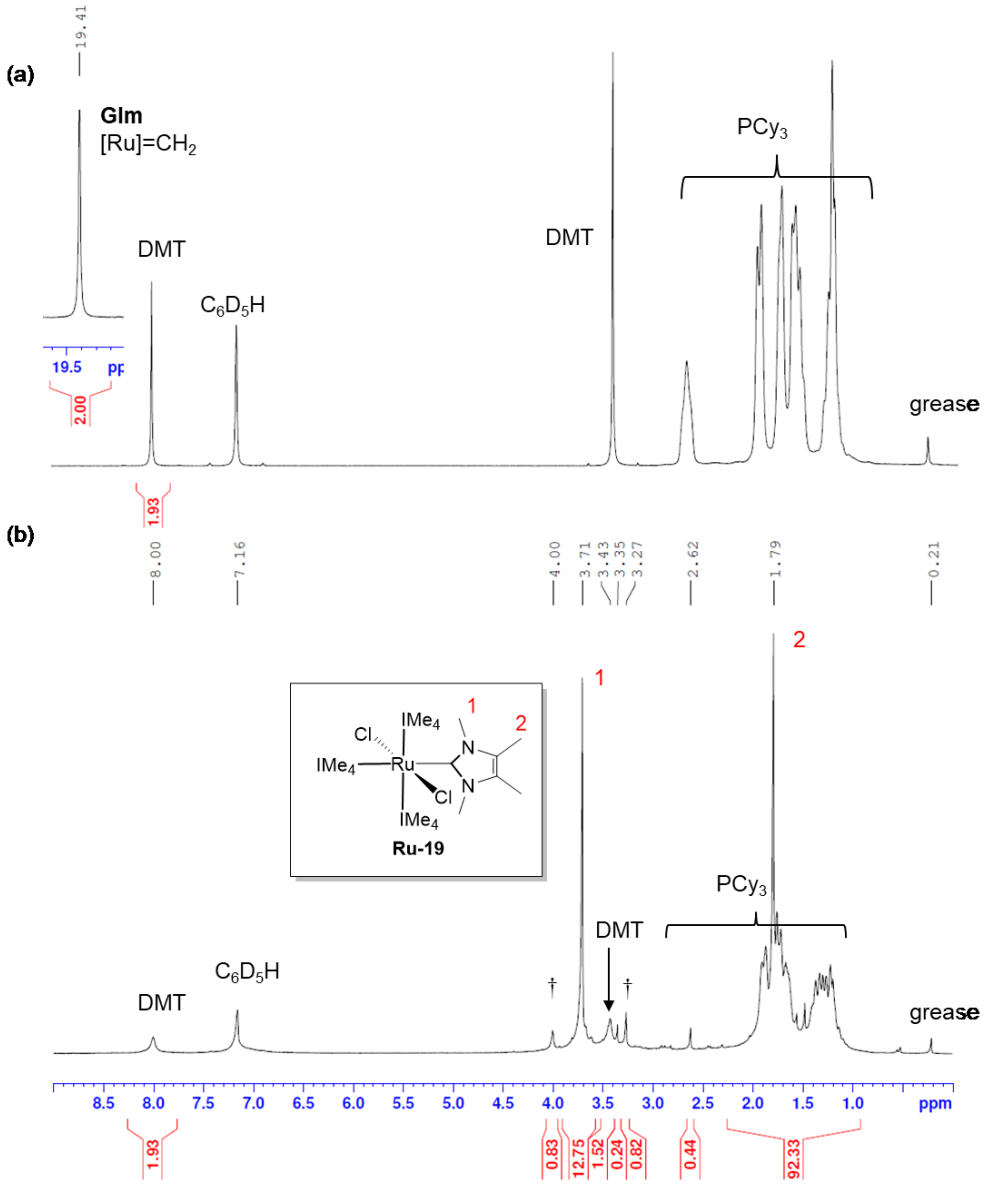

Figure A1. ^{1}H NMR spectra (300 MHz, C_6D_6) (a) of GIm; (b) after adding IMe_4 († = unassigned).

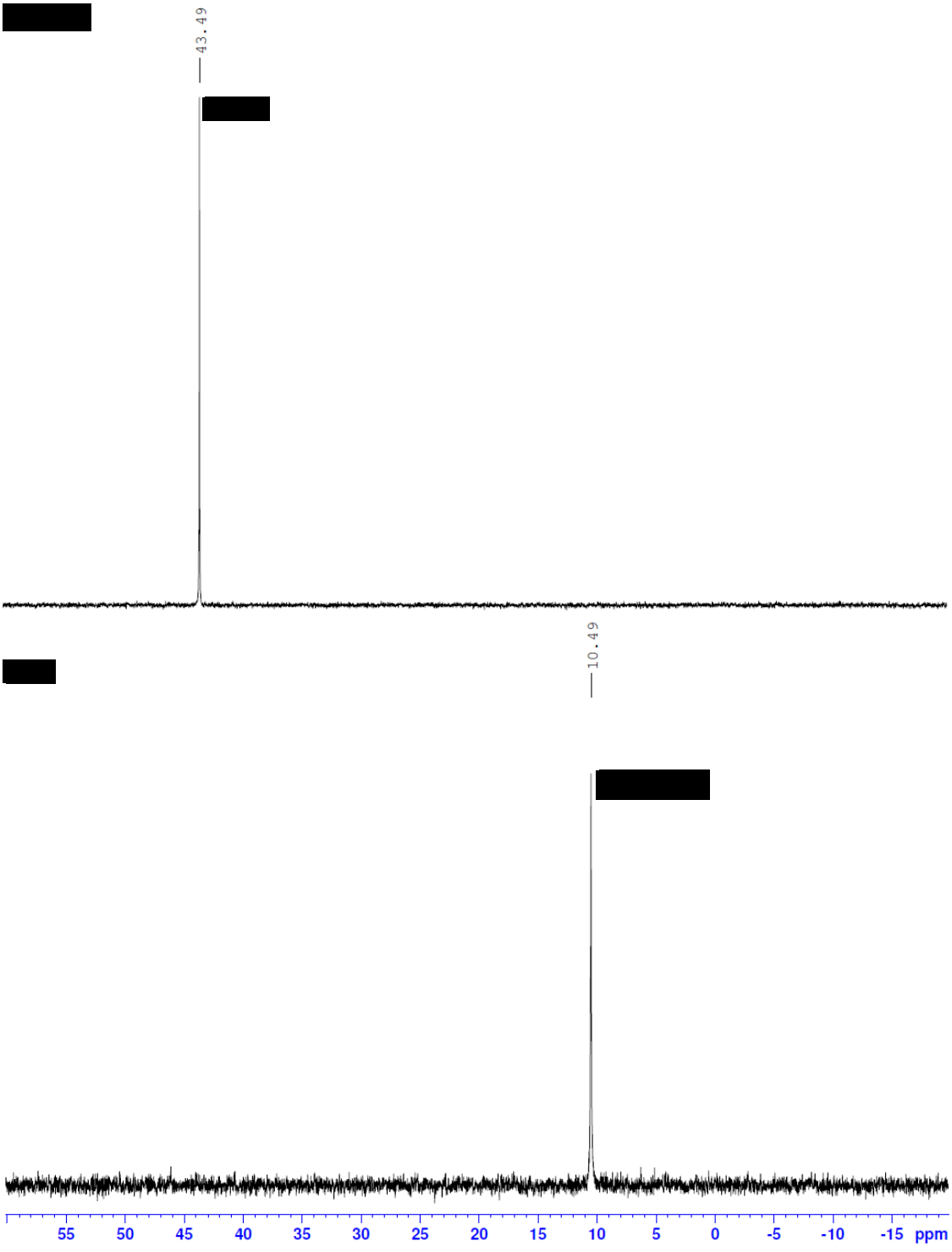

Figure A2. $^{31}P\{^{1}H\}$ NMR spectra (121 MHz, C_6D_6): (a) of GIm; (b) after adding IMe_4.

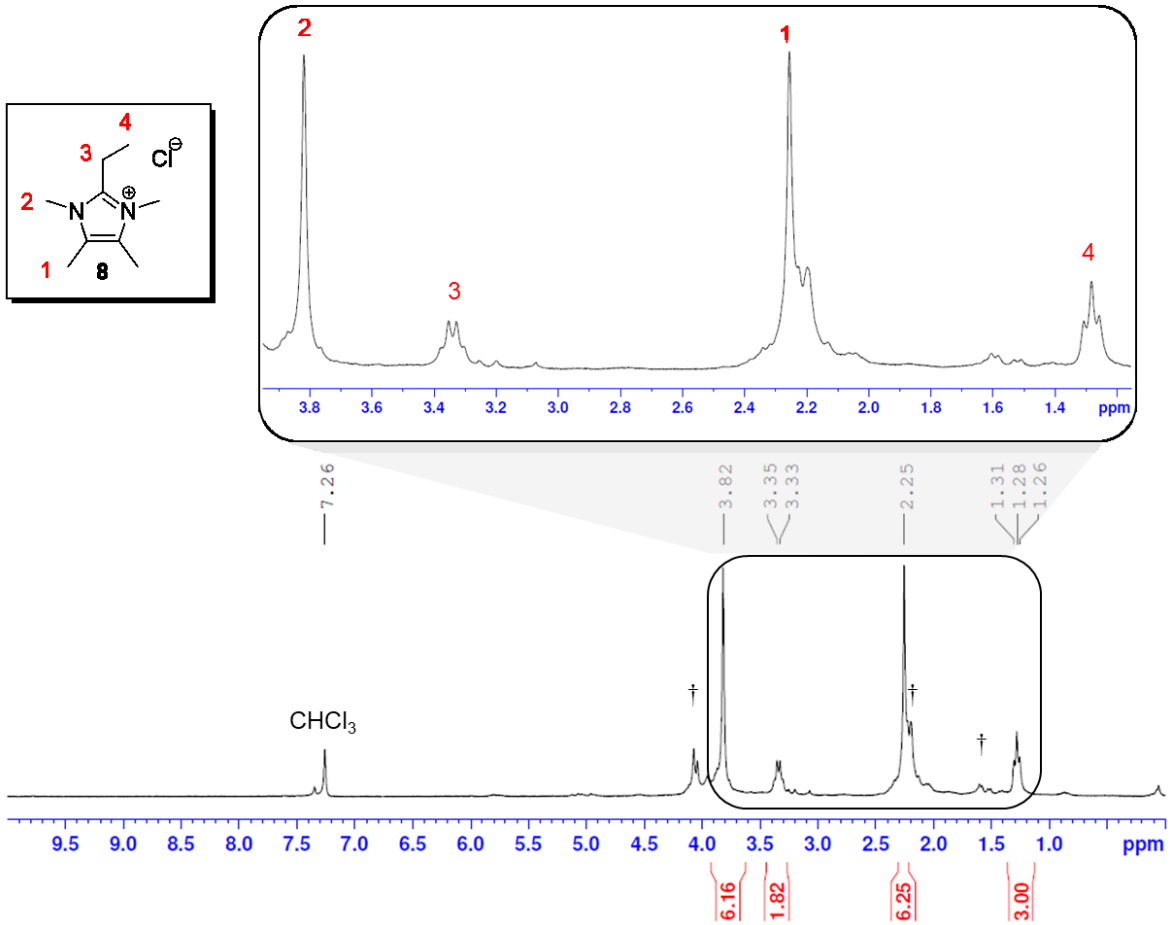

Figure A3. ^{1}H NMR spectrum (600 MHz, $CDCl_3$) of precipitate after washing (benzene, hexanes) and drying under vacuum. (†) designates unassigned signals; labelled in main spectrum only.

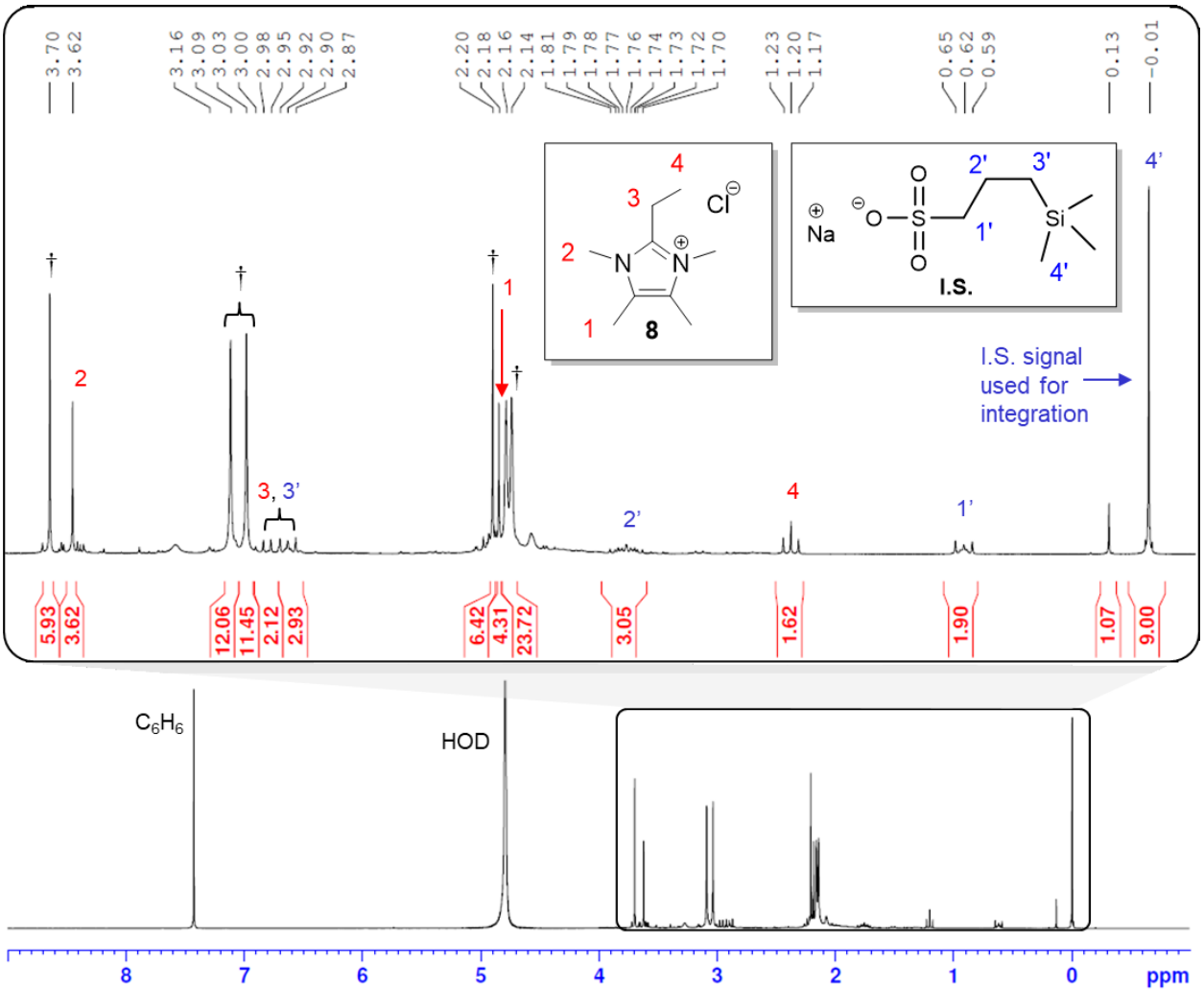

Figure A4. ^{1}H NMR spectrum (300 MHz, D_2O) for quantitation of [Et–IMe$_4$]Cl 8: product extracted into D_2O containing $NaO_3S(CH_2)_3SiMe_3$ as internal standard. Additional unassigned peaks marked (†) may reflect decomposition of the Ru co-product by water.

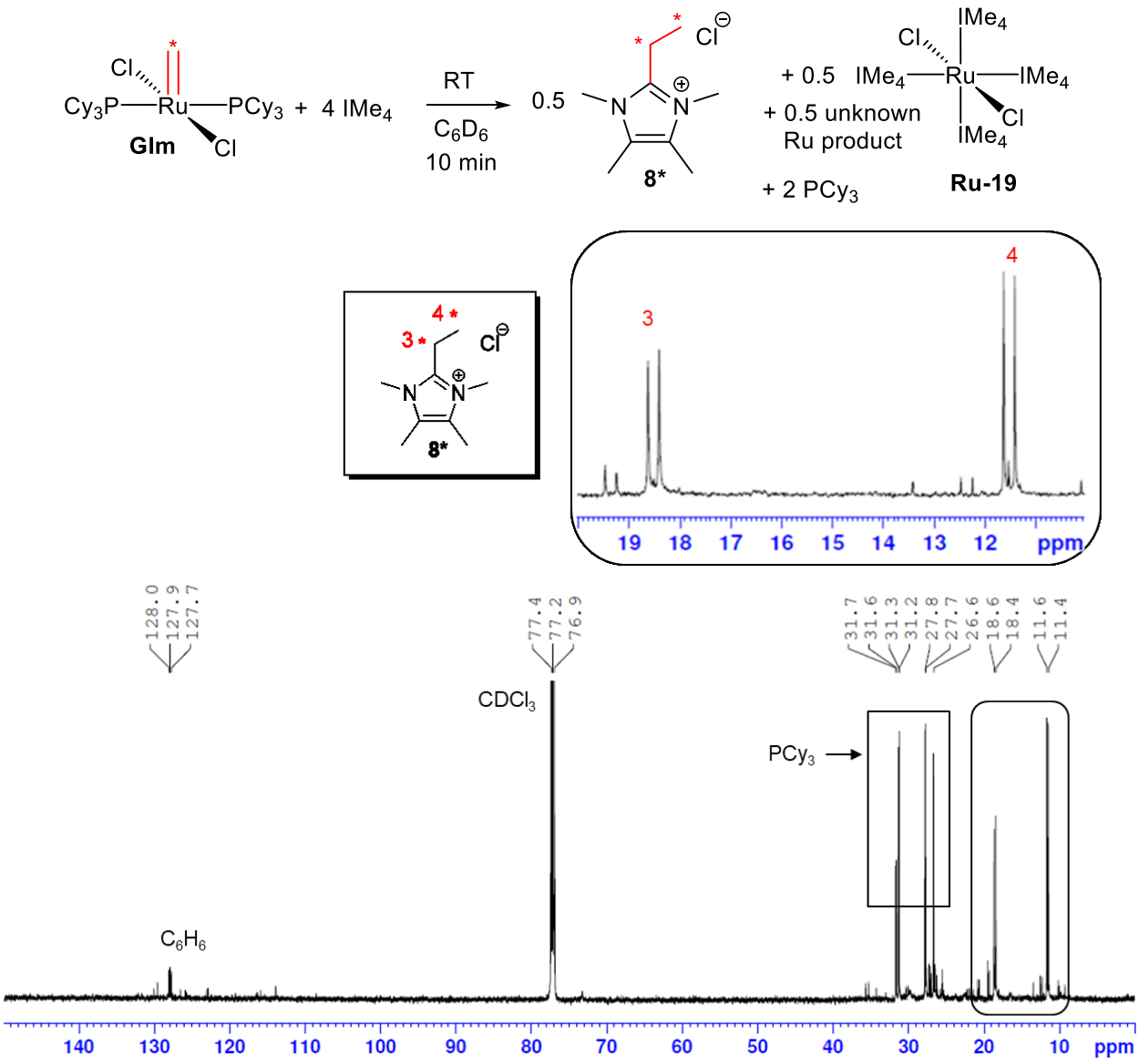

Figure A5. $^{13}C\{^{1}H\}$ NMR spectrum (151 MHz, $CDCl_3$) of products generated from the reaction of GIm* with IMe_4. Sample prepared by evaporating the benzene solvent and dissolving the residue in $CDCl_3$. The inset above shows the key signals for doubly-^{13}C-labelled 8*.

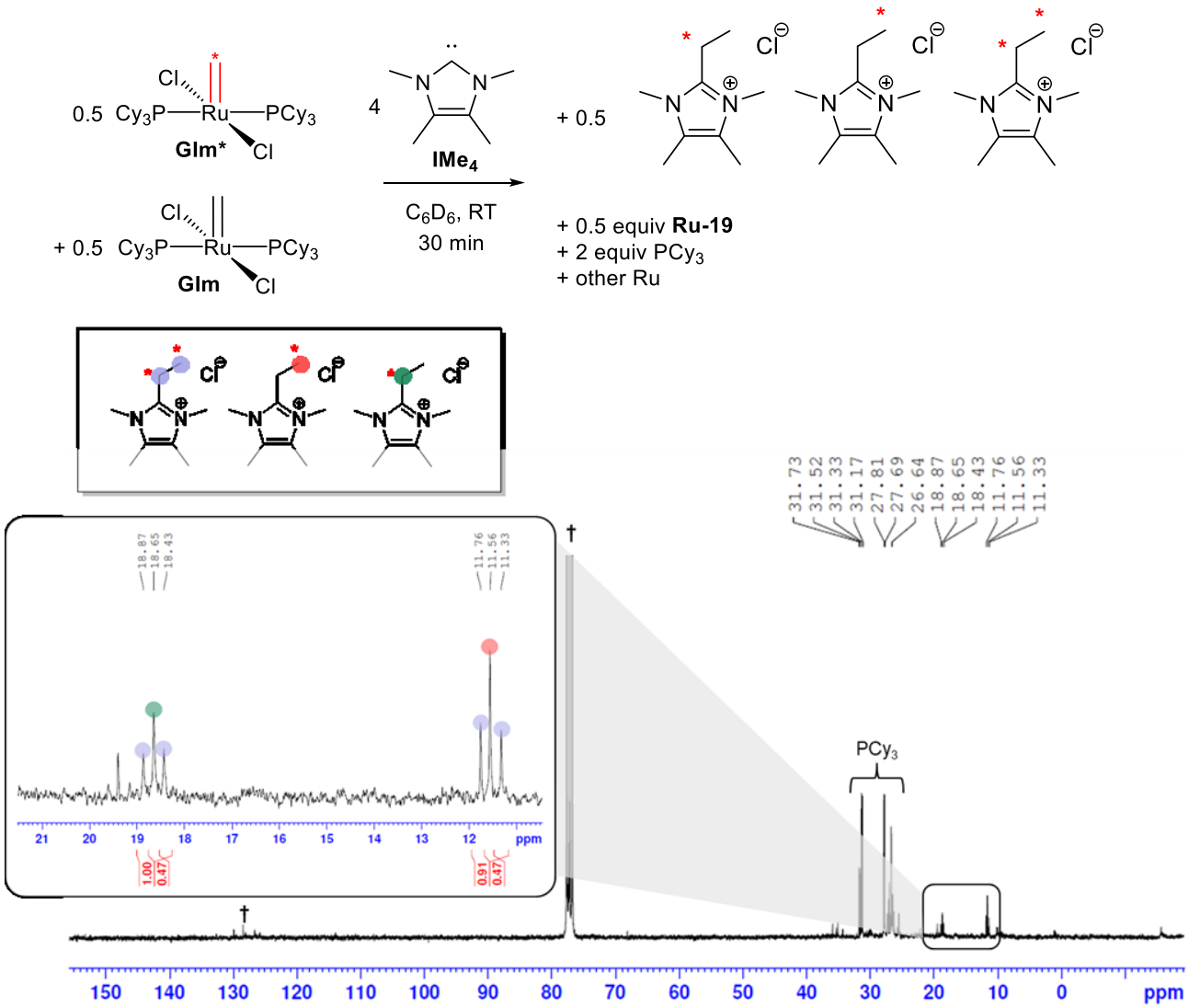

Figure A6. $^{13}C\{^{1}H\}$ NMR spectrum (151 MHz, $CDCl_3$) of products generated from the reaction of a 1:1 mixture of GIm* and GIm with IMe_4. Sample prepared by evaporating the benzene solvent and dissolving the residue in $CDCl_3$.

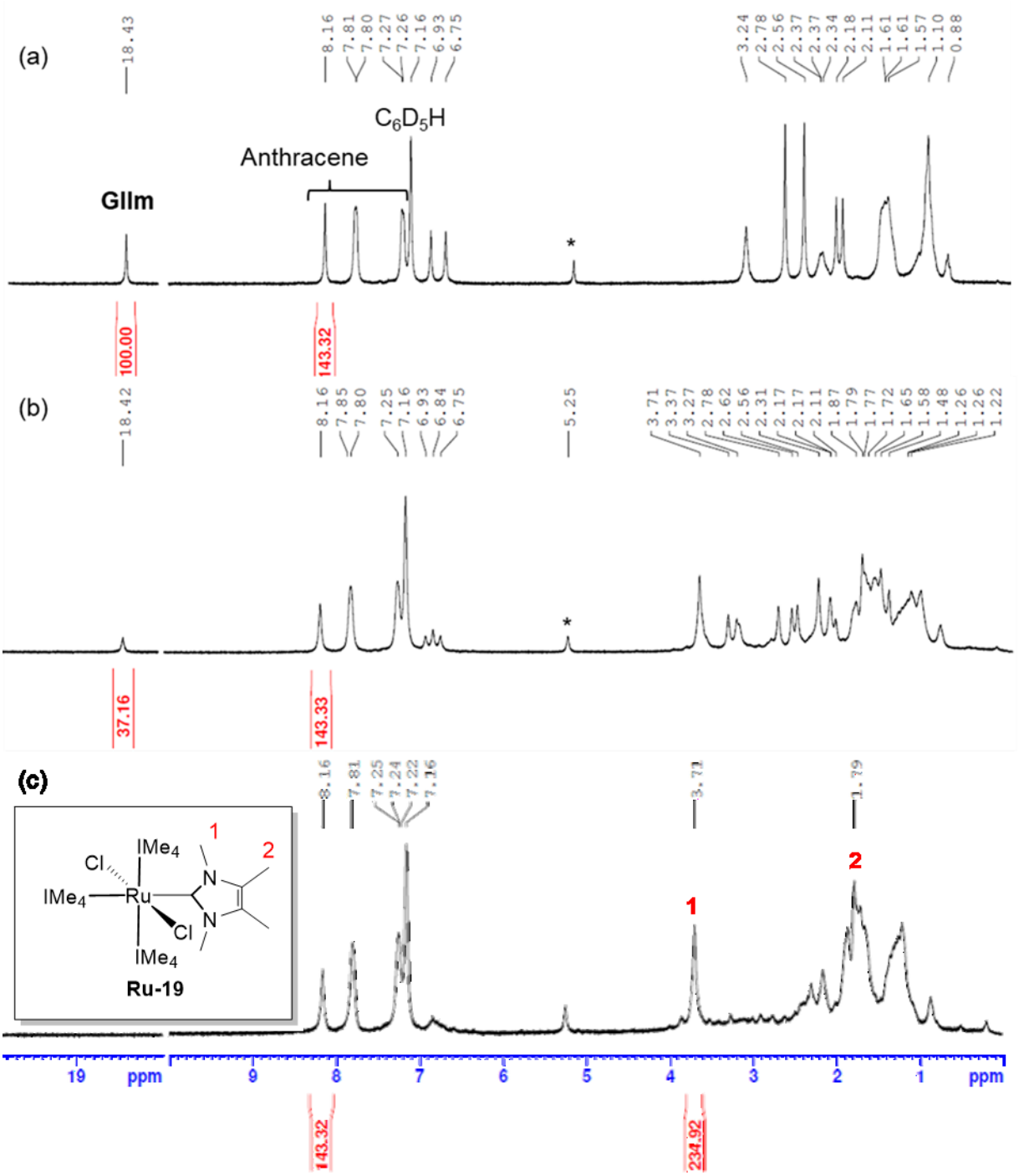

Figure A7. ^{1}H NMR spectra (C_6D_6, 300 MHz) for the decomposition of **GIIm** by IMe_4. (a) Initial spectrum, before adding IMe_4. (b) Spectrum 5 min after adding IMe_4, showing only ca. 40% **GIIm** remaining. (c) Spectrum after 24 h, showing complete consumption of **GIIm**. (*) denotes a CH_2Cl_2 impurity.

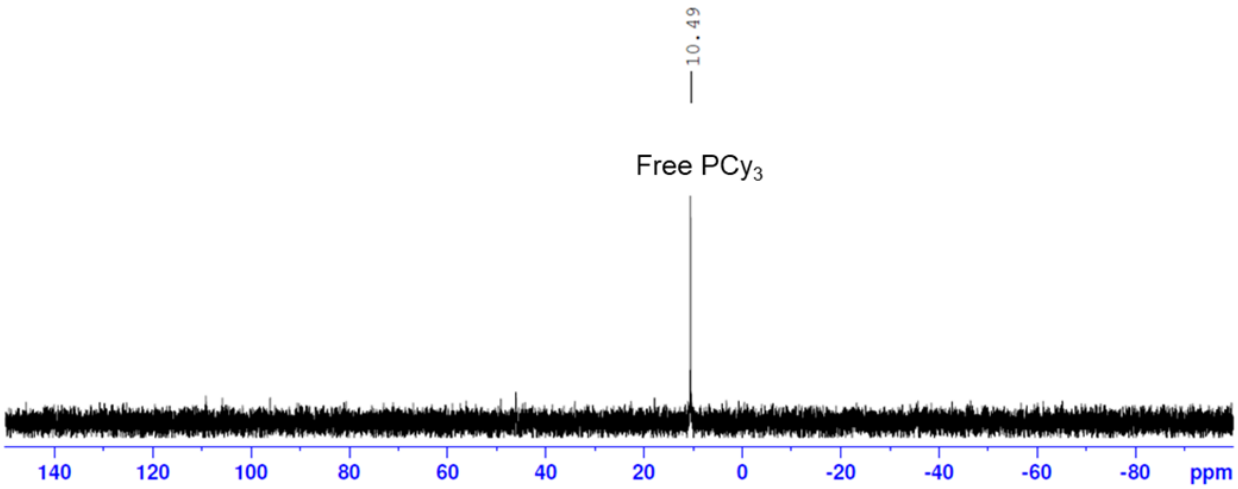

Figure A8. Final $^{31}P\{^{1}H\}$ NMR spectrum (C_6D_6, 121 MHz) for the experiment of Fig. A7, after 24 h.

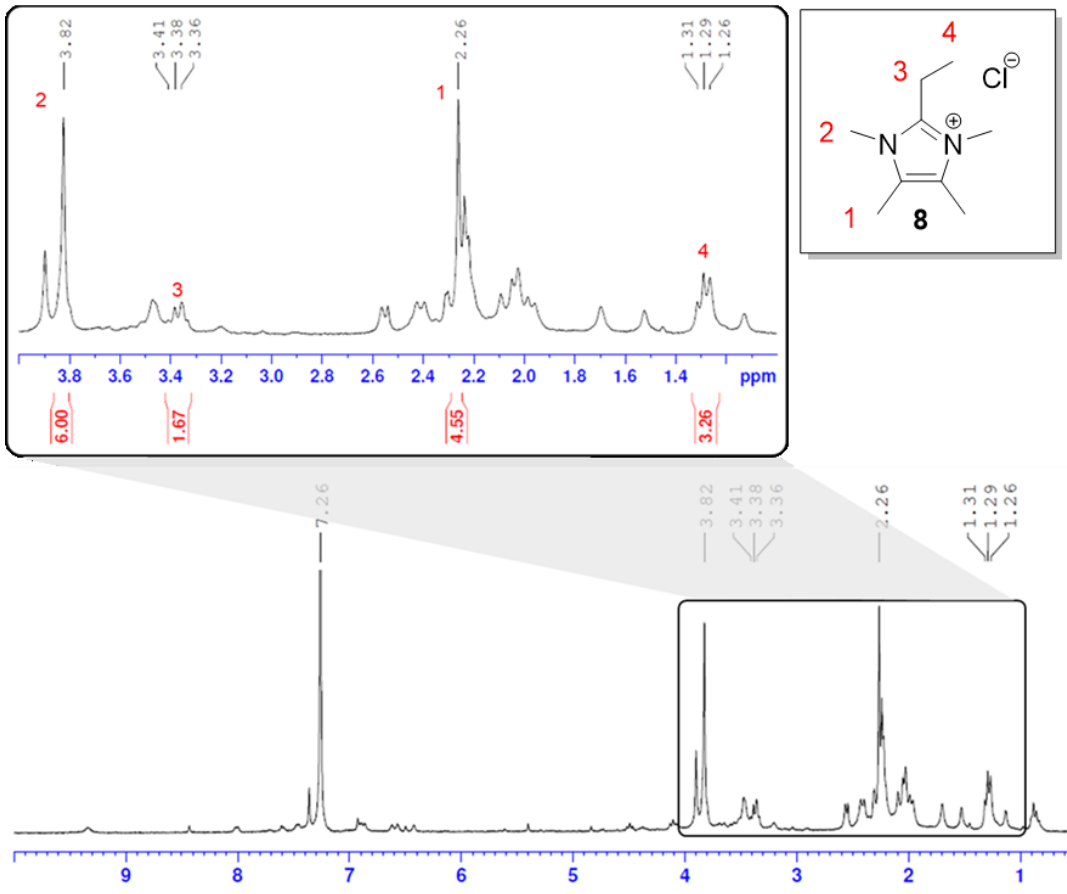

Figure A9. ^{1}H NMR spectrum ($CDCl_3$, 300 MHz) of precipitate from the experiment of Figure A7, showing signals for [EtIMe$_4$]Cl **8**.

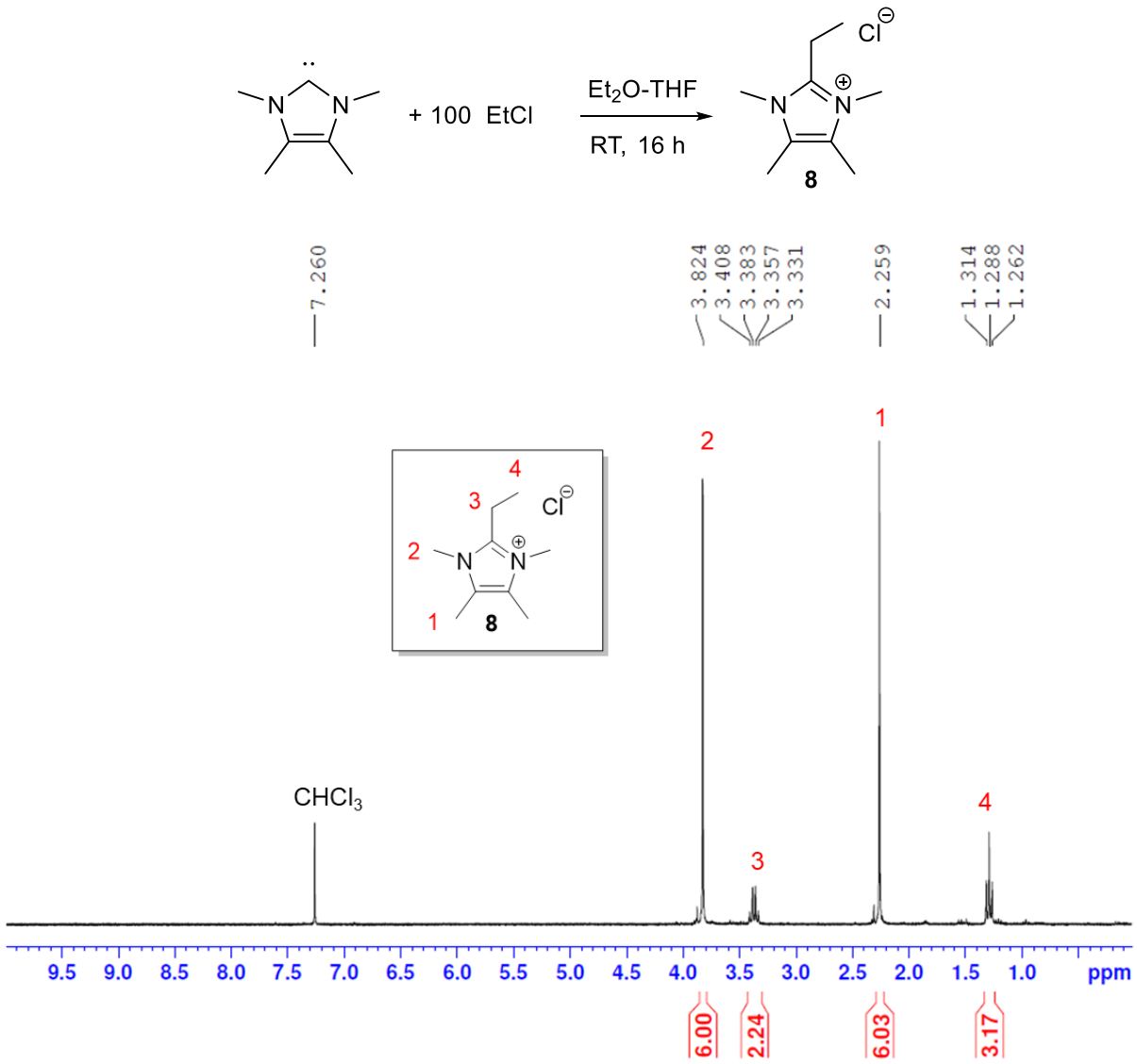

Figure A10. ^{1}H NMR spectrum (300 MHz, $CDCl_3$) of [Et–IMe$_4$]Cl, **8**.

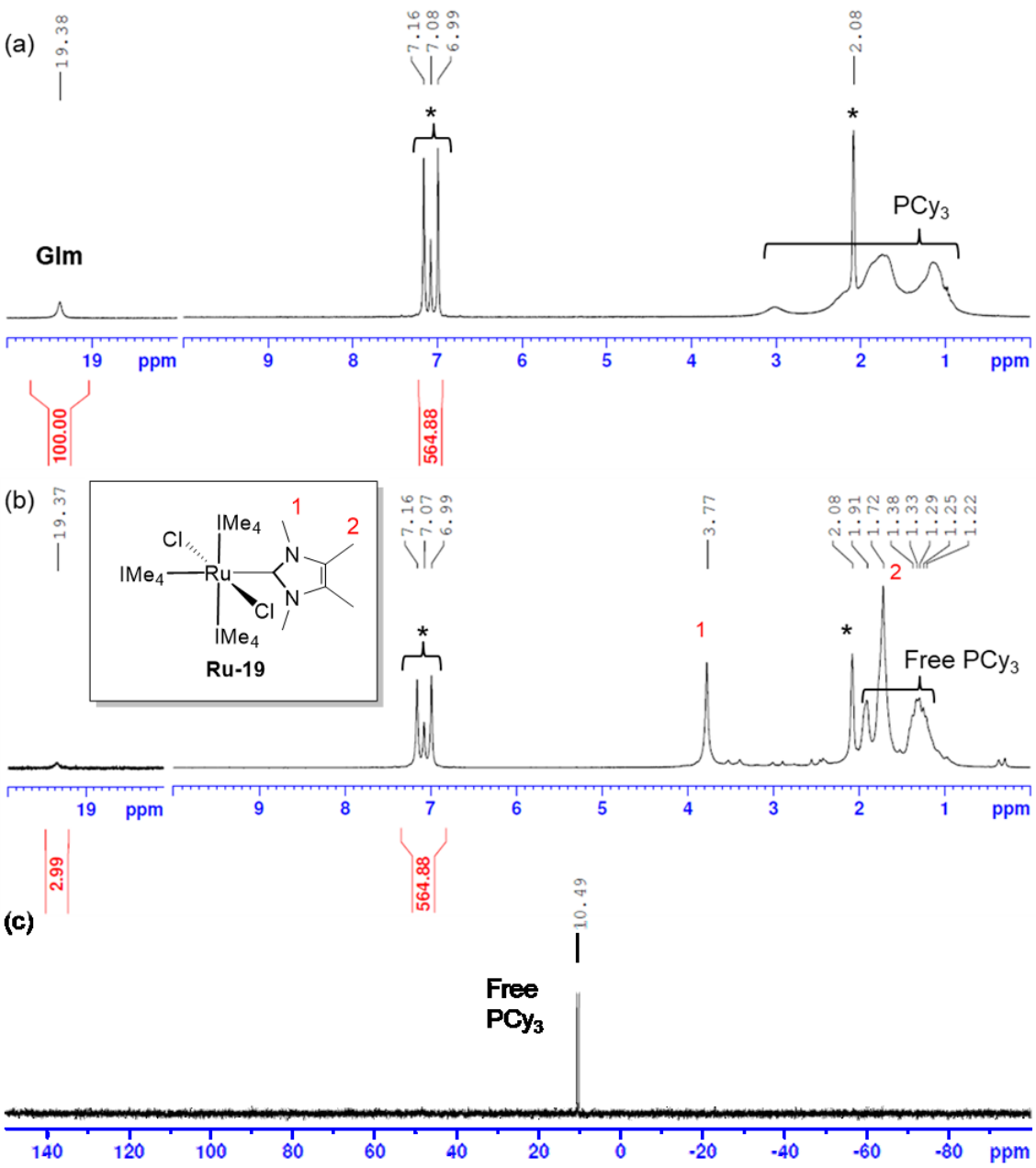

Figure A11. NMR spectra for decomposition of **GIm** at low temperature (–80 °C; C_7D_8). (a) ^1H NMR spectrum before adding IMe_4; (b) 5 min after adding IMe_4. (c) $^{31}P\{^1H\}$ NMR spectrum 10 min after adding IMe_4, showing only free PCy_3. (*) denotes signals for residual protio-toluene.

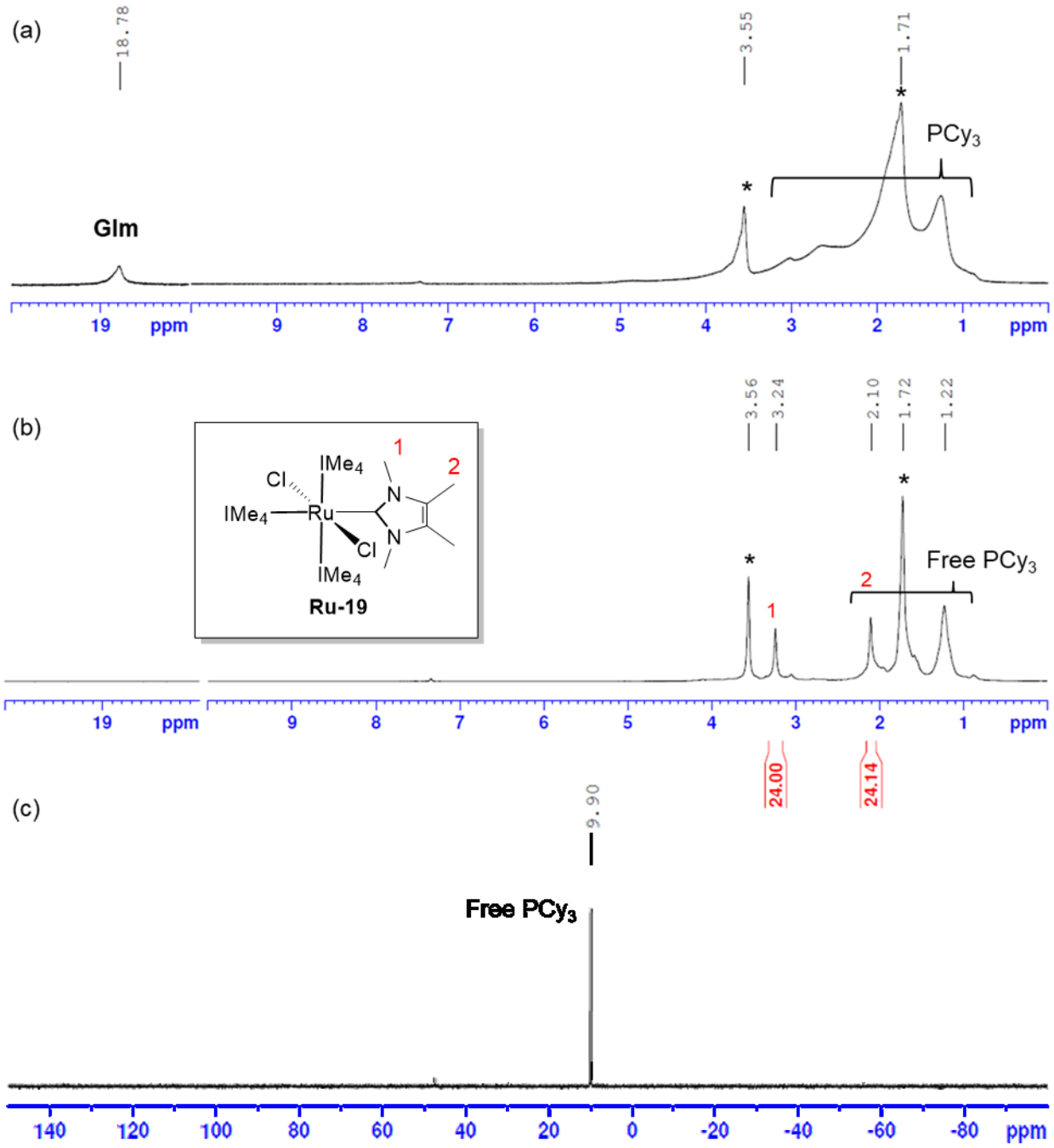

Figure A12. NMR spectra for the decomposition of **GIm** at low temperature (–80 °C) in THF-d8. (a) ^{1}H NMR spectrum before adding IMe_4; (b) 5 min after adding IMe_4. (c) $^{31}P\{^{1}H\}$ NMR spectrum after 10 min reaction, showing only free PCy_3. (*) denotes signals for residual protio-THF.

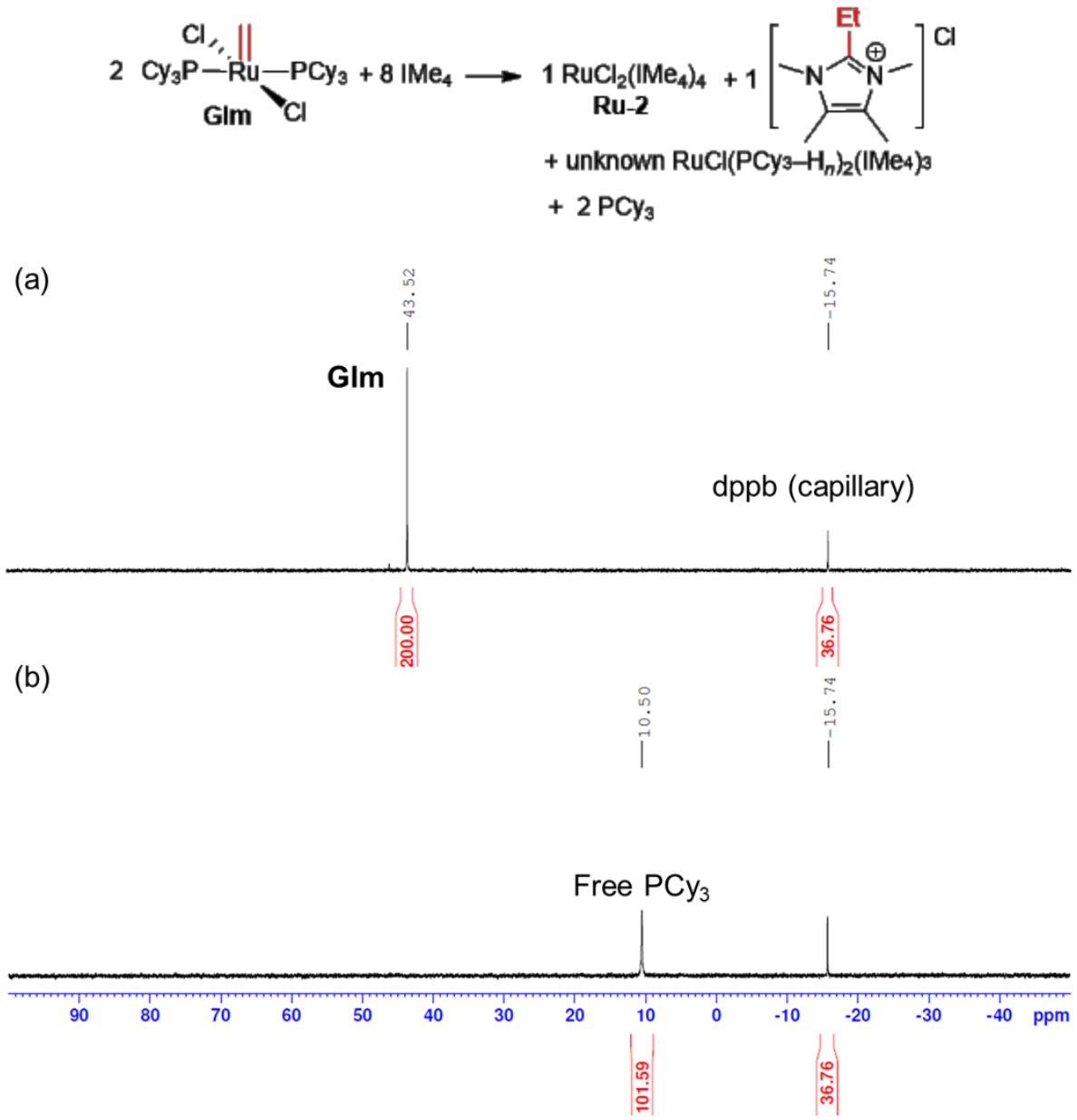

Figure A13. $^{31}P\{^{1}H\}$ NMR spectra (121 MHz, C_6D_6) measured using an inverse-gated 30° pulse sequence. (a) 60 s relaxation delay. (b) 20 s relaxation delay.

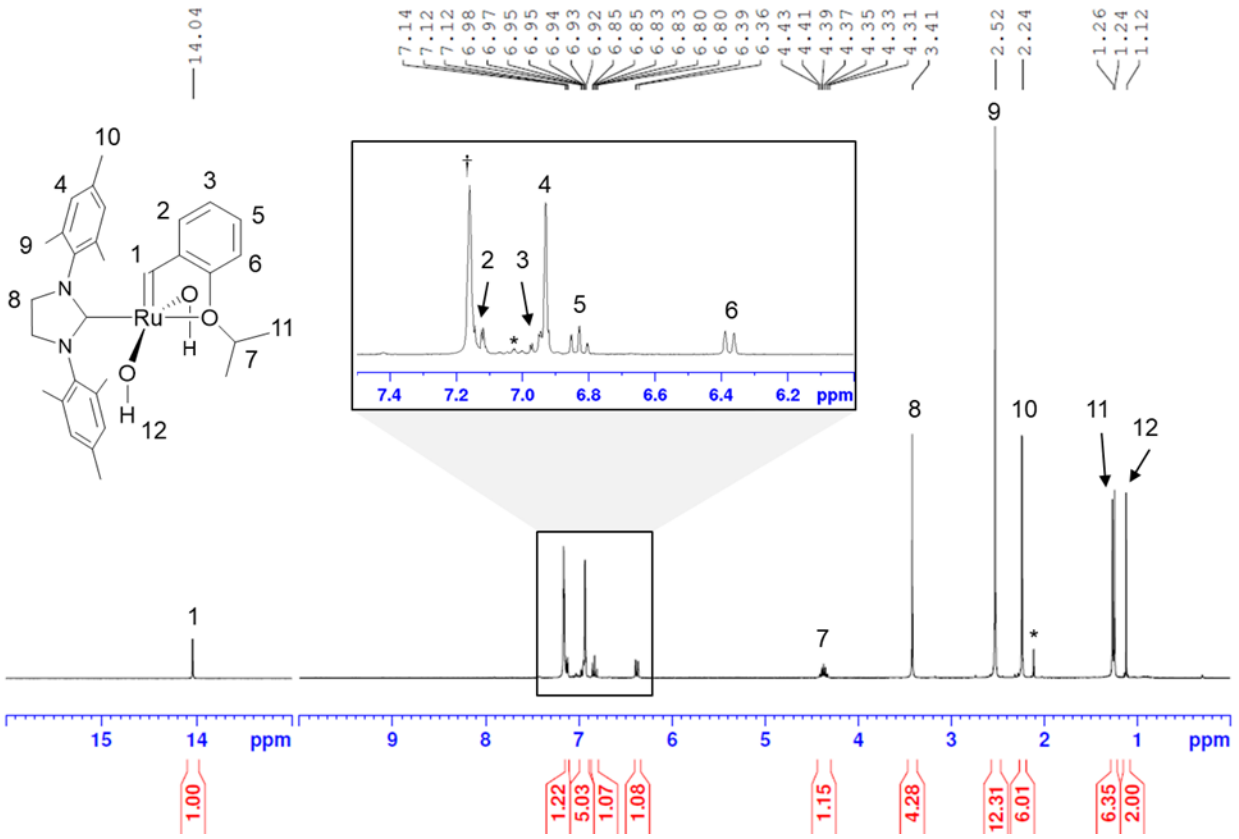

Figure A14. ^{1}H NMR (300 MHz, C_6D_6) spectrum of **HII-OH** (SW = 40 ppm, O^{1}P = 10 ppm). Inset is an enhancement of the aromatic region. The symbol (†) denotes residual C_6D_5H; (*) denotes residual toluene.

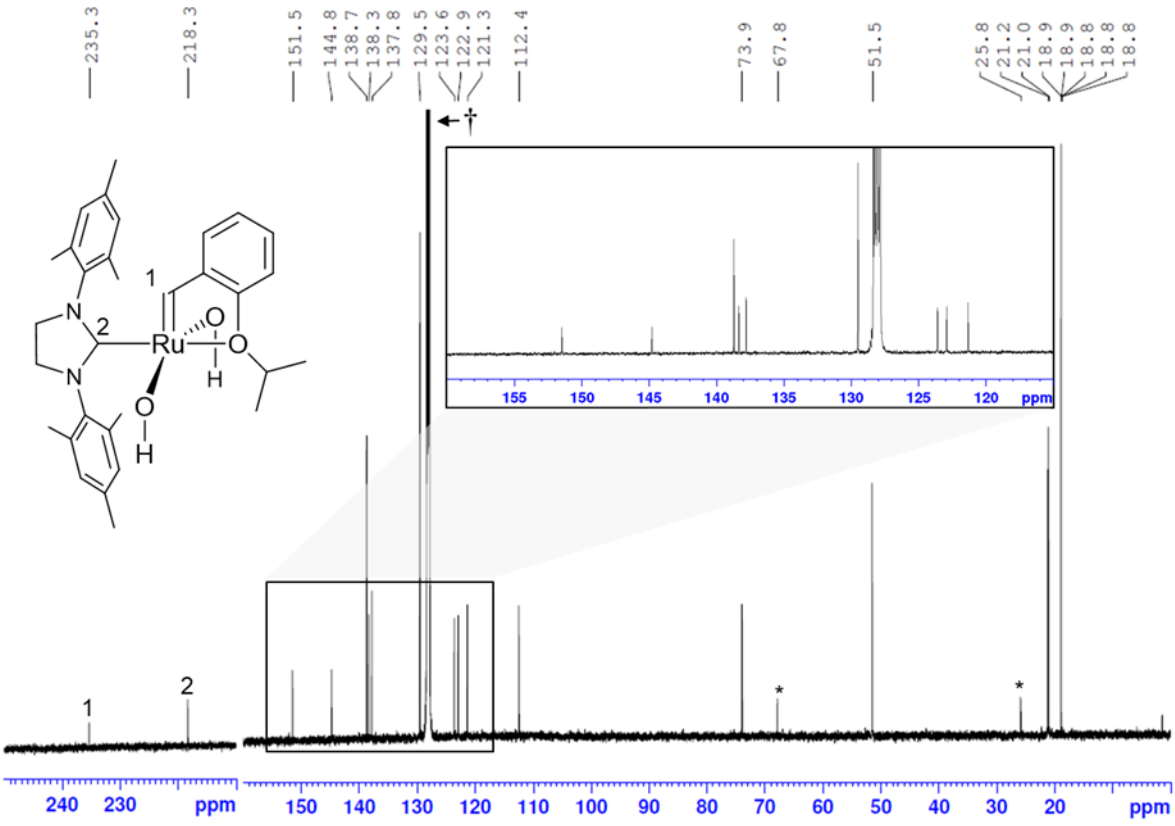

Figure A15. $^{13}C\{^{1}H\}$ NMR (125.5 MHz, C_6D_6) spectrum of **HII-OH** (SW = 500, O^1P = 100 ppm). Inset is an enhancement of the aromatic region. The symbol (†)denotes residual C_6D_5H; (*) denotes residual THF solvent.

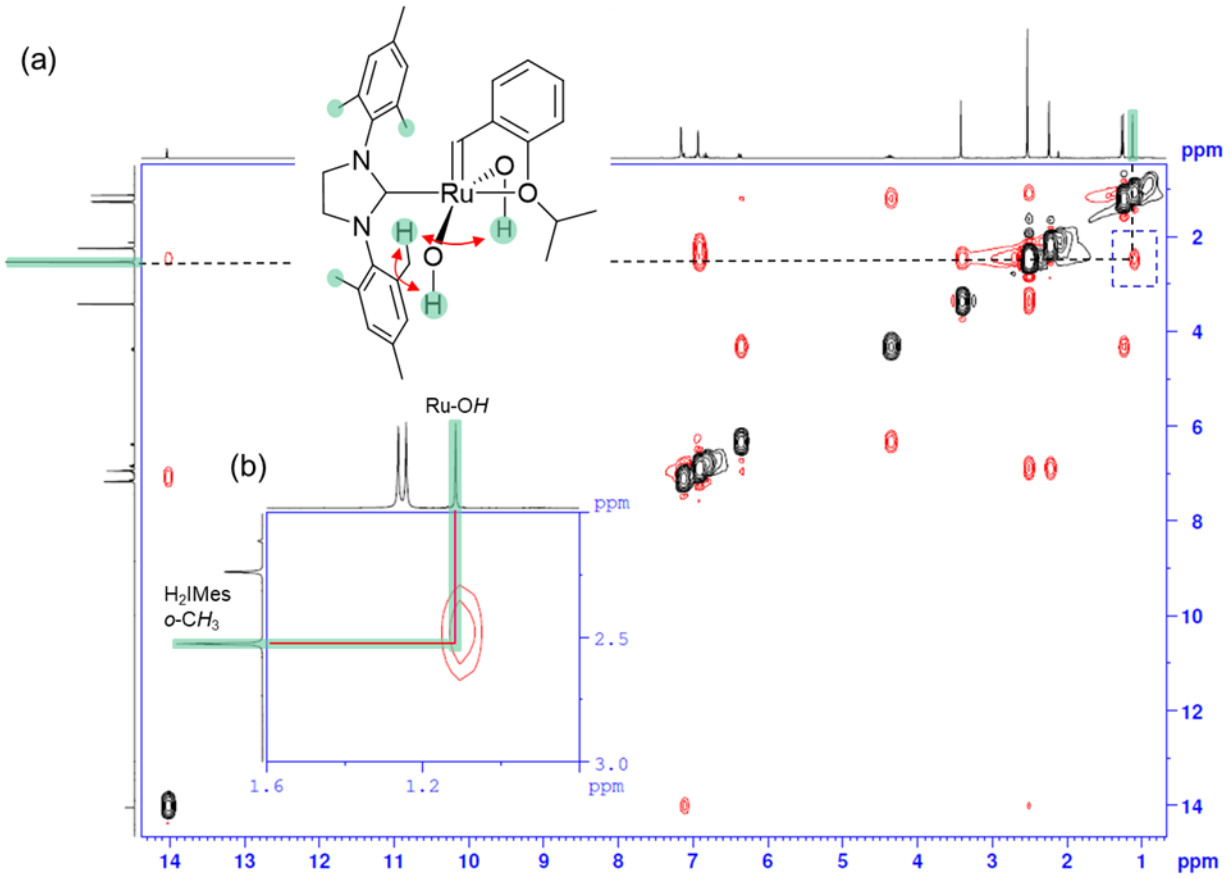

Figure A16. (a) ^{1}H-^{1}H NOESY spectrum (300 MHz, C_6D_6) of **HII-OH**. NOESY interactions are shown in red. (b) Inset is expanded region showing NOESY interaction between Ru-O*H* and H_2IMes *o*-C*H*$_3$ protons.

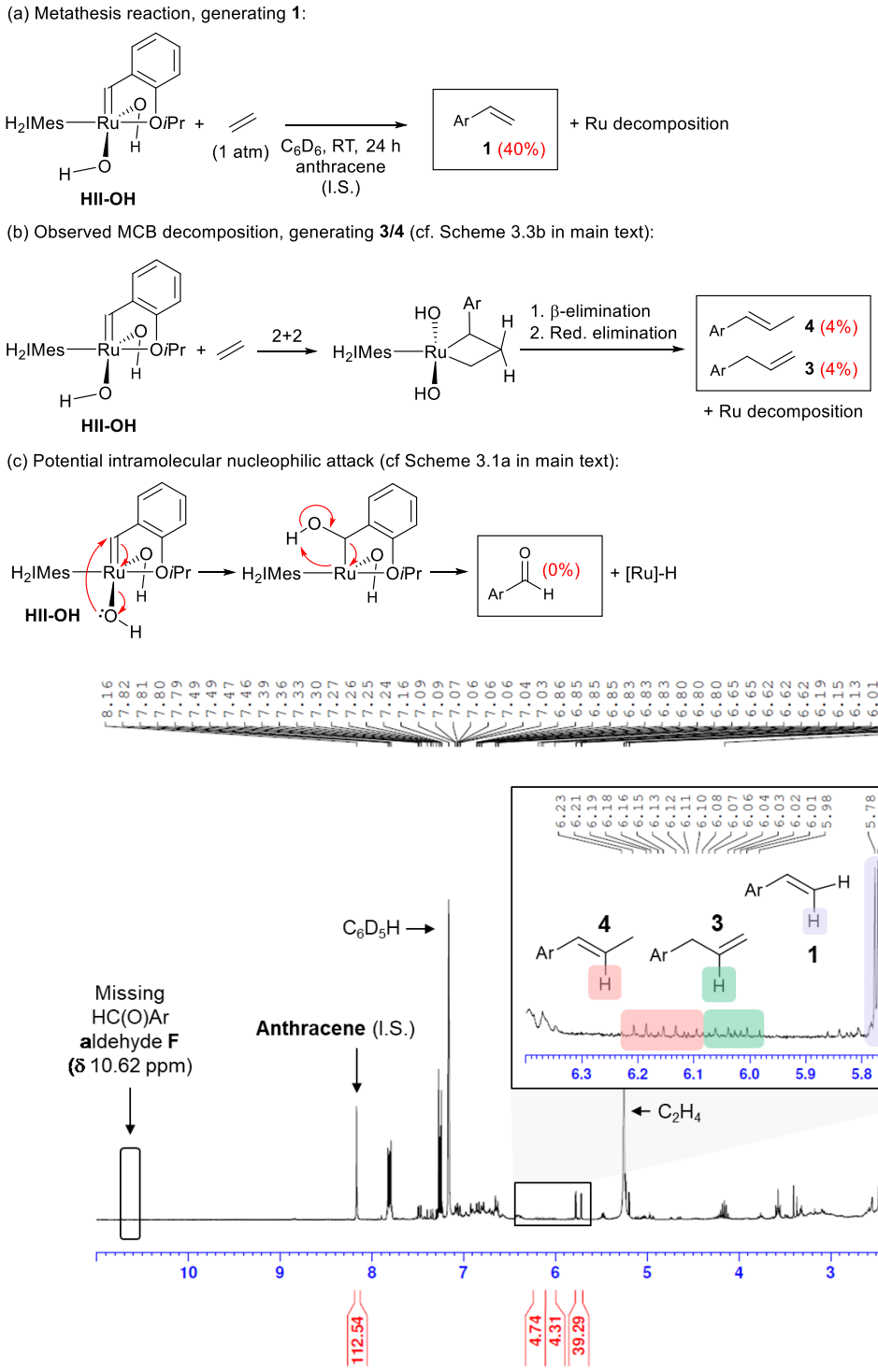

Figure A17. 1H NMR spectrum (C6D6, 300 MHz) of reaction of HII-OH with 1 atm C2H4 at RT. Spectrum shown is following complete decomposition of HII-OH (24 h). Inset shows important organic decomposition products, with the corresponding integrated protons highlighted in color. Integrations of only the internal standard and organic products provided for simplicity. All integration values are relative to starting HII-OH charge (100%).

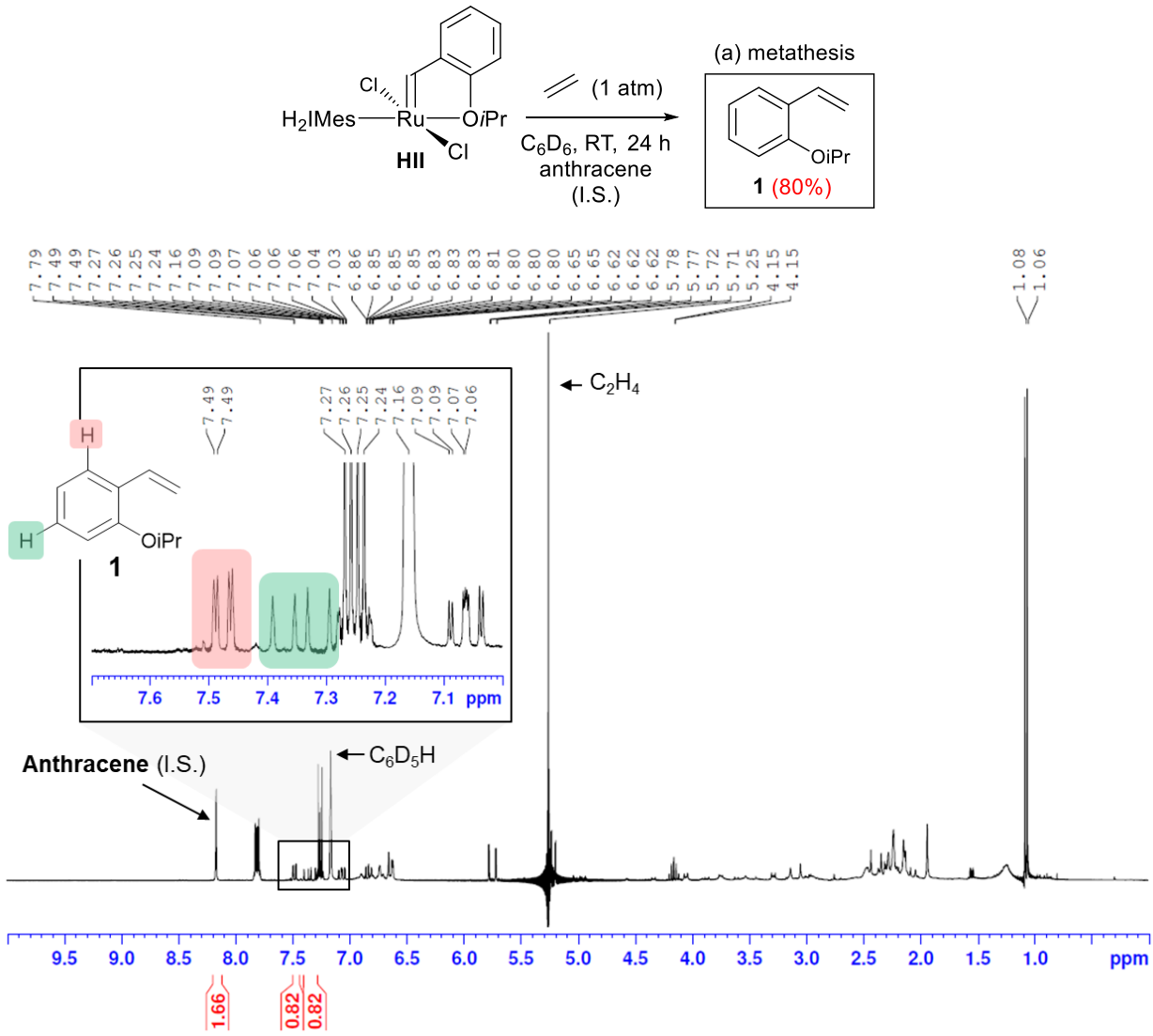

Figure A18. ^{1}H NMR (C_6D_6, 300 MHz) for the reaction of **HII** with 1 atm C_2H_4 at RT. Spectrum shown is following complete decomposition of **HII** (24 h). Inset shows important organic decomposition products, with the corresponding integrated protons highlighted in color. Integrations of only the internal standard and organic products provided for simplicity. All integration values are relative to starting **HII** charge (100%).

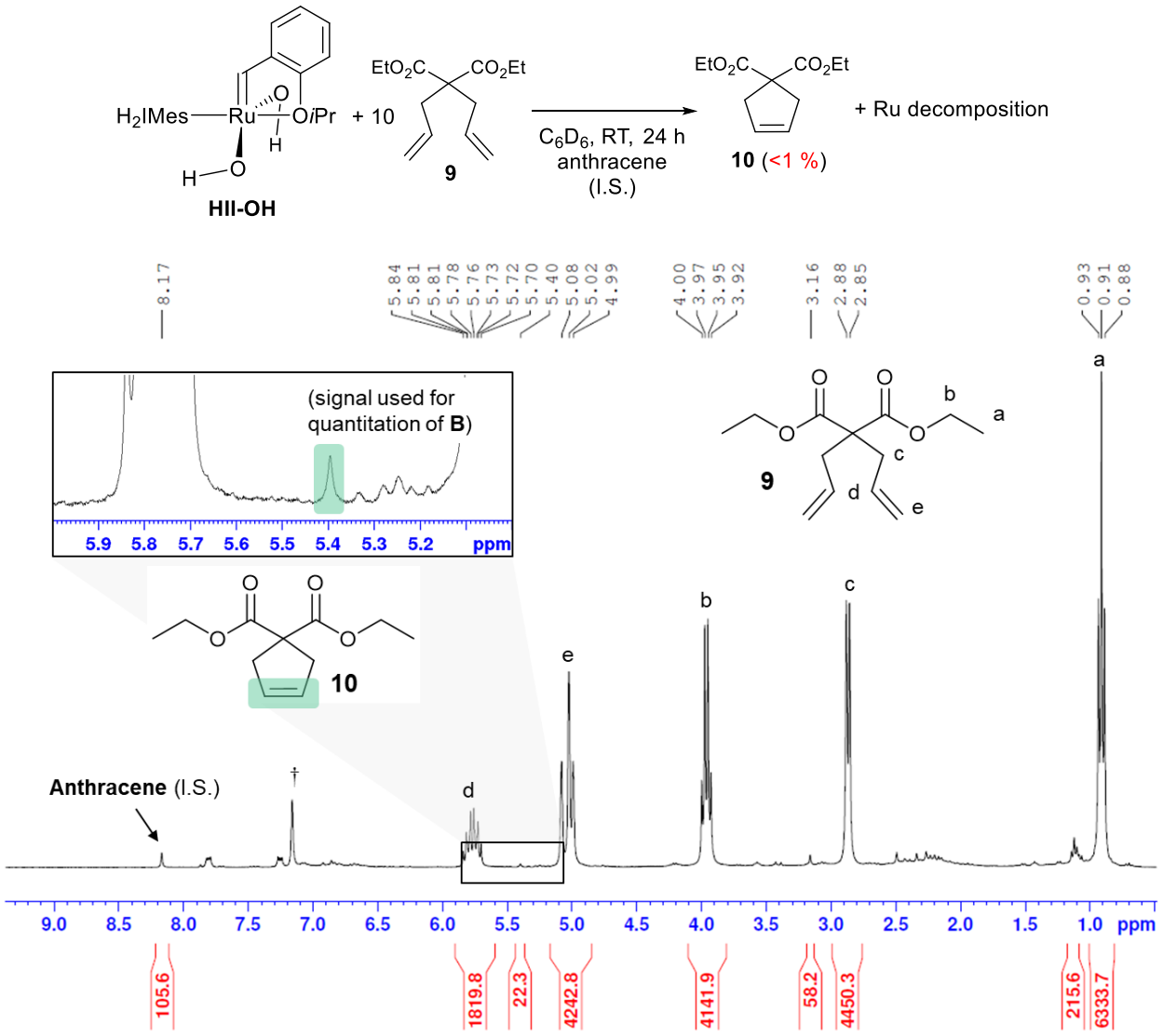

Figure A19. ^{1}H NMR spectrum (C_6D_6, 300 MHz) for the reaction of **HII-OH** with 10 equiv **9** at RT. Spectrum shown is following complete decomposition of **HII-OH** in solution (48 h). Inset shows signal used for integration of RCM products. Only important integrations shown for simplicity. All integrations indicated are relative to starting **HII-OH** charge (100%). The symbol (†) denotes residual C_6D_5H.

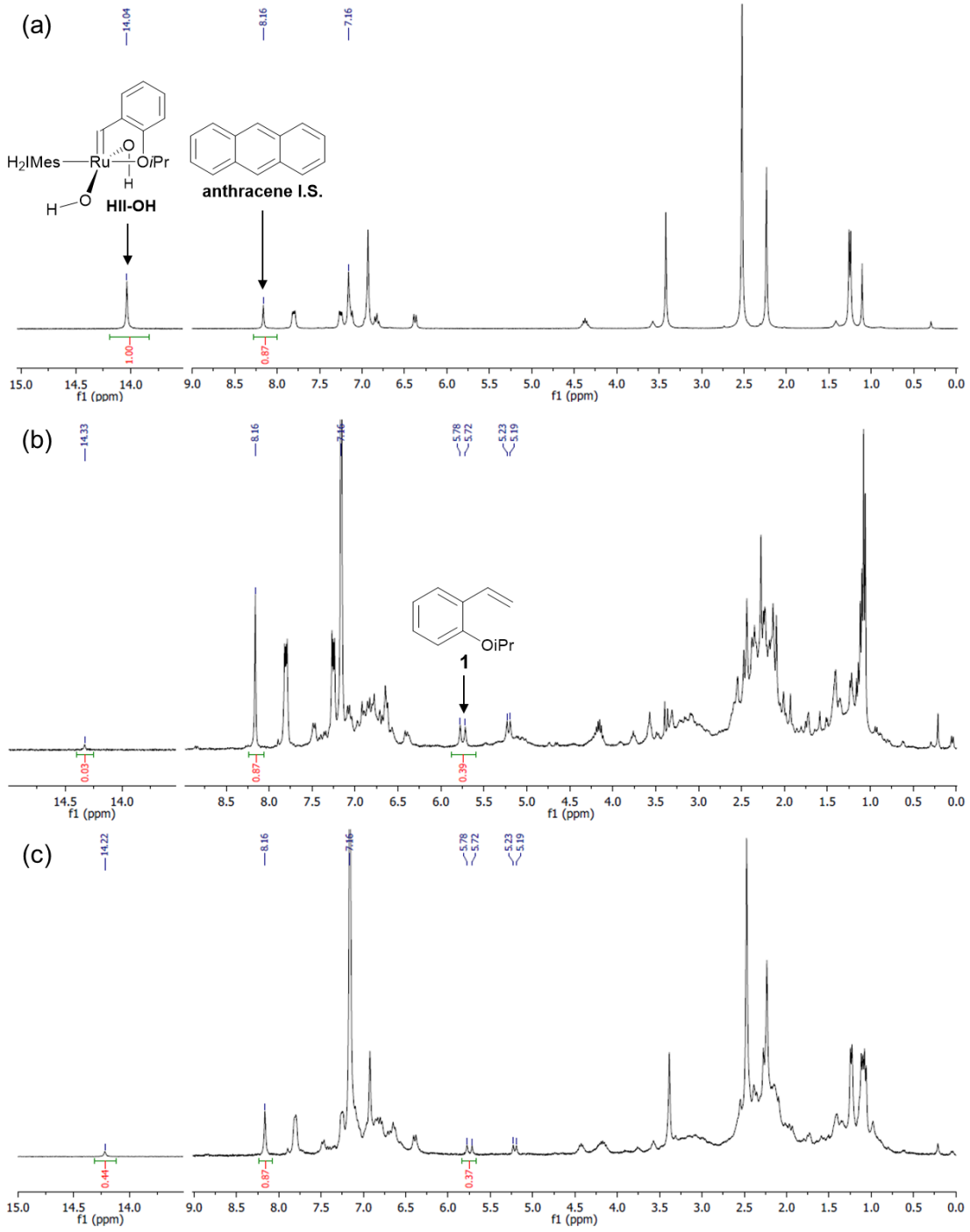

Figure A20. ^{1}H NMR spectra (C_6D_6, 300 MHz) for the autocatalytic decomposition of **HII-OH** at RT. (a) Initial spectrum, before adding C_2H_4 gas. (b) Spectrum following decomposition of **HII-OH** by C_2H_4 (22 hours, after degassing to remove excess C_2H_4 (δ 5.25 ppm). (c) Spectrum after 24 h following addition of fresh **HII-OH** (48 h total reaction time). Only important integrations shown for simplicity.

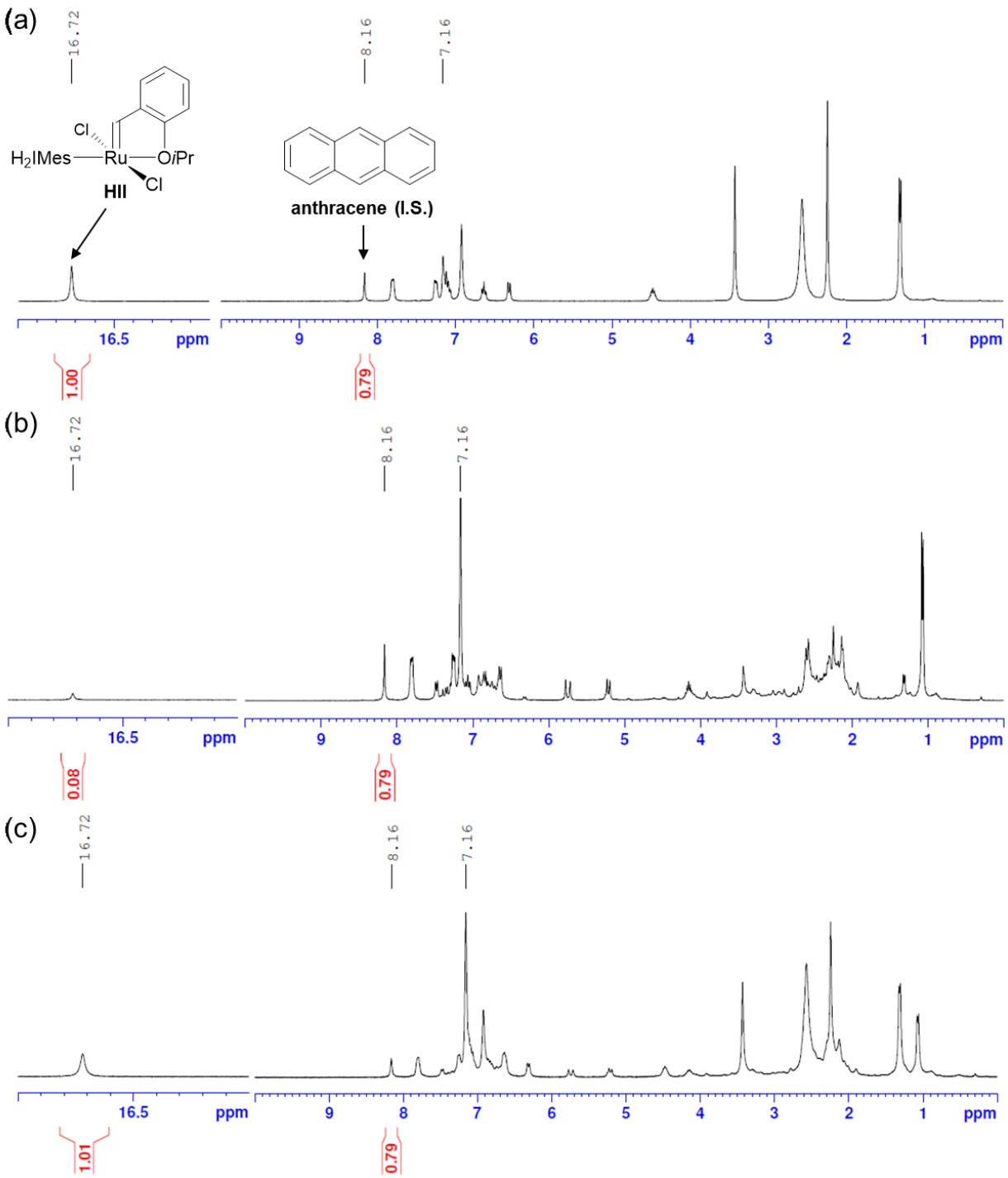

Figure A21. 1H NMR spectra (C6D6, 300 MHz) for the robustness of pristine **HII** in the presence of decomposed **HII**. (a) Initial spectrum, before adding C_2H_4 gas. (b) Spectrum following decomposition **HII** by C_2H_4 (22 hours, after degassing to remove excess C_2H_4 (5.25 ppm). (c) Spectrum after 24 h following addition of pristine **HII** (48 h total reaction time), no decomposition of HII is observed. Only important integrations shown for simplicity.

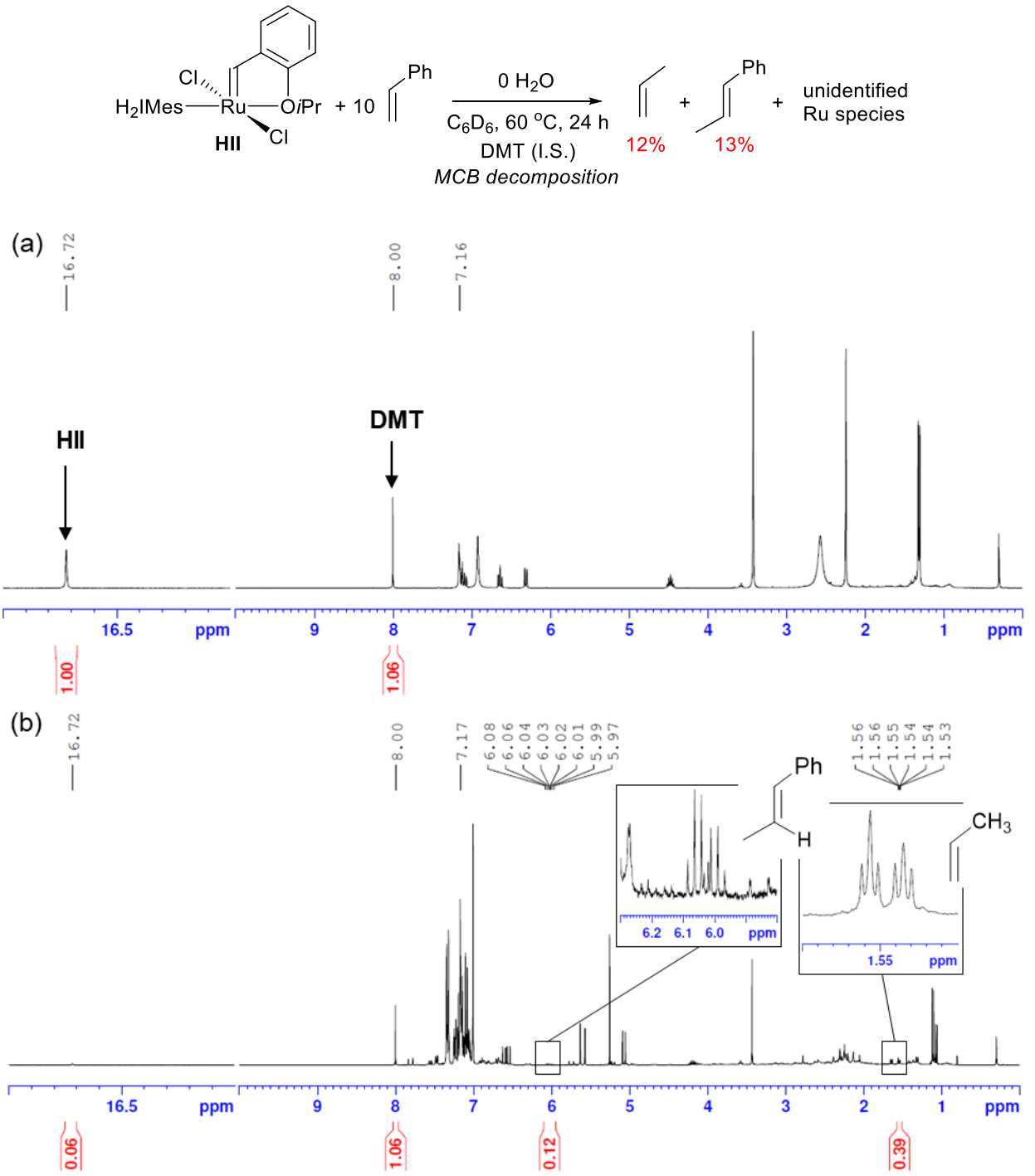

Figure A22. ^{1}H NMR spectra (C_6D_6, 300 MHz) for the reaction between **HII** and styrene at 60 °C without water. (a) Initial spectrum, before adding styrene (b) Spectrum after 24 h reaction. Insets show signals used for integration of organic markers derived from MCB decomposition.

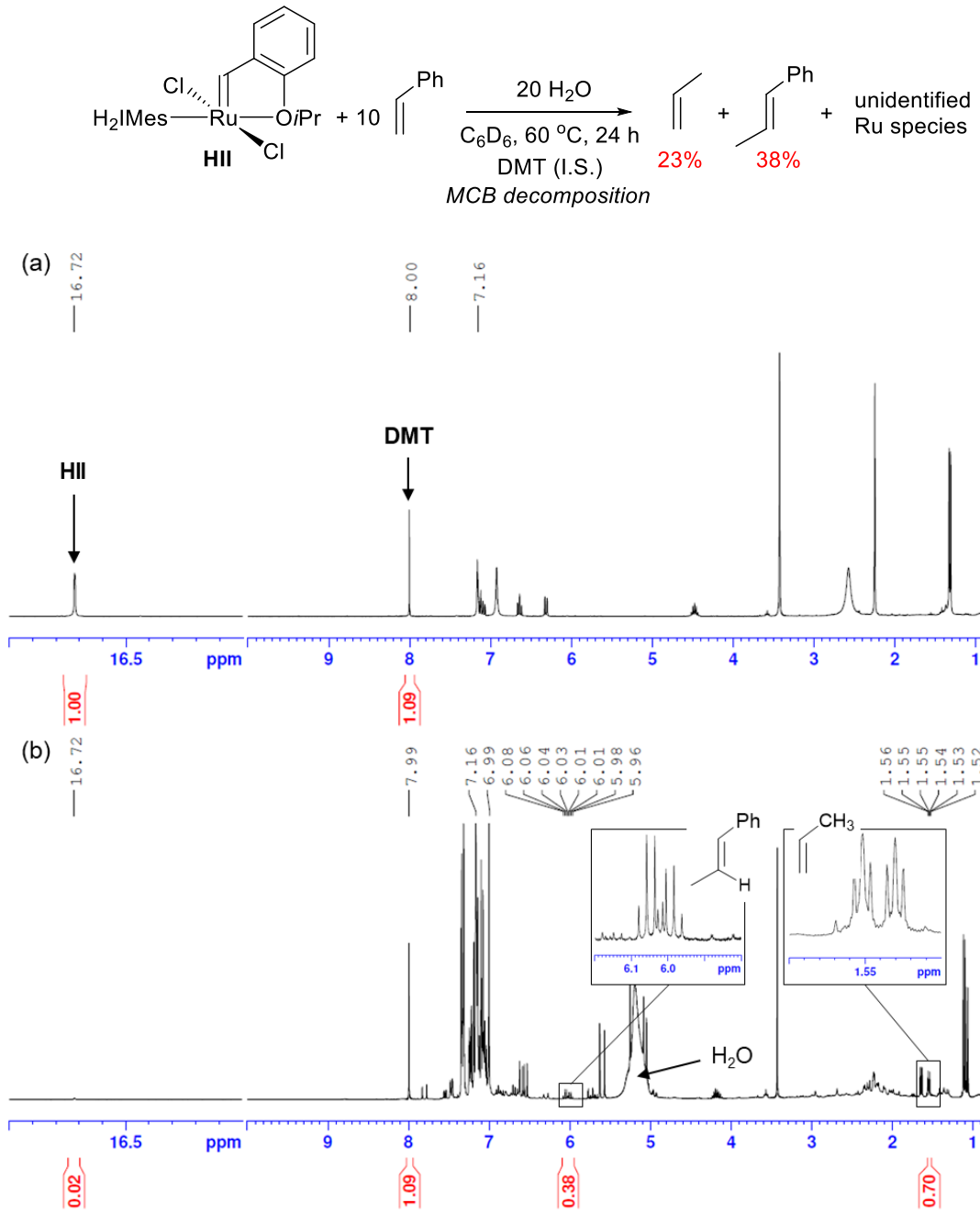

Figure A23. ^{1}H NMR spectra (C_6D_6, 300 MHz) for the reaction between **HII** and styrene at 60 °C with 20 equivalents H_2O added. (a) Initial spectrum, before adding styrene (b) Spectrum after 24 h reaction. Insets show signals used for integration of organic markers derived from MCB decomposition.

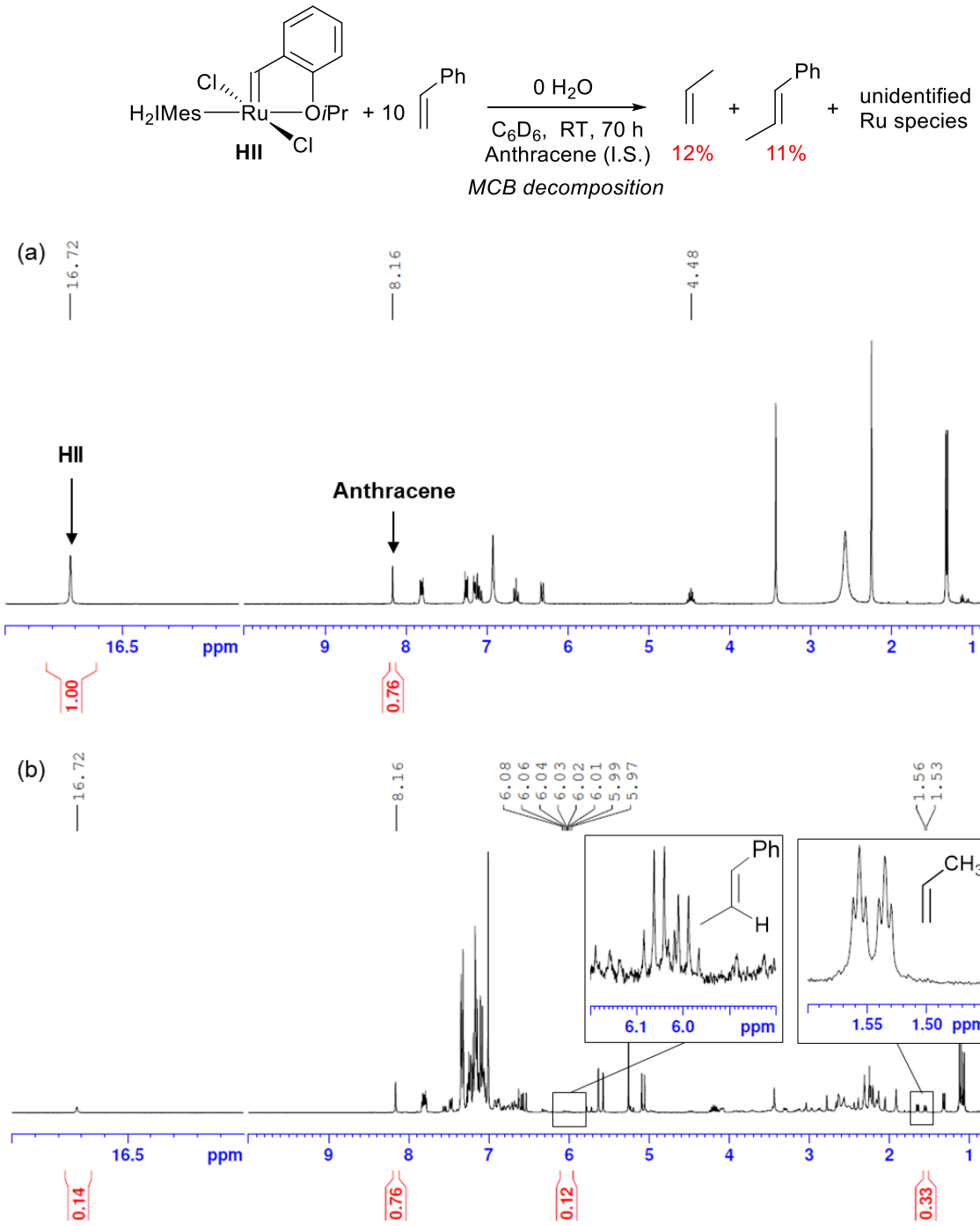

Figure A24. ^{1}H NMR spectra (C_6D_6, 300 MHz) for the reaction between **HII** and styrene at RT without water. (a) Initial spectrum, before adding styrene (b) Spectrum after 70 h reaction. Insets show signals used for integration of organic markers derived from MCB decomposition.

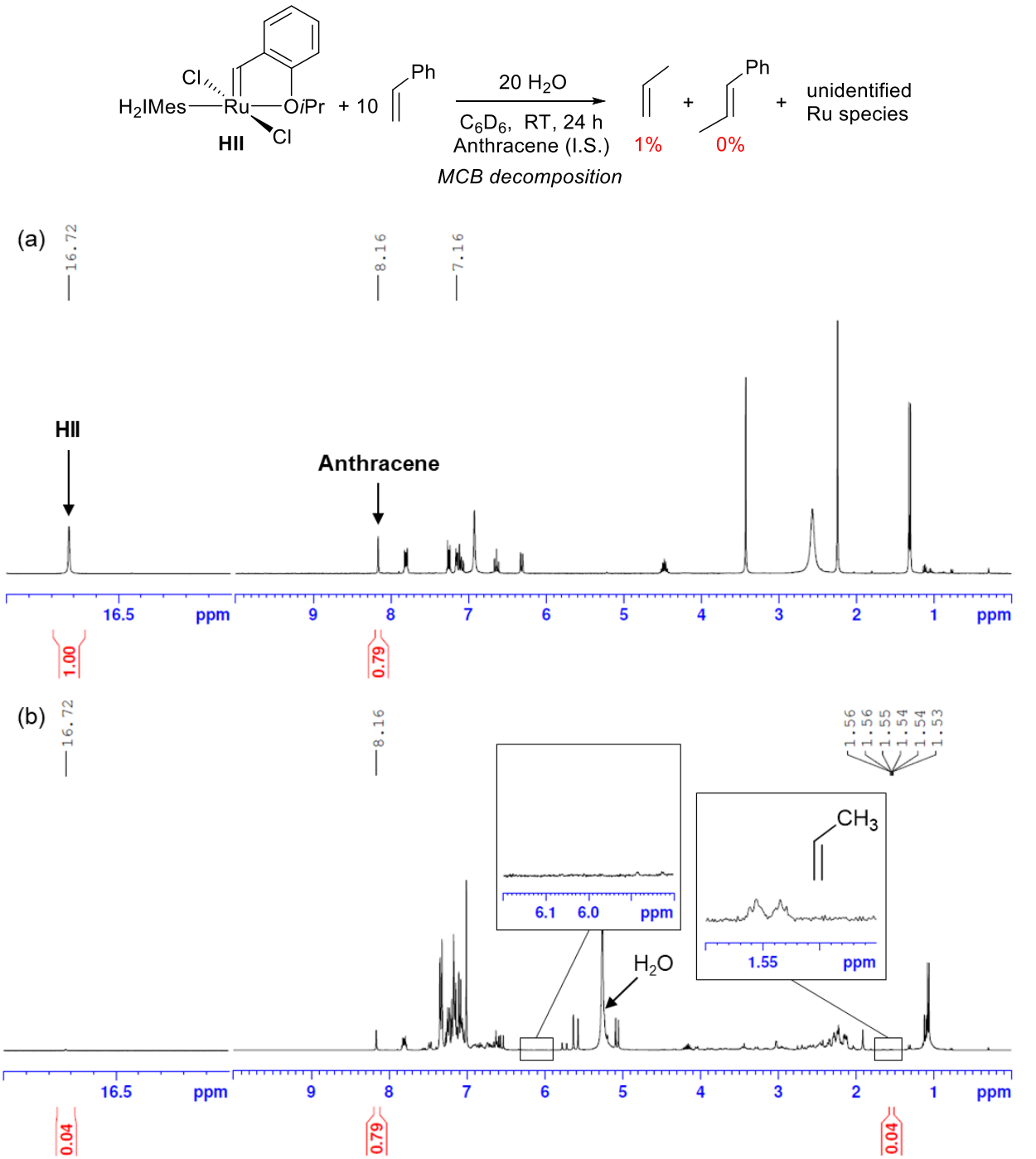

Figure A25. ^{1}H NMR spectra (C_6D_6, 300 MHz) for the reaction between **HII** and styrene at RT with 20 equivalents water. (a) Initial spectrum, before adding styrene (b) Spectrum after 24 h reaction. Left inset shows location where β-methylstyrene would appear. Right inset shows signals used for integration of propene, derived from MCB decomposition.

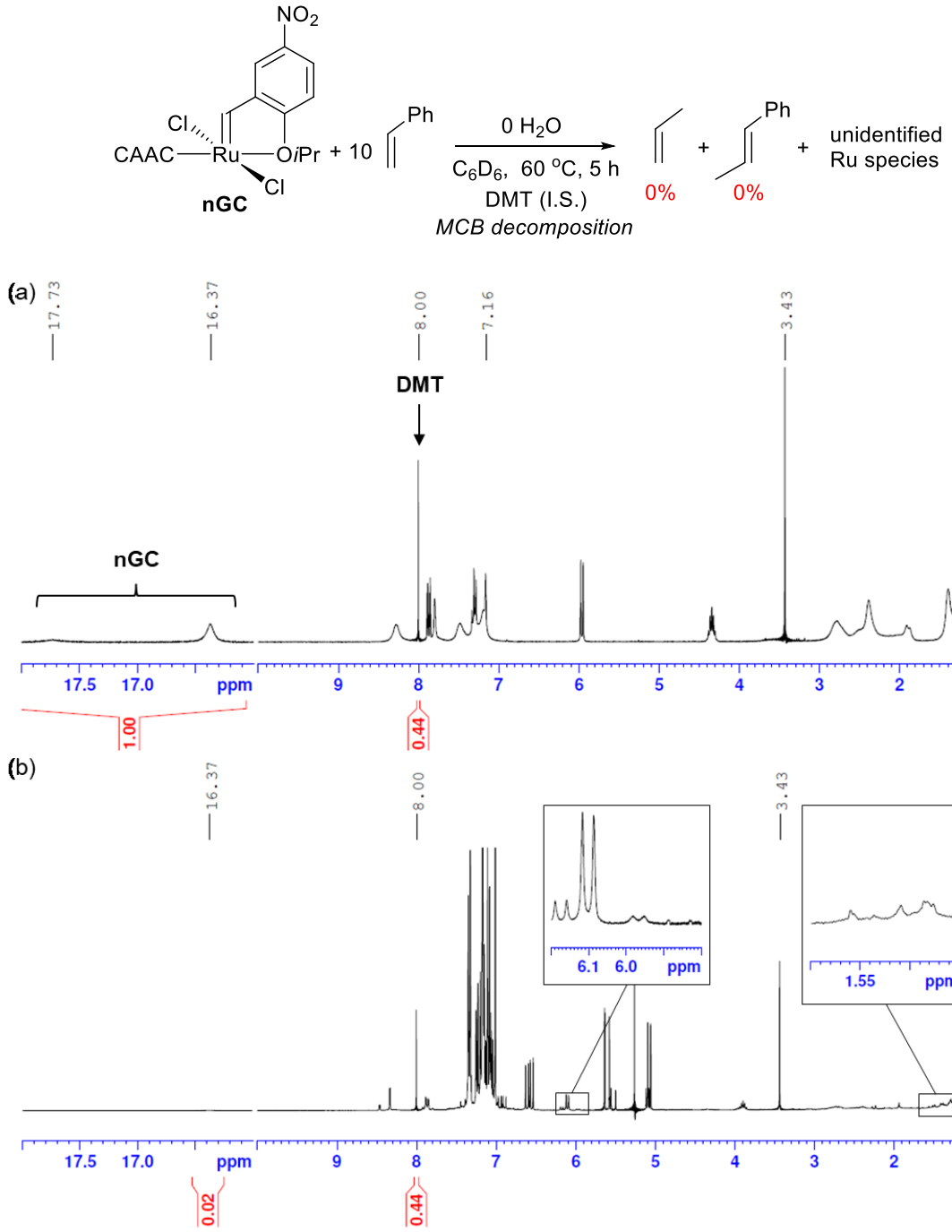

Figure A26. ^{1}H NMR spectra (C_6D_6, 300 MHz) for the reaction between **nGC** and styrene at 60 °C without water. (a) Initial spectrum, before adding styrene (b) Spectrum after 5 h reaction. Both insets show locations where β-methylstyrene and propene markers would appear.

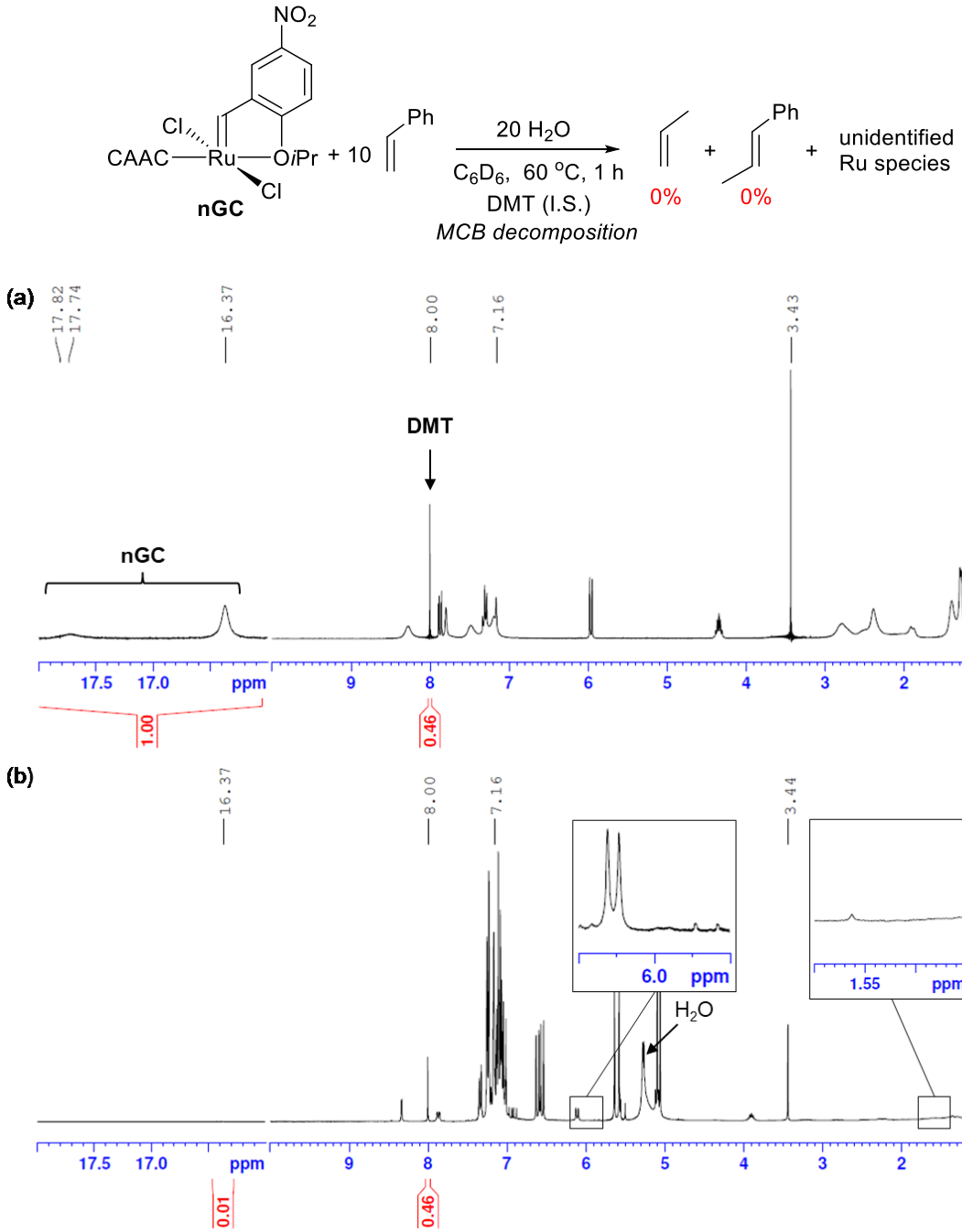

Figure A27. ^{1}H NMR spectra (C_6D_6, 300 MHz) for the reaction between **nGC** and styrene at 60 °C with 20 equivalents of water. (a) Initial spectrum, before adding styrene (b) Spectrum after 5 h reaction. Both insets show locations where β-methylstyrene and propene markers would appear.

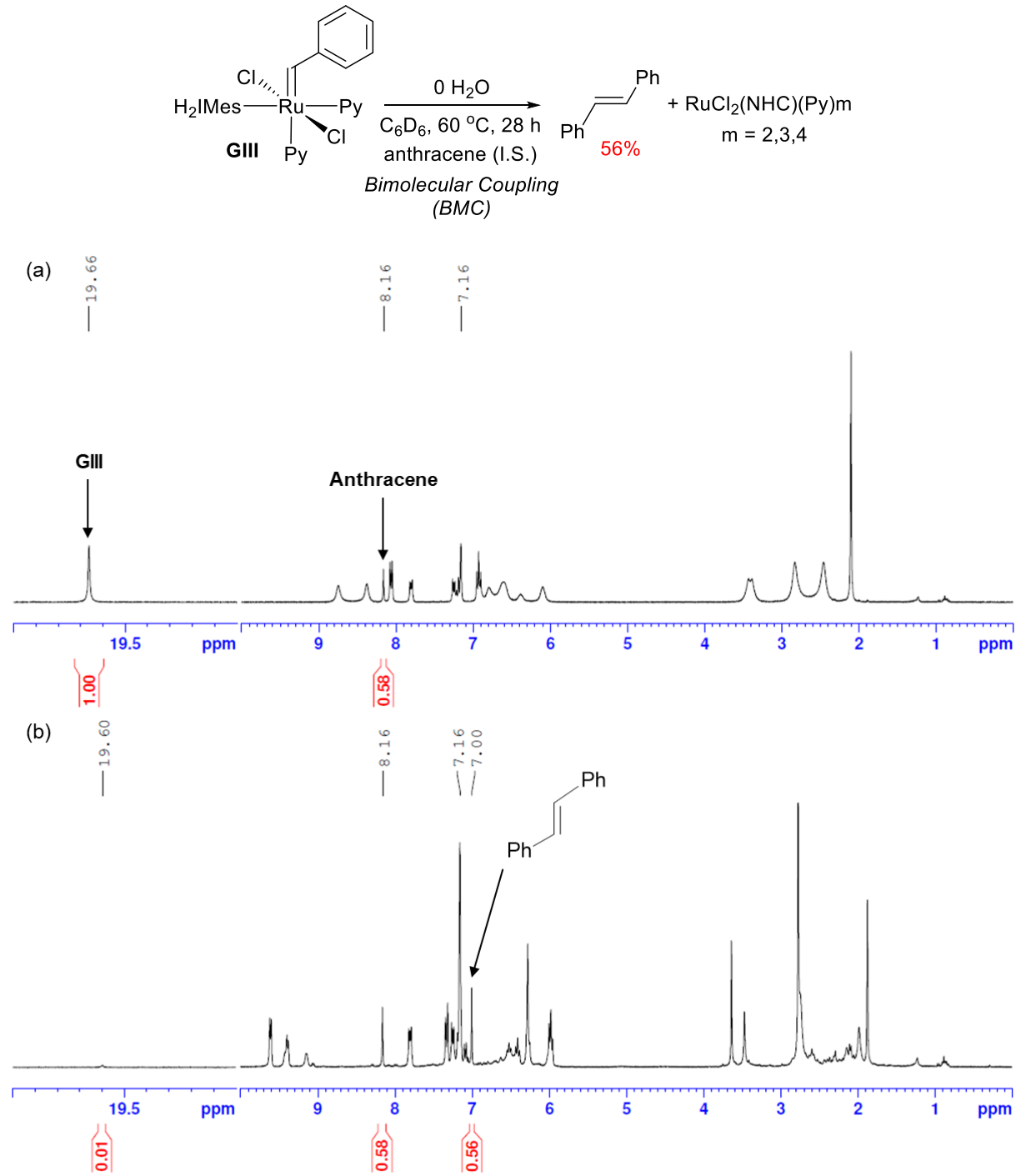

Figure A28. ^{1}H NMR spectra (C_6D_6, 300 MHz) for the thermolysis of **GIII** at 60 °C without water. (a) Initial spectrum, before heating (b) Spectrum after 28 h reaction.

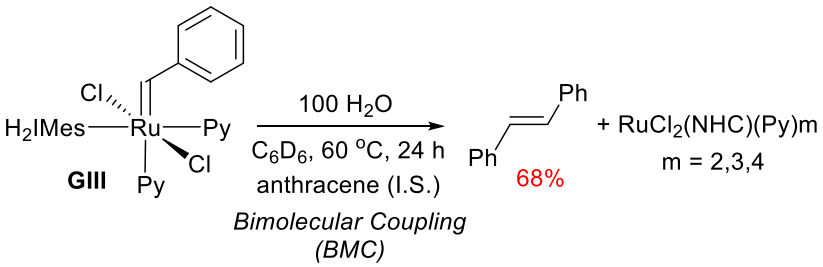

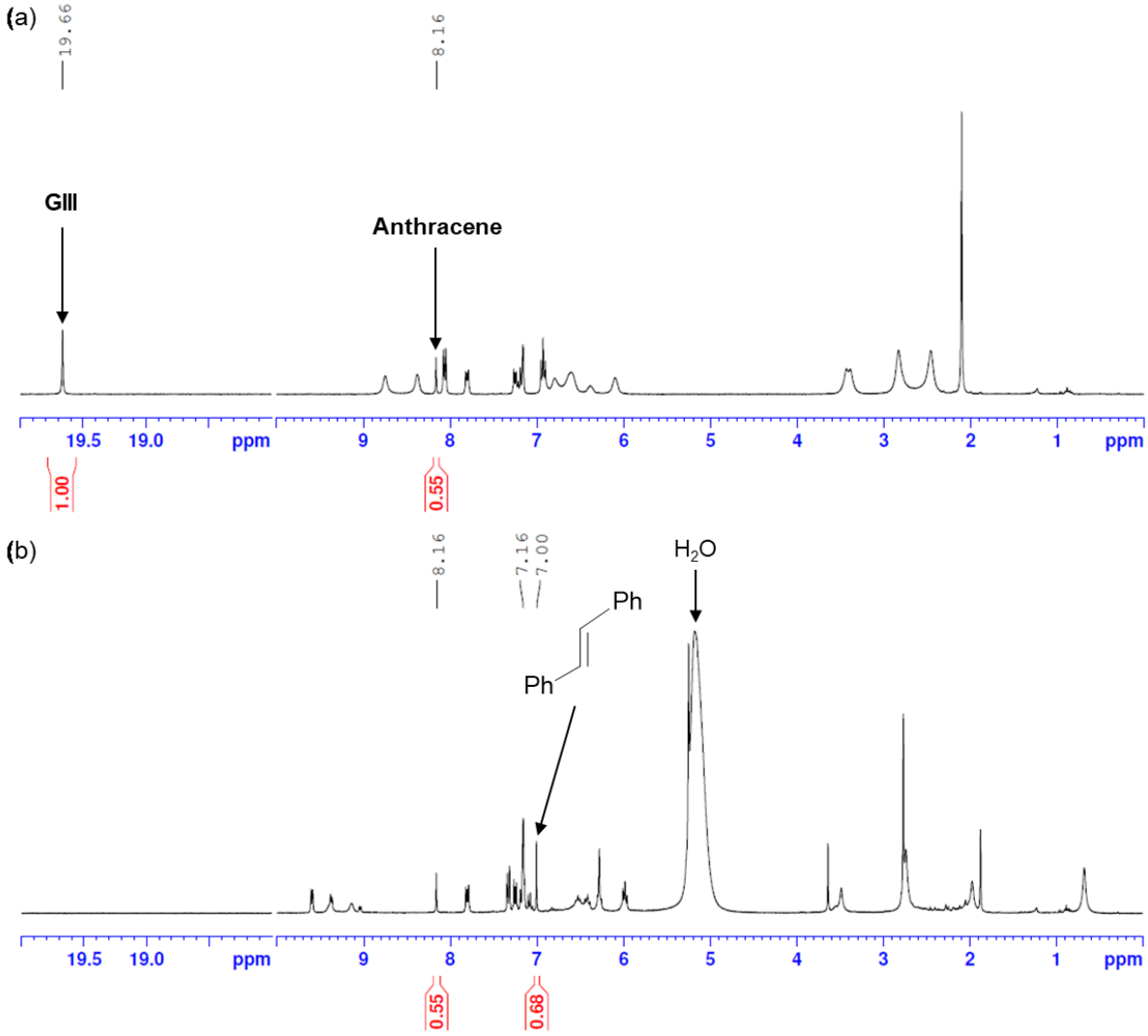

Figure A29. ^{1}H NMR spectra (C_6D_6, 300 MHz) for the thermolysis of **GIII** at 60 °C with 100 equivalents water. (a) Initial spectrum, before heating (b) Spectrum after 24 h reaction.

B. IR Spectra

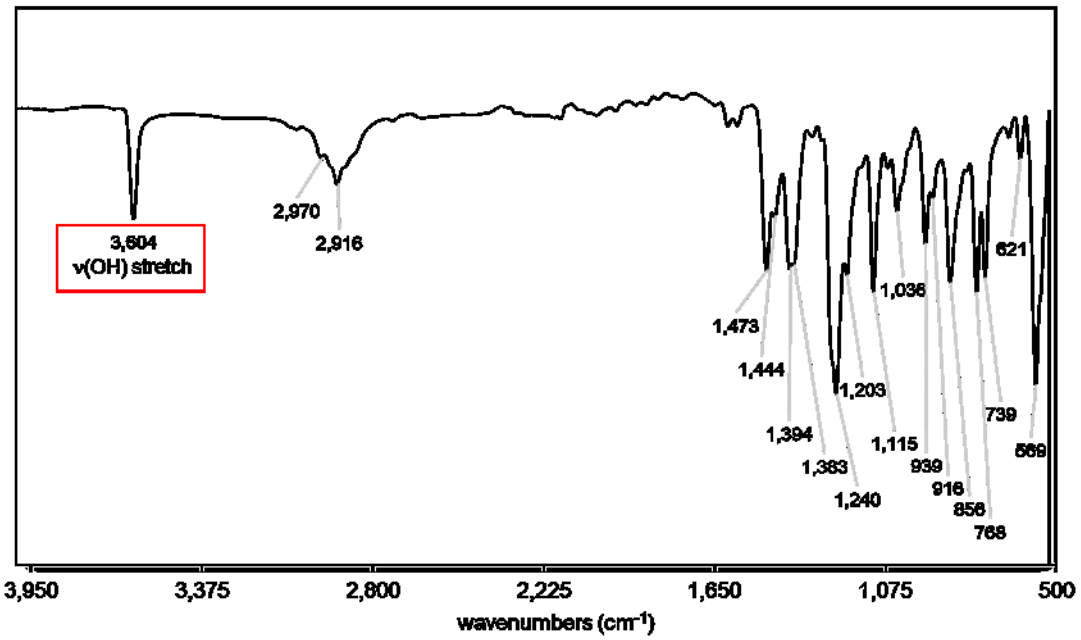

Figure B1. Infrared (IR) spectrum of **HII-OH**. Red box highlights diagnostic ν(OH) stretch at 3604 cm^{-1}.

C. Mass Spectra

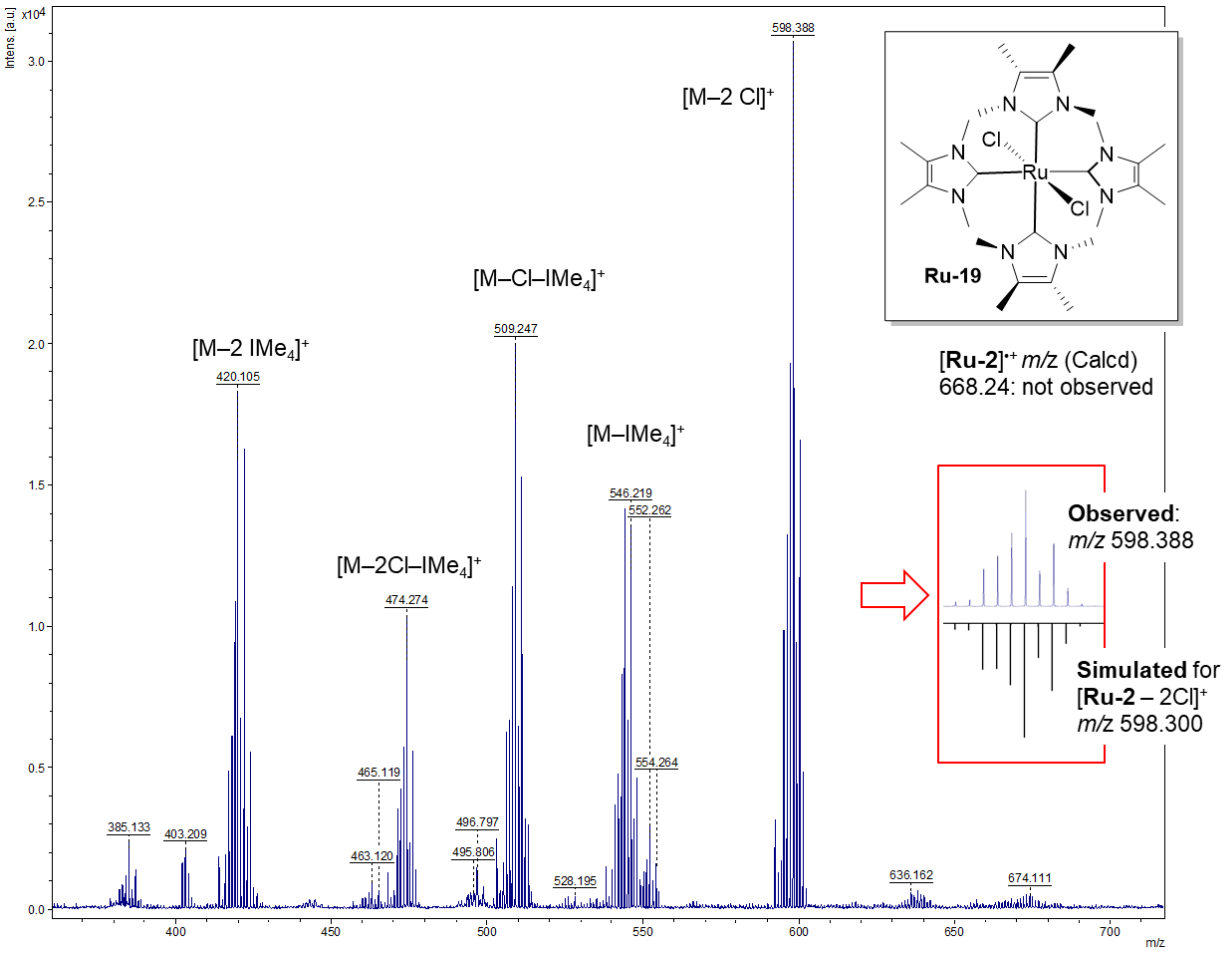

Figure C1. Anaerobic MALDI-TOF mass spectrum (pyrene matrix) of benzene-soluble products from the reaction of GIm with IMe_4 in benzene: evidence for formation of $[RuCl_2(IMe_4)_4]^{\bullet+}$. The molecular ion $[M]^{\bullet+}$ ($C_{28}H_{48}Cl_2N_8Ru$) is not observed.

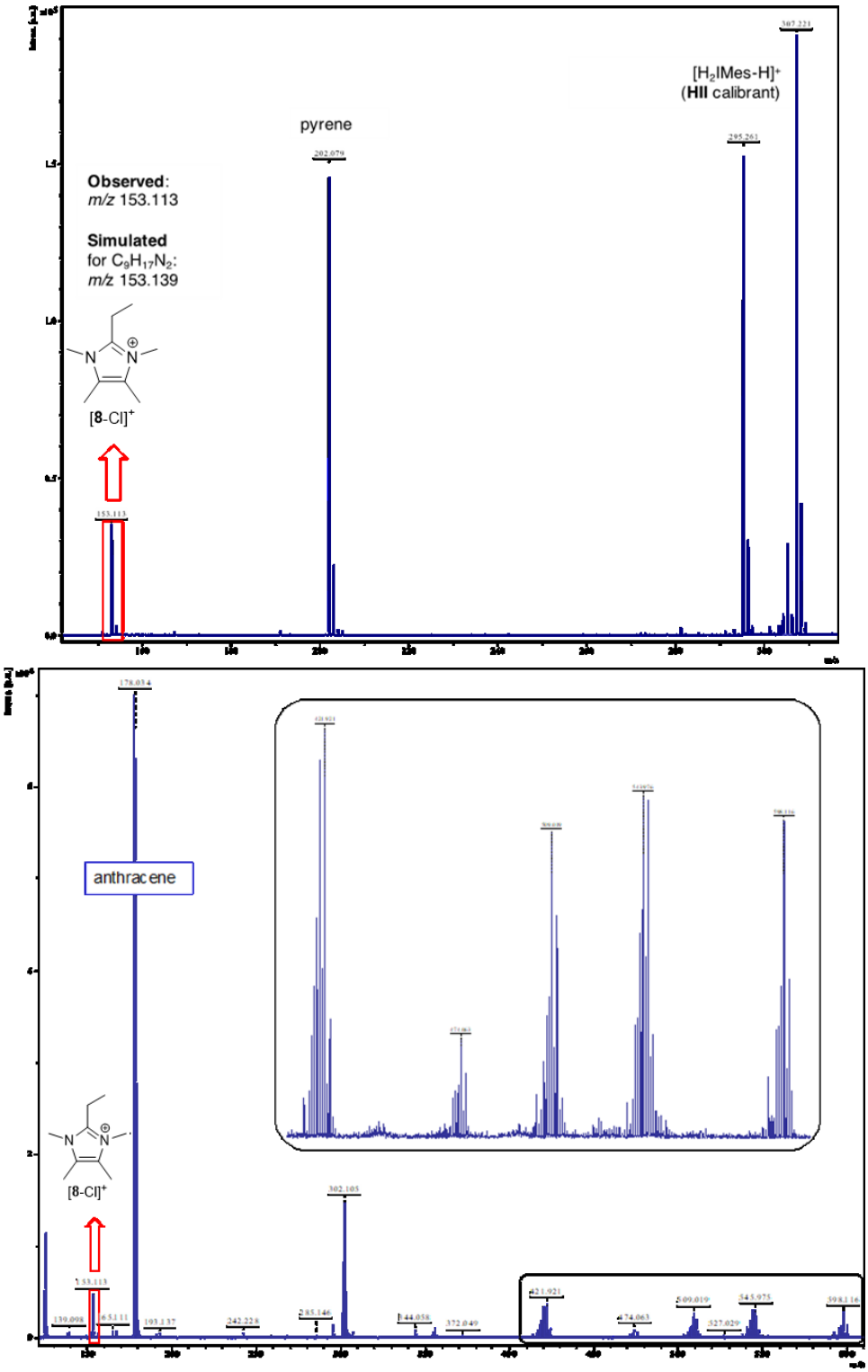

Figure C2. Anaerobic MALDI-TOF mass spectra of precipitate after washing with benzene and hexanes. Top (pyrene matrix; calibration vs **HII**): note signal for the cation $[8–Cl]^+$. Bottom (anthracene matrix; referenced to signal for $[8–Cl]^+$). Inset shows signals for Ru products, including Ru-19: cf. Fig. C1.

D. Computational Studies

D1. Computational Study for Chapter 2

Computational Methods

All density functional theory (DFT) calculations were performed with the Gaussian 09 suite of programs.[1] The computational methods were as described in our recent work,[2] except for a better integration grid, "finegrid" instead of "SG1", being used in the CPHF part of the analytical Hessian calculations and the use of benzene or toluene (vide infra) for the solvation corrections to the final energy (consistent with the experiments). The computational methods are described below.

Geometry Optimization.

Geometry optimization was performed using Head-Gordon's long-range- and dispersion-corrected hybrid density functional ωB97XD[3-5] as implemented in Gaussian 09. This functional was chosen as it provides geometries in good agreement with those from X-ray diffraction for ruthenium olefin metathesis catalysts and other homogeneous catalysts.[6] All atoms but ruthenium were described by Dunning's correlation-consistent valence double-ζ plus polarization basis sets (cc-pVDZ),[7,8] as retrieved from the EMSL basis set exchange database.[9,10] Ruthenium was described with the Stuttgart 28-electron relativistic effective core potential (ECP28MDF retrieved from the Stuttgart/Cologne Group website)[11,12] in combination with the correlation-consistent valence double-ζ plus polarization basis set (cc-pVDZ-PP)[11] retrieved from EMSL basis set exchange database.[9,10] Numerical integration was performed on the "ultrafine" grid. However, since this grid specification in Gaussian 09 defaults to the "SG1" grid for analytical Hessian calculations using the CPHF procedure, we explicitly specified an improved grid ("finegrid") in all analytical Hessian calculations used for vibrational analysis and thermochemical corrections. Before optimization of the geometry, all states were checked for internal instability. Wavefunctions found to be instable were re-optimized to real, spin-restricted or unrestricted solutions for spin singlet or multiplet states, respectively. Next, geometries were optimized using tight convergence criteria (max. force $1.5 \cdot 10^{-5}$ a.u., RMS force $1.0 \cdot 10^{-5}$ a.u., max. force $6.0 \cdot 10^{-5}$ a.u., RMS force $4.0 \cdot 10^{-5}$ a.u.), without symmetry constraints, using default convergence criteria for the self-consistent field (SCF) optimization procedure (RMS change in density matrix $< 1.0 \cdot 10^{-8}$, max. change in density matrix $= 1.0 \cdot 10^{-6}$).

All stationary points were characterized by the eigenvalues of the analytically calculated Hessian matrix, confirming the presence of only one (for transition-states) or no (for minima) imaginary frequencies. As stated above, these analytical Hessian calculations were performed using a better-than-default integration grid (the so-called "finegrid" of Gaussian 09), which usually prevents the curvature artifacts occasionally found with coarser grids.[13] The translational, rotational, and vibrational components of the thermal corrections to enthalpies and Gibbs free energies were calculated within the ideal-gas, rigid-rotor, and harmonic oscillator approximations, except that all frequencies below 100 cm^{-1} were shifted to 100 cm^{-1} when calculating the vibrational component of entropy (i.e. the quasi-harmonic oscillator approximation),[14,15] to prevent asymptotic behavior of the harmonic approximation with very low-frequency modes.

Single-Point Energy Calculations.

All single-point energy calculations were performed with the Gaussian 09 implementation of the generalized gradient approximation functional of Perdew, Burke and Ernzerhof (PBE)[16,17] including Grimme's D3 empirical dispersion term,[18] with revised Becke-Johnson damping (overall labelled PBE-D3M(BJ) for brevity).[19] Ruthenium was described by the ECP28MDF relativistic effective core potential[11] accompanied by a correlation-consistent valence quadruple-ζ plus polarization basis set (ECP28MDF_VQZ)[11] both obtained from the Stuttgart/Cologne Group website. Carbon and hydrogen atoms were described by valence quadruple-ζ plus polarization (EMSL: cc-pVQZ)[9,10] basis sets.[7] All other atoms were described by the valence quadruple-ζ plus polarization augmented with diffuse functions (EMSL: aug-cc-pVQZ),[7,9,10,20] Electrostatic and non-electrostatic solvation effects in benzene or toluene (vide infra) were taken into account by using the polarizable continuum model (PCM) in combination with the "Dis", "Rep", and "Cav" keywords and the built-in program values (dielectric constant, number density, etc.).[21-24] The solute cavity was constructed using the united atom topological model with atomic radii optimized for Hartree−Fock (termed "UAHF").[24-27] Numerical integrations were performed with the "ultrafine" grid of Gaussian 09 and the self-consistent field (SCF) density-based convergence criterion was set to 10^{-5} (RMS change in density matrix < $1.0\cdot10^{-5}$, max. change in density matrix = $1.0\cdot10^{-3}$).

Calculation of Gibbs Free Energies

Gibbs free energies were calculated at 298.15 K or 193.15 K according to equation 1:

$$G^{solvent}_{\text{PBE-D3M(BJ)}} = E^{solvent}_{\text{PBE-D3M(BJ)}} + \Delta G^{\text{T}}_{\varpi\text{B97XD;qh}} + \Delta G^{\text{T}}_{\text{1atm}\rightarrow\text{1M}} \qquad (1)$$

where $E^{solvent}_{\text{PBE-D3M(BJ)}}$ is the potential energies resulting from single-point calculations with PBE-D3M(BJ), including the contributions from the implicit solvation model; $\Delta G^{\text{T}}_{\varpi\text{B97XD;qh}}$ is the thermal correction to the Gibbs free energy calculated at the geometry optimization level with the quasi-harmonic approximation at the given temperature; and $\Delta G^{\text{T}}_{\text{1atm}\rightarrow\text{1M}}$ is the standard state correction corresponding to 1 M solution (but exhibiting infinite-dilution, ideal-gas-like behavior), which is equal to 1.89 kcal mol^{-1} (= RT·ln(24.46)) at room temperature. Tables S1 and S2 report these values, together with the single-point energy calculated at the geometry optimization level ($E^{solvent}_{\text{PBE-D3M(BJ)}}$), and the corresponding Gibbs free energy including thermal corrections from the harmonic approximation at specific temperatures (298.15 K and 193.15 K).

Exploration of the Reaction Network

The computational study focused on seven key potential events: i) ligand exchange, ii) nucleophilic attack of NHC (IMe_4 or H_2IMes) on the methylidene carbon to give $Ru–CH_2–NHC$, iii) coupling of two $Ru=CH_2$ units to give ethylene-containing species, iv) coupling of $Ru=CH_2$ with $Ru–CH_2–IMe_4$, v) nucleophilic attack of IMe_4 on the carbon atoms of Ru–(η^2-ethylene), vi) release of $H_2C=IMe_4$ from $Ru–CH_2–IMe_4$, and vii) nucleophilic attack of $H_2C=IMe_4$ on the

methylidene carbon of **GIm**. Given the presence of both PCy_3 and IMe_4, the number and nature of the dative ligands coordinating the metal center on which some of these events take place are ambiguous. To limit the study to a manageable scope, we sampled specific species along different reaction pathways, and calculated only the most important activation energies.

The reaction network starts with **M1** (Scheme S1), i.e., the experimental reactant **GIm**, which is taken to be the reference point against which all the other free energies are calculated. The dissociation of PCy_3 from **M1** to form 14-electron species **M2** is uphill by 16.4 kcal/mol. While the potential energy surface of this dissociation appears to have no pronounced maximum and a transition-state could not be located, the lower bound for the free energy barrier was estimated by assuming barrier-less coordination of free PCy_3 to **M2**.[28] Within this assumption (in the following referred to as the variational transition-state approximation), the coordination of PCy_3 is controlled by diffusion and typically has a rate constant of ca. $4 \cdot 10^9$ $M^{-1}s^{-1}$ in most solvents,[29] corresponding to a free energy barrier of 4.4 kcal/mol. Thus, the lower bound for the reverse step barrier, i.e., the dissociation of PCy_3 from **M1,** is estimated at 20.8 kcal/mol (TS_{VAR} in Scheme S1).

The small size, relatively planar geometry, and good donor properties of IMe_4 suggest associative or interchange-associative mechanisms for the substitution of PCy_3 by IMe_4 in **M1**. Coordination of IMe_4 to give the coordinatively saturated **M4** requires 21 kcal/mol via transition-state **M3**. However, further dissociation of PCy_3 via transition-state **M5** is more demanding (27.7 kcal/mol above **M1**). Thus, at room temperature, the dissociative substitution of PCy_3 for IMe_4 is preferred over the associative pathway (though see below). The resulting complex **M6** is more stable than **M1** by 8 kcal/mol, and further IMe_4 binding gives the significantly more stable complex **M10**, and ultimately **M11**. The particularly high stability of the tris(IMe_4) species **M11** is a result of IMe_4 being a small and excellent donor ligand.

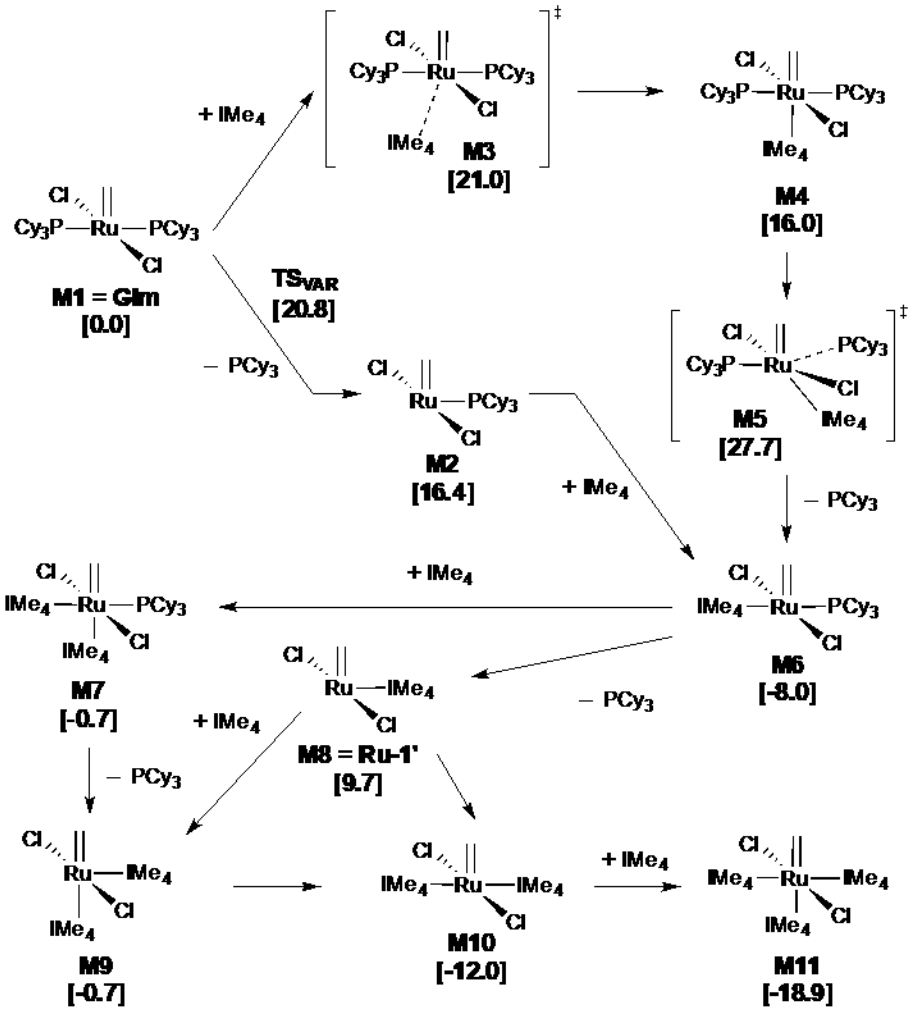

Scheme D1. Free energies (kcal/mol at 298.15K, relative to **M1** = **GIm**) of selected Ru=CH_2 species along ligand exchange pathways.

An alternative to ligand exchange is nucleophilic attack of free IMe_4 on the methylidene carbon of **M1**. The outer-sphere attack of IMe_4 on **M1** via transition-state **M12** corresponds to a barrier of 21.0 kcal/mol (Scheme S2). Notably, the lowest-energy barrier for this reaction mode is obtained for IMe_4-coordinated species to give a 16-electron product (i.e., outer-sphere attack on **M10** via **M20**, inner-sphere migration of IMe_4 onto the methylidene carbon via **M22**, and external nucleophilic attack of IMe_4 on the methylidene ligand of **M6** via **M14**). However, these pathways require complete replacement of the two PCy_3 ligands by three IMe_4 ligands: this in turn requires overcoming an initial barrier of at least 20.8 kcal/mol for loss of the first PCy_3 ligand from **M1**.

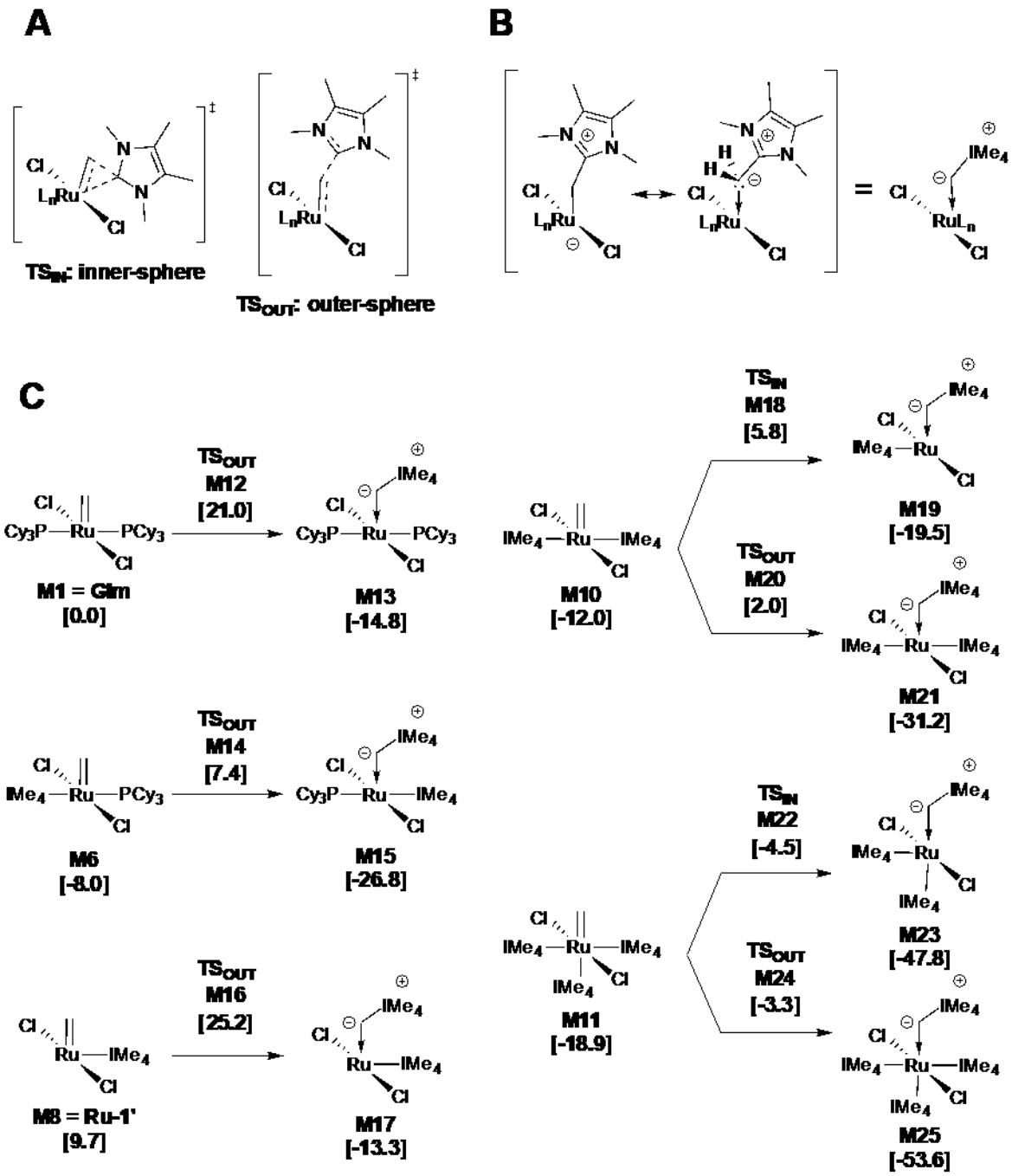

Scheme D2. A. General structures for inner- and outer-sphere nucleophilic attack of IMe_4 on $Ru{=}CH_2$. **B**. Representation of the ligand resulting from attack of IMe_4 on $Ru{=}CH_2$. **C.** Free energies (kcal/mol, relative to **M1** = **GIm**) of selected species along reaction pathways involving attack of IMe_4 on $Ru{=}CH_2$.

The outer-sphere nucleophilic attack on **M1** (via **M12**) and the dissociation of the first PCy_3 from **M1** are competing processes, with similar barriers at room temperature. However, the experimental evidence for immediate reaction at –80 °C (see main text) implies a fast reaction with

a barrier on the order of 15 kcal/mol at that temperature. This is compatible with direct attack of IMe_4 on methylidene via **M12**, but not with dissociation of PCy_3 via **M2** or **M5** (Scheme S3).

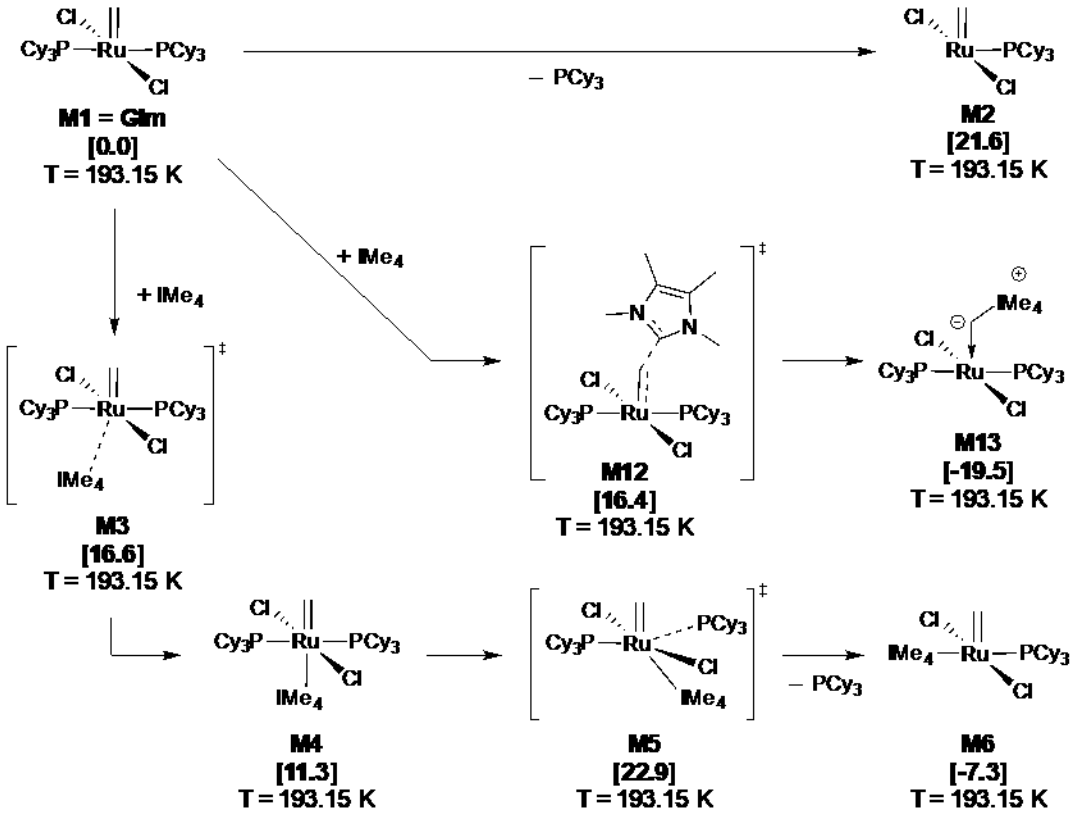

Scheme D3. Selected free energies (kcal/mol, relative to **M1** = **GIm**) calculated at 193.15 K in toluene.

Methylidene complex **M8** (Scheme S2) is the intuitive starting point for bimetallic coupling to form ethylene. This and other possibilities for ethylene formation via bimetallic coupling are explored below. It should be noted, however, that while the thermodynamics of these reactions is favorable, reaching **M8** and other starting points for coupling involves relatively high barriers (>20 kcal/mol) for initial ligand dissociation or exchange. These barriers are again inconsistent with the observed rapidity of reaction at –80 ºC.

Ethylene-containing diruthenium systems (as described in previous calculations)[2,30] can be achieved via Cl-bridging with, e.g., **M6** or **M10**. The most plausible products are shown in Scheme S4. In particular, the methylidene carbon atoms of **M27** (the formal dimer of **M8**) readily form a C–C bond via transition-state **M28** (6.6 kcal/mol above **M1**; barrier only 3.2 kcal/mol from **M27**). Cleavage of the chloride bridges and coordination of further IMe_4 would yield the monometallic complex tetrakis-IMe_4 **M29** and the η^2-ethylene complex **M30**.

Addition of one IMe_4 ligand to the Ru center that donates its methylidene π-electrons to the second Ru (see **M27**) is thermodynamically favorable, with the resulting complex **M34** at -22.4 kcal/mol relative to **M1**. Importantly, the presence of the additional IMe_4 breaks the π-component of the

$Ru{=}CH_2$ bond and forms a $Ru–CH_2–Ru$ bridge. The activation energy of C–C bond formation from **M34**, via transition-state **M35**, is almost 6 kcal/mol higher than between the methylidenes (via **M28**), but is still facile. Thus, the additional IMe_4 stabilizes the overall pathway, but does not give a lower barrier for coupling. Alternative combinations of phosphine and IMe_4 ligands in the bimetallic system have not been explored given the lower stability (with respect to **M34**) of sampled bimetallic, methylidene-containing intermediates **M26**, **M31, M32**, **M33**.

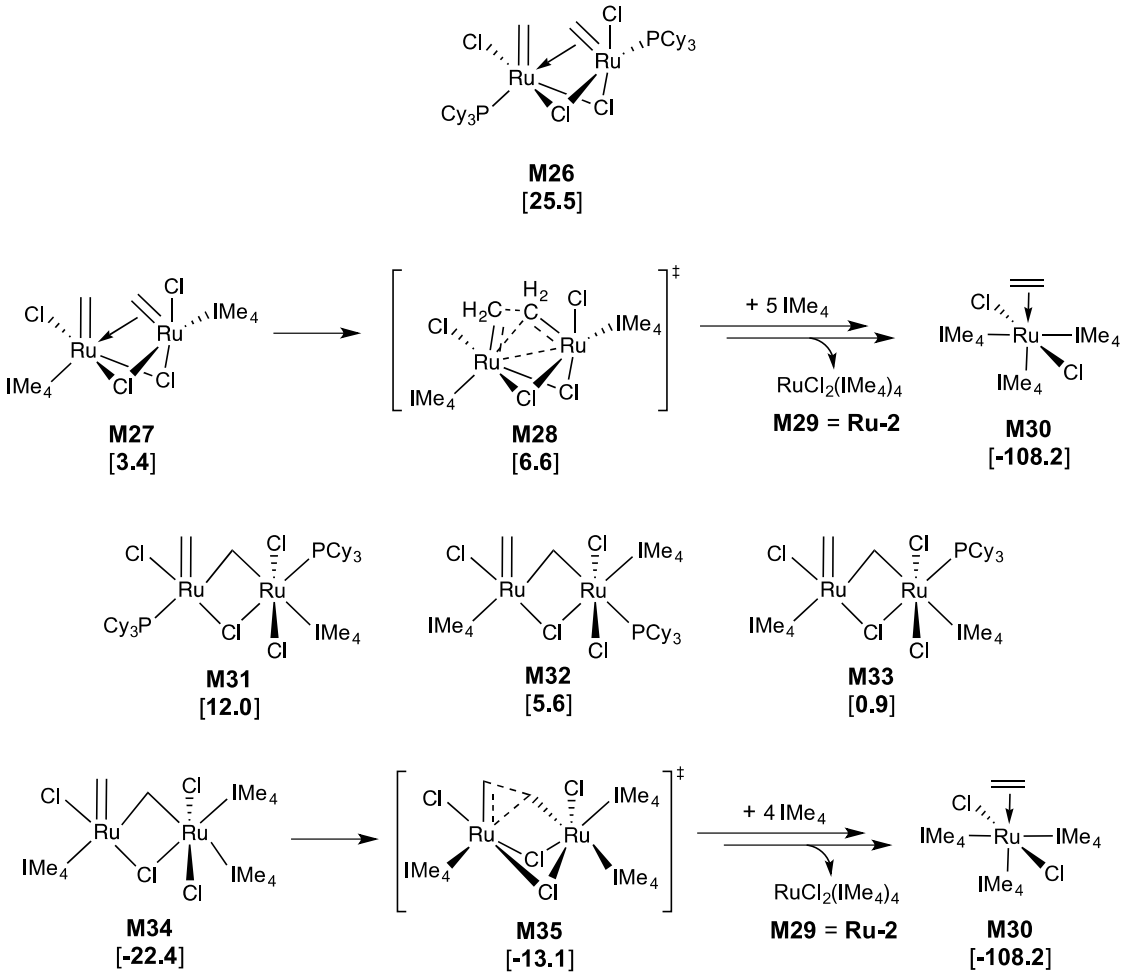

Scheme D4. Free energies (kcal/mol relative to **M1** = **GIm**) of bimetallic, methylidene-derived species and monometallic products resulting from coupling of methylidene complexes.

Liberation of ethylimidazolium salt **A** from an ethylene-bound complex requires attack of IMe_4 on the ethylene, followed by abstraction of a proton from an as-yet unidentified partner (likely a PCy_3 or IMe_4 ligand: see below). The attack on Ru-coordinated ethylene complexes is explored in Scheme S5. Again, we considered both outer- and inner-sphere possibilities with different numbers of IMe_4 ligands. In light of the much higher stability calculated for IMe_4 vs PCy_3 complexes (see the preceding schemes), the discussion below focuses on the former.

The activation energy for attack of IMe_4 on ethylene is in the range 14–28 kcal/mol (Scheme S5), vs 14–18 kcal/mol for attack on methylidene (Scheme S2). Thus, as an elementary step, attack on

ethylene is more demanding than attack on methylidene, and the lowest activation energy for the single step is estimated for the inner-sphere mechanism via **M45**. However, the excellent coordinating properties of IMe_4 justify the equilibration of the Ru(η^2-ethylene) species in Scheme S5 with the η^2-ethylene complex **M30** as the key intermediate. From there, inner-sphere (**M51**) vs outer-sphere (**M52**) attack differs by less than 2 kcal/mol, and represent the highest activation energy (e.g., 26.4 kcal/mol from **M30** to **M51**) encountered in starting from **M1** and proceeding through dissociative exchange of the first PCy_3 and bimolecular coupling. The result of this path, upon saturation of **M50** with IMe_4, is **M53**. This species is thermodynamically unstable with respect to **M30** where ethylene is intact but coordinated, and should evolve via protonation to finally release the ethylimidazolium salt.

The same endpoint – that is, $Ru(IMe_4)_4$ and $Ru–CH_2–CH_2–IMe_4$ (**M29** and **M53**, respectively) – can be reached by coupling the $Ru–CH_2–IMe_4$ ligand with a methylidene unit in the **M6**, **M10**, **M11** series (Scheme S6). Notably, the key feature of the bimetallic clusters prior to C–C bond formation (Scheme S4) is donation of π-electrons from a $Ru=CH_2$ to a vacant d-orbital of another Ru complex,[2] possibly followed by evolution of the π-donating methylidene into a methylene bridge. The same interaction can be realized between a $Ru=CH_2$ and a $Ru–CH_2–IMe_4$ center with a vacant site, such as **M17**. Formation of the bimetallic system is not expected to occur via association of the two monomers, i.e., **M8** and **M17**, but via gradual replacement of dative ligands from more stable intermediates. Among the resulting bimetallic complexes, **M56** is only ca. 6 kcal/mol less stable than **M25**, and can lead to formation of the C–C bond via insertion of the methylene bridge into the $Ru–CH_2IMe_4$ bond. This gives the $Ru–CH_2–CH_2–IMe_4$ skeleton and an unsaturated Ru center that can easily coordinate IMe_4, thus initiating rupture of the bimetallic cluster which can then evolve into **M29** and **M53**.

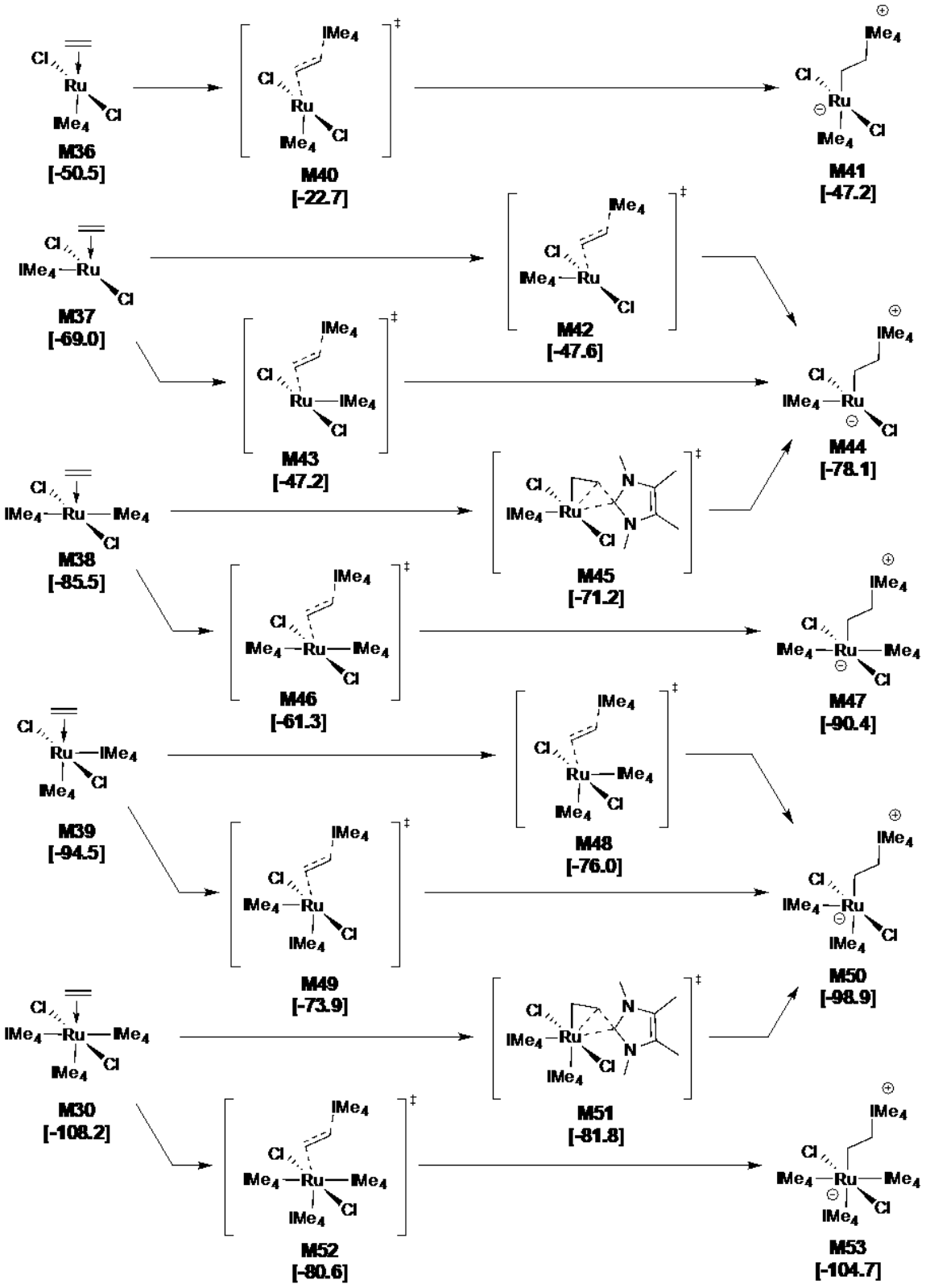

Scheme D5. Free energies (kcal/mol relative to **M1** = **GIm**) of selected species along reaction pathways involving attack of IMe_4 on Ru-bound ethylene.

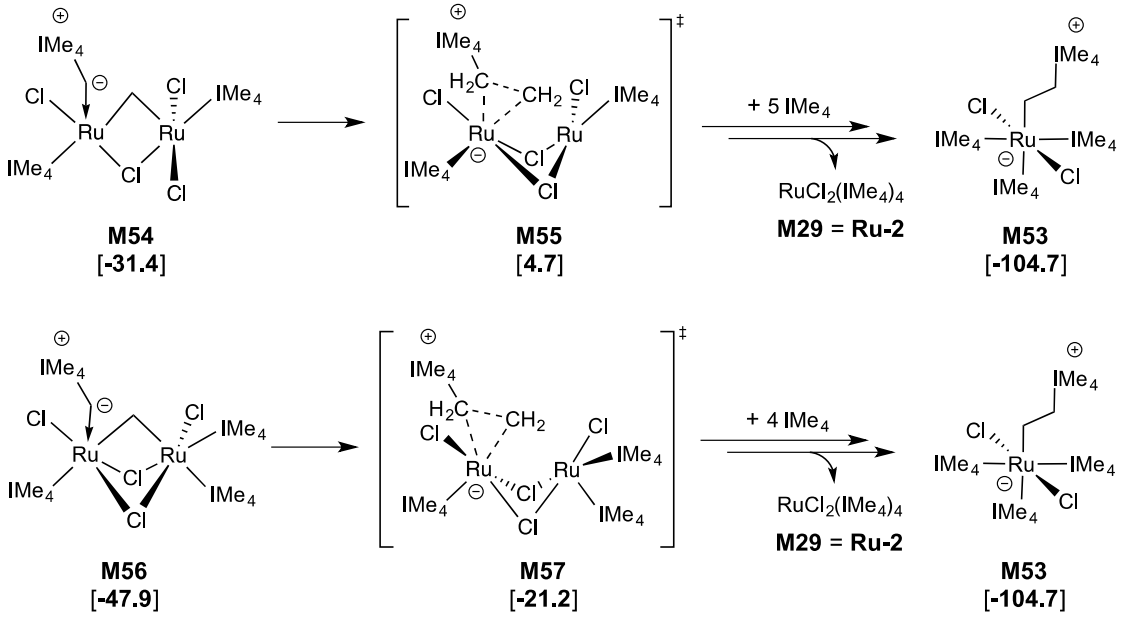

Scheme D6. Free energies (kcal/mol relative to **M1** = **GIm**) of selected species along reaction pathways involving coupling of methylidene and methylimidazolium ligands.

The barrier from **M25** to **M57**, the lowest-energy transition-state found for C–C bond formation between Ru–CH_2–IMe_4 and Ru=CH_2, is 32.4 kcal/mol, significantly higher than the 26.4 kcal/mol barrier for generation of **M53** via **M30**. In both cases, substantial energy is released on forming the intermediates **M29** and **M25** or **M30** (53.6 and 108.2 kcal/mol, respectively). The resulting thermal excitation of the system could be sufficient to overcome the barrier to pass via **M57**, but this effect would be more substantial for **M51** because of the higher-energy release (108 vs 54 kcal/mol) and the lower activation energy for **M51** than **M57**.

Summary of the Most Favorable Reaction Pathways

To summarize, the calculations are consistent with initial attack of IMe_4 on methylidene complex **M1**, over ligand exchange followed by formation of bimetallic species containing two Ru=CH_2 groups. Nucleophilic attack on **M1** is compatible with the experimental observation of fast reaction at –80 °C (see main text). However, formation of the C–C bond via coupling of the Ru–CH_2–IMe_4 and Ru=CH_2 species in **M57** is very demanding even at room temperature (32.4 kcal/mol), and the 38 kcal/mol barrier at low temperature (Table S2) cannot be reconciled with the experimental findings.

An alternative reaction for the Ru–CH_2–IMe_4 species can be identified, considering the nature of this functional group (see Scheme S7). The imidazolium ring changes the nature of the Ru-coordinating carbon atom, such that the total neutral fragment behaves as an *N*-heterocyclic olefin (NHO). This activated olefin is known to coordinate transition-metals as a two-electron σ-donor.[31] However, the decoordination of the NHO ligand **M59** from **M13** requires too much energy via transition-state **M58**. This pathway leads to **M60**, which is not the lowest energy model for the resulting tetra-coordinate Ru(II) species. Model **M61** and, in particular, the spin triplet **M62** are

significantly more stable than **M60**, which suggests the existence of other, yet to be investigated dissociation pathways, possibly involving the spin triplet surface.

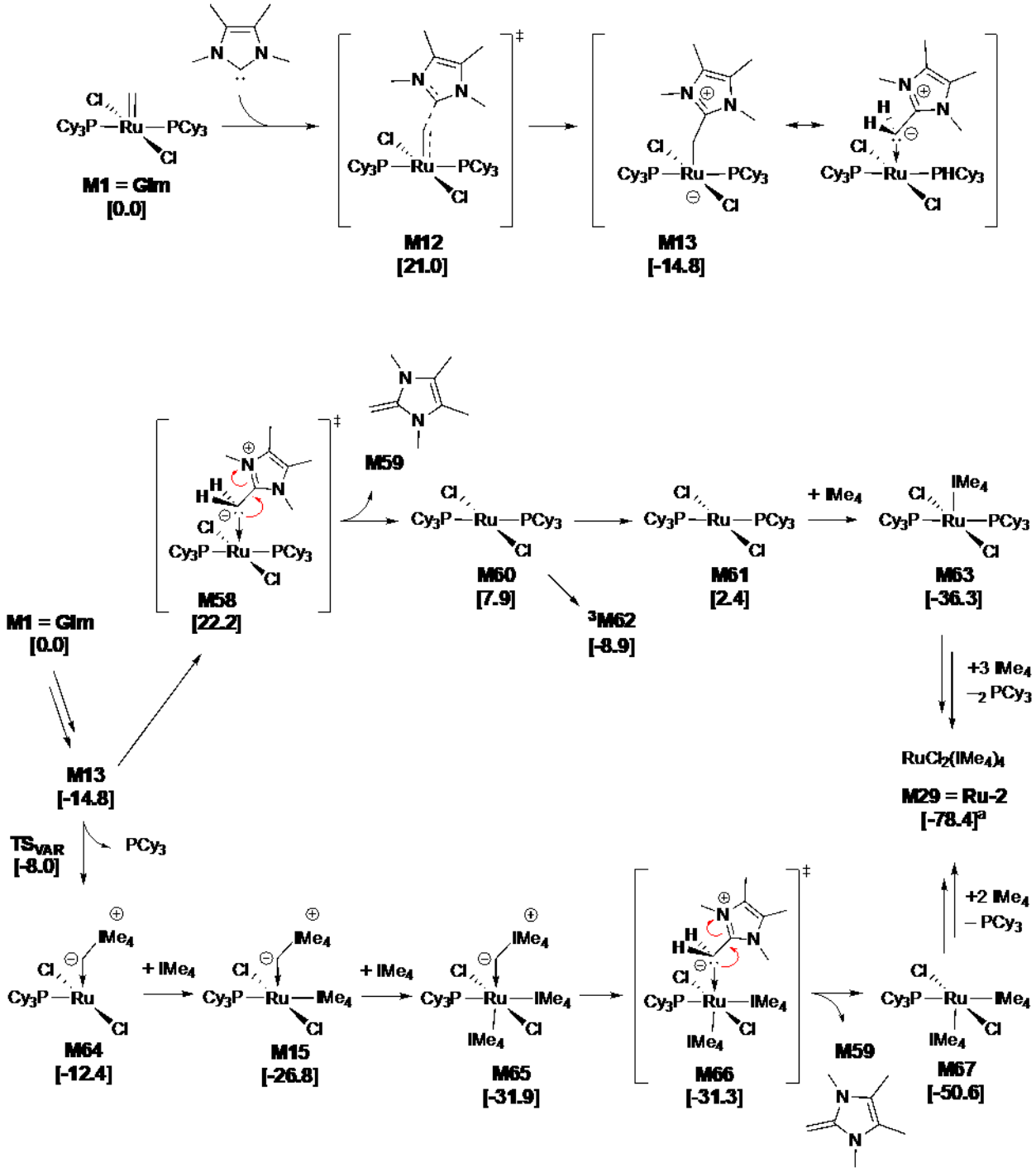

Scheme D7. Free energies (kcal/mol relative to **M1** = **GIm**) of selected species along reaction pathways involving release of *N*-heterocyclic olefin **M59**. [a] Free energy resulting from production of **M59** and **M29**.

Still, the dissociation of the NHO ligand requires significantly more energy than the competing dissociation of PCy_3 from **M13**. For the latter, the variational approximation estimates a lower bound free-energy barrier of ca. 7 kcal/mol to form the four-coordinate minimum **M64**, which can coordinate IMe_4 to form **M15**. The small size and excellent donor properties of IMe_4 permit further uptake of IMe_4 to form the 18-electron complex **M65**, which is even more stable than **M15**. From **M65** the release of **M59** requires less than 1 kcal/mol via transition-state **M66**, and is thermodynamically favored thanks to the stability of the 16-electron **M67**. The latter should bind further IMe_4 and release PCy_3 to yield **M29** and free PCy_3, both of which are observed experimentally.

NHO **M59** is a nucleophile, and its attack on the methylidene carbon of **M1** has a barrier (18 kcal/mol) lower than attack by the free IMe_4 carbene (i.e., 21 kcal/mol at **M12**). The resulting ethylimidazolium-coordinated center **M69** is slightly unstable with respect to **M1**, and its ethylimidazolium ligand is a true alkyl ligand, not a dative NHO ligand. The strong basicity of the alkyl ligand in ethylimidaziolium species such as **M69** precludes the simple decoordination seen for **M65**. Instead, given the experimental evidence for substantial amounts of free PCy_3, we expect that dissociation of PCy_3 gives **M70**, and eventually **M71**, which allows liberation of the ethylimidazolium chloride by protonolysis involving activation of a C–H bond in either PCy_3 or IMe_4.

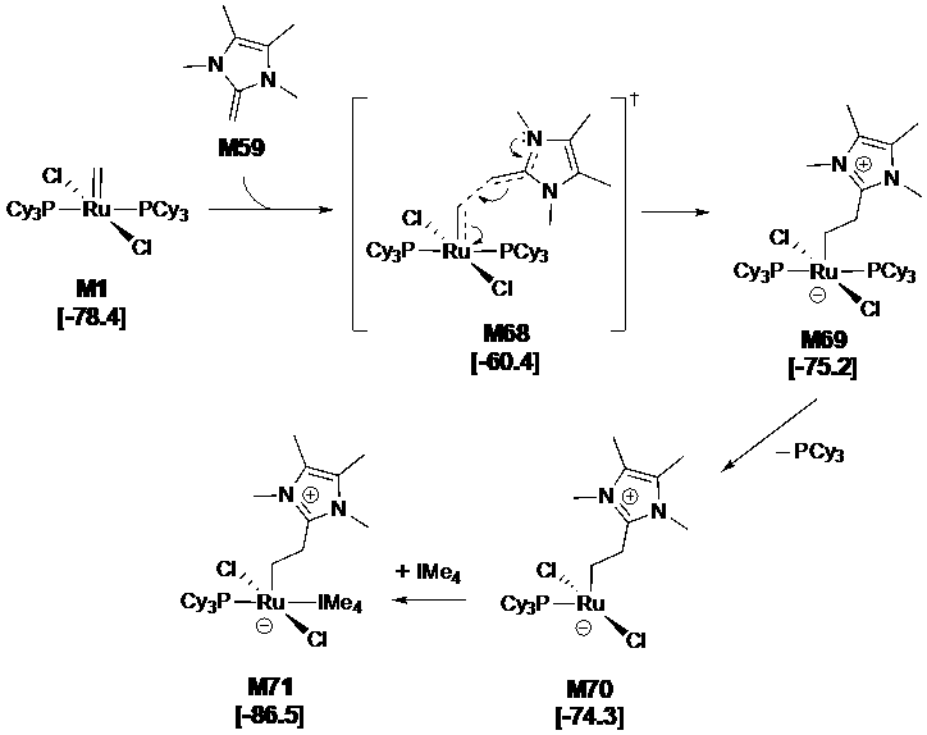

Scheme D8. Free energies (kcal/mol relative to the initial **M1** = **GIm** that generated **M59**; see Scheme S7) of selected species along the reaction path describing the attack of *N*-heterocyclic olefin on methylidene.

Finally, to explore the influence of steric bulk on the key nucleophilic attack on the Ru methylidene, we examined nucleophilic attack by H_2IMes on the methylidene carbon of **M1** (Scheme S9). H_2IMes is substantially more sterically demanding than IMe_4. The molecular model of the product resulting from nucleophilic attack (**M72**) reveals significant geometric strain, in particular bending of the bond angle around the N atoms of the H_2IMes fragment, and partial displacement of a PCy_3 ligand (the Ru–P bond distances are 2.34 Å and 2.68 Å). This strain explains the instability of **M72** with respect to **M1**, a striking contrast to the product (**M13**, -14.8 kcal/mol) resulting from the corresponding nucleophilic attack of IMe_4. Thus, the steric bulk of H_2IMes prevents attack on the **M1** methylidene, consistent with the fact that the second-generation Ru methylidene complex can be synthesized by addition of H_2IMes to the first-generation analogue.[1,2]

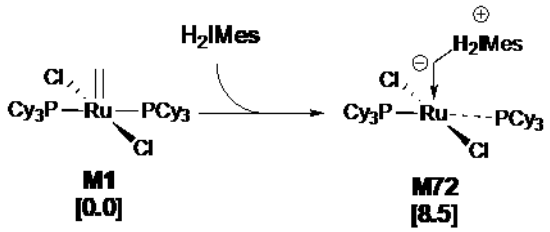

Scheme D9. Free energies (kcal/mol, relative to **M1** = **GIm**) of selected species along reaction pathways involving attack of H_2IMes on $Ru{=}CH_2$.

Table D1. Calculated Gibbs free energies at room temperature in benzene.

Mol. ID	$E_{\varpi\text{B97XD}}$ [a.u.]	$G^{\text{T=298.15K}}_{\varpi\text{B97XD}}$ [a.u.]	$\Delta G^{\text{T=298.15K}}_{\varpi\text{B97XD;qh}}$ [a.u.]	$E^{benzene}_{\text{PBE-D3M(BJ)}}$ [a.u.]	$G^{benzene}_{\text{PBE-D3M(BJ)}}$ [a.u.]	$G^{benzene}_{\text{PBE-D3M(BJ)}}$ w.r.t. **M1**	
						[a.u.]	[kcal/ mol]
M1 = GIm	-3148.540886	-3147.614821	-3147.605868	-3147.010619	-3146.072582	0.000000	0.0
M2	-2101.444613	-2100.984192	-2100.980498	-2100.545743	-2100.078609	0.026150	16.4
M3	-3531.889458	-3530.791870	-3530.778763	-3530.129531	-3529.015817	0.033490	21.0
M4	-3531.913127	-3530.807313	-3530.797107	-3530.142798	-3529.023759	0.025547	16.0
M5	-3531.885395	-3530.784291	-3530.771982	-3530.121585	-3529.005153	0.044154	27.7
M6	-2484.858664	-2484.224990	-2484.217843	-2483.738135	-2483.094296	-0.012812	-8.0
M7	-2868.243137	-2867.429092	-2867.421475	-2866.884070	-2866.059389	-0.001181	-0.7
M8 = Ru-1'	-1437.770239	-1437.601440	-1437.599923	-1437.271496	-1437.098161	0.015499	9.7
M9	-1821.157837	-1820.816312	-1820.812368	-1820.439951	-1820.091463	-0.001078	-0.7
M10	-1821.172411	-1820.831356	-1820.826069	-1820.458873	-1820.109512	-0.019127	-12.0
M11	-2204.575460	-2204.053281	-2204.048634	-2203.627025	-2203.097180	-0.030071	-18.9
M12	-3531.889094	-3530.787262	-3530.776161	-3530.131721	-3529.015770	0.033537	21.0
M13	-3531.964960	-3530.856692	-3530.847416	-3530.193420	-3529.072857	-0.023550	-14.8
M14	-2868.210184	-2867.403953	-2867.393555	-2866.866003	-2866.046355	0.011853	7.4
M15	-2868.280632	-2867.467918	-2867.459303	-2866.925273	-2866.100925	-0.042717	-26.8
M16	-1821.117852	-1820.775721	-1820.772490	-1820.398579	-1820.050199	0.040186	25.2
M17	-1821.196313	-1820.847290	-1820.844966	-1820.465905	-1820.111540	-0.021155	-13.3
M18	-1821.138682	-1820.799471	-1820.793928	-1820.428865	-1820.081092	0.009292	5.8
M19	-1821.197390	-1820.852991	-1820.848144	-1820.473725	-1820.121460	-0.031075	-19.5
M20	-2204.526242	-2204.009841	-2204.003254	-2203.589940	-2203.063933	0.003176	2.0
M21	-2204.593176	-2204.073070	-2204.067150	-2203.645818	-2203.116773	-0.049664	-31.2
M22	-2204.543308	-2204.021115	-2204.016604	-2203.604041	-2203.074318	-0.007209	-4.5
M23	-2204.615792	-2204.096770	-2204.090019	-2203.672055	-2203.143264	-0.076154	-47.8
M24	-2587.928621	-2587.232772	-2587.225667	-2586.755105	-2586.049133	-0.005299	-3.3
M25	-2588.018542	-2587.317968	-2587.311629	-2586.839133	-2586.129201	-0.085367	-53.6
M26	-4202.934453	-4201.986665	-4201.973694	-4201.132635	-4200.168857	0.040661	25.5
M27	-2875.585737	-2875.220848	-2875.214038	-2874.596620	-2874.221903	0.005417	3.4
M28	-2875.581098	-2875.215735	-2875.210229	-2874.590646	-2874.216758	0.010562	6.6
M29 = Ru-2	-2548.745340	-2548.070402	-2548.064212	-2547.591587	-2546.907440	-0.172447	-108.2
M29[a] = Ru-2	-2548.745340	-2548.070402	-2548.064212	-2547.591587	-2546.907440	-0.124998	-78.4
M30	-2243.913724	-2243.359401	-2243.355388	-2242.937305	-2242.375950	-0.172447	-108.2
M31	-4586.342088	-4585.214188	-4585.201002	-4584.311287	-4583.167182	0.019060	12.0
M32	-3922.658565	-3921.821983	-3921.811341	-3921.036453	-3920.186210	0.008934	5.6
M33	-3922.663689	-3921.827739	-3921.817840	-3921.042594	-3920.193726	0.001417	0.9
M34	-3259.006207	-3258.462350	-3258.455471	-3257.793458	-3257.239704	-0.035659	-22.4
M35	-3258.993580	-3258.448529	-3258.442253	-3257.779297	-3257.224952	-0.020907	-13.1
M36	-1477.066704	-1476.872939	-1476.869709	-1476.530513	-1476.330499	-0.080445	-50.5
M37	-1477.088418	-1476.890624	-1476.888831	-1476.562695	-1476.360089	-0.110035	-69.0
M38	-1860.490996	-1860.118782	-1860.114577	-1859.742446	-1859.363009	-0.136230	-85.5
M39	-1860.509701	-1860.137459	-1860.133726	-1859.756444	-1859.377450	-0.150672	-94.5
M40	-1860.383666	-1860.022487	-1860.013491	-1859.636087	-1859.262893	-0.036114	-22.7
M41	-1860.433695	-1860.067799	-1860.060174	-1859.678569	-1859.302030	-0.075251	-47.2
M42	-1860.410059	-1860.045175	-1860.038172	-1859.677584	-1859.302678	-0.075900	-47.6
M43	-1860.411228	-1860.046108	-1860.039625	-1859.676627	-1859.302005	-0.075227	-47.2
M44	-1860.470911	-1860.102499	-1860.095847	-1859.729328	-1859.351245	-0.124466	-78.1
M45	-1860.456274	-1860.085109	-1860.080865	-1859.718733	-1859.340305	-0.113526	-71.2
M46	-2243.807939	-2243.267627	-2243.258739	-2242.853398	-2242.301180	-0.097676	-61.3
M47	-2243.862333	-2243.319961	-2243.311009	-2242.901919	-2242.347577	-0.144073	-90.4
M48	-2243.833640	-2243.292718	-2243.284401	-2242.876831	-2242.324573	-0.121070	-76.0
M49	-2243.832180	-2243.290840	-2243.281995	-2242.874410	-2242.321207	-0.117703	-73.9
M50	-2243.879766	-2243.335616	-2243.327341	-2242.916563	-2242.361119	-0.157616	-98.9
M51	-2243.855715	-2243.305344	-2243.300882	-2242.891756	-2242.333905	-0.130401	-81.8
M52	-2627.232526	-2626.512501	-2626.502633	-2626.041655	-2625.308743	-0.128516	-80.6
M53	-2627.276035	-2626.553235	-2626.544700	-2626.081398	-2625.347044	-0.166816	-104.7

[a] Calculated according to the reaction path that generates **M58** (see Scheme E7).

Table D1 (continued).

Mol. ID	$E_{\varpi\text{B97XD}}$ [a.u.]	$G^{\text{T=298.15K}}_{\varpi\text{B97XD}}$ [a.u.]	$\Delta G^{\text{T=298.15K}}_{\varpi\text{B97XD;qh}}$ [a.u.]	$E^{benzene}_{\text{PBE-D3M(BJ)}}$ [a.u.]	$G^{benzene}_{\text{PBE-D3M(BJ)}}$ [a.u.]	$G^{benzene}_{\text{PBE-D3M(BJ)}}$ w.r.t. **M1**	
						[a.u.]	[kcal/ mol]
M54	-3259.034171	-3258.489231	-3258.481690	-3257.809545	-3257.254045	-0.050000	-31.4
M55	-3258.971864	-3258.426888	-3258.418969	-3257.752512	-3257.196598	0.007446	4.7
M56	-3642.439847	-3641.716903	-3641.708263	-3640.991653	-3640.257050	-0.076281	-47.9
M57	-3642.405577	-3641.686216	-3641.675964	-3640.947232	-3640.214601	-0.033831	-21.2
M58	-3531.897073	-3530.795833	-3530.784585	-3530.129454	-3529.013948	0.035359	22.2
M59	-422.647140	-422.473691	-422.472895	-422.414584	-422.238117	0.012567	7.9
M60	-3109.233899	-3108.332979	-3108.322981	-3107.712560	-3106.798623	0.012567	7.9
M61	-3109.228778	-3108.328378	-3108.318444	-3107.720704	-3106.807352	0.003838	2.4
M62	-3109.263871	-3108.364210	-3108.354669	-3107.737541	-3106.825321	-0.014130	-8.9
M63	-3492.681843	-3491.602579	-3491.591889	-3490.938665	-3489.845692	-0.057777	-36.3
M64	-2484.875654	-2484.239658	-2484.231962	-2483.748018	-2483.101308	-0.019824	-12.4
M65	-3251.685732	-3250.692270	-3250.683296	-3250.091302	-3249.085847	-0.050914	-31.9
M66	-3251.673130	-3250.685250	-3250.673915	-3250.086973	-3249.084739	-0.049807	-31.3
M67	-2829.005087	-2828.220444	-2828.210731	-2827.674817	-2826.877442	-0.080627	-50.6
M68	-3571.195018	-3570.069932	-3570.057552	-3569.422513	-3568.282029	-0.096328	-60.4
M69	-3571.244853	-3570.111102	-3570.100398	-3569.453084	-3568.305611	-0.119910	-75.2
M70	-2524.165359	-2523.502076	-2523.494427	-2523.010284	-2522.336333	-0.118455	-74.3
M71	-2907.557045	-2906.722339	-2906.710669	-2906.181810	-2905.332415	-0.137813	-86.5
M72	-4073.759071	-4072.428552	-4072.413623	-4071.653513	-4070.305046	0.013561	8.5
IMe_4	-383.336311	-383.187732	-383.187732	-383.128322	-382.976725	-	-
PCy_3	-1047.026249	-1046.587417	-1046.584822	-1046.409674	-1045.967823	-	-
H_2IMes	-925.143298	-924.778927	-924.770628	-924.613414	-924.246025	-	-

Table D2. Calculated Gibbs free energies at –80 °C in toluene.

Mol. ID	$E_{\varpi\text{B97XD}}$ [a.u.]	$G^{\text{T=193.15K}}_{\varpi\text{B97XD}}$ [a.u.]	$\Delta G^{\text{T=193.15K}}_{\varpi\text{B97XD;qh}}$ [a.u.]	$E^{toluene}_{\text{PBE-D3M(BJ)}}$ [a.u.]	$G^{toluene}_{\text{PBE-D3M(BJ)}}$ [a.u.]	$G^{toluene}_{\text{PBE-D3M(BJ)}}$ w.r.t. **M1**	
						[a.u.]	[kcal/ mol]
M1 = GIm	-3148.540886	-3147.575730	-3147.570008	-3147.014954	-3146.042386	0.000000	0.0
M2	-2101.444613	-2100.958030	-2100.955673	-2100.548496	-2100.057866	0.034420	21.6
M3	-3531.889458	-3530.745360	-3530.736971	-3530.134669	-3528.980492	0.026434	16.6
M4	-3531.913127	-3530.762628	-3530.756104	-3530.147621	-3528.988908	0.018018	11.3
M5	-3531.885395	-3530.738841	-3530.730965	-3530.126618	-3528.970498	0.036428	22.9
M6	-2484.858664	-2484.191462	-2484.186890	-2483.741881	-2483.068417	-0.011591	-7.3
M12	-3531.889094	-3530.741898	-3530.734799	-3530.136698	-3528.980713	0.026213	16.4
M13	-3531.964960	-3530.812116	-3530.806185	-3530.198441	-3529.037976	-0.031050	-19.5
M25	-2588.018542	-2587.279181	-2587.275125	-2586.843296	-2586.098189	-0.097845	-61.4
M29	-2548.745340	-2548.032691	-2548.028730	-2547.595540	-2546.877240	-0.190932	-119.8
M30	-2243.913724	-2243.327009	-2243.324445	-2242.940810	-2242.349841	-0.190932	-119.8
M51	-2243.855715	-2243.272498	-2243.269643	-2242.895322	-2242.307560	-0.148651	-93.3
M57	-3642.405577	-3641.641538	-3641.634966	-3640.952243	-3640.179942	-0.037413	-23.5
M65	-3571.195018	-3570.022923	-3570.015002	-3569.427571	-3568.245865	0.020720	13.0
M59	-422.647140	-422.457587	-422.457078	-422.415951	-422.224199	-	-
IMe_4	-383.336311	-383.172826	-383.172826	-383.129715	-382.964540	-	-
PCy_3	-1047.026249	-1046.566166	-1046.564513	-1046.411874	-1045.950101	-	-

D2. Computational Study for Chapter 3

Computational Details

All calculations were implemented in Gaussian16. Gas-phase geometries and thermodynamic corrections were computed with the B3LYP functional. Ru atoms were described with the relativistic effective core potential (ECP28MDF) in combination with the correlation-consistent double-ζ plus polarization (cc-pVDZ-PP) basis set. Non-Ru elements were treated using cc-pVDZ. Single-point energy refinements used PBE in tandem with D3M(BJ) dispersion corrections. In these energy calculations, ruthenium was described with ECP28MDF and a quadruple-ζ basis set (cc-pVQZ-PP). Carbon and hydrogen atoms were described using cc-pVQZ, with all other atoms using aug-cc-pVQZ. Benzene solvation was treated implicitly using the polarized continuum model (PCM) in the single point calculation.

Calculations for the reaction of **HII-OH** and C_2H_4 were undertaken using a van der Waals complex of the precatalyst and small olefin. Results stemming from this reference point have been shown to be in better agreement with experimental findings.[32]

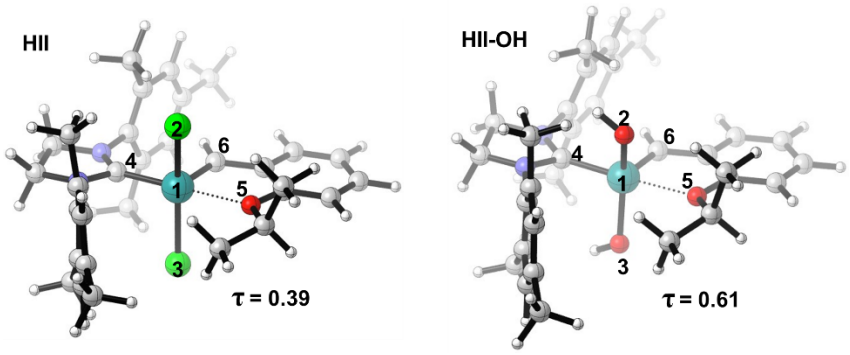

Figure D1. Comparing the optimized geometries for **HII** and **HII-OH**. Values of τ are calculated based on angles shown in Table D3, below.

Table D3.Comparing important bond lengths and angles between **HII** and **HII-OH**. The τ parameter is calculated according to (β-α)/60.[33]

Bond length (Å)	**HII**	**HII-OH**
Ru_1-O_5	2.33	2.28
Ru_1-C_4	1.96	1.93
Ru_1-C_6	1.84	1.85
Ru_1-X (X = Cl or O)	2.37	1.98
Bond angle (°)		
X_2-Ru-X_3 (X = Cl or O)	155.1	139.6
C_4-Ru_1-O_5	178.6	176.2
τ	0.39	0.61

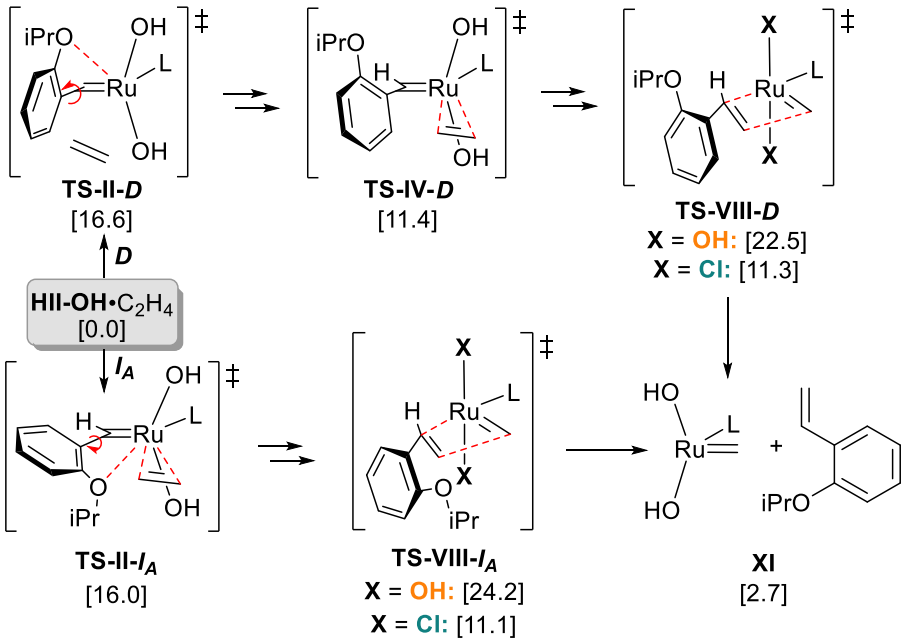

Scheme D10. Comparing the transition-state energies (in kcal/mol) required for initiation and cycloaddition in the reaction of **HII** (green, X = Cl)) and **HII-OH** (orange, X = OH) with ethylene.

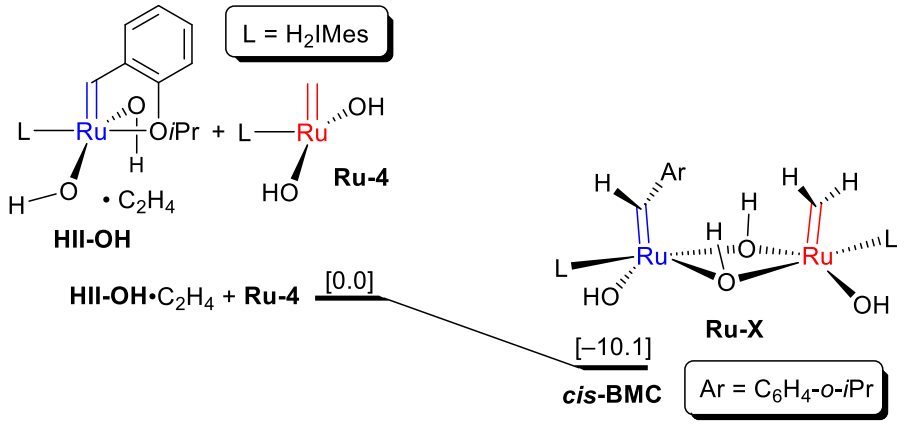

Scheme D11. Computed Gibbs free energy profile (kcal/mol) for the bimolecular coupling of **HII-OH** with **Ru-4**. The chosen geometry is analogous to that considered by Fogg and co-workers.[2]

E. References

(1) Frisch, M. J.; Trucks, G. W.; Schlegel, H. B.; Scuseria, G. E.; Robb, M. A.; Cheeseman, J. R.; Scalmani, G.; Barone, V.; Mennucci, B.; Petersson, G. A.; Nakatsuji, H.; Caricato, M.; Li, X.; Hratchian, H. P.; Izmaylov, A. F.; Bloino, J.; Zheng, G.; Sonnenberg, J. L.; Hada, M.; Ehara, M.; Toyota, K.; Fukuda, R.; Hasegawa, J.; Ishida, M.; Nakajima, T.; Honda, Y.; Kitao, O.; Nakai, H.; Vreven, T.; Montgomery Jr., J. A.; Peralta, J. E.; Ogliaro, F.; Bearpark, M. J.; Heyd, J.; Brothers, E. N.; Kudin, K. N.; Staroverov, V. N.; Kobayashi, R.; Normand, J.; Raghavachari, K.; Rendell, A. P.; Burant, J. C.; Iyengar, S. S.; Tomasi, J.; Cossi, M.; Rega, N.; Millam, N. J.; Klene, M.; Knox, J. E.; Cross, J. B.; Bakken, V.; Adamo, C.; Jaramillo, J.; Gomperts, R.; Stratmann, R. E.; Yazyev, O.; Austin, A. J.; Cammi, R.; Pomelli, C.; Ochterski, J. W.; Martin, R. L.; Morokuma, K.; Zakrzewski, V. G.; Voth, G. A.; Salvador, P.; Dannenberg, J. J.; Dapprich, S.; Daniels, A. D.; Farkas, Ö.; Foresman, J. B.; Ortiz, J. V.; Cioslowski, J.; Fox, D. J. *Gaussian 09*, Revision D.01; Gaussian, Inc.: Wallingford, CT, USA, 2009.

(2) Bailey, G. A.; Foscato, M.; Higman, C. S.; Day, C. S.; Jensen, V. R.; Fogg, D. E., Bimolecular Coupling as a Vector for Decomposition of Fast-Initiating Olefin Metathesis Catalysts. *J. Am. Chem. Soc.* **2018**, *140*, 6931–6944.

(3) Becke, A. D., Density-functional thermochemistry. V. Systematic Optimization of Exchange-Correlation Functionals. *J. Chem. Phys.* **1997**, *107*, 8554–8560.

(4) Wu, Q.; Yang, W., Empirical Correction to Density Functional Theory for van der Waals Interactions. *J. Chem. Phys.* **2002**, *116*, 515–524.

(5) Chai, J.-D.; Head-Gordon, M., Long-Range Corrected Hybrid Density Functionals with Damped Atom-Atom Dispersion Corrections. *Phys. Chem. Chem. Phys.* **2008**, *10*, 6615–6620.

(6) Minenkov, Y.; Singstad, Å.; Occhipinti, G.; Jensen, V. R., The Accuracy of DFT-Optimized Geometries of Functional Transition Metal Compounds: A Validation Study of Catalysts for Olefin Metathesis and Other Reactions in The Homogeneous Phase. *Dalton Trans.* **2012**, *41*, 5526–5541.

(7) Dunning, T. H., Gaussian Basis Sets for Use in Correlated Molecular Calculations. I. The Atoms Boron Through Neon and Hydrogen. *J. Chem. Phys.* **1989**, *90*, 1007–1023.

(8) Woon, D. E.; Dunning, T. H., Gaussian Basis Sets for Use in Correlated Molecular Calculations. III. The Atoms Aluminum through Argon. *J. Chem. Phys.* **1993**, *98*, 1358–1371.

(9) Feller, D., The Role of Databases in Support of Computational Chemistry Calculations. *J. Comput. Chem.* **1996**, *17*, 1571–1586.

(10) Schuchardt, K. L.; Didier, B. T.; Elsethagen, T.; Sun, L.; Gurumoorthi, V.; Chase, J.; Li, J.; Windus, T. L., Basis Set Exchange: A Community Database for Computational Sciences. *J. Chem. Inf. Model.* **2007**, *47*, 1045–1052.

(11) Peterson, K. A.; Figgen, D.; Dolg, M.; Stoll, H., Energy-Consistent Relativistic Pseudopotentials and Correlation Consistent Basis Sets for the 4d Elements Y–Pd. *J. Chem. Phys.* **2007**, *126*, 124101.

(12) http://www.tc.uni-koeln.de/PP/clickpse.en.html, visited October, 2 2018.

(13) Martin, J. M. L.; Bauschlicher, C. W.; Ricca, A., On the Integration Accuracy in Molecular Density Functional Theory Calculations Using Gaussian Basis Sets. *Comput. Phys. Commun.* **2001**, *133*, 189–201.

(14) Zhao, Y.; Truhlar, D. G., Computational Characterization and Modeling of Buckyball Tweezers: Density Functional Study of Concave–Convex π···π Interactions. *Phys. Chem. Chem. Phys.* **2008**, *10*, 2813–2818.

(15) Ribeiro, R. F.; Marenich, A. V.; Cramer, C. J.; Truhlar, D. G., Use of Solution-Phase Vibrational Frequencies in Continuum Models for the Free Energy of Solvation. *J. Phys. Chem. B* **2011**, *115*, 14556–14562.

(16) Perdew, J. P.; Burke, K.; Ernzerhof, M., Generalized Gradient Approximation Made Simple. *Phys. Rev. Lett.* **1996**, *77*, 3865–3868.

(17) Perdew, J.; Burke, K.; Ernzerhof, M., Erratum to ref 16. *Phys. Rev. Lett.* **1997**, *78*, 1396–1396.

(18) Grimme, S.; Ehrlich, S.; Goerigk, L., Effect of the Damping Function in Dispersion Corrected Density Functional Theory. *J. Comput. Chem.* **2011**, *32*, 1456–1465.

(19) Smith, D. G. A.; Burns, L. A.; Patkowski, K.; Sherrill, C. D., Revised Damping Parameters for the D3 Dispersion Correction to Density Functional Theory. *J. Phys. Chem. Lett.* **2016**, *7*, 2197–2203.

(20) Kendall, R. A.; Dunning, T. H.; Harrison, R. J., Electron Affinities of the First-Row Atoms Revisited. Systematic Basis Sets and Wave Functions. *J. Chem. Phys.* **1992**, *96*, 6796–6806.

(21) Cossi, M.; Scalmani, G.; Rega, N.; Barone, V., New Developments in the Polarizable Continuum Model for Quantum Mechanical and Classical Calculations on Molecules in Solution. *J. Chem. Phys.* **2002**, *117*, 43–54.

(22) Scalmani, G.; Frisch, M. J., Continuous Surface Charge Polarizable Continuum Models of Solvation. I. General Formalism. *J. Chem. Phys.* **2010**, *132*, 114110.

(23) Tomasi, J.; Mennucci, B.; Cammi, R., Quantum Mechanical Continuum Solvation Models. *Chem. Rev.* **2005**, *105*, 2999–3093.

(24) Tomasi, J.; Persico, M., Molecular Interactions in Solution: An Overview of Methods Based on Continuous Distributions of the Solvent. *Chem. Rev.* **1994**, *94*, 2027–2094.

(25) Tomasi, J., Thirty Years of Continuum Solvation Chemistry: A Review, and Prospects for the near Future. *Theor. Chem. Acc.* **2004**, *112*, 184–203.

(26) Cramer, C. J.; Truhlar, D. G., Density Functional Theory for Transition Metals and Transition Metal Chemistry. *Phys. Chem. Chem. Phys.* **2009**, *11*, 10757–10816.

(27) Klamt, A.; Mennucci, B.; Tomasi, J.; Barone, V.; Curutchet, C.; Orozco, M.; Luque, F. J., On the Performance of Continuum Solvation Methods. A Comment on "Universal Approaches to Solvation Modeling". *Acc. Chem. Res.* **2009**, *42*, 489–492.

(28) McMullin, C. L.; Jover, J.; Harvey, J. N.; Fey, N., Accurate Modelling of Pd(0) + PhX Oxidative Addition Kinetics. *Dalton Trans.* **2010**, *39*, 10833-10836.

(29) Fernández-Ramos, A.; Miller, J. A.; Klippenstein, S. J.; Truhlar, D. G., Modeling the Kinetics of Bimolecular Reactions. *Chem. Rev.* **2006**, *106*, 4518-4584.

(30) Engel, J.; Smit, W.; Foscato, M.; Occhipinti, G.; Törnroos, K. W.; Jensen, V. R., Loss and Reformation of Ruthenium Alkylidene: Connecting Olefin Metathesis, Catalyst Deactivation, Regeneration, and Isomerization. *J. Am. Chem. Soc.* **2017**, *139*, 16609–16619.

(31) Powers, K.; Hering-Junghans, C.; McDonald, R.; Ferguson, M. J.; Rivard, E., Improved Synthesis of N-Heterocyclic Olefins and Evaluation of their Donor Strengths. *Polyhedron* **2016**, *108*, 8–14.

(32) Ashworth, I. W.; Hillier, I. H.; Nelson, D. J.; Percy, J. M.; Vincent, M. A., Olefin Metathesis by Grubbs–Hoveyda Complexes: Computational and Experimental Studies of the Mechanism and Substrate-Dependent Kinetics. *ACS Catal.* **2013**, *3*, 1929-1939.

(33) Addison, A. W.; Rao, T. N.; Reedijk, J.; Van Rijn, J.; Verschoor, G. C., Synthesis, Structure, and Spectroscopic Properties of Copper(II) Compounds Containing Nitrogen-Sulfur Donor Ligands. *J. Chem. Soc., Dalton Trans.* **1984**, 1349–1356.